UNIVERSITÀ
DI PARMA

Chemical Sciences XXXII Cycle Ph.D.

Pharmaceutical and environmental applications of coordination chemistry: innovative design of chelating agents and metal complexes with biological activity

Ph.D. Student: Jennifer Bartoli

Supervisors: Prof. Rogolino Dominga
Prof. Carcelli Mauro

2016-2019

"It was the secrets of heaven and earth that I desired to learn;
and whether it was the outward substance of things or the inner spirit of nature
and the mysterious soul of man that occupied me,
still my inquiries were directed to the metaphysical, or in its highest sense,
the physical secrets of the world."

Mary Shelley

Summary

Thiosemicarbazone derivatives as anti-aflatoxigenic agents 9

1.Introduction 10
- 1.0 Premise 11
- 1.1 *Aspergillus Flavus* 13
- 1.2 Aflatoxins biosynthesis 14
- 1.3 Aflatoxigenic inhibitors 18
  - 1.3.1 Phenylpropanoids 19
  - 1.3.2 Terpenoids and Alkaloids 20
  - 1.3.3 Plant-signaling compounds 22
  - 1.3.4 Phytic and Hydroxamic acids 22
  - 1.3.5 Calcium signaling disruptors 23
  - 1.3.6 Antibiotics and cyclic dipeptides 24
- 1.4 A new class of inhibitors: the thiosemicarbazone ligands 24

2.Experimental section 29
- 2.1 Materials and methods 30
- 2.2 Chemistry 30
- 2.3 Biological analysis 38
  - 2.3.1 Aflatoxins accumulation and fungal growth 38
  - 2.3.2 Cytotoxicity 39
  - 2.3.3 Genotoxicity on human cells 40
  - 2.3.4 Mutagenicity on bacteria and cytotoxicity on plants 40

3. Results and Discussion 42
- 3.1 High lipophilic thiosemicarbazones 43
  - 3.1.1 Synthesis and Characterization 43
  - 3.1.2 Anti-aflatoxigenic and antifungal activity 47
  - 3.1.3 Cyto- and genotoxicity 48
  - 3.1.4 Conclusion 53
- 3.2 Bis-vanillin scaffold derivatives 54
  - 3.2.1 Synthesis and Characterization 54
  - 3.2.2 Evaluation of antioxidant activity 57
  - 3.2.3 Anti-aflatoxigenic and antifungal activity 58

Thiosemicarbazones and Cu(II)-complexes as antitumor agents 59

1.Introduction 60
- 1.0 Premise 61
- 1.1 *cis*Platin and platinum-containing drugs 64
  - 1.1.1 *cis*Platin analogues 67
- 1.2 Copper complexes as antitumor compounds 70
  - 1.2.1 Copper and its role in biological systems 70
  - 1.2.2 Copper homeostasis 71

1.2.3 Copper and its role in neoplasms 73
1.3 Copper complexes as an alternative to platinum-based drugs in anticancer therapy 75
1.4 Mechanism of action of copper complexes 76
1.4.1 Copper complexes as topoisomerase inhibitors 77
1.4.2 26S proteasome inhibitors 78
1.5 S-donor systems: thiosemicarbazones (TSCs) 80

2. Experimental section 83
2.1 Materials and methods 84
2.1.1 Chemistry 84
2.1.2 crystallography 84
2.2 Chemistry 85
2.3 Studies in solution 89
2.4 *In vitro* biological assays 90
2.4.1 Experiments with human cells 90
2.4.2 Cell cultures 91
2.4.3 Spheroid cultures 91
2.4.4 MTT assay 91
2.4.5 Acid Phosphatase (APH) Assay 91
2.4.6 Cellular accumulation and distribution 92
2.4.7 Comet Assay 92
2.4.8 Proteasome activity 93
2.4.9 Quantification of thiols 93
2.4.10 Total and oxidized intracellular glutathione 93
2.4.11 Protein disulfide isomerase (PDI) activity 94
2.4.12 Transmission electron microscopy (TEM) analysis 94
2.4.13 Nuclear DNA fragmentation 94
2.5 Experiments with animals 94

3. Results and Discussion 96
3.1 Cu(II)-thiosemicarbazone complexes 97
3.1.1 Synthesis and crystal structure analysis 97
3.1.2 Studies in solution 101
3.1.3 Evaluation of the *in vitro* cytotoxicity 105
3.1.4 Evaluation of cellular uptake 108
3.1.5 Mechanistic studies of Cu(II)-thiosemicarbazones complexes 109
3.1.6 *in vivo* preliminary studies of **FM4** 112
3.2 Water-soluble Cu(II) complexes 113
3.2.1 Synthesis and crystal structure analysis 113

2,3-dihydro-6,7-dihydroxy-1H-isoindol-1-ones as Influenza virus PA_N endonuclease inhibitors 117

1. Introduction 118
1.0 Premise 119
1.1 Influenza virus 120

1.1.1 Influenza virus structure 120
1.1.2 Influenza virus lifecycle 121
1.2 Treatment of Influenza virus infections 123
1.2.1 M2 ion channel blockers 123
1.2.2 NA protein inhibitors 124
1.2.3 RNA polymerase or endonuclease inhibitors 125
1.3 PA_N endonuclease as a new attractive target 127
1.4 PA_N endonuclease inhibitors 132
1.4.1 α,β-diketo acids family 132
1.4.2 Flutimide and its derivatives 133
1.4.3 N-hydroxamic acids family and catechins 134
1.4.4 3-hydroxypyridinone and analogues 135

2. Experimental section 139
2.1 Materials and methods 140
2.1.1 Chemistry 140
2.1.2 Protein expression and purification 140
2.1.3 Endonuclease activity assay 141
3.2 Chemistry 142

3. Results and Discussion 153
3.1 2,3-dihydro-6,7-dihydroxy-1H-isoindol-1-one-based inhibitors 154
3.1.1 Synthesis and Characterization 154
3.2 Biological assays 162
3.2.1 FRET-based endonuclease assay 162

Thiosemicarbazone derivatives as anti-aflatoxigenic agents

1.INTRODUCTION

1.0 PREMISE

Since ancient times, global economy has been mostly based on agriculture, in particular cereal crops like corn or wheat. Agriculture is at the heart of the economy of most developing countries; in the last decades, a relevant problem has acquired more and more importance: about 40% of worldwide food is spoiled or lost. This is primarily caused by climate changes[1] that have occurred over the past 30 years: it is well known worldwide that the Earth is overheating due to the air pollution caused by progress, provoking drastic climate changes, with dry winters and rainy summers becoming more common every year, affecting the cultures and causing serious losses to farmers. The increase of the amount of CO_2 in the atmosphere also "stresses" crops and provokes, among many other effects, the proliferation of different classes of fungi, like *Aspergillus*, *Fusarium* and *Penicillium genera*.[2] As a consequence, fungal contamination of crops and food has become a crucial problem worldwide.

Among all, the *Aspergillus genera* is responsible of the production of beneficial secondary metabolites, such as antibiotics and other pharmaceuticals[3]: for example, *A. terreus* produces lovastatin, which is used as a potent cholesterol-lowering drug. However, this kind of fungi also produce secondary metabolites, called mycotoxins, that are toxic for plants, humans and animals. Such compounds are not essential for fungal survival, but it is just a way to respond to the extreme condition at which they're exposed. There are several kind of fungal toxins, and they can be classified on the basis of the side effects that they can provoke. They are generally divided into: a) cytotoxic poisons, b) neurotoxins, c) gastrointestinal irritant, d) toxin similar to Antabuse, a drug use in cases of alcoholism addiction. Among all mycotoxins, the most important are aflatoxins (AFs): these metabolites are produced by *Aspergillus genera*, in particular the *Aspergillus flavus* fungus. Such compounds result to be extremely toxic and it is really important to prevent food contamination, also considering the thermal stability of AFs, that can be found also in processed food. The aim of the work discussed in this chapter is to impair the production of these secondary metabolites, and food contamination as a consequence, without damaging the microbiome of the fungus. In order to do that, the thiosemicarbazones class has been explored, together with different

[1] Oerke, E. C. & Dehne, H. W. ; *Crop Protection* 23, 275–285 (**2004**).

[2] Tournas, V. H. ; *Critical reviews in microbiology* 31(1), 33–44 (**2005**).

[3] Brakhage, A.A.; Schuemann, J.; Bergmann, S.; Scherlach, K.; Schroeckh, V.; Hertweck, C. ; *Prog. Drug Res*. 66, 3–12 (**2008**).

related metal complexes, as potential anti-aflatoxigenic agents. Biological assays have been developed to evaluate their activity against *AF*s proliferation, together with cyto-/genotoxicity test on both human and plant cells.

1.1 ASPERGILLUS FLAVUS

A. flavus (Figure 1) belongs to *Trichocomaceae familia*, which includes about 200 molds; it is present preferably in environments rich in CO_2 and it proliferates in different kind of food and crops, particularly if rich in amid, like cereals, cotton, groundnuts, peanuts, etc.

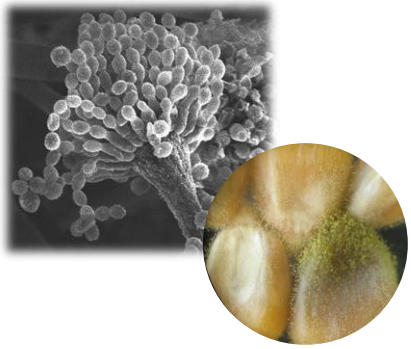

Figure 1.Aspergillus flavus on corn seeds as seen by trasmission electron microscopy

This is the most economically important fungus because it is the most abundant soil-borne mold on earth; its notoriety is due to production of AFs. This fungus is stable from 12°C to 48°C, but the perfect range of growing is between 28-37°C, therefore its growth is favored in hot and humid climates. The *A. flavus* toxins were first identified as the cause of a severe animal poisoning incident in England in 1960, called the Turkey X disease[4,5]. The five major aflatoxins are highlighted in Figure 2; the most dangerous one is aflatoxin B1. Chronic exposure to aflatoxins can result in suppressed immune response, malnutrition, proliferation of the bile duct, centrilobular necrosis and fatty infiltration of the liver, hepatic lesions, and even hepatomas. In addition to aflatoxins B_1 and B_2, *A. flavus* also produces many other mycotoxins such as cyclopiazonic acid, kojic acid, beta-nitropropionic acid, aspertoxin, aflatrem and aspergillic acid[6].

[4] Allcroft, R.; Carnaghan, R.B.A.; Sargeant, K.; O'Kelly, J. ; *Vet. Rec*. 73, 428–429 (**1961**).

[5] Lancaster, M.D.; Jenkins, F.P.; Philip, J.M. ; *Nature* 192, 1095–1096 (**1961**).

[6] Goto, T.; Wicklow, D.T.; Ito, Y. ; *Appl. Environ. Microbiol*. 62, 4036–4038 (**1996**).

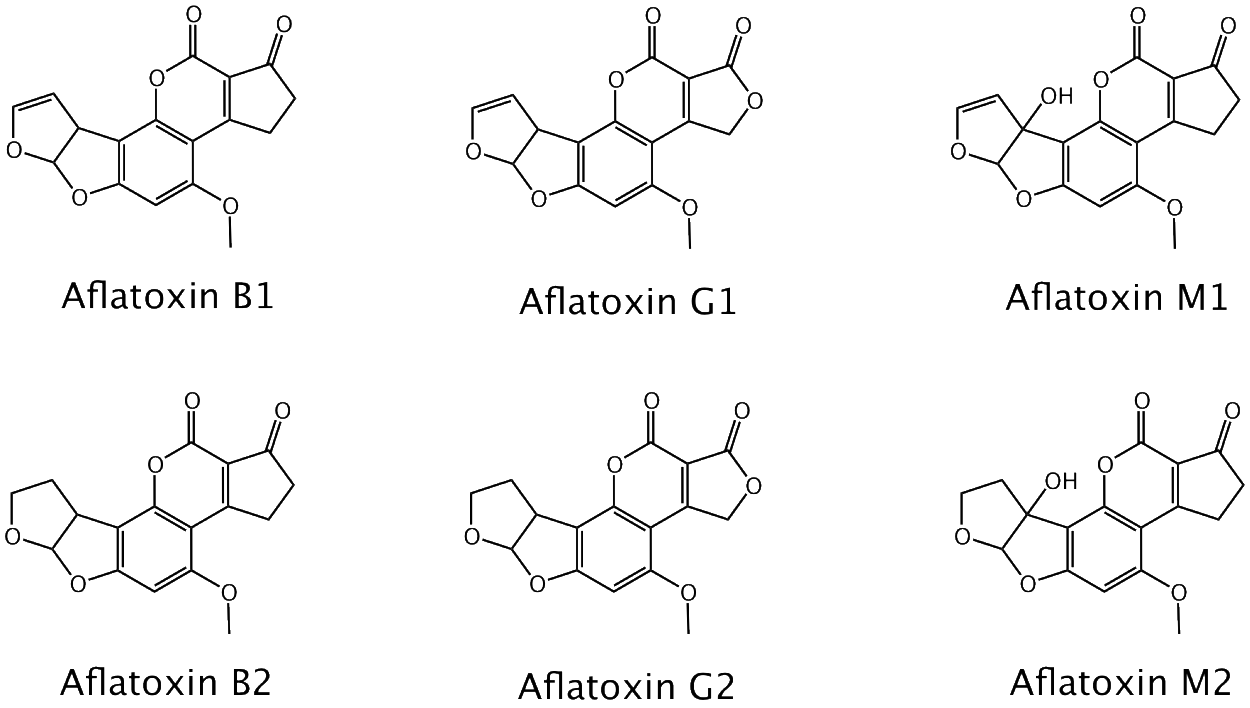

Figure 2. Molecular structure of the most common AFs.

Contamination by mycotoxins could occur both pre-harvest and post-harvest and it is frequent in developing countries, both for climate conditions and for uncorrected agricultural practices. These compounds have a good stability: they persist to thermal treatments and are found in processed food; moreover, they can be found in milk and milk-derived food of animals feed with contaminated crops. Therefore, it would be possible to find aflatoxins in common aliments that we consume every day, especially nuts, corn, baked products and cheese.

1.2 AFLATOXINS BIOSYNTHESIS

Extensive efforts have been made to better understand AFs biosynthesis during the years,[7,8,9] but it has been a really difficult challenge, since the synthetic pathway involves numerous steps (Figure 3).

[7] Papa, K.E. ; *Mycologia* 68, 159–165 (**1976**).

[8] Bennett, J.W.; Goldblatt, L.A. ; *Sabouraudia* 11, 235–241 (**1973**).

[9] Jiujiang Yu; *Toxin* 4; 1024-1057 (**2012**).

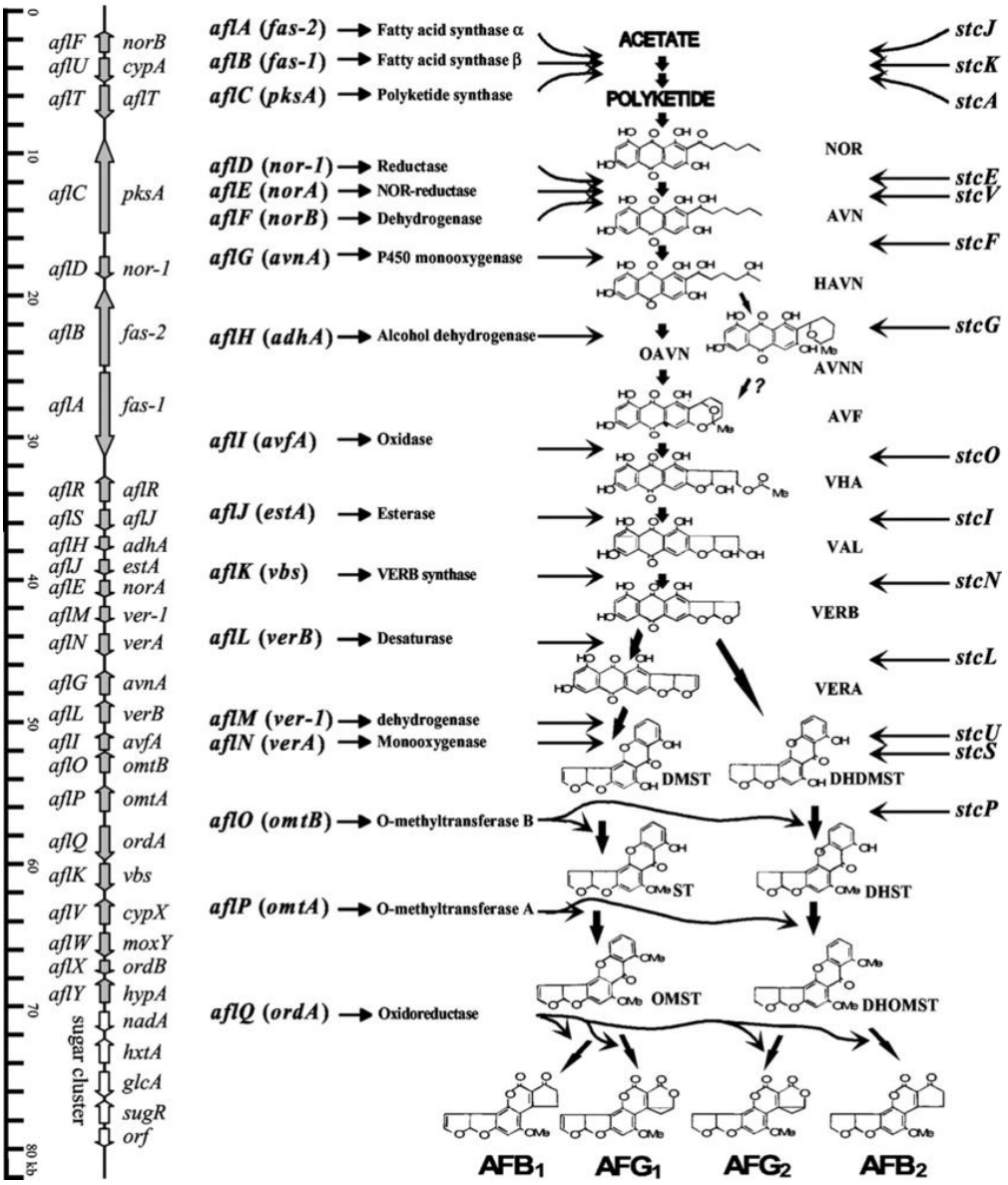

Figure 3.Biosynthetic pathway of aflatoxins and scheme of the 30 gene cluster (on the left).

Different studies have highlighted that the first stable precursor of AFs biosynthesis is NOR (norsolorinic acid).[10,11] Other precursors have been identified so far and it was stated that biosynthesis of these mycotoxins includes a gene cluster (30 genes), discovered in *A. parasiticus/flavus*[12], that is controlled by a complex regulatory network that involves multiple proteins and complexes (Figure 4).

10 Bennett, J.W.; Chang, P.K.; Bhatnagar, D. ; *Adv. Appl. Microbiol*. 45, 1–15 (**1997**).

11 Dutton, M.F. ; *Microbiol. Rev*. 52, 274–295 (**1988**).

12 Yu, J.; Chang, P.K.; Cary, J.W. et al. ; *Appl. Environ. Microbiol*. 61, 2365-2371(**1995**).

Starting from an hexanoyl unit, which is the initial substrate for AFs synthetic pathway[13] (Figure 4), polyketide is synthesized thanks to two synthases (FAS) and a polyketide synthase (NR-PKS, PksA); seven malonyl-derived ketide extension are necessary to produce norsolorinic acid anthrone[14], which is converted to NOR through a monooxygenase. Then three enzymatic steps convert NOR to averufin (AVF) which is a key intermediate for AFs biosynthesis: NOR is converted into AVN by a reductase, to HAVN by a monooxygenase and to AVF by a second dehydrogenase. Averufin is subjected to an oxidation, then a hydrogenation to give versional (VAL), which is converted to VER-B by a cyclase: this is the last intermediate of the pathway that different AFs have in common, then this compound would be subjected to various reactions to provide different aflatoxin scaffolds like B1, B2, G1 and G2. To these, two more are added, M1 and M2: they are mammalian AFs derived from a conversion of the respective B forms (Figure 2).

Proteins and complexes respond to different stimuli such as carbon and nitrogen sources, temperature, light, pH, amino acids in the environment, reactive oxygen species, hypoxic conditions, biofilm formation, iron availability, but also stimuli derived from another organism.[15,16,17]

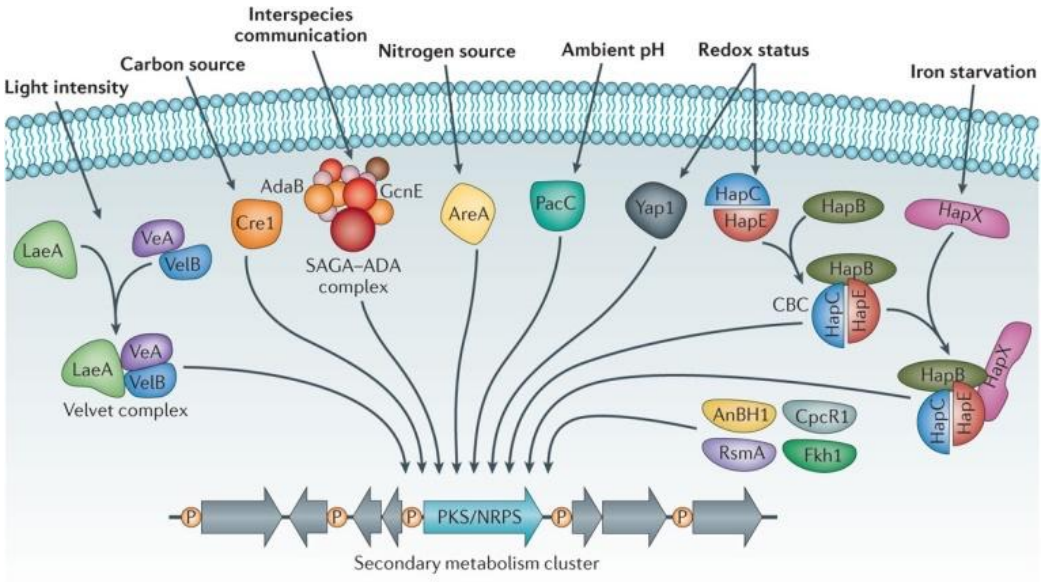

Figure 4.Global regulatory proteins involved in the regulation of gene clusters in various fungi. [Taken from A.A. Brachage][18]

13 Hsieh, D.P.; Mateles, R.I. ; *Biochem. Biophys. Acta* 208, 482-486 (**1970**).

14 Crawford, J.M. et al. ; *Science* 320, 243–246 (**2008**).

15 A.A. Brakhage, et al. ; *Phytochemistry*, 70, 1801-1811 (**2009**).

16 S. Bruns, et al. ; *Proteomics* 10, 3097-3107 (**2010**).

17 M. Vodisch, et al. ; *J. Proteome Res*. 10, 2508-2524 (**2011**).

18 A.A. Brakhage ; *Nat. Rev. Microbiol.* 11, 21-32 (**2013**).

There are different factors that can influence the synthetic pathway: a) nutritional factors like nitrogen and carbon sources; b) water activity and temperature[19]; c) pH and bioactive agents[20,21,22]. One important aspect influencing AFs production is related to oxidative stress conditions: for instance, it has been revealed[23] that treating *A. flavus* with H_2O_2 induces significant increase of production of mycotoxins by the fungus; other studies proved that hydrolysable tannins[24] can inhibit AFs biosynthesis because gallic acid, a decomposition product with antioxidant activity, is able to reduce the expression of the gene cluster involved in the assembly of the toxins. It has also been verified that if supplying antioxidant compounds, like ascorbic or caffeic acid, to an oxidatively stressed fungus, AFs synthesis is decreased, without effecting normal fungal growth.

Nowadays, different approaches are applied to limit aflatoxins proliferation: they are classified into pre-harvest or post-harvest ones. There's a third category, the least used, which involved the rotation of the cultivated land: this technique reduces the stress of the crops, limiting proliferation of fungi, causing the decreasing of AFs productions. Pre/post-harvest strategies focus on the use of chemical substances known as pesticides. These are defined by FAO as "any substance, single or mixed with others, designed to destroy or control any harmful organism or prevent damage".[25] The use of this class of compounds provokes different kinds of problems: first, they are not specific for fungi as the *Aspergillus*, so they can completely destroy the plant microbiome; secondary, pesticides can persist both in the environment and on the crops, contaminating also the processed food. Because of all these aspects, there is an urgent need of finding new compounds that are able to contain aflatoxin contamination and at the same time are safe for humans and the environment. With these premises, it is necessary to find compounds that have a good anti-aflatoxigenic activity, but that do not interfere with fungal growth. This is an important aspect to evaluate, since the capability of an aflatoxigenic inhibitor to suppress AFs biosynthesis and accumulation in a selective way, allows to preserve the presence of fungi, which is not negative itself, without affecting the

19 Peng Wang et al.; *International Journal of Food Microbiology* 310; 108313 (**2019**).

20 Kale, S.P.; Cary, J.W.; Bhatnagar, D.; Bennett, J.W. ; *Appl. Environ. Microbiol*. 62; 3399–3404 (**1996**).

21 Kale, S.; Bennett, J.W. ; Bhatnagar, D., Lillehoj, E.B., Arora, D.K., Eds.; Tylor and Francis: New York, NY, USA, **1991**; Volume 5, pp. 311–332.

22 Yabe, K.; Nakamura, H.; Ando, Y.; Terakado, N.; Nakajima, H.; Hamasaki, T. ; *Appl. Environ. Microbiol*. 54; 2096–2100 (**1988**).

23 Kim, J.H.; Campbell, B.C.; Molyneux, R.; Mahoney, N.; Chan, K.L.; Yu, J. et al. ; *Mycotoxin Res*. 22; 3–8 (**2006**).

24 Mahoney, N.; Molyneux, R.J. ; *J. Agric. Food Chem*. 52; 1882–1889 (**2004**).

25 http://www.fao.org/environmental-social-standards/en/

plant microbiome. With the aim to find a good candidate, different natural compounds have been tested and are described in the literature as AFs inhibitors, in particular essential oils: it is well known that such compounds have a good antimicrobic activity combined with a safe profile for humans and animals.

1.3 AFLATOXIGENIC INHIBITORS

Three different strategies of AFs' synthesis inhibition have been highlighted so far: a) altering the physiological environment; b) interfering with the gene cluster expression; c) blocking the enzymatic activity of an enzyme (Figure 5). Most inhibitors' mode of action is still unknown, but studies have demonstrated that they may act before the first important step of the biosynthesis. There is also some evidence of inhibition of single enzyme activities, but the best inhibitors are the ones acting on physiological and environmental factors, such as ROS concentration and pH.

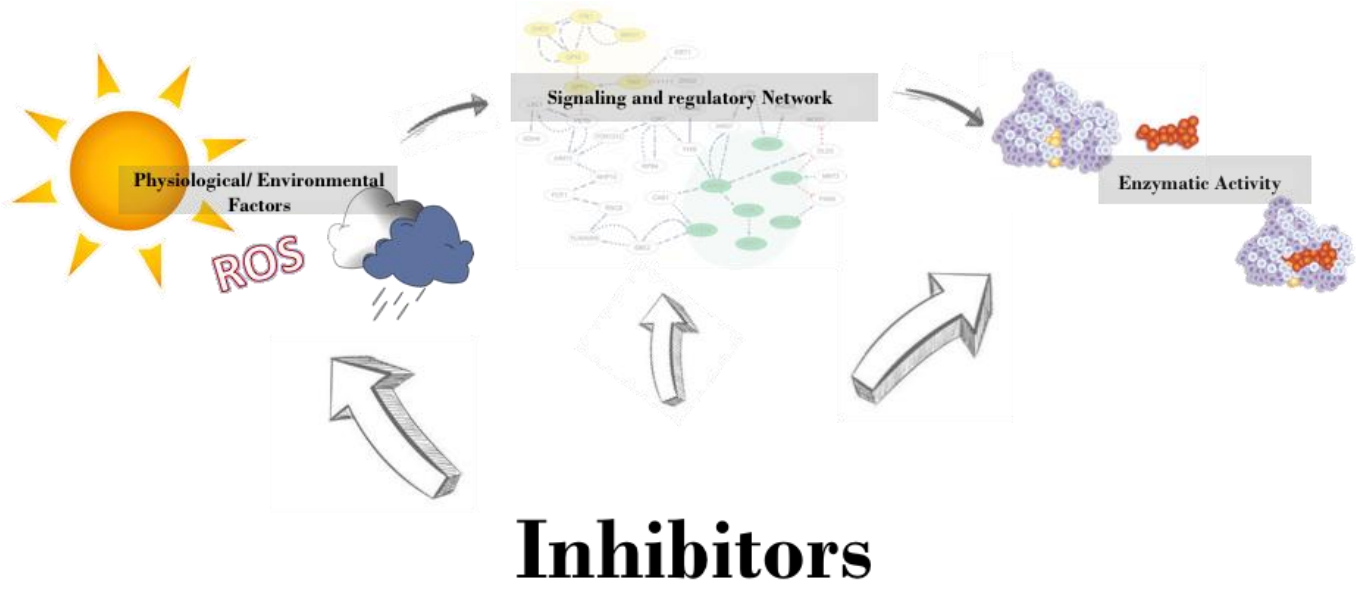

Figure 5.Scheme showing the potential mode of action of an inhibitor.

Since 1960, diverse compounds, both natural and synthetic, have been screened for their ability to block AFs biosynthesis: the most important classes of inhibitors are briefly described in the following paragraphs.

1.3.1 Phenylpropanoids

Recent studies have demonstrated that there is a correlation between oxidative stress and ROS production: in order to survive to oxidative stress, the organism has to keep under control the concentration of ROS inside the cell, and the presence of a high content of such compounds is a prerequisite to AFs biosynthesis. It has been also demonstrated that a reduction of ROS production can be induced by aflatoxins inhibitors with antioxidant activity. Because of that, a different number of antioxidant compounds have been considered for their anti-aflatoxigenic activity: phenylpropanoids are some of these. They are organic molecules produced by plants from phenylalanine and tyrosine and many of them show an antioxidant activity. However, because of their complex structure, the uptake, interaction with enzymes and intracellular mobility could be difficult. This class includes phenols and flavonoids. An example is eugenol (Figure 6), which is found in cloves and cinnamon. This compound seems to inhibit aflatoxins production[26] but, in some cases, the opposite behavior was observed: depending on the time of exposure of crops to eugenol, it can increase the percentage of AFs that are produced. Ferulic acid, a building block of lignin, which has an important defense role in the plants, has also been studied[27], but there is still debate about its real anti-aflatoxigenic activity; vanillylacetone, which acts at the biosynthesis level, shows a better activity that vanillin or vanillic acid[28]. Non-plant phenolics have been tested, like the food additives butylated hydroxyanisole and butylated hydroxytoluene, and they have revealed a really good activity[29].

---

26 Hitokoto H. , Morozumi S. , Wauke T. , Sakai S. , Kurata H. ; *Appl Environ Microbiol* 39; 818–822 (**1980**).

27 Chipley J.R., Uraih N.; *Appl Environ Microbiol* 40; 352–357 (**1980**).

28 Aziz N.H. et al. ; *Microbios* 93; 43–54 (**1998**).

29 Rusul G, Marth E.H. ; *Mycopathologia* 101; 13–23 (**1988**).

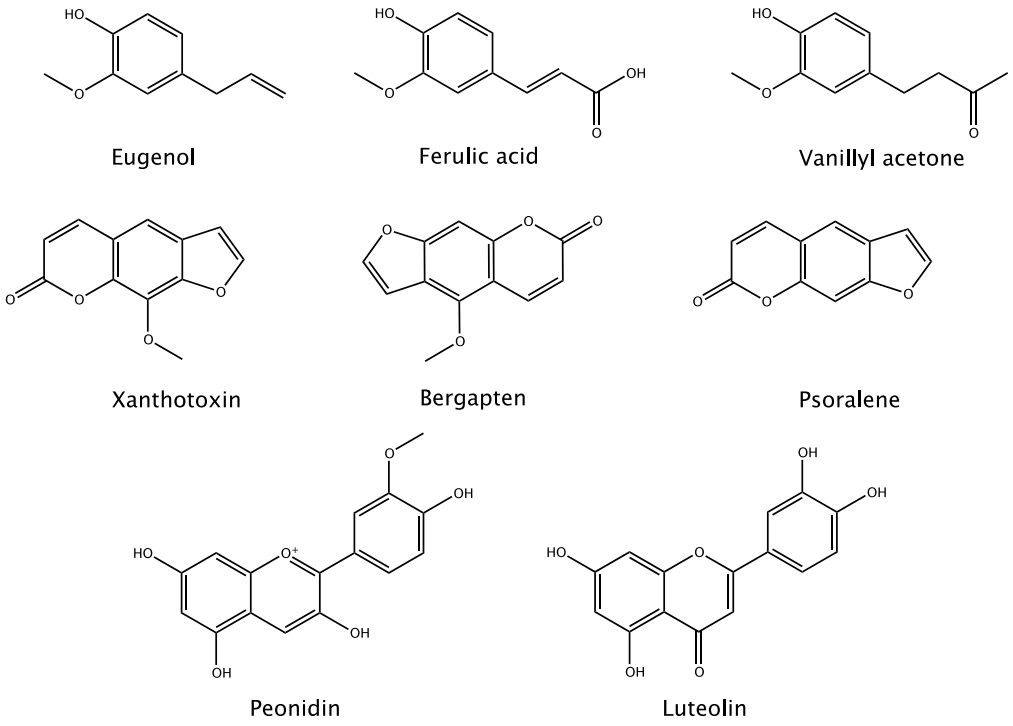

Figure 6.Molecular structure of the most important phenylpropanoids

Cumarins, like xanthotoxin, bergapten and psoralene, can inhibit AFs production at millimolar concentration, provoking a reduction in fungal growth, but their mechanism of action is still unknown. Flavonoids (peonidin, luteolin…) are active at really high concentration levels; luteolin acts differently on *A. flavus* and *A. parasiticus* and this probably depends on the different response of fungi to oxidative stress exposure.

1.3.2 Terpenoids and Alkaloids

Terpenoids, also called isoprenoids, are natural compounds derived from terpene; some of them, illustrated in Figure 7, have been found to inhibit AFs biosynthesis, with the exception of limonene, with IC_{50} values below 0.5 mM. In particular, α-carotene is able to block the production of NOR, preventing all the pathway regulation. Among all of them, lutein is the most powerful, with IC_{50} value of 1.1 μM[30], while camphene has just a modest inhibitory power[31].

[30] Norton R.A. ; *Phytopathology* 87; 814–821 (**1997**).

[31] Mahmoud A.L.E. ; *Lett Appl Microbiol* 19; 110-113 (**1994**).

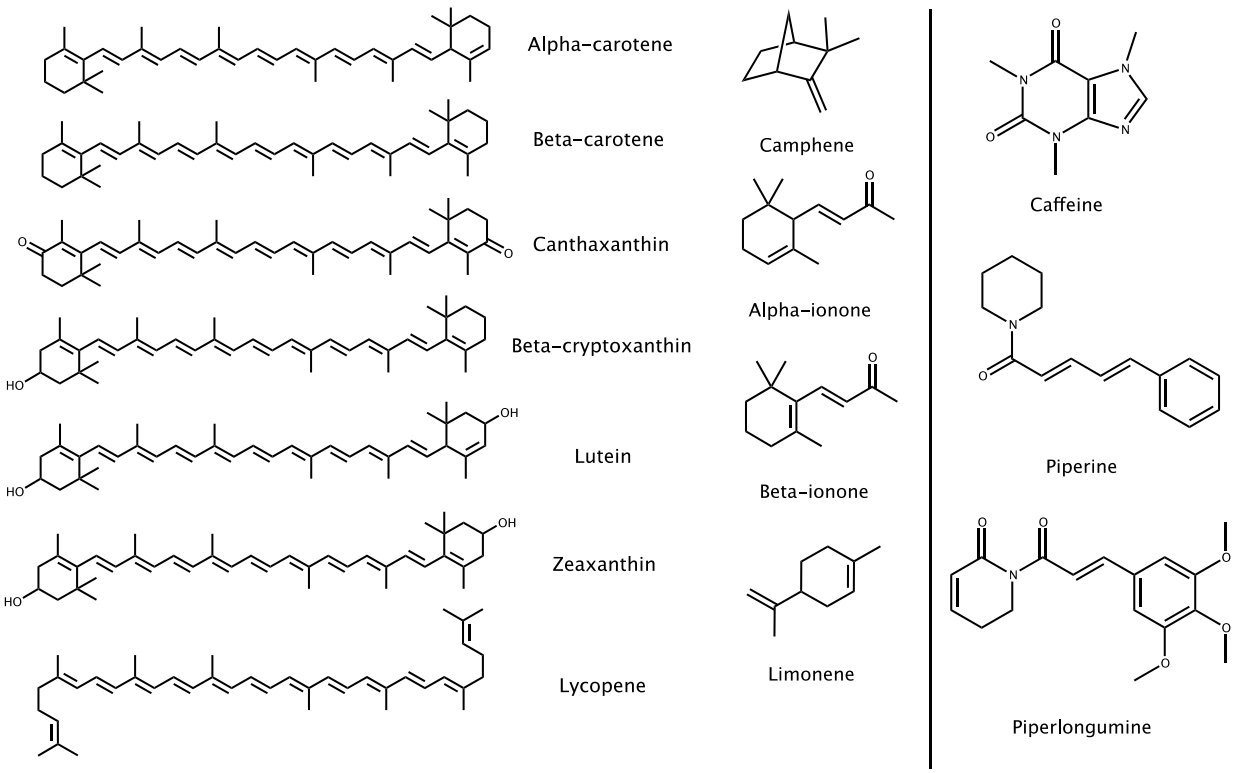

Figure 7. Molecular structures of terpenoids (left) and alkaloids (right) that have been tested for AFs inhibition on A. flavus.

Another important category of compounds that have been tested for the ability to block AFs biosynthesis is that of alkaloids: the most powerful were found to be caffeine and spices derived from black pepper. When coffee powder is added to the culture's medium of fungi like *A. flavus*, it inhibits the production of mycotoxins; [32] to validate obtained data, decaffeinated coffee powder was used, and a higher concentration of AFs was found in the medium: this demonstrated that the presence of caffeine is crucial to obtain inhibition. Piperine, on the other hand, is able to reduce the concentration of produced mycotoxins but it causes a reduction in fungal growth[33]. Among alkaloids, the most promising in term of antiaflatoxigenic activity was discovered to be piperlongumine (Figure 7), that doesn't influence at the same time the fungal growth. Anyway, the mode of action of these compounds is still unknown.

32 Buchanan R.L.; Lewis D.F. ; *Appl Environ Microbiol* 47; 1216–1220 (**1984**).

33 Madhyastha M.S., Bhat R.V. ; *Appl Environ Microbiol* 48; 376–379 (**1984**).

1.3.3 Plant-signaling compounds

Jasmonic acid and its derivatives are signaling molecules involved in various plant processes, including production of viable pollen, root growth, plant response to abiotic stress, and defenses against insects and pathogens. These compounds are produced by LOX (lipoxygenase) starting from linoleic and linolenic acid.

It has emerged that some jasmonate derivatives are able to inhibit the synthetic pathway of mycotoxins. Methyl jasmonate derivatives, 9*S*-hydroperoxy-trans-10,*cis*-12-octadecadienoic acid, 13*S*-hydroperoxy-cis-9,*trans*-11-octadecadienoic acid and 13*S*-hydroperoxy-cis-9,trans-11,cis-15-octadecatrienoic acid can decrease the amount of synthesized aflatoxins, without damaging fungal growth. LOX also produces volatile alkanals and alkenals, which are able to reduce the biosynthesis of AFs with low IC_{50} values and the most potent one is *trans*-2-nonenal. The problem of these compounds is that they also damage fungal growth, so they don't seem to be specific for aflatoxigenic activity, with the exception on nonyl aldehyde. The activity of ethylene has also been evaluated and it has been demonstrated that it is able to reduce AFs production at concentrations around 0.1 ppm, with no effect of fungal development.

1.3.4 Phytic and Hydroxamic acids

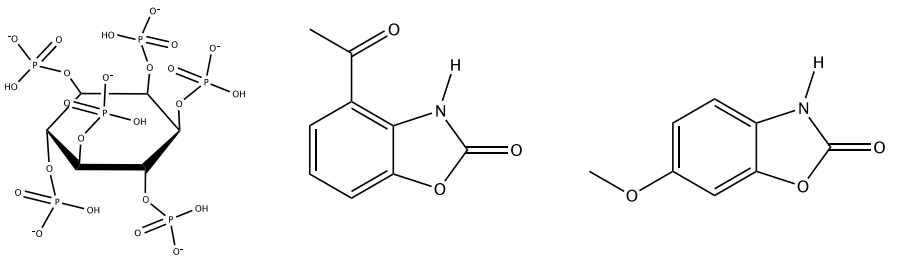

Figure 8.Molecular structure of phytic acid and of the most common hydroxamic acid used as AFs inhibitors.

Phytic acid (Figure 8) is a chelator for divalent ions, especially zinc, normally present in cereals. Since it can sequestrate several essential cations, limiting their absorption, it has important antinutritive effects: it is therefore preferable to consume cereals with low percentage of phytic acid. Soybean powder, which is the aliment with the highest quantity of this compound, has been used[34] to study its effect on AFs biosynthetic pathway. It has emerged that the breakdown of phytic acid, and the

[34] Gupta S.K. et al.; *Appl Environ Microbiol* 29; 834–836 (**1975**).

consequent release of Zn, provokes an enhancement in AFs concentration in the medium. In order to verify if the increase in AFs production is ascribable to the presence of the metal ion, zinc sulfate has been added to soybeans powder. It was registered a stimulation in mycotoxins' production which is reduced of about 87% on adding phytic acid that can subtract the cation to the solution. Studying the effect of this acid, Erlich and Ciegler[35] have discovered that its effect depends on the pH value of the medium: for pH around 6.6 it acts like a potent inhibitor but, decreasing it to 4, phytic acid loses its inhibitory power. This is probably related to the coordinating ability that varies with pH.

Another class with interesting anti-aflatoxigenic properties is that of hydroxamic acids: two of the stronger inhibitors of this class are 4-acetyl-benzoxazolin-2-one (4-ABOA) and 6-methoxy-benzoxazolin-2-one (MBOA), reported in Figure 9. The last one is able to decrease AFs production without damaging fungal growth at 2.5 mM concentration while 4-ABOA can reach IC_{50} value of about 50 mM. A third compound, that belongs to this class, need to be remembered: benzoxazolin-2-one; its strong inhibitory ability has been reported by Miller[36].

1.3.5 Calcium signaling disruptors

Recent studies[37] have reported that calmodulin phosphorylation/dephosphorylation seems to be really important in AFs production. An antagonist of this enzyme has been identified in trifluoroperazine (TFP) (Figure 9) and its activity has been evaluated in fungi at different age stages: TFP is able to completely inhibit fungal growth at concentration above 10 mM, reducing aflatoxins synthesis of about 18.4%; in 1-day-old cultures it affects little on fungal progress, inhibiting AFs at 42%. It is interesting what happens in 7-days-old culture: TFP does not influence fungal growth, but it is able to completely inhibit mycotoxins production. Since this compound is also antagonist of other calcium binding protein, it is still unknown if its activity is due to its influence on calmodulin activity; as an example, it can interfere with acetyl CoA carboxylase activity, reducing it 3.8-fold adding 0.14 mM TFP.

35 Ehrlich K. , Ciegler A. ; *Mycopathologia* 87; 99–103 (**1984**

36 Miller J.D.; Fielder D.A. et al. ; *Biochem. Syst. Ecol.* 24; 647–658 (**1996**).

37 Jayashree T.; Praveen J.;Subramanhyam C.; *FEMS Microb. Lett.* 183; 215-219 (**2000**).

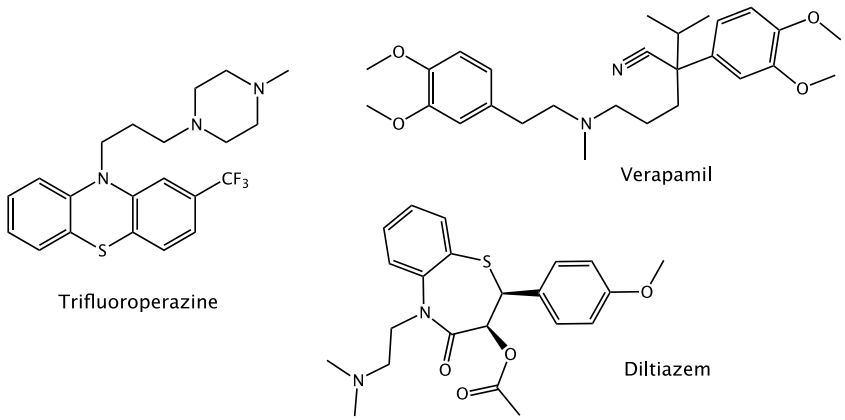

Figure 9. Molecular structures of common Calcium signaling disruptors.

Different reports[38] have also related the activity of calcium ion transport activity to AFs production; verapamil and diltiazem (Figure 9), two Ca^{2+} channel blockers, have been tested and they can reduce the quantity of aflatoxins, acting better on G type than on B one.

1.3.6 Antibiotics and cyclic dipeptides

It is known that bacteria are a rich source of anti-aflatoxigenic and fungistatic compounds[39]. An example is the bacterium *Achromobacter xylosoxidans*, that can inhibit accumulation of AFs' precursors like NOR: the dipeptide cyclo(L-leucyl-L-propyl) seems to be responsible for its activity; there are two other dipeptides, cyclo(D-leucyl-D-propyl) and cyclo(L-propyl-L-valyl), that have a good inhibition on fungi. Aflastatin A (AsA), a polyketide, seems to be very active, with IC_{50} values below 0.1 μM; its activity mechanism has been investigated and NOR production effects have been evaluated: it was reported that AsA provokes perturbation in the primary fungal metabolism[40]. Recently, dioctatin A has been revealed to inhibit AFs accumulation with IC_{50} of about 4 μM, without influencing fungal growth when concentration remains below 50 μM.

1.4 A NEW CLASS OF INHIBITORS: THE THIOSEMICARBAZONE LIGANDS

Most of the inhibitors that are listed above present as a common feature an antioxidant activity that is probably related to the ability of impairing aflatoxins biosynthesis[41]. Different studies have in fact demonstrated the presence of high percentage of ROS, lipid peroxidation and activity of antioxidant

38 Rao J.P.; Subramanyam C.; *Lett. Appl. Microbiol*. 28; 85–88 (**1999**).

39 Palumbo J.D.; Baker J.L.; Mahoney N.E.; *Microb. Ecol*. 52; 45–52 (**2006**).

40 Yoshinari T.; Akiyama T.; Nakamura K. et al.; *Microbiology* 153; 2774 (**2007**).

41 Fanelli C., Fabbri A.A., Brasini S., De Luca C., Passi S.; *Nat. Toxins* 3; 109–113 (**1995**).

enzymes in fungi that accumulate high percentage of AFs, but it is still unknown which is the correlation between these toxins production and oxidative stress.

It was supposed that the fungus needs to detoxify the cell from ROS accumulation, so it synthesizes such compounds, even because six oxidative steps are involved in AFs biosynthesis[42]. It has also been confirmed by Jayashree and Subramanyam[43] that oxidative stress is necessary for mycotoxins production: their accumulation is important to maintain the cell oxidative status at levels that can less afflict the fungus. Recently, a new class of compounds known for their chemical and biological activity, thiosemicarbazones (Figure 10),[44] has been studied as AFs inhibitors.

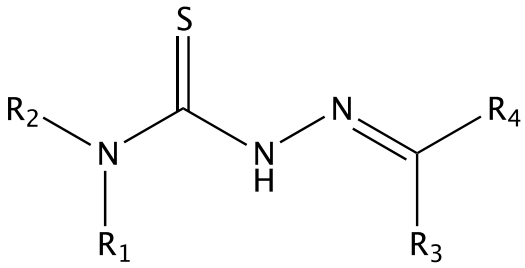

Figure 10. General molecular structure of thiosemicarbazones.

This class of compounds is well known for their antitumor[45], antiviral and antifungal activity[44]. They are also extremely versatile: in fact, there are different sites that can be functionalized in order to get molecules with the required features, modulating, for instance, lipophilicity or solubility in water. The presence of the sulfur atom could make them be involved in redox mechanisms, which makes this class more reactive than the carbazones one. Thanks to the possibility to introduce donor atoms on the organic scaffold, they could also have good chelating ability towards metal ions such as copper, zinc and nickel. The presence of such metals can enhance the antioxidant activity of the free ligand, making the metal-based compounds better inhibitors candidates. Moreover, inactivation of metalloenzymes involved in ROS production[46] can occur as a consequence of metal-cofactor sequestration. To mention an example, iron is an essential element and it plays a key role in diverse biological processes[47]: thiosemicarbazone derivatives are able to chelate non-heme iron

42 Narasaiah K.V.; Sashidar R.B.; Subramanyam C.; *Mycopathologia* 162; 179-189 (**2006**).

43 T. Jayashree, C. Subramanyam; Free Rad. Biol. Med. 10; 981-985 (**2000**).

44 G. Grover, S.G. Kini; Eur. J. Med. Chem. 41; 256-262 (**2006**).

45 Sîrbu A., Palamarciuc O. et al.; *Dalton trans.* 46; 3833 (**2017**).

46 Nguyen D.T., Le T.H., Bui T.T.T.; *Eur. J. Med. Chem.* 60; 199-207 (**2012**).

47 R.P. Tenorio; *Quimica Nova* 28; 1030-1037 (**2005**).

ions of several iron-dependent enzymes, like ribonucleotide reductase, which is essential for fungal survival[48].

Data on some thiosemicarbazones derivatives and related copper complexes as antifungal and anti-aflatoxigenic agents have been recently reported by our research group[49] (Figure 11):

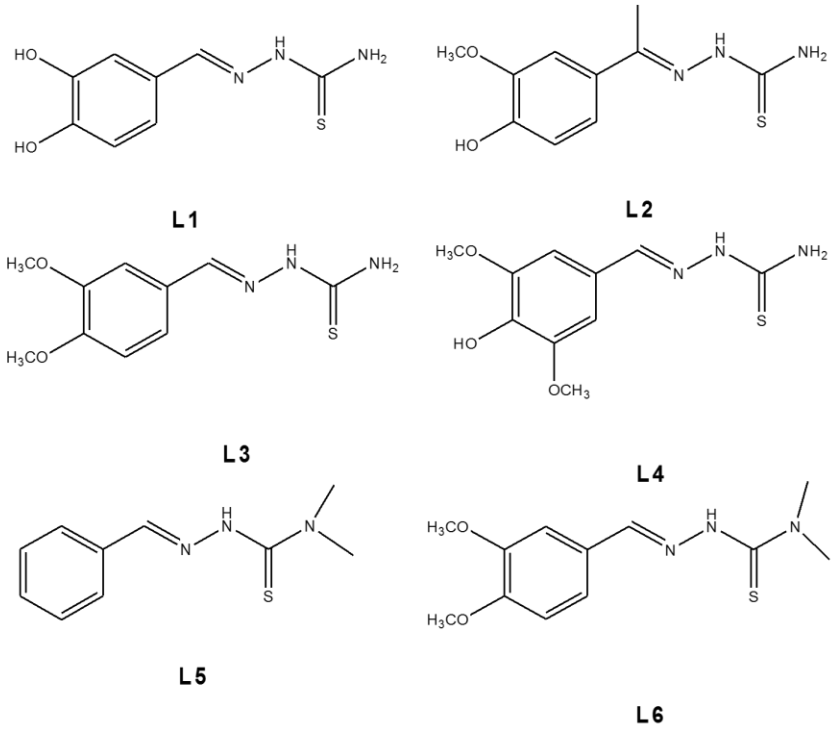

Figure 11.Thiosemicarbazone derivatives analyzed in a previous work[49].

starting from natural molecules such as vanillin and its isomers, the thio- group has been insert in order to improve their ability to chelate metal ions such as copper. This metal ion has a powerful antifungal profile and can work in synergy with the thiosemicarbazone ligand, leading to higher activity.

Copper complexes have been synthesized, and both ligands and complexes have been subjected to antiviral and anti-aflatoxigenic analysis, followed by geno- and cytotoxic ones. Compounds revealed a very good anti-aflatoxigenic activity but, unfortunately, copper complexes are cytotoxic. Therefore, this class of compounds seems very promising, but needs a careful evaluation of the safety profile for future developments. From a preliminary analysis of data, it emerges that there seems to be a correlation between the lipophilic character of the products and their anti-

48 R.O.A. Soares, et al.; *Experimental Parasitology* 129; 381-387 (**2011**).

49 Rogolino D.; Gatti A. et al.; *Sci. Rep.* 7: 11214 (**2017**).

aflatoxigenic activity: the most active derivatives turn out to be those that have a greater lipophilicity.

AIM OF THE PROJECT: Based on the data obtained from the previous analysis[47], lipophilicity could be considered a good target feature to be pursued to obtain effective AFs inhibitors. With this purpose, a new panel of molecules (Figure 12) with a good lipophilicity profile has been synthesized, and a model ligand has been chosen to synthesize the relative copper complex.

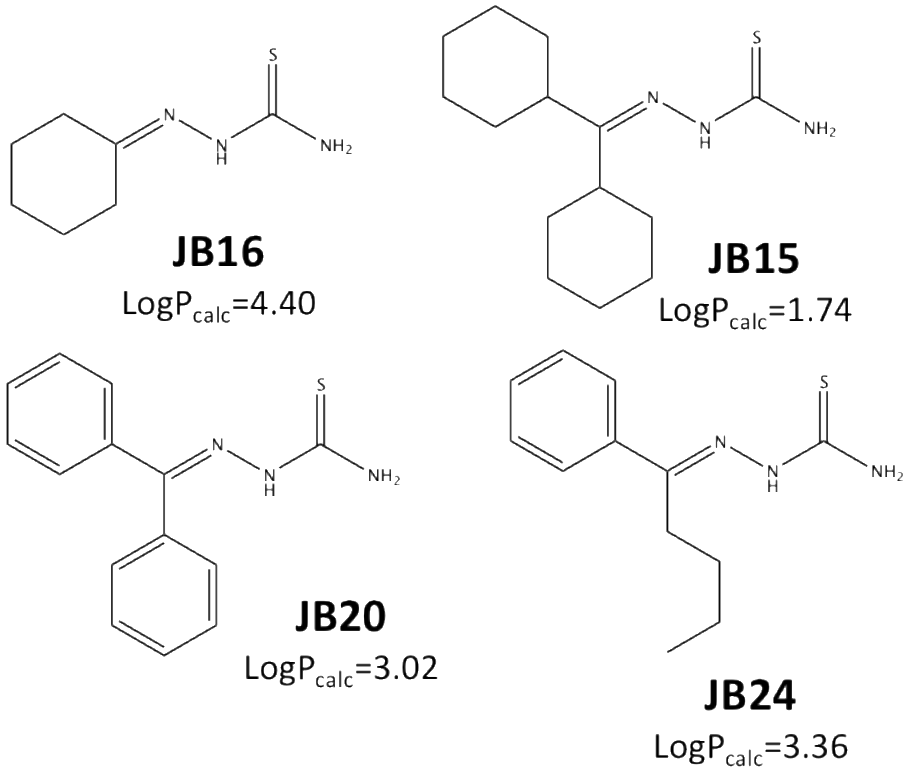

Figure 12.Molecular structure of new thiosemicarbazone inhibitors with good lipophilic character.

To improve the inhibitory power of vanillin derivatives, a second panel of compounds with a bis-vanillin scaffold (Figure 13) has been synthesized, together with the relative zinc and copper complexes.

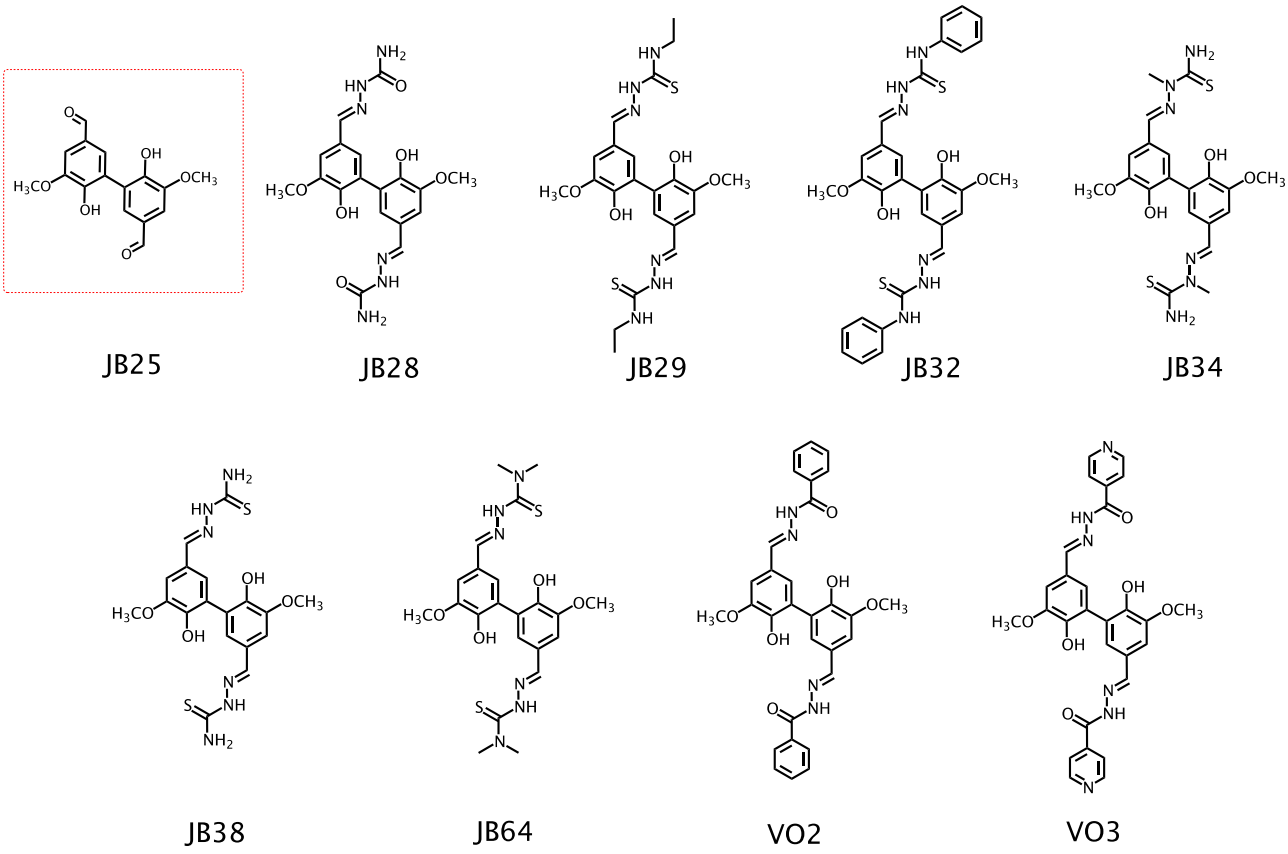

Figure 13. Bis-vanillin based thiosemicarbazone derivatives.

The synthetized molecules have been tested on *A. flavus* to verify their anti-aflatoxigenic and fungistatic activity. Two of them resulted to be good inhibitors without compromising the fungal growth, so their genotoxicity on diverse human cells has been evaluated, followed by cytotoxicity test on *Allium cepa* to attest their safety regards to genetic mutations on plants.

2. EXPERIMENTAL SECTION

2.1 MATERIALS AND METHODS

Chemicals were purchased from Sigma-Aldrich srl (Milano, Italy). Dulbecco's Modified Eagle's medium (DMEM) and RPMI-1640 medium were purchased from Lonza Group Ltd (Basel, Switzerland); Ham's Nutrient Mixture F-12 and Fetal bovine serum (FBS) were purchased from EuroClone s.p.a. (Milano, Italy). Hs27(ATCC, CRL1634), CRL 1790 (ATCC, CCD 841 CoN) and HFL1(ATCC, CCL-153) were obtained from the American Type Culture Collection (ATCC). U937 cells were obtained from the American Tissue Culture Collection (Rockville, MD). CellTiter96® AQ_{ueous}One Solution Cell Proliferation Assay was purchased from Promega Corporation, Madison, WI, USA. The purity of the compounds was determined by elemental analysis and verified to be ≥95%. $^{1}H/^{13}C$-NMR spectra were obtained in a 5 mm NMR precision tube at 298 K on a Bruker Avance 400 FT spectrophotometer. The ATR-IR spectra were recorded by means of a Nicolet-Nexus (Thermo Fisher) spectrophotometer by using a diamond crystal plate in the range of 4000–400 cm−1. Electrospray mass spectral analyses (ESI-MS) were performed with an electrospray ionization (ESI) time-of-flight Micromass 4LCZ spectrometer. Samples were prepared in methanol. The MS spectra were recorded in methanol and acquired in positive EI mode by means of a DEP-probe (Direct Exposure Probe) mounting on the tip of a Re-filament with a DSQII Thermo Fisher apparatus, equipped with a single quadrupole analyzer. ICP data were obtained by mean of an emission spectrometer JY 2501 with coupled plasma induction in radial configuration HORIBA Jobin Yvon (Kyoto, Japan), ULTIMA2 model. Instrumental features: monochromator Model JY 2501; focal length 1 m; reso- lution 5 pm; nitrogen flow 2 l/min. ICP source: nebulizer Meinhard, cyclonic spraying chamber; argon flow 12 l/min; wavelengths range 160– 785 nm; optical bench temperature 32 °C. The wavelength used for quantitative analysis was chosen by examining the emission line with greater relative intensity, ensuring that there was no spectral interference with the Argon emission lines. Acquisition parameters: wavelength Cu (nm): 224.700; Voltage (V): 580; gain: 100. The quantita- tive analysis was performed after the acquisition of a calibration line using standard solutions in HNO3 at 2%, to simulate the final acidity of the samples; the concentration range of the standards varied from 1 mg/L to 100 mg/L. Compounds were dissolved in 10 mL of CH3OH (2% HNO3). Data acquisition and processing were performed using the ICP JY v 5.2 software (Jobin Yvon).

2.2 CHEMISTRY

Cyclohexanone thiosemicarbazone, **JB16**: cyclohexanone (342 µL, 3.30 mmol) is dissolved in ethanol (20 mL), together with few drops of glacial acetic acid. After 15 min, thiosemicarbazide (300 mg, 1 eq, 3.30 mmol) is added to the solution, which is heated up to reflux and it is left reacting for 2 days and monitored by TLC (Hex:AcOEt, 7:3). The solution is concentrated and cooled to 4°C to promote precipitation of the product. The solid is isolated by filtration and dried by vacuum to give a pale yellow solid (yield = 31%). ^{1}H-NMR (DMSO-d_6, 25°C, 400 MHz), ppm: 10.12 (s, 1H, NH), 7.93(s, 1H, NH_2), 7.50 (s, 1H, NH_2), 2.40 (t, 2H, CH_{alif}), 2.23 (t, 2H, CH_{alif}), 1.63-1.56 (m, 6H, CH_{alif}). IR (ATR, cm^{-1}): ν_{NH2}= 3374 ; ν_{NH} = 3205, 3143; ν_{CH}= 2940 ; $\nu_{C=N}$= 1582; $\nu_{C=S}$= 1073, 1035, 831. MS-EI: m/z= 171.1 (100, M^+). M.p.: 170-171 °C.

Dicyclohexylketone thiosemicarbazone, **JB15**: dicyclohexylmethanone (650 µL, 3.30 mmol) is dissolved in ethanol (20 mL) together with few drops of glacial acetic acid; after 15 min thiosemicarbazide (297.51 mg, 1 eq, 3.26 mmol) is added and the solution is heated up to reflux and it is left reacting for 2 days and monitored by TLC (Hex:AcOEt , 7:3). The solvent is removed, and the solid residue is purified by column chromatography (Hex:AcOEt, 7:3) to give a yellow solid (yield=15%). ^{1}H-NMR (DMSO-d_6, 25°C, 400 MHz), ppm: 10.21 (s, 1H, NH), 8.03 (s, 1H, NH_2), 7.41 (s, 1H, NH_2), 3.03 (t, 1H, HC-C=N), 2.25 (t, 1H, HC-C=N), 1.69-1.15 (20H, CH_{alif}). IR (ATR, cm^{-1}): ν_{NH2}= 3430; ν_{NH}= 3276, 3230, 3140; ν_{CH}= 2921 ; $\nu_{C=N}$= 1693; $\nu_{C=S}$= 1081, 843. MS-EI: m/z= 255.3 (80, M^+). M.p.: 169-170 °C.

Benzophenone thiosemicarbazone, **JB20**: benzophenone (0.722 g, 1.2 eq, 3.96 mmol) is dissolved in n-propanol (20 mL) together with few drops of glacial acetic acid; the mixture is heated up to reflux. After 15 min, thiosemicarbazide (298.64 mg, 1 eq, 3.277 mmol) is added and the mixture is left reacting for 2 days and monitored by TLC (Hex:AcOEt, 7:3). The solution is concentrated and cooled to 4°C to promote precipitation of the residual reagent, which is removed by filtration. Then,

all solvent is removed, and the solid residue is recrystallized from ethanol to give the product as a white solid (yield=15%). ^{1}H-NMR (DMSO-d_6, 25°C, 400 MHz), ppm: 8.66 (s, 1H, NH), 8.40 (d, 2H, NH_2), 7.76-7.65 (m, 5H, CH_{arom}), 7.42-7.34 (5H, CH_{arom}). IR (ATR, cm^{-1}): ν_{NH2}= 3430 ; ν_{NH}= 3276, 3236, 3141; ν_{CH}= 2922 ; $\nu_{C=N}$= 1693; $\nu_{C=S}$= 1081, 844. MS-EI: m/z= 235.3, M^+. M.p.: 172-173 °C.

***Valerophenone thiosemicarbazone,* JB24**: Thiosemicarbazide (300 mg, 3.29 mmol) is dissolved in ethanol (40 mL) and it is heated up to reflux; then valerophenone (658 µL, 1.2 eq, 3.95 mmol) is added together with few drops of glacial acetic acid. The mixture is left reacting for 3 days monitoring by TLC (Hex:AcOEt , 8:2). The mixture is filtrated, and the solvent removed; the solid residue is purified by column chromatography to get a white powder (yield = 23%).

^{1}H-NMR ((DMSO-d_6, 25°C, 400 MHz), ppm: 10.34 (s, 1H, NH), 8.24 (s, 1H, NH), 8.90-7.88 (3H, NH+CH_{arom}), 7.38-7.39 (3H, CH_{arom}), 2.87 (t, 2H, H_2C-C=N), 1.37 (t, 4H, CH_{alif}), 0.88 (t, 3H, CH_{alif}). IR (ATR, cm^{-1}): ν_{NH2}= 3378; ν_{NH}= 3226, 3149; ν_{CH}= 2957, 2929 ; $\nu_{C=N}$= 1588; $\nu_{C=S}$= 1066, 847. MS-EI: m/z= 267.5 (100, M^+).

***$Cu_2(HL)(L)_2$,* HL: *Cyclohexanone thiosemicarbazone,* JB21**: **JB16** (229.64 mg, 2 Eq, 1.34 mmol) is dissolved in a Schlenk flask in degassed ethanol (20 mL) under nitrogen atmosphere; $CuCl_2 \cdot 2H_2O$ (114.29 mg, 1 eq, 0.67 mmol) is dissolved in a second Schlenk flask degassed ethanol. The solution of the metal salt is slowly added to the ligand one and the reaction mixture is stirred at room temperature for 20 hours. The precipitate is collected by filtration under nitrogen atmosphere and it is dried by vacuum to give a green powder (yield=66%). ^{1}H-NMR (DMSO-d_6, 25°C, 400 MHz), ppm: 10.52 (s, 1H, NH); 7.64, 8.47 (2s, br, 1H+1H, NH_2); 2.60 (s, br, CH_{alif}); 1.58-1.69 (m, br, CH_{alif}). IR (ATR, cm^{-1}): ν_{NH2}= 3436; ν_{NH}= 3248, 3165; ν_{CH}= 2932, 2856 ; $\nu_{C=N}$= 1604; $\nu_{C=S}$= 1034. ESI-MS (CH_3OH): pos cone 50 m/z=701, $[Cu_2(HL)_2L+H]^+$; m/z=405, $[Cu(HL)L+H]^+$; m/z=234, $[Cu(HL)]^+$. ICP: Cu found 20.3% ± 0.7%, calcd for $Cu_2(L)_2(HL)$: 19.8 %.

***Bis-vanillin,* JB25**: 4-hydroxy-3-methoxybenzaldehyde (500 mg, 3.29 mmol) is dissolved in water (100 mL) together with iron(II) sulfate (16.68 mg, 1.67 eq, 109.8 μmol) and the mixture is heated up to 50°C and left reacting for 10 min. Then, sodium thiosulfate (385 mg, 37 eq, 2.44 mmol) is added and the solution becomes purple, then brown. The reaction mixture is left reacting for 4 days at 50°C. The formed beige precipitate is isolated by filtration and dried by vacuum. 2M NaOH is added until all the solid is dissolved; then, 2M HCl is added to the basic solution until a precipitate is formed. The solid is isolated by filtration and dried by vacuum to give a beige solid (yield = 38%). ^{1}H-NMR (DMSO-d_6, 25°C, 400 MHz), ppm: 9.82 (s, 1H, CH), 9.79 (s, br, OH), 7.44 (s, 1H, CH_{arom}), 7.43 (s, 1H, CH_{arom}), 3.94 (s, 3H, OCH_3). ^{13}C-NMR (DMSO-d_6, 25°C, 400 MHz), ppm: 191.64, 150.87, 148.61, 128.59, 128.21, 125.03, 109.64, 56.50. IR (ATR, cm^{-1}): ν_{OH}= 3254; ν_{CH}= 2969; $\nu_{C=O}$= 1671. M.p.: 250°-252°C, dec.

***Bis(vanillin-semicarbazone),* JB28**: Semicarbazide hydrochloride (148 mg, 1.32 mmol) is dissolved into 2.5 ml of 1M KOH in methanol. **JB25** (200 mg, 0,662 mmol) is added to the semicarbazide together with few drops of acetic acid and ethanol (25 mL) is added to the mixture, which is heated up to reflux and it is left reacting for 24 hours. The solution is then allowed to return to r.t. and the formed precipitate is isolated by filtration and dried by vacuum to give the product as a beige solid (yield = 47.5%). ^{1}H-NMR (DMSO-d_6, 25°C, 400 MHz), ppm: 9.98 (s, 1H, NH), 7.75 (s, 1H, CH), 7.35 (s, 1H, CH_{arom}), 6.97 (s, 1H, CH_{arom}), 6.42 (s, 2H, NH_2), 3.87 (s, 3H, OCH_3). ^{13}C-NMR (DMSO-d_6, 25°C, 400 MHz), ppm: 157.36, 148.67, 146.40, 140.58, 125.84, 125.51, 123.68, 107.92, 56.46. ESI-MS: cone 50 m/z= 439, $[HL+Na]^+$. IR (ATR, cm^{-1}): ν_{NH}= 3464; ν_{OH}= 3205; $\nu_{C=O}$= 1672; $\nu_{C=N}$= 1577. M.p.: 260°-261°C, dec.

***Bis(vanillin-4-ethyl-thiosemicarbazone),* JB29**: 4-ethyl-thiosemicarbazide (157.64 mg, 1.32 mmol) is dissolved in water (30 mL) at room temperature; **JB25** (200 mg, 0. 66 mmol) is dissolved in ethanol (30 mL) at room temperature and it is added to the solution of 4-ethylthiosemicarbazide, together

with few drops of acetic acid as catalyst; the mixture is heated up to 96°C and it is left reacting for 24 hours. It is then concentrated and cooled to promote precipitation of the product; the formed precipitate is isolated by filtration and dried by vacuum to give the product as a beige solid (yield = 48.7%). ^{1}H-NMR (DMSO-d_6, 25°C, 400 MHz), ppm: 11.26 (s, 1H, NH), 8.93 (s, 1H, OH), 8.41 (t, 1H, NH-Et), 7.99 (s, 1H, CH), 7.36 (s, 1H, CH_{arom}), 7.14 (s, 1H, CH_{arom}), 3.92 (s, 3H, OCH_3), 3.59 (m, 2H, CH_2), 1.14 (t, 3H, CH_3). ^{13}C-NMR (DMSO-d_6, 25°C, 400 MHz), ppm: 176.70, 148.34, 146.63, 143.33, 125.90, 125.02, 123.98, 109.33, 56.63, 38.67, 15.21. ESI-MS: cone 50 m/z= 505, $[HL+H]^+$. IR (ATR, cm^{-1}): ν_{NH}= 3517; ν_{OH}= 3344; $\nu_{C=N}$= 1547; $\nu_{C=S}$= 1046, 619.

Bis(vanillin-4-phenyl-thiosemicarbazone), **JB32**: **JB25** (200 mg, 0.66 mmol) and 4-phenyl-thiosemicarbazide (223 mg, 1.33 mmol) are dissolved into ethanol (30 mL) together with few drops of acetic acid as catalyst; it is heated up to reflux and it is left reacting or 3 days. the solution is then allowed to return to room temperature; the formed precipitate is isolated by filtration and dried by vacuum (yield = 71.6%). ^{1}H-NMR (DMSO-d_6, 25°C, 400 MHz), ppm: 11.65 (s, 1H, NH), 9.99 (s, 1H, NH), 8.92 (s, br, OH), 8.10 (s, 1H, HC=N), 7.53 (m, 3H, CH_{arom}), 7.36 (m, 2H, overlapping signals), 7.22 (m ,2H, overlapping signals), 3.92 (s, 3H, OCH_3). ^{13}C-NMR (DMSO-d_6, 25°C, 400 MHz), ppm: 176.0, 167.29, 148.47, 146.92, 144.32, 139.71, 128.50, 126.61, 125.77, 124.87, 109.31, 56.71. ESI-MS: cone 80 m/z= 601, $[HL+H]^+$. IR (ATR, cm^{-1}): ν_{NH}= 3499; ν_{OH}= 3310; $\nu_{C=N}$= 1550; $\nu_{C=S}$= 1193, 744.

Bis(vanillin-2-methyl-thiosemicarbazone), **JB34**: **JB25** (216.91 mg, 0.72 mmol) is dissolved into ethanol (30 mL) together with few drops of acetic acid as catalyst; the mixture is heated up to reflux and it is left reacting for 10 min. 2-methyl-thiosemicarbazide (151.69 mg, 1.44 mmol) is added to the solution and it is left reacting for 24 hours; the solution is then allowed to return to room temperature and it is cooled to promote precipitation. The formed precipitate is isolated by filtration and dried by vacuum to give the product as a pale solid (yield = 66.4%). ^{1}H-NMR ((DMSO-d_6, 25°C, 400 MHz), ppm: 8.92 (s, 1H, OH), 8.29 (s, 2H, NH_2), 7.84 (s, 1H, CH), 7.59 (s, 1H, CH_{arom}),

7.22(s, 1H, CH_{arom}), 3.92 (s, 3H, OCH_3), 3.75 (s, 3H, NCH_3). ^{13}C-NMR (DMSO-d_6, 25°C, 400 MHz), ppm: 180.43, 148.45, 146.65, 142.55, 125.69, 125.63, 125.36, 108.99, 56.71, 33.33. ESI-MS: cone 50 m/z= 477, $[HL+H]^+$. IR (ATR, cm^{-1}): ν_{NH}= 3412; ν_{OH}= 3276; $\nu_{C=N}$= 1676; $\nu_{C=S}$= 1050, 777.

Bis(vanillin-thiosemicarbazone), **JB38**: **JB25** (402 mg, 1.33 mmol) is dissolved in ethanol (30 mL) together with few drops of acetic acid as catalyst. Thiosemicarbazide (210.37 mg, 2.3 mmol) is added and the solution is heated up to reflux and it is left reacting for 24 hours, monitoring with TLC (Hex:AcOEt, 7:3). The solution is allowed to return to room temperature and the precipitate is isolated by filtration and dried by vacuum to give a pale solid (yield = 80%). ^{1}H-NMR (DMSO-d_6, 25°C, 400 MHz), ppm: 11.28 (s, 1H, OH), 8.92 (s, 1H, NH), 8.08 (s, 1H, NH_2), 7.98 (s, 2H, CH+NH_2), 7.48 (s, 1H, CH_{arom}), 7.02 (s, 1H, CH_{arom}), 3.90 (s, 3H, OCH_3). ^{13}C-NMR (DMSO-d_6, 25°C, 400 MHz), ppm: 177.85, 148.53, 146.53, 142.5, 125.53, 125.14, 57.32.

JB42: **JB38** (200mg, 0.48 mmol) is dissolved into distilled THF (35 mL) in a Schlenk flask, under nitrogen flux; $CuCl_2 \cdot 2H_2O$ (77.75 mg, 0,45mmol) is dissolved into degassed ethanol (7 mL) and added to the ligand solution. The mixture is left reacting for 3 hours at room temperature; it is then concentrated and cooled to promote precipitation of the product. The precipitate is isolated by filtration and dried by vacuum. ^{1}H-NMR (DMSO-d_6, 25°C, 400 MHz), ppm: 11.39 (s, br, OH), 8.23 (s, 2H, NH_2), 8.01 (s, 1H, CH), 7.49 (s, 1H, CH_{arom}), 7.07 (s, 1H, CH_{arom}), 3.91 (s, 3H, OCH_3). ICP: Cu found 17.8 %., calcd. for $Cu_2(H_2L)_3Cl_4$: 17.72%.

JB47: **JB38** (200.38 mg, 0.48 mmol) is dissolved into THF (25 mL) under nitrogen atmosphere in a Schlenk flask; $Zn(CH_3COO)_2$ $2H_2O$ (100 mg, 0.55mmol) is dissolved in methanol (5 mL) under nitrogen; the metal solution is slowly added to the ligand one and it is left reacting at room temperature for 4 hours. The formed precipitate is isolated by filtration and dried by vacuum. ^{1}H-NMR (DMSO-d_6, 25°C, 400 MHz), ppm: 11.29 (s, br, OH), 8.06 (t, 3H, NH_2+CH), 7.48 (s, 1H, CH_{arom}),

7.21 (s,1H, CH_{arom}), 4.37 (s, 3H, OCH_3), 1.85 (s,3H, CH_3). ICP: Zn found 10.90%, calcd for $Zn(H_2L)(CH_3COO)_2$: 10.35%.

JB54: **JB38** (204.45 mg, 0.49 mmol) is dissolved into distilled THF (50 mL) in a Schlenk under nitrogen flux; $Zn(CH_3COO)_2 \cdot 2H_2O$ (204.33 mg, 0.93 mmol) is dissolved into methanol (10 mL) in a second Schlenk. The metal solution is added dropwise to the ligand and it is left reacting at room temperature for 3 hours. The solution is concentrated by vacuum and cooled to promote precipitation; the formed solid is isolated by filtration under inert atmosphere and it is dried by vacuum. ^{1}H-NMR (DMSO-d_6, 25°C, 400 MHz), ppm: 11.23 (s, br, OH), 8.00 (d, br, NH_2), 7.94 (s, 1H, CH), 7.45 (s, 1H, CH_{arom}), 7.18 (s, 1H, CH_{arom}), 3.82 (s, 3H, OCH_3), 1.83 (s, 3H). ICP: Zn found 11.40%, calcd for $Zn(HL)(CH_3COO)$: 11.43%.

JB55: **JB38** (262.97 mg, 0.63 mmol) is dissolved into distilled THF (30 mL) in a Schlenk under nitrogen atmosphere; in a second Schlenk, $CuCl_2 \cdot 2H_2O$ (200mg, 1.18 mmol) is dissolved into ethanol (10 mL) and it is added dropwise to the ligand solution. The mixture is left reacting at r.t. for 3 hours. The formed precipitate is filtered and dried by vacuum. ^{1}H-NMR (DMSO-d_6, 25°C, 400 MHz), ppm: 11.71 (s, br, OH), 9.03 (s, br, NH), 8.59 (s, br, NH_2), 8.05 (s, 1H, CH), 7.52 (s, 1H, CH_{arom}), 7.13 (s, 1H, CH_{arom}), 3.90 (s, 3H, OCH_3). ^{13}C-NMR (400 MHz, DMSO-d^6), ppm: 148.49, 147.22, 146.55, 125.59, 124.45, 56.66, 19.09. ICP: Cu found 9.6%, calcd for $Cu(HL) \cdot 2EtOH$: 10.46%.

JB59: **JB38** (200.81 mg, 0.482 mmol) is dissolved into THF (20 mL) in a Schlenk under nitrogen atmosphere; in a second Schlenk $Cu(CH_3COO)_2 \cdot H_2O$ (90 mg, 0.45 mmol) is dissolved into ethanol (10 mL) and it is added dropwise to the ligand solution; the mixture is left reacting at r.t. for 4 hours. The solution is concentrated by vacuum and cooled to promote precipitation; the formed solid is isolated by filtration under inert atmosphere and it is dried by vacuum. ^{1}H-NMR (DMSO-d_6, 25°C, 400 MHz), ppm: paramagnetic. ICP: Cu found 13.60%.

JB62: **JB38** (199.08 g, 0.48 mmol) is dissolved into distilled THF (20 mL) under nitrogen atmosphere; $Cu(CH_3COO)_2 \cdot H_2O$ (178.09 g, 0.90 mmol) is dissolved in ethanol (10 mL) and the metal solution is added dropwise to the ligand; the mixture is left reacting for 4 hours at r.t. The solution is concentrated by vacuum and cooled to promote precipitation. The precipitate is isolated by filtration under inert atmosphere and dried by vacuum. ^{1}H-NMR (DMSO-d_6, 25°C, 400 MHz), ppm: paramagnetic. ICP: Cu found 16.47%

***Bis(vanillin-4,4-dimethyl-thiosemicarbazone),* JB64**: 4,4-dimethyl-thiosemicarbazide (163 mg, 1.37 mmol) is dissolved into 5% Acetic Acid (THF solution) at room temperature, under nitrogen atmosphere. **JB25** (198.28 mg, 0.65 mmol) is added and it is heated up to 50°C for 4 hours. The solution is allowed to return to room temperature, and it is cooled to 0°C. The precipitate is isolated by filtration under nitrogen atmosphere and dried by vacuum (yield = 48.7%). ^{1}H-NMR (DMSO-d_6, 25°C, 400 MHz), ppm: 10.88 (s, 1H, OH), 8.15 (s, 1H, CH), 7.21 (s, 1H, CH_{arom}), 7.00 (s, 1H, CH_{arom}), 3.87 (s, 3H, OCH_3), 3.35 (s, 6H, $N(CH_3)_2$). IR (ATR, cm^{-1}): ν_{NH}= 3676; ν_{OH}= 3194; $\nu_{C=N}$= 1550; $\nu_{C=S}$= 1066, 785.

***Bis(vanillin-benzohydrazone),* VO2**: **JB25** (200 mg, 0.66 mmol) is dissolved in ethanol (30 mL) together with few drops of acetic acid as catalyst; benzo-hydrazide (180 mg, 1.32 mmol) is added and solution is heated up to reflux and it is left reacting for 20 hours. The precipitate is isolated by filtration and dried by vacuum (yield = 70%). ^{1}H-NMR (DMSO-d_6, 25°C, 400 MHz), ppm: 11.73 (s, 1H, NH), 9.03 (s, br, OH), 8.39 (s, 1H, CH), 7.91 (d, 2H, CH_{arom}), 7.53 (m, 1H, CH_{arom}), 7.52 (t, 2H, CH_{arom}), 7.36 (s, 1H, CH_{arom}), 7.10 (s, 1H, CH_{arom}), 3.92 (s, 3H, OCH_3). ^{13}C-NMR (DMSO-d_6, 25°C, 400 MHz), ppm: 177.58, 163.33, 150.24, 149.92, 144.44, 134.28, 131.92, 128.88, 127.98, 127.53, 125.02, 124.86, 107.35, 56.30. IR (ATR, cm^{-1}): ν_{NH}= 3513; ν_{OH}= 3207; $\nu_{C=O}$= 1632; $\nu_{C=N}$= 1572.

***Bis(vanillin-isonicotinhydrazone),* VO3**: **JB25** (200 mg, 1 Eq, 662 µmol) is dissolved in ethanol (30 mL), together with few drops of acetic acid as catalyst; isonicotin-hydrazide (181 mg, 2 eq, 1.32

mmol) is added and the mixture is heated up to reflux and it is left reacting for 20 hours. The formed precipitate is isolated and dried by vacuum (yield=70%). ^{1}H-NMR (400 MHz, DMSO-d_6), ppm: 12.01 (s, 1H, NH), 9.08 (s, br, OH), 8.77 (d, 2H, CH_{arom}), 8.42 (s, 1H, CH), 7.83 (d, 2H, CH_{arom}), 7.37 (s, 1H, CH_{arom}), 7.13 (s, 1H, CH_{arom}), 3.93 (s, 3H, OCH_3). ^{13}C-NMR (400 MHz, DMSO-d_6), ppm: 161.85, 150.72, 150.05, 148.63, 147.10, 141.15, 125.51, 125.06, 122.02, 108.12, 56.62. IR (ATR, cm^{-1}): ν_{NH}= 3633; ν_{OH}= 3214; ν_{CH}= 3068; $\nu_{C=O}$= 1651; $\nu_{C=N}$= 1648.

2.3 BIOLOGICAL ANALYSIS

2.3.1 Aflatoxins accumulation and fungal growth

***Aspergillus flavus* strains.** The toxigenic strain CR10 and the atoxigenic strain TOϕ, isolated from corn kernels sampled in the Po Valley were used.

Effect on aflatoxin accumulation. The high throughput procedure described in previous works[49] was used to assess aflatoxin accumulation in a coconut-milk derived medium (CCM). Briefly, suspensions of conidia were diluted and brought to the final concentration of 5×10^2 conidia⁄ well; cultures were set in a final volume of 200 µL/well of CCM medium added with molecules at 25, 50 or 100 µM. DMSO (0.25%, 0.5% and 1% respectively) was used as control. The plates were incubated in the dark under stationary conditions for 6 days at 25 °C. Aflatoxin accumulation was monitored by fluorescence emission determination: readings were performed directly from the bottom of wells of the culture plate with a microplate reader (TECAN SpectraFluor Plus, Männedorf, Switzerland) using the following parameters: λ_{ex} = 360 nm; λ_{em} = 465 nm; manual gain = 83; lag time = 0 µs; number of flashes = 3; and integration time = 200 µs. Samples were inoculated in quadruplicate.

Effect on fungal growth. Once assessed the AF accumulation rate as described above, mycelia from single wells were recovered at the 6th day of incubation, slightly dried on hands paper, and weighted. Biomass measures were then converted in percentage inhibition respect to controls (DMSO-treated cultures).

Effect on sclerotia biogenesis. A 5 µl aliquot of aflatoxigenic strain CR10 spore suspension, containing approximately 10^6 conidia/ml, was point-inoculated in the center of Petri dishes (Ø = 5 cm) poured with Czapek Dox Agar (CZA) medium added with 100 µM thiosemicarbazones. Control plates were added with 1 % (v/v) DMSO. Plates were replicated in triplicate and incubated at 30˚C

in darkness; after two weeks of incubation, sclerotia were manually scraped from the colonies surface and washed with a 70% ethanol solution to completely remove conidia, then dried for three days at 60 °C. Dry weight was assessed. Thiosemicarbazones inhibition rate on sclerotia production was expressed as percentage respect to the control. Plates were inoculated in triplicate.

Statistical analysis. For statistical analyses one-way analysis of variance (ANOVA) was used in the Past 3.x software. Results of mycelial growth, aflatoxin accumulation and sclerotia production were analyzed by Tukey's test; differences were considered significant at $p< 0.05$.

2.3.2 Cytotoxicity

The biological activity of the new active molecules with antifungal potential was assessed on normal cells: human fibroblast cell line Hs27 (ATCC, CRL1634), human lung epithelial cell line HFL1 (ATCC, CCL-153), human colon epithelial cell line Crl1790 (ATCC, CCD 841 CoN). These cell lines represent the human districts related to possible xenobiotic ways of interaction with the human body, to investigate the exposition risks. We also performed toxicological assays on human histiocytic lymphoma cell line U937 (ATCC, CRL-3253). Hs27 and CRL1790 were cultured in DMEM; HFL1were cultured in Ham's Nutrient Mixture F-12; U937 cells were cultured in RPMI-1640. All media were supplemented with 10% (v/v) fetal bovine serum (FBS), 1% penicillin (100 U/ml)/streptomycin (100 µg/ml) and 1% L-Glutamine (2 mM). Flasks and plates were maintained at 37°C and 5% CO_2 in a humidified atmosphere. Culture medium was refreshed every two or three days during sub-culturing. Hs27, CRL1790 and HFL1cells were used between passage numbers 5 and 20. MTS assay (CellTiter96® AQueous One Solution Cell Proliferation Assay) was performed to identify the antiproliferative effect of the compounds. Briefly, 100 µL of a suspension of cells in exponential growth (5 ×104/mL in complete medium without phenol red supplemented with 5% FBS) were added into 96-well plates 24h before treatment. Plates were incubated at 37 °C in a humidified 5% CO_2 incubator. After this recover period, increasing concentrations of compounds (0.5-1.0-5.0-10.0-50.0-100.0 µM) were added to the medium and cells were left exposed for 24-48-72h. Negative control was represented by 100 µM DMSO. After treatment period, 20 µl of MTS reagent was added to each well. At the end of exposure time, the absorbance at 485 nm was measured by a microwell plate reader (TECAN SpectraFluor Plus, Männedorf, Switzerland).

The cytotoxicity response parameters GI50, drug concentration inducing a 50% reduction of the cell number in comparison to untreated control cells cultured in parallel, were extrapolated from concentration-response curves.

2.3.3 Genotoxicity on human cells

To assess primary DNA damage, the alkaline version of Comet assay was performed with U937 cells as described in a previously published work [49]. U937 cells were seeded 24h before treatment at a concentration of 1 x 105 cell/mL in 1 mL of complete medium. Cells were treated with increased concentrations (25.0-50.0-75.0-100.0) of the compounds for 1h and 24h. DMSO (100 µM) and ethylmethanesulfonate (EMS) (2 mM) were used as positive and negative controls, respectively. After treatment period at 37 °C, the percentage of live cells was assessed by Trypan blue exclusion method: cells were resuspended in complete medium and Trypan blue was added. 100 cells for each concentration were counted manually using a hemocytometer. Only the treatments that had a viability higher than 70% have been processed in the Comet assay, as described by Buschini and coworkers[50]. DNA was stained with 75 µL ethidium bromide (10 µg/mL) before the examination at 400× magnification under a Leica DMLS fluorescence microscope (excitation filter BP 515–560 nm, barrier filter LP 580 nm), using an automatic image analysis system (Comet Assay IV – Perceptive Instruments Ltd, UK). Percentage of DNA in the tail region of the comet (TI, tail intensity) provided representative data on genotoxic effects. For each sample, coded and evaluated blind, 100 cells were analyzed.

The "IBM SPSS Statistics 24" software was used to analyze statistical differences between samples. The mean values from the repeated experiments were used in a one-way analysis of variance (ANOVA). If significant F-values ($P<0.05$) were obtained, Student's t test (Bonferroni's version) was performed.

2.3.4 Mutagenicity on bacteria and cytotoxicity on plants

Ames test: molecules were dissolved in a compatible solvent (DMSO) and assayed with the *Salmonella*/microsome test (Ames test) at increasing doses (0.1, 1, 10, 50, 100 µM/plate), with *S. typhimurium* TA98 and TA100 strains, with and without metabolic activation (S9 mix) to highlight the presence of indirect and direct mutagenic activity. The experimental procedure was the standard plate incorporation method. Salmonella TA98 strain detects frame-shift mutagens and TA100 strain responds to base-pair substitution. Positive controls were 2-nitrofluorene (10 µg/plate) and sodium azide (10 µg/plate) for TA98 without S9 and TA100 without S9, respectively, and 2-aminofluorene (20 µg/plate) for both strains with S9. DMSO was tested as negative control.

[50] Buschini A.; Pinelli S.; Pellacani C.; Giordani F.; Ferrari M.B.; Bisceglie F.; Giannetto M.; Pelosi G.; Tarasconi P.; *J. Inorg. Biochem.* 103; 666-677 (**2009**).

The data obtained were shown as revertants per plates, computed by means of three replicates with their relative standard deviation. Moreover, the results were expressed as mutagenicity ratio (RM) dividing the revertants/plate by spontaneous mutation rate. The results of the test were considered positive if two consecutive dose levels or the highest non-toxic dose level produced a response at least twice that of the solvent control and at least two of these consecutive doses showed a dose-response relationship.

Allium cepa test: a preliminary toxicity assay was performed and 12 equal-sized young onion bulbs was exposed for 96 hours in the dark to different concentrations of molecules dissolved in DMSO changing the sample solution every day. Root length was used to calculate the EC_{50} value of each compound and to identify the concentration to undergo the *Allium cepa* genotoxicity assay being the highest dose correspondent to the EC_{50} value identified (the concentration that gives a 50% reduction in root growth). Other macroscopic parameters (turgescence, consistency, change in color, root tip shape) were used as toxicity indexes.

Two *Allium cepa* genotoxicity tests were carried out to detect chromosome aberrations (namely buds, bridges, binucleate cells, laggard or lost chromosomes, fragments, c-mitosis polar slip, rings and multipolar cells) and micronuclei. Both tests were performed using six equal-sized young bulbs per sample. After 72-hour pre-germination in Rank solution the bulbs were exposed to samples for 24 hours, then the roots were fixed in acetic acid and ethanol (1:3) for 24 hours and lastly stored in 70% ethanol for the chromosome aberrations (CA) test. In the micronuclei (MN) test the bulbs, after exposure, were replaced in saline solution (Rank's solution) for 44 hours of recovery time, to cover two rounds of mitosis so that damage induced in chromosomes during mitosis to be visible as micronuclei in interphase cells. Then the roots were fixed in acetic acid and ethanol (1:3) for 24 hours and lastly stored in 70% ethanol[51]. The negative control was DMSO in Rank solution (the dose of DMSO corresponding to volume of samples) and positive control was maleic hydrazide (10 mg/l, 6h exposure). Five roots of each sample were considered for microscopic analysis: 1000 cells/slide (5000 cells/sample) were scored for mitotic index (as a measure of cell division and hence of sample toxicity), 200 in mitosis cells/slide (1000 cells/sample) for chromosomal aberrations and 2000 in interphase cells/slide (10000 cells/sample) were scored for micronuclei frequency.

Statistical analysis was performed using Chi-square test for mitotic index and chromosomal aberrations, the analysis of variance and Dunnett's t-test were performed for MN. All experiments were performed in duplicate (two independent assays).

[51] Cabaravdic M.; *Med. Arh.* 64; 215–218 (**2010**).

3.RESULTS and DISCUSSION

3.1 HIGH LIPOPHYLIC THIOSEMICARBAZONES

3.1.1 Synthesis and Characterization

A previous work[49] carried out by our research group has highlighted that it is possible to tune the antiaflatoxigenic activity against *A. flavus* by varying substituents on the N4 of the ligand or by changing the nature of the starting aldehyde or ketone. Previous results also have confirmed that the sulfur atom is crucial for activity: the replacement of the sulfur atom of the thiosemicarbazones with an oxygen one leads to inactive compounds, underling the importance of the presence, in the molecular scaffold, of a donor atom which can be involved into redox processes. In figure 14 it is shown the molecular structure of previously studied compounds. Analysis of available data seems to suggest that there is a correlation between the lipophilic character of the inhibitor and its antiaflatoxigenic activity: the most active compounds, in fact, present higher lipophilic character. Therefore, in order to enlarge the panel of studied compounds and to confirm a structure-activity relationship, a new panel of molecules has been designed, starting from ketones that already have a good hydrophobic character (Figure 14).

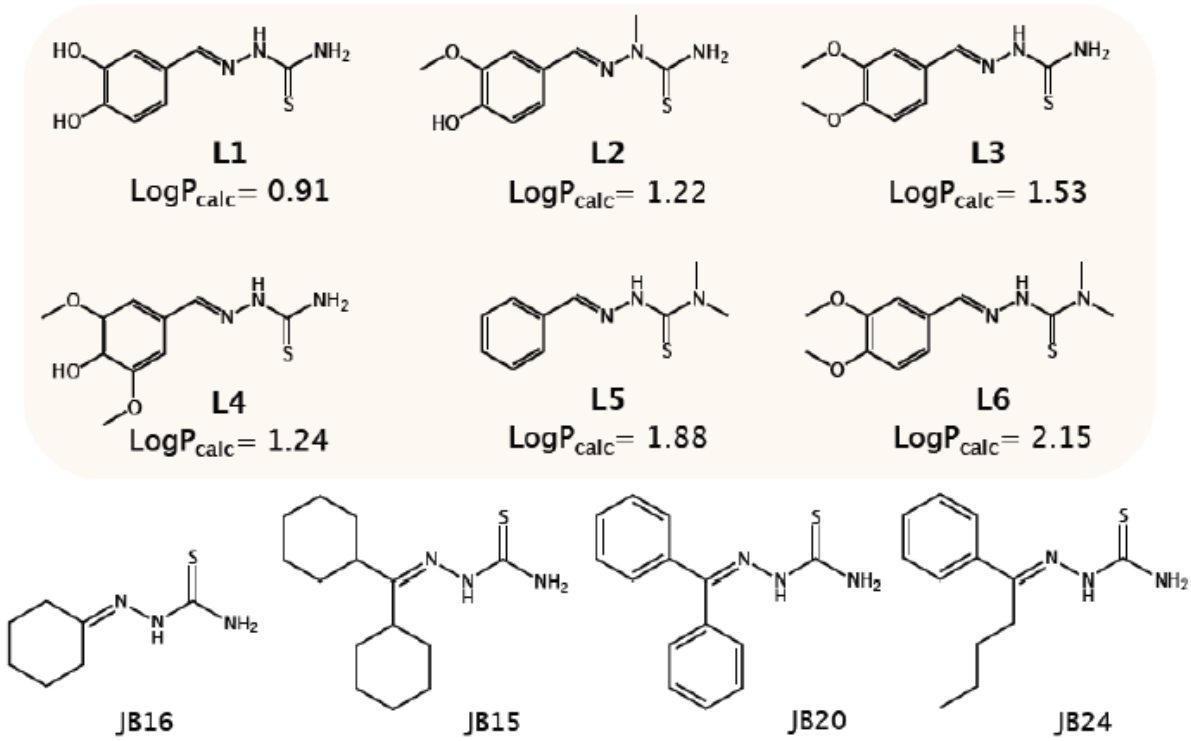

Figure 14. Molecular structure of the inhibitors: the first , on the top, and the new ones, with higher lipophilic character, on the bottom, with the respective calculated LogP[52].

[52] www.molinspiration.com/cgi-bin/properties

All derivatives have been synthesized by condensation reaction: the ketone is dissolved in ethanol with a catalytic amount of glacial acetic acid. An equimolar quantity of thiosemicarbazide is added an it is left reacting overnight; the final products have been isolated either by precipitation or purification by column chromatography (Hex:AcOEt) to get white to pale yellow powders. All the obtained products have been characterized by ATR-IR, ^{1}H-NMR, ^{13}C-NMR, EI-MS. In Figure 15 it has been reported the IR spectrum of **JB16** as an example.

The bands relative to the stretching vibration of NH and NH_2 groups are visible at 3430 and 3140 cm^{-1}, respectively. The stretching band around 1800 cm^{-1}, which are relative to the carbonylic group of the starting ketone, disappears and a new band, relative to the stretching of the C=N bond, appears at about 1693 cm^{-1}. The C=S group stretching bands are visible at about 1035-1080 cm^{-1} and 830-950 cm^{-1}. In Figure 15 it is evident the presence of CH stretching bands at about 2800 cm^{-1} to 3100 cm^{-1}.

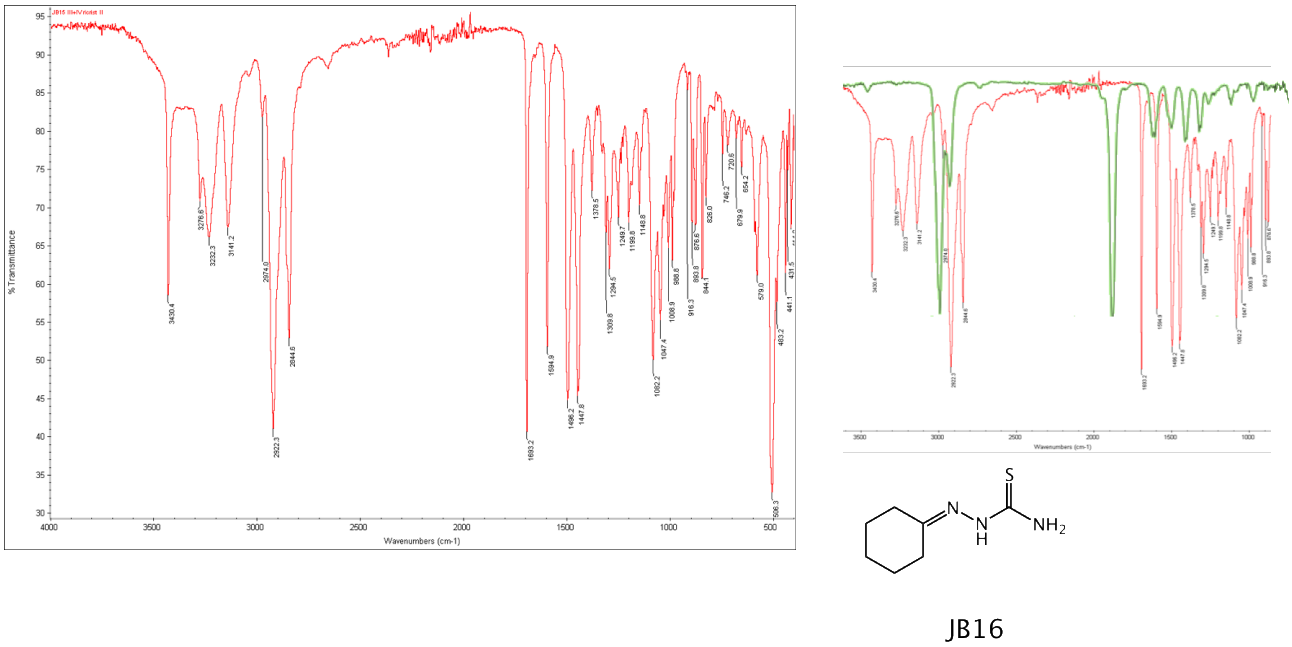

*Figure 15. ATR-IR spectra of **JB16** (on the left) and the comparison between the ketone (green) and the final ligand (red).*

In the ^{1}H-NMR spectra (DMSO-d_6, 400 MHz, 25°C) the resonances of the hydrazonic NH and of NH_2 are clearly visible (10.3-8.6 and 7.4-8.4 ppm, approximately). Such class of compounds are known to give a thione-thiol equilibrium in solution: from the proton NMR spectra (Figure 16) we can see that only the thione form is present in solution. In previous studies[47] developed by our laboratory team, it has been evaluated the idea that coordination to copper ions could gain the bio-disponibility of the metal ion, favoring adsorption into lipid membranes and thus promoting a better anti-

aflatoxigenic activity. The focus on copper ions is due to the wide application of this metal in agriculture as antifungal and antibacterial agent. Therefore, we choose **JB16** as a model ligand and investigated its coordination properties towards the copper(II) ion.

JB16 has been made reacting with an equimolar amount of $CuCl_2 \cdot 2H_2O$ under inert atmosphere. It is well known from literature that thiosemicarbazones can undergo oxidative cyclization reaction when there is the presence of bases, oxidants or a metal that can catalyze redox processes[53]. During complexation reaction, copper(II) is reduced to copper(I) and, as a consequence, in presence of a d^{10} diamagnetic nucleus, it has been possible to collect ^{1}H-NMR data, as reported in Figure 3. As far as the ligand, on the basis of the IR and ^{1}H NMR spectra, it is possible to say that a cyclized form of the ligand is absent. Looking at the IR spectrum, we can clearly see intense bands between 3500-3000 cm^{-1}, which belong to the stretching mode of NH and NH_2. The stretching band relative to C=N bond is shifted to higher wavenumbers respect to the free ligand (from 1582 to 1604 cm^{-1}), which indicates that it is involved into the coordination of the metal ion. The C=S stretching band in the complex is shifted as well respect to the free organic molecule, from 1073 cm^{-1} to 1034 cm^{-1}, respectively. Different studies reported in literature highlight the possibility to isolate polynuclear copper(I) complexes, like in the case of (-)-carvone and (+)-camphor thiosemicarbazones[47]; in our specific case, data analysis suggests a 2:3 metal to ligand stoichiometry: defining **JB16** as HL, it is possible to propose the formula $Cu_2(HL)(L)_2$ for complex **JB21** and this hypothesis is confirmed also by the ESI-MS mass (Figure 16) and ICP analysis.

[53] Chattopadhyay S.K. , Mak T.C.W.; *Inorganic Chemistry Communications* 3; 111–113 (**2000**).

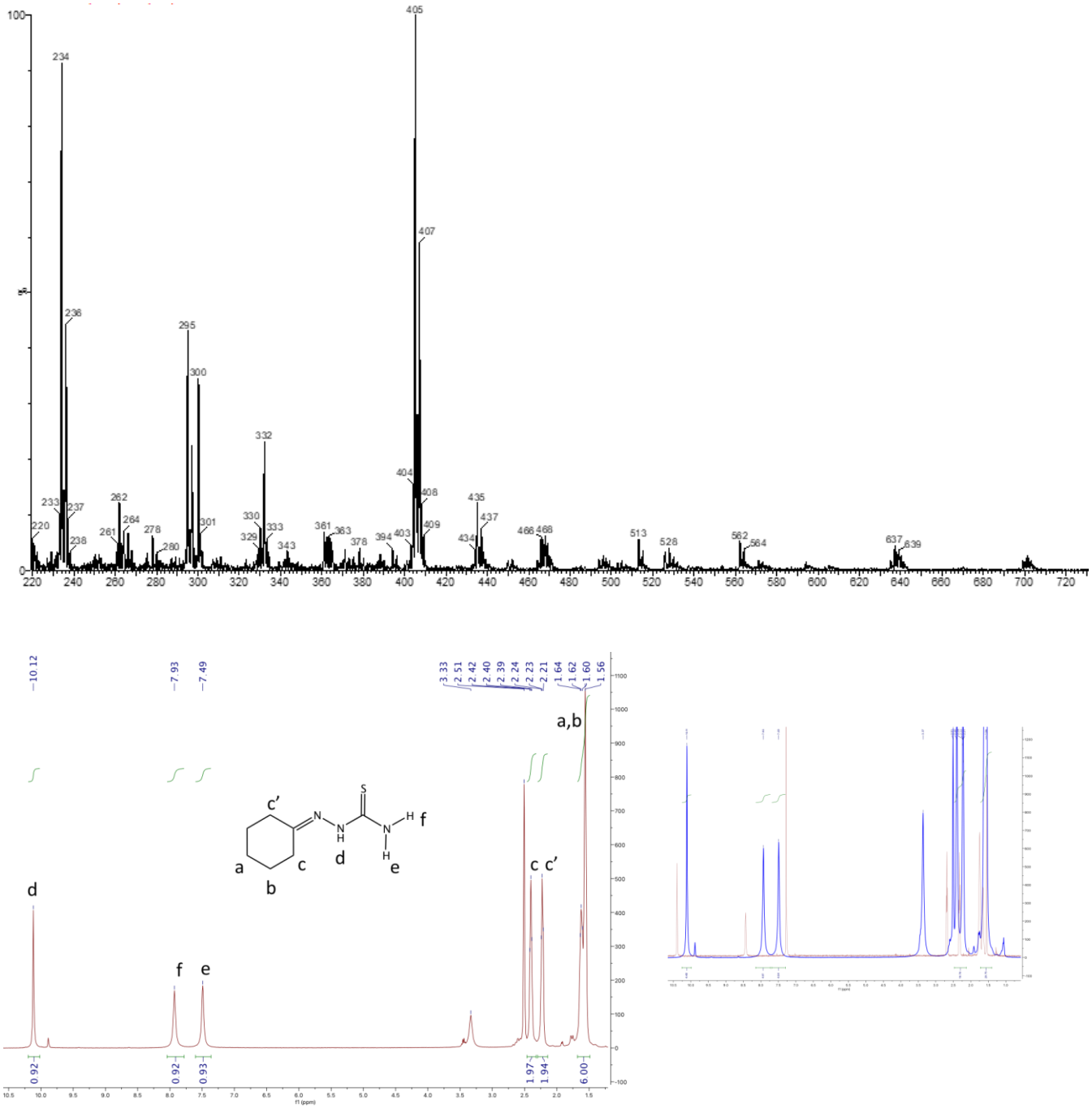

*Figure 16. ESI-MS of **JB21**, on the top, and ^{1}H-NMR spectra (bottom) of **JB16** (on the left) and the comparison with the one of the copper complex **JB21** (in blue on the right).*

3.1.2 Anti-aflatoxigenic and antifungal activity

Derivatives **JB16**-**JB24** and the copper complex (**JB21**) have been tested to evaluate their ability to reduce aflatoxins accumulation and fungal growth, by using a procedure described in detail in previous works[54,55].

As can be inferred by looking at Figure 17, **JB16** weakly inhibits aflatoxins production and it does not seem to affect fungal growth. Its copper(I) complex (**JB21**) has a better inhibiting profile than the free ligand, as expected, but it doesn't seem to have a dose-dependent response. **JB15** is able to halve the accumulation of mycotoxins, but it engraves on fungal growth, inhibiting its progress of about 80%. Better results are obtained with derivatives **JB20** and **JB24**, which inhibit AFs accumulation of 41% and 55% at 100 μM respectively, with low percentage of inhibition of fungal growth, resulting to be the best compounds of the panel: therefore, they were chosen for further analysis. As already mentioned in the introduction, in fact, poor antifungal activity together with inhibition of aflatoxins production is a highly desirable parameter, since this can ensure the preservation of the environmental microbiota while providing the protection from toxic secondary metabolites.

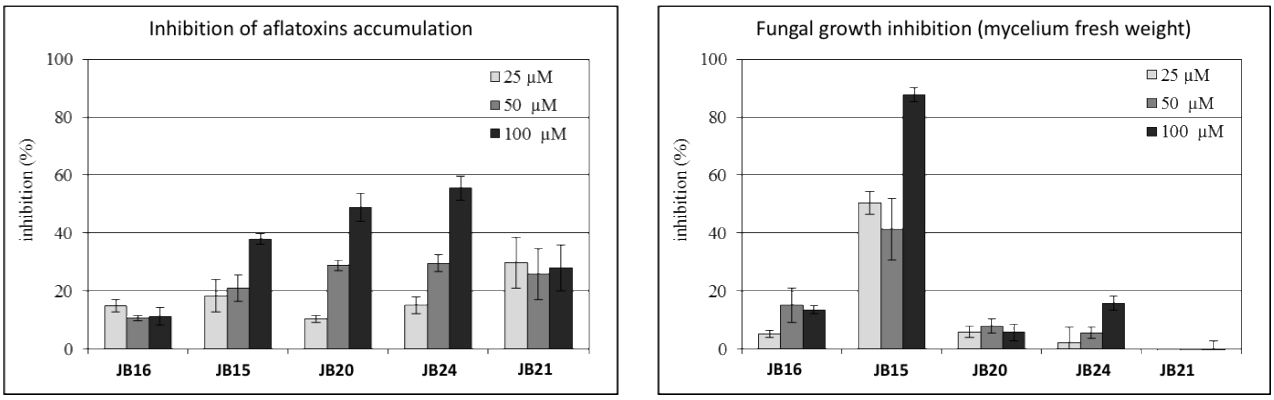

*Figure 17. Antifungal and anti-aflatoxigenic activities of compounds **JB16-JB21** at 25, 50 and 100 μM concentration. Results referred to aflatoxin accumulation (A) and mycelium fresh weight (B) in CCM medium; they are expressed as mean percentage inhibition in comparison with controls (0.25%, 0.5% and 1% DMSO respectively). Error bars indicate the standard deviations of four replications (p-value < 0.05).*

During the most part of their life, fungi exist as mycelia or conidia-asexual spores-but, under unfavorable conditions, such as oxidative stress, mycelia convert into more resistant forms, which are able to independently survive in bad conditions, and these are called sclerotia. Since it is well

[54] Degola, F.; Berni, E.; Restivo, F. M.; *Int. J. Food Microbiol.* 146; 235-243 (**2011**).

[55] Degola, F.; Dall'Asta, C.; Restivo, F. M.; *Letters in applied microbiology* 55; 82-89 (**2012**).

known that AFs biosynthetic pathway shares diverse regulatory steps with processes involved into the secondary metabolism, like sclerotia production, an evaluation of the effect of the aflatoxigenic inhibitors on such structure biogenesis is important to take into account. We therefore assed the ability of the most active compounds to affect sclerotia development.

Sclerotia formation was induced by culturing *A. flavus* CR10, an aflatoxigenic and sclerotigenic strain, in CZA solid medium added with 100 µM of **JB20** and **JB24** and 1% DMSO as negative control. The presence of the thiosemicarbazones derivatives in the culture medium reduced the formation of sclerotia and, as expected, no mycelium growth inhibition has been observed; the exposure to **JB20** and **JB24** has reduced the sclerotia biogenesis to 30% and 86% respectively, with respect to the control (Figure 18). These results coincide with what we have observed for other thiosemicarbazonic derivatives, which were effective in reducing AFs accumulation, with a slight action on fungal development and that strongly impair sclerotia formation in *A. flavus*.

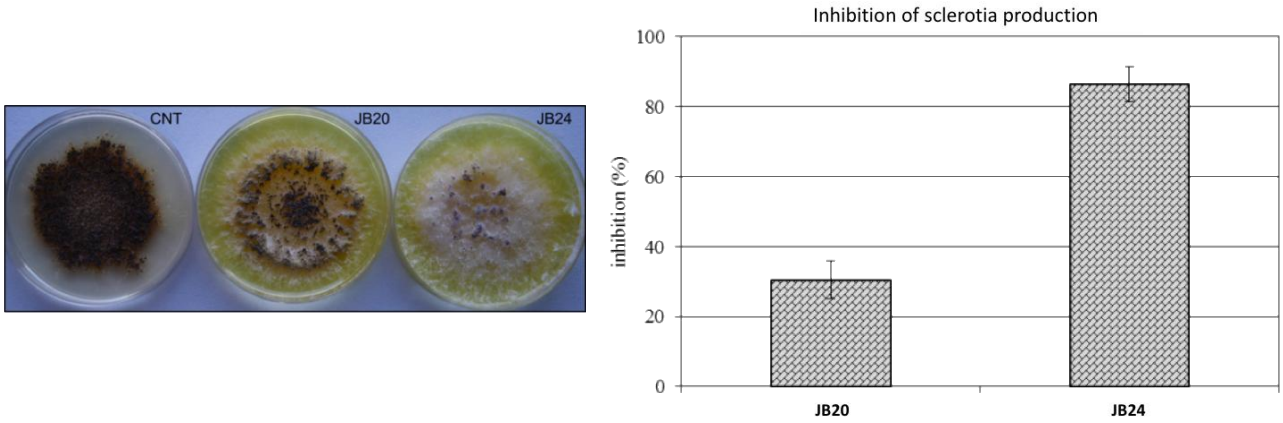

*Figure 18. Effects of **JB20** and **JB24** on sclerotia biogenesis. Assessments were performed in Czapek-Agar solid medium amended with 100 µM thiosemicarbazones or 1% DMSO as control (CNT). Error bars indicate the standard deviations of three replications (p value <0.05).*

3.1.3 Cyto- and genotoxicity

Since synthetized compounds have been designed to be used as antiaflatoxigenic agents on crops, their toxicity on human and plants have been evaluated. Three normal healthy cell lines were chosen to carry out the tests on **JB20** and **JB24**: colon epithelial cells (CRL1790), skin fibroblast (Hs27), and lung epithelial cells (HFL1); they are representative of diverse kind of exposure: epidermal contact (Hs27), inhalation (HFL1) and ingestion (CRL1790).

It was also tested a human histiocytic lymphoma cells line, U937, which is a good model that is used worldwide to identify cytotoxicity.

MTS assay protocol has been followed to determine GI (growth inhibition) and data are obtained as mean of four independent experiments (Table 1).

	CRL1790	Hs27	HFL1	U937
JB20	>100.0	>100.0	>100.0	73.0
JB24	>100.0	79.5	>100.0	58.0

Table 1. GI_{50} value (μM), concentration of compound that causes a 50% reduction of cell proliferation, obtained after 24h treatment in human healthy cell lines CRL1790 (colon epithelial cells), Hs27 (skin fibroblast), HFL1 (lung epithelial cells), and U937 (histiocytic lymphoma cells) cancer cell line.

Compound **JB20** shows no cytotoxicity on healthy cells and derivative **JB24** seems to mildly act only on Hs27. Since they show a good cytotoxicity profile, they have been evaluated for genotoxicity and mutagenicity on bacteria, plants and human cells.

The Alkaline Comet Assay has been performed on U937 cells to evaluate the genotoxicity of **JB20** and **JB24**; such test is able to verify the entity of DNA damage and also to detect alkali-labile sites, together with single and double strand breaks. The DNA percentage expressed as TI% (tail of the comet) indicates genotoxic effects of the considered compounds. Cells have been treated with diverse doses of compounds (25.0 - 50.0 - 75.0 - 100.0 μM) for 1 hour and 24 hours; results are reported in Figure 19.

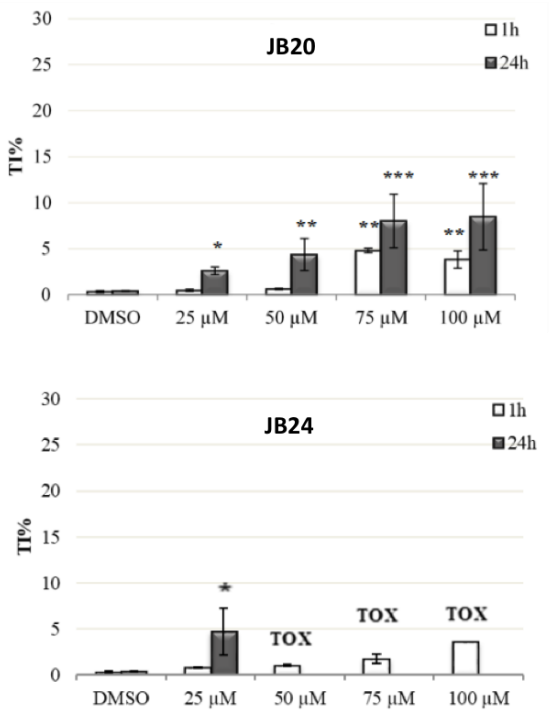

*Figure 19.Genotoxic activity of compounds **JB20** and **JB24**, using the Alkaline Comet Assay on U937 cells treated for 1 h and 24 h. *p < 0.05; **p < 0.01; ***p < 0.001. TOX: viability <70%*

Compound **JB20** has a dose-dependent activity on the selected cells in both treatment (1h and 24h); on the contrary, compound **JB24** has a toxic effect even after 1-hour treatment for concentration of 75.0 and 100.0 µM, while after 24h it was genotoxic already at 25.0 µM.

Ames test has been performed on both **JB20** and **JB24**, and results (Table 2) show no mutagenic effect in both *Salmonella typhimurium* strain TA98 and TA100.

	Doses (µM/plate)	TA 98		TA98+S9		TA 100		TA100+S9	
		mean ± SD	MR	mean ± SD	MR	mean ± SD	MR	mean ± SD	MR
JB20	0,1	14,5 ± 0,7	1,0	22,3 ± 4,11	1,0	94,5 ± 19,1	1,2	108,0 ± 0,0	1,2
	1	18,5 ± 2,1	1,2	30,0 ± 1,41	1,3	92 ± 7,1	1,1	99,5 ± 10,6	1,1
	10	11,5 ± 0,7	0,8	20,5 ± 0,71	0,9	96,5 ± 20,5	1,2	83,5 ± 6,4	0,9
	50	19,0 ± 2,8	1,2	22,0 ± 0,0	0,9	100,5 ± 7,8	1,2	86,5 ± 14,8	0,9
	100	16,5 ± 0,7	1,1	20,5 ± 6,36	0,9	95,5 ± 7,8	1,2	79,0 ± 17,0	0,9
JB24	0,1	12,0 ± 4,2	0,8	15,5 ± 6,36	0,7	75,5 ± 12,0	0,9	86,0 ± 17,0	0,9
	1	17,5 ± 12,0	1,1	26,0 ± 0,71	1,1	77,5 ± 12,0	1,0	86,5 ± 3,5	0,9
	10	15,5 ± 4,9	1,0	16,0 ± 2,12	0,7	74 ± 5,7	0,9	101,5 ± 16,3	1,1
	50	14,5 ± 0,7	1,0	22,0 ± 6,36	0,9	82 ± 1,4	1,0	92,5 ± 10,7	1,0
	100	17,5 ± 3,5	1,1	22,0 ± 3,54	0,9	75 ± 9,9	0,9	75,5 ± 3,5	0,8
Negative controls (DMSO)		15,25 ± 4,11		23,3 ± 10,6		81,5 ± 4,65		91,3 ± 11,32	

Table 2. Results of the Ames test expressed as revertants/plate and as mutagenicity ratio (MR). Negative control: DMSO, 100 µM/plate. Positive control –S9: TA98 10 µg/plate 2-nitrofluorene; TA100 10 µg/plate sodium azide; positive control +S9: TA98, TA100 20 µg/plate 2-aminofluorene. Positive control results: TA 98±S9 > 1,000 revertants/plate; TA100±S9 > 1,000 revertants/plate.

Different results are observed from the exposure of *Allium cepa* roots to **JB20** and **JB24**: the last one shows high level of toxicity at the lowest concentration; therefore, it has not been possible to carry out genotoxicity tests. Conversely, **JB20** has been subjected to genotoxicity analysis: the corresponding EC_{50} value at 50 μM has been determined, but it seems to have mild toxicity at 100 μM dose. Chromosomal aberration in *Allium cepa* have been determined at the lowest concentration tested (Table 3).

		1st experiment			2nd experiment		
	Doses (µM)	**Mitotic index (%)**	**Cromosomal Aberration AC (%)**	**p values***	**Mitotic index (%)**	**Cromosomal Aberration AC (%)**	**p values***
JB20	10	12,6	3,5	< 0.01	13,3	3,7	< 0.01
	25	11,6	4,5	< 0.01	11,2	4,6	< 0.01
	50	10,3	4,7	< 0.01	10,0	5,1	< 0.01
	100	12,3	7,4	< 0.01	11,8	7,4	< 0.01
C-		10,5	1,2		9,9	1,9	
C+		7,2	8,8		8,7	10,1	

*Table 3. Allium cepa chromosomal aberrations test on compound **JB20**: mitotic index and total chromosomal aberrations in metaphase root cells. C-: 100 µM DMSO; C+: maleic hydrazide (10-2M)*
** Statistically significant according to $\chi 2$ test*

The linear trend analysis has been developed and it clearly shows that a dose-response statistically significant ($p<0.05$) does exist (Figure 20).

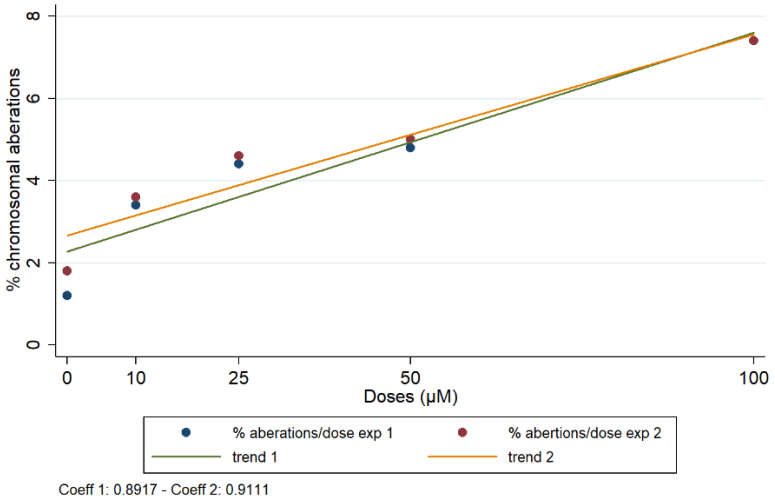

*Figure 20. Allium cepa root cells, tested with **JB20**, chromosomal aberrations linear trends.*

Analysis on micronuclei in the interphase cells have been developed and results have highlighted that there is no increase in comparison with negative control for **JB20** (Table 4).

		1st experiment		*2nd experiment*	
	Doses (µM)	**Mitotic index (%)**	**MCN (mean±DS)**	**Mitotic index (%)**	**MCN (mean±DS)**
JB20	10 µM	11,5	0,03 ± 0,03	11,8	0,03 ± 0,07
	25 µM	11,4	0,03 ± 0,03	11,5	0,04 ± 0,04
	50 µM	9,6	0,08 ± 0,03	10,4	0,07 ± 0,07
C-		12,5	0,04 ± 0,07	12,6	0,02 ± 0,04
C+		7,6	16,8 ± 8,4	7,2	17,2 ± 12,0

*Table 4. Allium cepa micronuclei test on compound **JB20** mitotic index and total chromosomal aberrations in metaphase root cells. C-: negative control, DMSO; C+: positive control, maleic hydrazide (10-2M). MCN, micronuclei frequency.*

3.1.4 Conclusions

In conclusion, we have investigated the ability of new thiosemicarbazone derivatives to inhibit AFs biosynthesis, rather than to impair fungal growth: valerophenone thiosemicarbazone (**JB24**) and benzophenone thiosemicarbazone (**JB20**) seem to be the most promising of the proposed panel of molecules. They also showed no antiproliferative activity on lung, skin and colon cell lines, and they have showed no mutagenic activity on bacteria. However, the Alkaline Comet Assay on U937 cells revealed that they do provoke DNA damages; **JB24** results to be toxic for *Allium cepa* roots and, the test of chromosomal aberrations has highlighted that **JB20** has a genotoxic activity even at the lowest doses. *Allium cepa* micronuclei test has been carried out on the benzophenone derivative and it resulted to be negative: **JB20** does not provoke disturbance in mitotic cycle, but it does directly cause DNA damage.

Overall, we can say that **JB20** and **JB24** revealed to be promising hit compounds, even if efforts have to be devoted to investigating the action mechanisms of the anti-aflatoxigenic thiosemicarbazones and, at the same time, control their genotoxic character.

3.2 BIS-VANILLIN SCAFFOLD DERIVATIVES

3.2.1 Synthesis and Characterization

Previous studies in our laboratory have reported that vanillin-thiosemicarbazones have a good anti-aflatoxigenic activity[47]. We decided to further investigate modifications of the vanillin scaffold, in order to improve the ability to inhibit mycotoxins accumulation in fungi. A new panel of molecules, bearing a bis-vanillinin scaffold, has been design and synthetized, as reported in Figure 21.

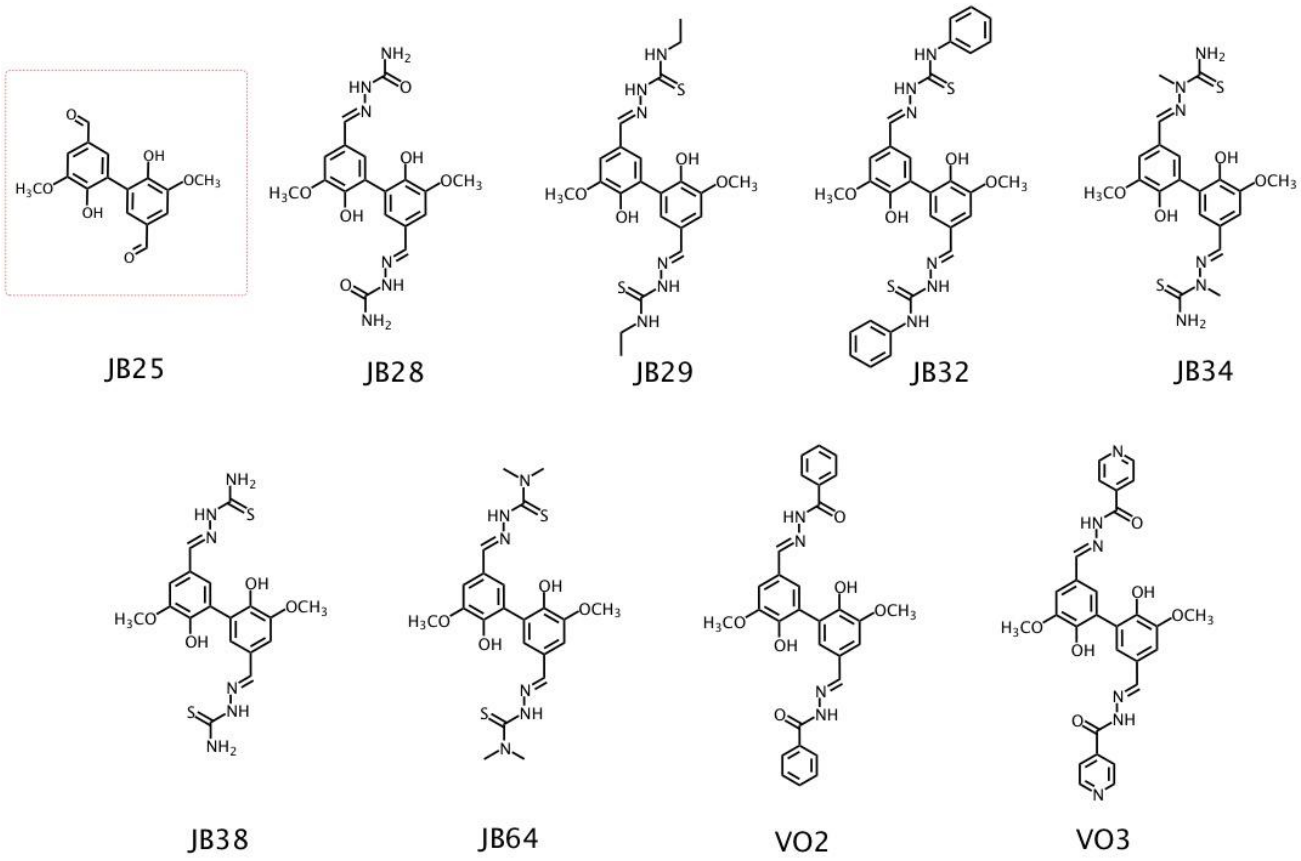

Figure 21. Bis-vanillin semi/thiosemicarbazones derivatives.

Starting from vanillin, the central core of the scaffold has been first isolated (**JB25**), and then we moved to functionalization using diverse semi/thiosemicarbazides. To get **JB25** a literature procedure has been slightly modified: 1 eq. of vanillin was reacted in presence of catalytic amount of $FeSO_4$ and 0.6 eq. of $Na_2S_2O_3$ for four days. The resulting bis-vanillin **JB25** has been isolated and fully characterized. It was then reacted with 2 eq. of the corresponding semi/thiosemicarbazide, in presence of catalytic amount of glacial acetic acid, to get the desired set of molecules, characterized by usual spectroscopic tools. Thiosemicarbazone derivatives are known to have a *cis*/*trans*

isomerism around the iminic bound: proton NMR analysis confirms that in such ligands only the *trans* isomer is present in solution (Figure 22).

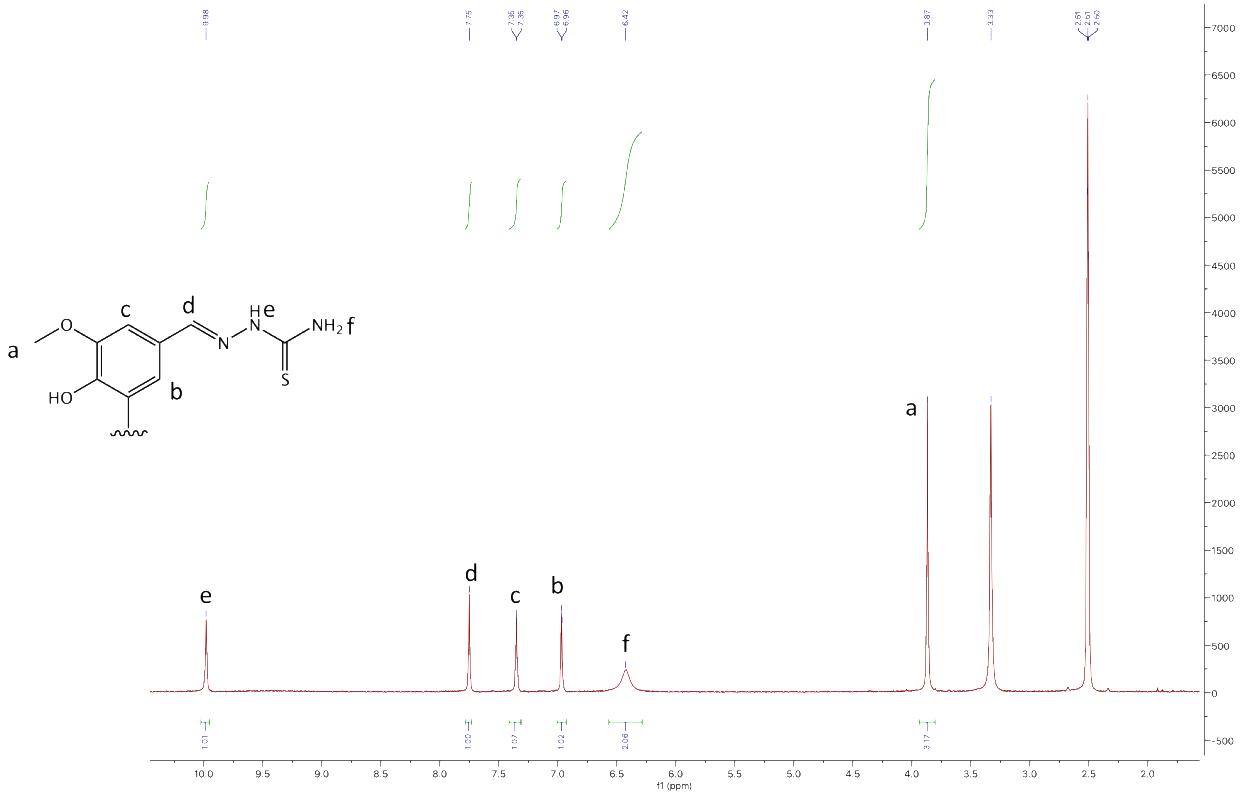

*Figure 22. ^{1}H-NMR of **JB38** (d_6-DMSO, 400 MHz, 25°C).*

A different synthetic pathway has been followed to get **JB64**: in this case, the approach used for all the other compounds has not make possible the isolation of the pure final compound. We have been able to isolate the designed ligand reacting **JB25** with 2 eq. of 4,4-dimethyl-3-thiosemicarbazide in a high-pressure vessel, using a 5% solution of acetic acid prepared in THF. After 3 hours we were able to collect the JB64 by filtration under inert atmosphere and ^{1}H-NMR has confirmed the success of the synthetic approach (Figure 23).

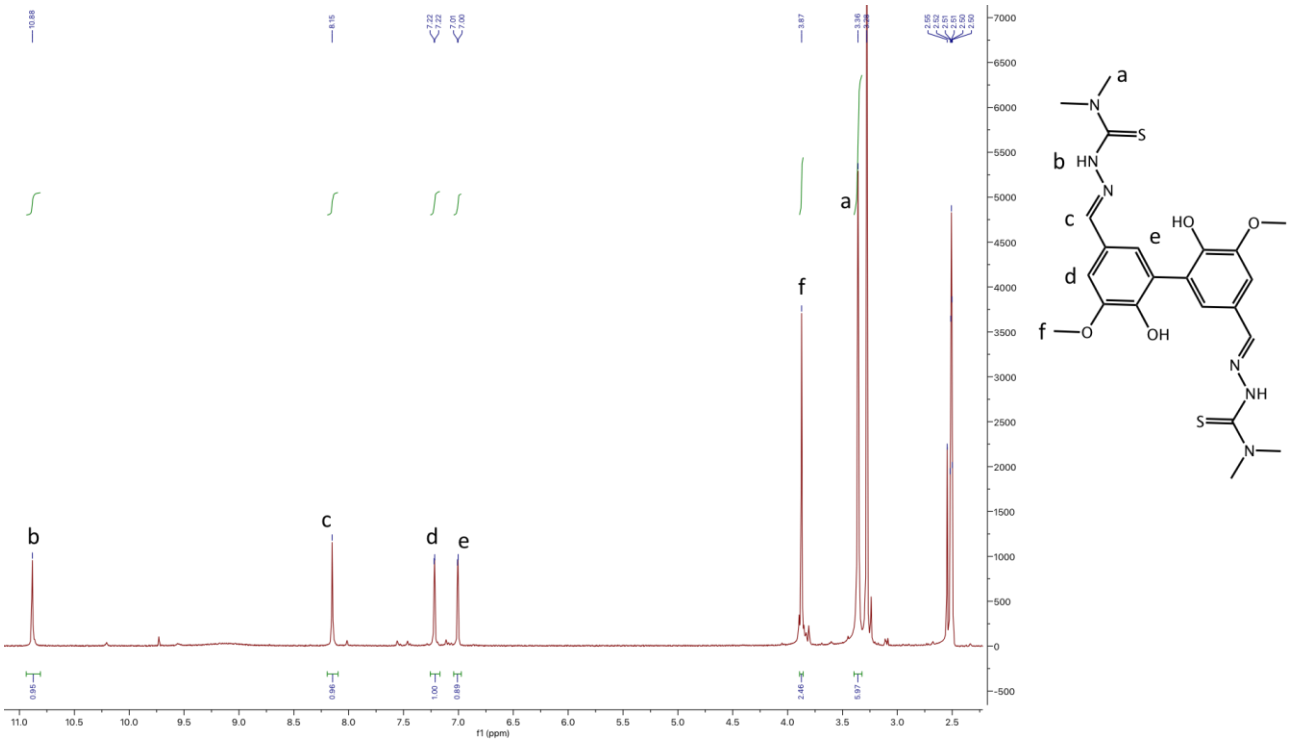

*Figure 23. ^{1}H-NMR spectrum (400 MHz, DMSO) of **JB64**.*

The spectrum highlights the presence of only one specie, demonstrating that the condensation reaction has occurred at both the aldehydic group of the central core.

We have, then, chosen **JB38** (H_2L) to study the ability of such molecular scaffold to complex metal ions: different reactions have been made, not just by varying the stoichiometric ratios between the metal and the ligand, but by using different metal ions and diversifying the counterion (Table 5).

	M^{2+}	Counterion	Stoichiometry	ICP_{det}	Proposed Formula
JB42	Cu^{2+}	Cl^-	H_2L:M , 1:1	7.6%	$Cu_2(H_2L)_3Cl_4$
JB55	Cu^{2+}	Cl^-	H_2L:M , 1:2	9.6%	Cu(HL) 2EtOH
JB59	Cu^{2+}	CH_3COO^-	H_2L:M , 1:1	13.60%	/
JB62	Cu^{2+}	CH_3COO^-	H_2L:M , 1:2	16.5%	/
JB47	Zn^{2+}	CH_3COO^-	H_2L:M , 1:1	10.90%	$Zn(H_2L)(CH_3COO)_2$
JB54	Zn^{2+}	CH_3COO^-	H_2L:M , 1:2	11.40%	$Zn(HL)(CH_3COO)$

*Table 5. Metal complexes of derivative **JB38** and relative ICP values.*

All compounds have been synthesized by adding a methanolic solution of the metal ion (1 eq. or 2 eq.) to a solution of the ligand under inert atmosphere; the mixture has been left reacting for about 4 hours and the formed precipitate has been isolated by filtration under nitrogen atmosphere. Preliminary assessments on the nature of the solids are made by ^{1}H-NMR.

In effect, a distinction has to be made in the case of copper complexes: the ones that have the acetate as counterion resulted to be paramagnetic copper(II) complexes; the others, instead, deriving from copper chloride, are diamagnetic copper(I) coordination compounds: the variation of pH of solution due to different ions can afflict the redox activity of copper(II), which is reduced to Cu^{+}. In the case of both zinc complexes, there is the presence of a singlet at 1.85 ppm, which is relative to the counterion, which is involved in coordination. On the basis of ICP analysis it has been possible to hypothesize a molecular formula; unfortunately, because of the high fragmentation during ESI-MS analysis, it has not been possible to find confirms of them by mean of this technique. Different crystallization attempts have been made but it has still not been possible to isolate single crystals of the complexes.

3.2.2 Evaluation of antioxidant activity

As we have previously discussed, there's seems to be a correlation between the antioxidant activity of a molecule and the relative anti-aflatoxigenic capability: therefore, we decided to perform an evaluation of the antioxidant capacity of **JB38** by using 2,2-diphenyl-1-picrylhydrazyl (DPPH) according to a reported literature procedure[56]. Such assay gives an indication of the antioxidant activity of a compound by monitoring the UV-visible absorption band at 517 nm of the radical; compounds with such characteristic are able to donate a proton to the radical, provoking a discoloration of DPPH solution, from dark purple to orange/yellow, based on the "antioxidant power" of the derivative.

A methanolic solution (1% DMSO because of solubility) of **JB38** is added at different concentrations (5-4-3-2-1 µM in cuvette) to an 80 µM methanolic solution of DPPH, left the final solutions (all in triplicate) incubating for 2.5 hours. UV-vis spectra were collected and obtained data were analyzed, in order to find the IC_{50} value, which is the concentration value of **JB38** able to halve the absorbance of DPPH, and it turned out to be 0.4 µM: the value results to be even lower than the one of ascorbic acid (IC_{50}=20.38 µM), revealing the good antioxidant character of the thiosemicarbazone ligand.

[56] Sharma O.P., Bhat T.K.; *Food Chemistry* 113; 1202-1205 (**2009**).

3.2.3 Anti-aflatoxigenic and antifungal activity

All derivatives have been tested in order to evaluate their anti-aflatoxigenic and antifungal activity. Unfortunately, such a scaffold is able to scree the fluorescence of aflatoxins at the wavelength at which analysis are performed. It was therefore not being possible to verify their ability to inhibit aflatoxin accumulation and, as a consequence, we did not perform further analysis on this set of compounds.

Notes: Biological assay for the evaluations of the activity of the thiosemicarbazones derivatives on fungal growth and aflatoxin accumulation, together with the estimation of the effect on sclerotia biosynthesis have been developed by professor Francesco Restivo and co-workers (University of Parma, SCVSA Department); cytotoxic studies on human cell lines have been advanced by professor Annamaria Buschini and collaborators (University of Parma, SCVSA Department). Professor Donatella Ferretti and professor Claudia Zani (University of Brescia, Department of Medical and Surgical Specialities, Radiological Sciences and Public Health) have studied the cyto/genotoxic activity of this class of compounds on plant and bacteria.

This study was supported by a grant from “Fondazione Cariplo” (Project No. 2014-0555, http://aflatox.it).

Thiosemicarbazones and Cu(II) complexes as Antitumor Agents

1.INTRODUCTION

1.0 PREMISE

Metals are essential components of cellular lifecycle, indispensable for normal biological processes that daily happen in the organism: they are present as cofactors in many enzymes, like iron in hemoglobin or zinc in "zinc-fingers" proteins, and they are able to bind different proteins and, also, DNA[57]. It is therefore not surprising that metals have been used since ancient times as remedies in medicine[58]: only to cite some examples, in 3000 B.C. copper was used for water sterilization in Egypt and gold was employed in different drugs in Arabia and China. Hippocrates, the pioneer father of medicine, started using mercury (400 B.C.), that years later, in the Renaissance in Europe, was used as salt (Hg_2Cl_2) as diuretic[1]. In 1500 A.C., Paracelsus (father of the modern "metallotherapy") discovered that mixtures of heavy metals such as iron, cadmium, mercury, arsenic and antimony were successful in treating the most diverse diseases, including cancer[59]. At the beginning of the 20th century, Ehrlich discovered an arsenic-based compound to prevent syphilis[1] (*Salvarsan*), which has been then discovered to be a mixture of different cyclic species (Figure 1), and Koch used gold cyanide (AuCN) to cure tuberculosis; in 1912 it was discovered that the use of antimony is useful to treat leishmaniosis and an iron-based compound[60], *Deferoxamine*, for malaria.

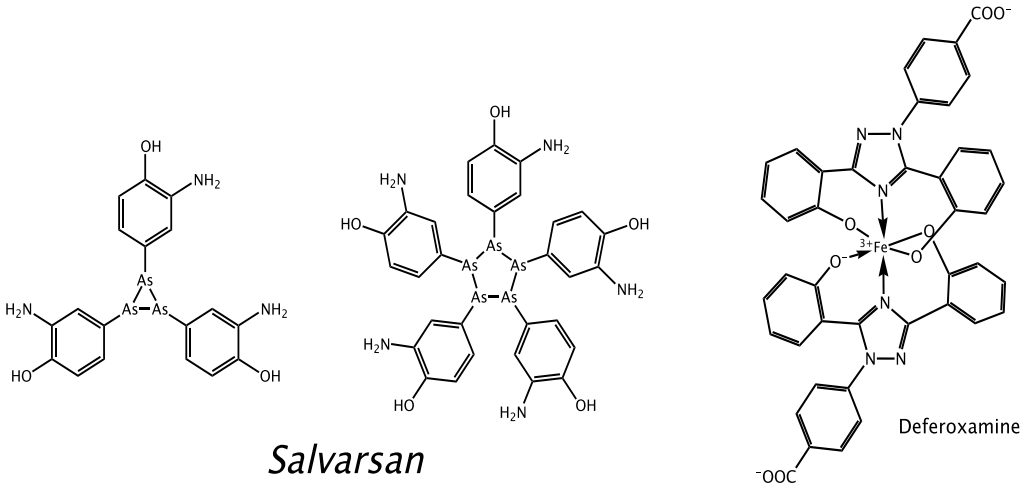

Figure 23. Molecular structure of some metal-based drugs.

57 Orvig C, Abrams MJ.; *Chem Rev.* 99(9):2201-4 (**1999**).

58 Chen D, Milacic V, Frezza M, Dou QP.; *Curr. Pharm. Des.* 15(7):777-91 (**2009**).

59 Williams DR.; *Educ Chem.* 124-127 (**1974**).

60 Sadler PJ.; *Adv. Inorg. Chem*. 36:1-48 (**1991**).

Nowadays, different metal complexes are used in therapy, like silver sulfadiazine and antimony N-methylglucamine as anti-infectives or *Auranofin*, a gold-based compound, used since 1935 to treat rheumatoid arthritis. It is known that the most widely used drugs are actually compounds based on organic molecules, but metal-based drugs are becoming increasingly common. Coordination and organometallic compounds present in fact several advantages: the coordination bond is more labile *vs* the covalent one, allowing ligand-exchange reactions in biological fluids. Moreover, the opportunity of using different kinds of ligands could modulate the bioavailability of the metal. Most important, the oxidation state and the redox activity of the metal ion play a crucial role in many processes. Overall, different oxidation states, variety in coordination geometry and charge, lipophilicity and rate of ligands exchange make metal-based drugs a challenging task for the development of novel and efficient drugs. Obviously, the comprehension of the mechanism of action of this class of compounds and the relative targets is important for the elaboration of new effective molecules.

The use of coordination complexes as chemotherapeutic agents goes back up to 1965, with the casual discover of a well-known small molecule by Rosenberg: *cis*-diamminedichloroplatinum(II), also called *cis*platin (Figure 2). This discovery represents a milestone in the fight against cancer and, still nowadays, *cis*platin represents the drug of choice in many clinical regimens. However, it presents many drawbacks and scientific research is trying to find effective alternatives with improved pharmacological profiles and reduced side-effects. In this scenario, copper-based compounds are attracting much attention for their promising anticancer properties[61]. With these considerations in mind, we have developed the work discussed in this chapter: the aim is to find metal-based antitumor agents, exploring the use of a metal ion such as copper, in order to explore an alternative to platinum-based drugs. In order to do that, we have decided to use the thiosemicarbazone molecular scaffold as chelating motif: it is well known that such class of compounds has good antiviral, antitumor and antifungal activity[189]. We focused our attention on the 2,3-dihydroxy- and 2-hydroxy-3-methoxy-benzaldehyde thiosemicarbazone derivatives; the copper(II) complexes were characterized in solution by means of UV-visible spectrophotometric titrations, and in the solid state, also by means of X-ray diffraction analysis. Antitumor properties of both ligands and complexes were assayed *in vitro* on a panel of cell lines, and in preliminary *in vivo* experiments. Detailed

[61] Gullino P.M.; *Anticancer Res*. 6(2); 153-8 (**1986**).

investigations on the mechanism of action of the copper(II) complexes are also reported, unveiling new possible biological targets so far unexplored. Here it is reported a brief introduction on *cis*platin and its analogues, together with an overview on the mechanism of action; then we describe the use of copper-based compounds in medicine and why they could be a possible good alternative strategy to platinum-based derivatives, so as to introduce our work.

1.1 *cis*PLATIN and PLATINUM-CONTAINING DRUGS

*Cis*platin is widely used in the treatment of diverse types of cancers, like testicular, ovarian, cervical, breast, bladder, head and neck, esophageal, lung, and brain. This coordination compound was first prepared by M. Peyrone in 1844, but elucidations about its structure were given in 1893 by Alfred Werner. In 1965, Rosenberg discovered that some electrolysis byproducts of platinum mesh electrodes, afterwards founded to be *cis*platin, were able to potently block cell proliferation in *Escherichia coli*. Nowadays, *cis*platin is still the most used anticancer drug in chemotherapy. It is made of a central metallic core, Pt(II), with a planar square coordination geometry: it has two chlorine and two ammonia ligands in *cis* position, respectively.

Even if *cis*platin has been used as treatment for about 40 years, its mechanism of action is partly still unclear; it is certain that just the *cis* isomer is active and that the presence of platinum as metal core is crucial to obtain antitumor activity. An important feature of this complex is in fact the nature of the bond between the metal and the leaving ligands: it requires less energy to be broken than a single/double covalent one; on the other side, platinum is an inert metal and the exchange reactions in solution are slow (hours vs μs/ns)[62]. *Cis*platin is generally administered as saline solution by injection or infusion; it diffuses quickly in tissues and it has a high affinity for plasmatic protein, like albumin: the complex, in fact, easily interacts with sulphur/thiols present in plasma proteins; about 90% of cisplatin is sequestered by albumin, which renders the drug inactive[63]. The residual 10% can enter the cell via passive diffusion[64] or, as recently discovered, by active transport mediated by OTs (Organic cations Transporters) and hCtr1 (human Copper transporter 1)[65]. Holzer et al.[66] have demonstrated that there is a correlation between the intracellular copper concentration and the platinum one: by mutating the CTR1 gene, which means an inhibition in copper transport, a lower copper internalization is observed together with low concentration of platinum and this means that there is a correlation between the mechanism of transport of these two metal ions inside the cell; contrariwise, an increase of platinum entering the cells is detected with an overexpression of the gene.

---

62 Kostova I. *Anticancer Agents Med Chem*. 6(1); 19-32 (**2006**).

63 Cepeda V., Fuertes M.A., Castilla J., Alonso C., Quevedo C., Pérez J.M.; *Anticancer Agents Med. Chem.* 7(1); 3-18 (**2007**).

64 Gately DP, Howell SB.; *Br J Cancer*. 67(6); 1171-6 (**1993**).

65 Jung Y, Lippard SJ.; *Chem Rev.* 107(5); 1387-407 (**2007**).

66 Holzer A.K. et al.; *J. Inorg. Biochem*. 98(10); 1607-1613 (**2004**).

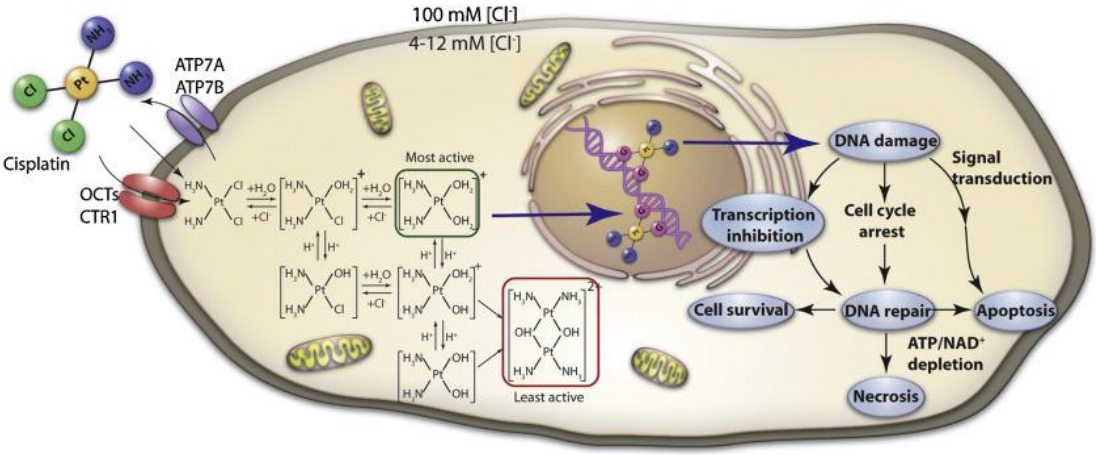

Figure 2. Scheme of the mechanism of internalization and interaction of cisplatin with DNA[67].

The chloride ions concentration is about 100 mM in the bloodstream and it radically decreases inside the cell to 3-4 mM: this provokes an hydrolysis (Figure 3) of the complex with a release of Cl^- ions that are substituted by water molecules or OH^- ions in a multi-step reaction that leads to mono/diaquo complexes.

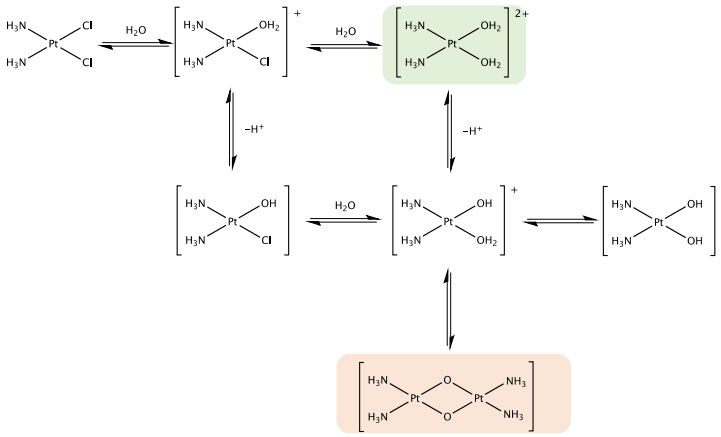

Figure 3. Multi-step reaction undergone by cisplatin inside the cells: in evidence the most reactive specie (green) and the least one (orange).

Such form is 1000-fold more reactive than the parent compound[68]: it has, now, better leaving groups so that the central metal core can easily react with nucleophile substrates.

DNA is the principal target of cisplatin: it interacts in particular with the purine nucleobases, because of the high nucleophilic character of the imidazole group. N(3) and N(7) of guanine and adenine are available to establish coordination bonds with the metal; N(7) is the preferred attack site because

[67] Ping'an M. et al; *Materials Today* 18(10); 554-564 (**2015**).

[68] Daley-Yates P.T., McBrien D.C.; *Chem Biol Interact.* 15; 777-782 (**1967**).

of its exposure in the major groove (Figure 4). It has to be taken into account that once *cis*platin is inside the cell, it can interact with various components of the lipidic bilayer, like phospholipids and phosphatidylserine; moreover, thiols of peptides, proteins, RNA, glutathione and metallothionein are all able to interact with the metal centre[69,70], so that just 1% of drug that enters the cell is able to interact with DNA[71]. Of this, 10% forms interstrand bonds between guanines of different helices, while the 90% establishes intrastrand bonds between adjacent guanines or between guanine and adenine (Figure 4)[72,73]. In the intrastrands bonds, Pt functions as a bridge by coordinating two nitrogen atoms of the imidazolic moiety of two guanines (GpG) or guanine-adenine (GpA) with the purinic moieties having a head-head orientation, resulting to be perpendicular as a consequence of the planar square geometry of platinum(II). A hydrogen bond between the NH_3 ligand and 5'-phosphate additionally stabilizes the supramolecular complex. These interactions are supposed to be responsible of the cytotoxic activity of *cis*platin: they cause a 35° distortion of the helices, with a consequent bending; few coordination intrastrand bonds are sufficient to activate the apoptosis process.

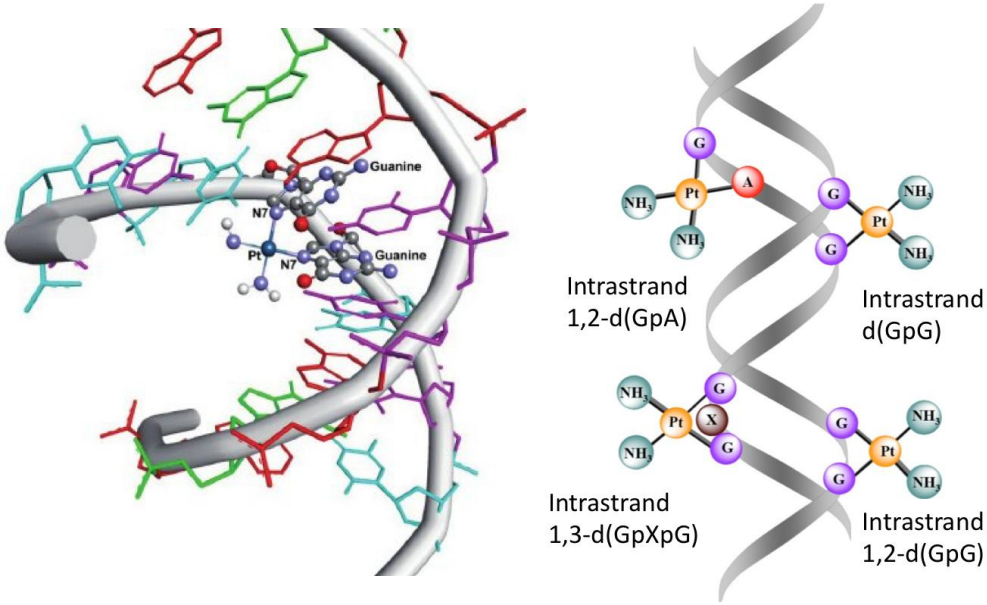

Figure 4. Reproduction of the coordination of the active form of cisplatin to the N7 atoms of guanines of the major groove (on the left) and scheme of the possible GpG and GpA intrastrand bonds (on the right).

69 Burger K.N., Staffhorst R.W., De Kruijff B.; *Biochim Biophys Acta*. 1419(1); 43-54 (**1999**).

70 Fuertes M.A., Alonso C., Pérez J.M.; *Chemical Reviews* 103(3); 645-662 (**2003**).

71 Daley-Yates P.T., McBrien D.C.; *Chem Biol Interact*. 15; 777-782 (**1967**).

72 Malinge J.M., Pérez C., Leng M.; *Nucleic Acids Res*. 22(19); 3834-9 (**1994**).

73 Natile G., Coluccia M.; *Coord Chem Rev.* 216-217; 383-410 (**2001**).

*Cis*platin is a potent anticancer drug, but presents many drawbacks, since the side effects are often severe. Among the most common and limiting effects there is nephrotoxicity. But *cis*platin can also provoke neurotoxicity, nausea, vomiting, toxicity, electrolyte disturbance, anemia. Another aspect to take into account is relative to resistance phenomena, a problem that has been driving research to the development of novel anticancer drugs. With the aim of reducing side effects and, possibly, resistance phenomena, many platinum-based compounds have been prepared and tested, but just nine entered clinical trials, like carboplatin, oxaliplatin, ormaplatin, nedplatin and enloplatin (Figure 5). In the following paragraph the second-and third-generation analogues of *cis*platin are briefly described.

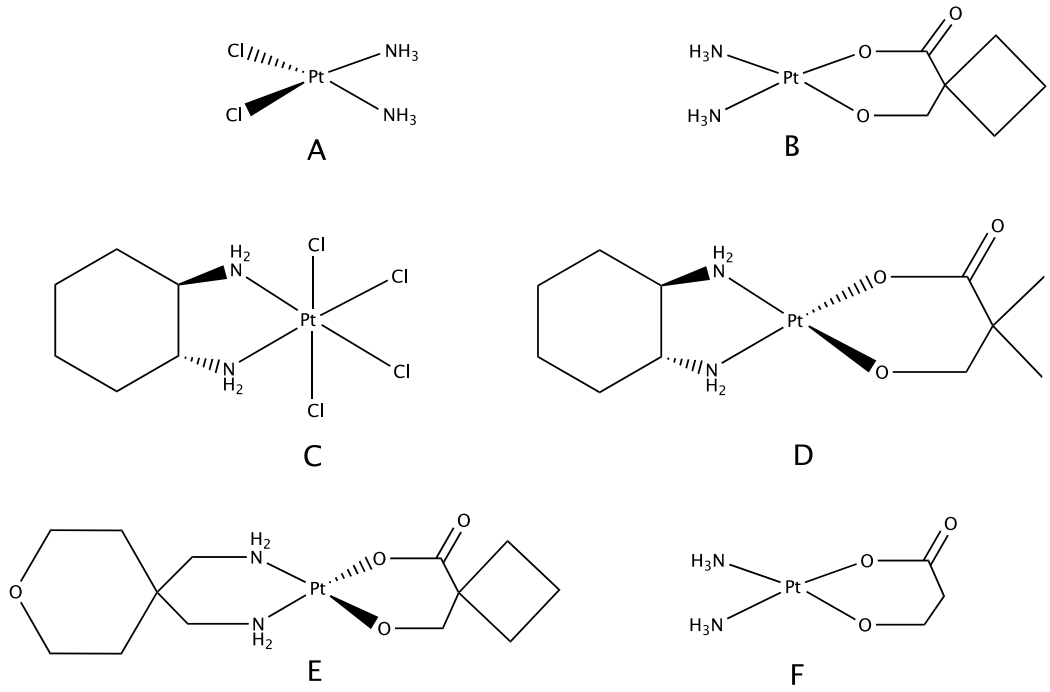

Figure 5. Molecular structure of cisplatin (A) and some of its derivatives: (B) carboplatin, (C) oxaliplatin, (D) ormaplatin , (E) enloplatin and (F) nedaplatin[74].

1.1.1 *Cis*platin Analogues

Carboplatin, is used to treat ovaries, lung, head and neck cancer; it differs from *cis*platin by a chelating cyclobutyldicarboxilato ligand in place of two chloride ones and it is often used as a prodrug of *cis*platin[75]. Its activity results to be lower and the DNA binding kinetic is slower: the supposed mechanism[76] considers that a ring opening occurs followed by binding of DNA but

74 Dasari S. et al.; *European Journal of Pharmacology* 740; 364-378 (**2014**).

75 Tinker, N.D.; Sharma, H.L. McAuliffe, C.A.; *In Platinum and Other Metal Complexes in Cancer Chemotherapy*, M. Nicolini Ed.; Martinus Nijhoff: Boston, MA, (**1988**); pp 144-159.

76 Frey, U.; Ranford, J.D.; Sadler, P.J.; *Inorg. Chem.* 32; 1333-1340 (**1993**).

carboplatin can undergo alternative action mechanisms[77]. The use of this derivative allows to avoid nephrotoxicity, but it has an important myelo suppressive effect[78]. Despite all these good premises, carboplatin results to be four times less potent than its parent compound.

Oxaliplatin (Figure 5), synthesized by Kidani et al, has been the first analogue able to overcome *cis*platin resistance[79,80]. Unlike carboplatin, in this compound the amino ligands are replaced by the bidentate (*1R,2R*)-cyclohexane-1,2-diamine. The FDA (*Food* and *Drug Administration*) has approved in 2009 the use of this platinum derivative, combined with folinic acid and 5-fluorouracil (5-FU) to treat adjuvant and metastatic colorectal cancers[81], and clinical trials are still ongoing to extend its use for metastatic gastric and esophagogastric adenocarcinoma[82].

Nedaplatin, developed by Shionogi & Co., presents a solubility in water tenfold higher than cisplatin and it provokes significant reduced nephrotoxic side effects when compared to *cis*platin and carboplatin[83,84]; it has better anticancer activity than carboplatin, but it also results to have a similar potency as *cis*platin, with fewer collateral effects. This compound, in combination with other drugs like docetaxel, paclitaxel and irinotecan, has completed phase I and phase II clinical trials in treatment of esophageal squamous cell carcinoma, giving promising results[85].

Even if second generation analogues have shown good profiles of activity, development of new derivatives is still ongoing, with the main purpose of reducing adverse side effects.

In the third generation of *cis*platin analogues, it is possible to found two coordination compounds like Lobaplatin and Heptaplatin (Figure 6).

---

77 Natarajan G., Malathi R., Holler E.; *Biochem. Pharmacol* 58; 1625-1629 (**1999**).

78 Canetta R. et al; *Cancer Treat. Rev.* 12 (Suppl. A); S125-S136 (**1985**).

79 Armand, J.P.; Bolgie, V.; Raymond, E.; Fizazi, K.; Faivre, S.; Ducreux, M.; *Semin. Oncol*. 27; 96-104 (**2000**).

80 Zarate, R.; Rodriguez, J.; Bandres, E.; Patino-Garcia, A.; Ponz- Sarvise, M.; Viudez, A.; Ramirez, N.; Bitarte, N.; Chopitea A.; Gacia-Foncillas, J.; *Br. J. Can.* 102; 987-994 (**2010**).

81 Sweetman S.C.; *Ed Martindale. The complete drug reference; 35th ed.; Pharmaceutical Press: London* (**2007**).

82 Lordick, F.; Luber, B.; Lorenzen, S.; Hegewisch-Becker, S.; Folprecht, G.; Woll, E.; Decker, T.; Endlicher, E.; Rothling, N.; Schuster, T.; Keller, G.; Fend, F.; Peschel, C.; *Br. J. Can*. 102; 500-505 (**2010**).

83 Kuwahara, A.; Yamamori, M.; Nishiguchi, K.; Okuno, T.; Chayahara, N.; Miki, I.; Tamura, T.; Inokuma, T.; Takemoto, Y.; Nakamura , T.; Kataoka, K.; Sakaeda, T.; *Int. J. Med. Sci*, 6; 305-311 (**2009**).

84 Alberto, E.M.; Lucas, M.F.A.; Pavelka, M.; Russo, N.; *J. Phys .Chem. B.* 113; 14473- 14479 (**2009**).

85 Huiping Z. et al.; *Oncology Letters* 17; 594-602 (**2019**).

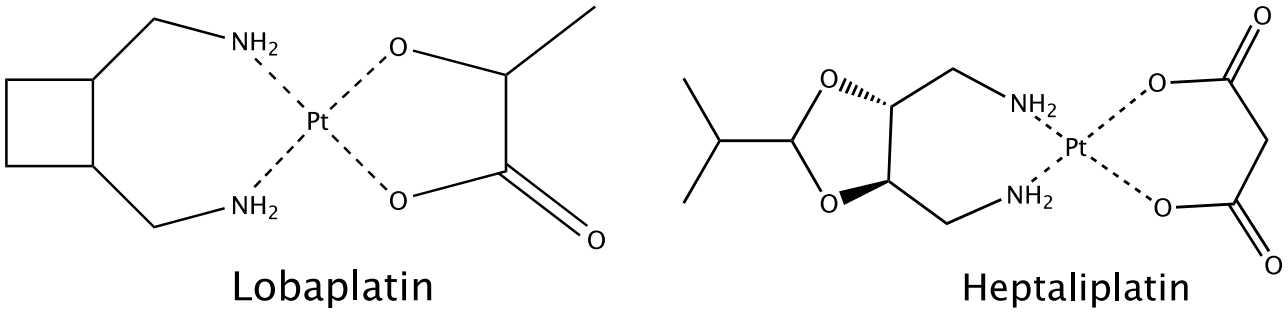

Figure 6. Lobaplatin and Heptaplatin chemical structures.

Lobaplatin is a diastereomeric mixture of platinum(II) complexes containing a 1,2-bis(aminomethyl)cyclobutane ligand and lactic acid as the leaving group, as depicted in Figure 6. It is in use to treat small cell lung cancer, leukemia and inoperable metastatic breast cancer[86]; it is also used combined with vinorelbine for late-stage non-small cell lung cancer, without showing any kind of improvement compared to *cis*platin/vinorelbine combination. Remarkable results have been obtained, instead, in the case of advanced breast cancer[87]; moreover, phase III clinical trials have been carried out in combination with 5-FU and leucovorin as treatment of recurrent/metastatic esophageal carcinoma[88]. Apart from alopecia[89], Lobaplatin provokes different side effects: neuro/renal ototoxicity has been observed[90,91], as well as anemia, nausea and vomiting[92] and also thrombocytopenia is a common side effect[93,94]. Heptaplatin (Figure 6) has a better in *vitro*/in *vivo* cytotoxicity than *cisplatin* in diverse carcinogenic cell lines[95,96,97]. It consists of a (4R,5R)-4,5-bis(aminomethyl)-2-isopropyl-1,3-dioxolane hydrophobic group, while the leaving group is a malonate; as well as a high stability in solution[30], it has a potent antitumor activity in *cis*platin resistant cell lines[23] with no severe toxicity[29,30]. This analogue is now in use to treat gastric

86 A. I. Limited, Drugs R&D 4; 369-372 (**2003**).

87 Wheate, N.J. et al.; *Dalton Trans*. 39; 8113-8127 (**2010**).

88 Shchepinov, M.S. et al.; *Nucleic Acids Res.* 29; 3864-3872 (**2001**).

89 Gietema, J.A. et al; *Anti-Cancer Drugs* 4; 51-55 (**1993**).

90 Gietema, J.A. et al; *Br. J. Cancer* 71; 1302-1307 (**1995**).

91 Kavanagh, J.J. et al; *Gynecol. Oncol.* 58; 106-109 (**1995**).

92 Gietema, J.A. et al; *Br. J. Cancer* 67; 396-401 (**1993**).

93 Manegold, C. et al; *Onkologie* 19; 248-251 (**1996**).

94 Sternberg, C.N. et al; *Ann. Oncol.* 8; 695-696 (**1997**).

95 Kim, D.K. et al.; *J. Med. Chem. 37*; 1471- 1485 (**1994**).

96 Kim, D.K. et al.; *Cancer Chemother. Pharmacol. 37*; 1-6 (**1995**).

97 Kim, D.K. et al.; *Cancer Chemother. Pharmacol. 35*; 441-445 (**1995**).

cancer[98,99]: a phase III clinical trial is still ongoing to evaluate the effect of a combination of heptaplatin and 5-FU/leucovorin on stomach carcinoma. The advantages of using this analogue instead of *cis*platin are the lower levels of neutropenia, proteinuria and emesis[100].

1.2 COPPER COMPLEXES AS ANTITUMOR COMPOUNDS

Although *cis*platin has excellent antitumor activity, its analogues have innumerable side effects that cannot be overlooked. The antitumor research has made a step forward in order to find innovative metal-based candidates, evaluating as a target alternative pharmacological mechanisms that can possibly interfere with the tumor development. Among all studied metals, copper emerges for its role in carcinogenic cells: levels of this ion are altered in tumor cells and it has an important role in angiogenesis[101]. Copper, in fact, promotes proliferation and migration of human endothelial cells, it induces transcription of mRNA and the protein expression of VEGF (*vascular endothelial growth factor*)[102,103]. The importance of copper for various angiogenesis regulators synthesis[104,105] makes this metal very attractive for the development of novel antitumor compounds, in consideration of the crucial role of angiogenesis for tumor growth, invasion and metastasis[106,107]. Moreover, copper is an endogenous metal: replacing exogenous platinum with copper could be an optimal strategy in order to reduce the occurrence of side effects. The advantages in using copper for the development of anticancer drugs are discussed in the following paragraphs.

1.2.1 Copper and its role in biological systems

Copper is an essential micronutrient for organisms that live in oxygen rich environments and it is an important cofactor of various enzymes, like cytochrome C oxidase, superoxide dismutase, lysis oxidase.[108,109,110]. It is a redox-active metal, that can switch from Cu(II) to Cu(I) and vice versa and

98 Lee, J.W. et al.; *Anti-Cancer Drugs 17*; 377-384 (**2006**).

99 Kim, N.K. et al.; Cancer *91*; 1549-1556 (**2001**).

100 Lee, K.H. et al.; *Cancer Res. Treat*. *41*; 12–18 (**2009**).

101 Gullino P.M.; *Anticancer Res.* 6(2); 153-8 (**1986**).

102 Sen C.K. et al.; *Physiol Heart Circ Physiol.* 282(5); 1821-7 (**2002**).

103 Frangoulis M., Georgiou P., Chrisostomidis C. et al.; *Plast Reconstr Surg*. 119(3); 837-43 (**2007**).

104 Brem S., Wotoczek-Obadia M.C.; AACR Special Conference: Angiogenesis and Cancer Research, Orlando, USA, January 24-28, **1998**, Abs. A-16.

105 Theophanides T., Anastassopoulou J.; *Crit Rev Oncol Hematol*. 42(1); 57-64 (**2002**).

106 Yoshii J. et al.; *Int J Cancer.* 94(6); 768-73 (**2001**).

107 Schmitt S.M., Frezza M., Dou Q.P.; *Front Biosci (Schol Ed)*. 4; 375-391 (**2013**).

108 Gaetke L.M., Chow C.K.; *Toxicology* 189(1-2); 147-63 (**2003**).

109 Tapiero H., Townsend D.M., Tew K.D.; *Biomed Pharmacother*. 57(9); 386-98 (**2003**).

110 Gupte A., Mumper R.J.; *Cancer Treat Rev*. 35(1); 32-46 (**2009**).

according to the oxidation state, it can form complexes with a large variety of donor atoms, like carboxylic oxygen, imidazole nitrogen, thiol of cysteine, sulphur atom of thioether groups.[111] The ability of the copper ion to easily donate/accept an electron makes this metal a useful tool in redox processes and in scavenging free radicals[112]. In force of its ability to easily react with O_2 and produce ROS (reactive oxygen species), the concentration level of the free ion inside the cell has to be kept really low (10^{-18}-10^{-13} M)[59], since when present in high concentration it is toxic, especially for small organisms.

The principal cause of copper toxicity is related to its ability to form ROS species. When Cu(II) is exposed to superoxide ion ($^{\bullet}O_2^-$) or reducing agents like ascorbic acid, it can be reduced to Cu(I); in this form it is then able to catalyze hydroxylic radical formation ($^{\bullet}OH^-$) starting from hydrogen peroxide, according to Haber-Weiss reaction[113]. $^{\bullet}OH^-$ is extremely reactive and it can interfere with many biological molecules provoking oxidative damages to the cell[114,115] . ROS formation contributes to the development of different pathologies, including tumors and aging. Cu(II) forms thiol radicals ($^{\bullet}$RS), but also Cys-Cu Met-Cu complexes, inducing formation of disulphurs RSSR that are potentially toxic; moreover, copper exerts its toxicity by replacing other metal co-factors: the substitution of Zn(II) in *zinc finger* domain of DNA makes the protein defective, altering its role in hormone-dependent signal transduction[116]. Because of all these effects, a tightly-regulated homeostasis of copper is necessary for cell survival[117].

1.2.2 Copper homeostasis

The quantity of copper inside the human body is about 80-120 mg and the liver accumulate the 10% of the total amount[118]; copper homeostasis is strictly regulated thanks to a class of proteins that contain copper coordinating domains, rich in cysteine, methionine and histidine[119].

The homeostatic process is divided into 3 phases: absorption, distribution and elimination. Absorption occurs in the duodenum, with efficiency of about 12-60%[120] depending on different

111 Tisato F., Marzano C., Porchia M., Pellei M., Santini C.; *Med Res Rev*. 30(4); 708-49 (**2010**).

112 Linder M.C., Hazegh-Azam M.; *Am J Clin Nutr*. 63(5); 797S-811S (**1996**).

113 Bremner I.; *Am. J. Clin.Nutr*. 67; 1069S-1073S (**1998**).

114 Powell S.R.; *J. Nutr.* 130; 1447S-1454S (**2000**).

115 Galaris D., Evangelou A.; *Crit. Rev. Oncol. Hematol*. 42(1); 93-103 (**2002**).

116 Predki P.F., Sarkar B.*; J Biol Chem*. 267; 5842–6 (**1992**).

117 Turnlund J.R., Keyes W.R., Peiffer G.L., Scott K.C.; *Am J Clin Nutr*. 67; 1219S-25S (**1998**).

118 Iakovidis I., Delimaris I., Piperakis S.M.; *Mol Biol Int.* 2011; 594529 (**2011**).

119 Safaei R., Holzer A.K., Katano K., Samimi G., Howell S.B.; *J. Inorg. Biochem*. 98(10); 1607-1613 (**2004**).

120 Turnlund J.R., Keyes W.R., Anderson H.L., Acord L.L.; *Am J Clin Nutr*. 49(5), 870-8 (**1989**).

factors: for example, the oral uptake of zinc or iron can decrease copper internalization. It has been observed[121] that high level of copper corresponds to low iron concentration, while high level of iron can lead to systematical deficiency of copper, provoking anemia, neutropenia and osteoporosis[73]. hCTR1 is the protein responsible of the metal ion uptake inside the enterocytes (Figure 7); the first studies date back to the nineties, when *Saccharomices cerevisiae* was used as model[122]: it was demonstrated that CTR1 and CTR3 mediate copper transport; such proteins contain His, Cys and Met residual[123] that can chelate the metal ion.

Copper enters the cell by a pore in the plasmatic membrane[124]: the ion is directed to the extracellular N-terminal domain, it crosses the membrane and exits in the intracellular environment, probably bound to carboxylic moieties, then it reaches the target protein[57] (Figure 7). hCTR1 is expressed in liver, kidneys, heart and intestine; the up/down regulation is monitored by the SP1 protein and its activity depends on copper concentration levels[125]. During the internalization process, Cu(II) is reduced to Cu(I) by various proteins, like *Steap protein*[126] and *Dcytb protein*[127]. Different studies have reported that copper chaperons are able to bind only the Cu(I) form[128], therefore it is expected that a reductase in the apical membrane intervenes in the uptake process.

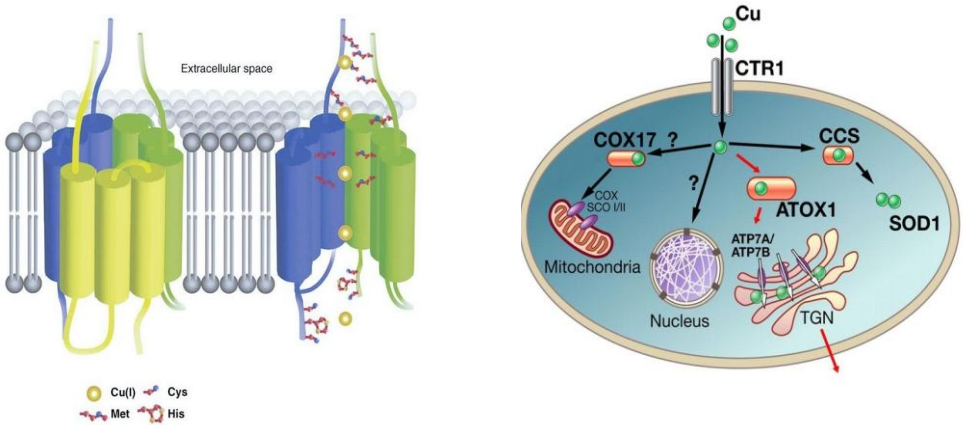

Figure 7. Copper uptake by hCTR1, on the left, and its intracellular distribution, on the right.

121 Ha J.H., Doguer C., Wang X., Flores S.R., Collins J.F.; *PLoS One*. 11(8); 0161033 (**2016**).

122 Dancis A., Yuan D.S., Haile D., Askwith C., Eide D., Moehle C., Kaplan J., Klausner R.D.; *Cell.* 76(2); 393-402 (**1994**).

123 Puig S., Lee J., Lau M., Thiele D.J.; *J Biol Chem.* 277(29); 26021-30 (**2002**).

124 Cheng-Yu Tsai, Christopher A. Larson, Roohangiz Safaei, Stephen B. Howell. *Biochem Pharmacol*. 90(4); 379–387 (**2014**)

125 Yan D., Aiba I., Chen H.H., Kuo M.T.; *J Inorg Biochem.* 161; 37-9 (**2016**).

126 Ohgami R.S., Campagna D.R., McDonald A., Fleming M.D.; *Blood*. 108(4); 1388-94 (**2006**).

127 McKie A.T. et al.; *Science* 291(5509); 1755-9 (**2001**).

128 Eisses J.F., Stasser J.P., Ralle M., Kaplan J.H., Blackburn N.J.; *Biochemistry*. 39(25); 7337-42 (**2000**).

hCTR1 has been considered for long time the only protein responsible of copper internalization; recently, it has been discovered that Cu(II) could be conveyed by DMT1, a bivalent metal ions transporter, which is involved also in iron(II) transport[129,130]. Once inside the enterocytes, the copper ion binds Atox1, a copper-chaperon which has an essential role in copper homeostasis: it takes the ion to ATP7A, which allows it to enter the circulatory system. Once in the circulatory system, copper, as Cu(II), binds albumin (10-12%), L-histidine and transcupreine[131,132]. When the metal ion reaches the liver, it is quickly internalized in the hepatocytes by hCTR1 thanks to the action of a reductase. In the cell copper is bound by glutathione (GSH) and metallothioneins (MT), that constitute the copper reservoir of the cell.[133] Several copper-chaperons, small cytosolic proteins, are responsible for the transport inside the cell, guiding copper towards the appropriate receiving protein: CCS1 is responsible for copper transport to SOD enzyme, which is involved into oxidative stress defense process in the cytoplasm[134]; Cox17 takes copper to cytochrome C oxidase (CCO) which is located in the inner mitochondrial membrane and Atox1 transports copper to ATP7B, by which the metal is incorporate inside ceruloplasmin (Cp): copper bound to Cp is available for the uptake from the organism tissues[57]. To avoid an excessive accumulation of the metal, the cell involves two ATP-ases, ATP7A and ATP7B which mediate copper cell outflow: ATP7A is responsible for eliminating the copper at the level of the enterocyte, while ATP7B works at the level of the hepatocyte, removing the excess of the metal through the bile[135].

1.2.3 Copper and its role in neoplasms

The role of copper in tumor growth has been intensely studied in the past decades; it has been highlighted that in carcinogenic cells there is a change in terms of copper levels and absorption, transport, metabolism and elimination of the metal[136]. In particular, copper levels result altered in

129 Arredondo M., Uauy R., González M.; *Biochim Biophys Acta* 1474(2); 169-76 (**2000**).

130 Tennant J., Stansfield M., Yamaji S., Srai S.K., Sharp P.; *FEBS Lett.* 527(1-3); 239-44 (**2002**).

131 Lau S.J., Sarkar B.; *J Biol Chem*. 246(19); 5938-43 (**1971**).

132 Wang T., Guo Z.; *Curr Med Chem*. 13(5); 525-37 (**2006**).

133 Freedman J.H., Ciriolo M.R., Peisach J.; *J Biol Chem*. 264(10); 5598-605 (**1989**).

134 Culotta V.C, Klomp L.W., Strain J., Casareno R.L., Krems B., Gitlin J.D.; *J Biol Chem*. 272(38); 23469-72 (**1997**)

135 Arredondo M., Núñez M.T.; *Mol Aspects Med*. 26(4-5); 313-27 (**2005**).

136 Linder M.C., Hazegh-Azam M.; *Am J Clin Nutr*. 63(5); 797S-811S (**1996**).

Hodgkin lymphoma, sarcoma, cervical, prostate, liver, lung, brain and breast cancer[137,138,139,140]. Studies have evidenced that hematic copper concentrations can be correlated to tumor incidence, progression and appearance of recurrence[141,102]. Different tumors, like lymphoma, present really elevated hematic ceruloplasmin levels[60], its synthesis and secretion increase in presence of tumor[89] and it is correlated to tumor stadium; hematic analysis of this protein is useful to define the diagnosis, establish the prognosis and chemotherapy efficacy. Copper seems therefore to play a role in tumor genesis, growth and metastasis, particularly because of its involvement in various angiogenic factors synthesis, crucial for cell proliferation and migration, like VEGF, angiogenin, bFGF, TNF-a[142,60].

When it is present in normal concentration, copper induces oxidative phosphorylation and it has an antioxidant activity; on the contrary, when present in excess, it takes to neurodegeneration and angiogenesis[143]. An angiogenesis overregulation is index of a pathogenic condition and it occurs also during solid state tumor progression: actually, new blood vessels form a new entry way for nutrients, growth and signaling factors which are important for tumor development[144]. The role of copper in this biological process has been underlined for the first time by McAuslan and Reilly in 1980, when they noticed that Cu-based salts were the most common species present in tumor extracts[145]. It has also been demonstrated that copper is able to fortify the bound between angiogenin and receptors of endothelial cells of pulmonary artery of calf[146].

For all these reasons this metal could be a good target for the development of new antitumor drugs[147,148].

First attempts were made in order to control copper levels[149]; studies have revealed that copper binding systems can be suitable to this purpose. Three different compounds have been investigated (Figure 8): tetrathiomolibdate (TM), trienine and D-penicillamine (D-pen). They have all reached out

137 Winder A.J., Harris H.; *Eur. J. Biochem*. 198; 317−326 (**1991**).

138 Chen H.H., Yan J.J., Chen W.C., Kuo M.T., Lai Y.H., Lai W.W., Liu H.S., Su W.C.; *Lung Cancer*. 75(2); 228- 34 (**2012**).

139 Wee N.K.Y., Weinstein D.C., Fraser S.T., Assinder S.J.; *The International Journal of Biochemistry & Cell Biology*. 45(5); 960-963 (**2013**).

140 Gandin V., Tisato F., Dolmella A., Pellei M., Santini C., Giorgetti M., Marzano C., Porchia M.; *J Med Chem.* 57(11); 4745-60 (**2014**).

141 Díez M., Arroyo M., Cerdàn F.J., Muñoz M., Martin M.A., Balibrea J.L.; *Oncology*. 46(4); 230-4 (**1989**).

142 Lowndes S.A., Harris A.L.; *J Mammary Gland Biol Neoplasia*. 10(4); 299-310 (**2005**).

143 Bharathi Devi S.R., Dhivya M.A., Sulochana K.N.; *J Biosci*. 41(3); 487-96 (**2016**).

144 Turski M.L., Thiele D.J.; *J Biol Chem*. 284(2); 717-21 (**2009**).

145 McAuslan B.R., Reilly W.; *Exp Cell Res*. 130(1); 147-57 (**1980**).

146 Soncin F., Guitton J.D., Cartwright T., Badet J.; *Biochem Biophys Res Commun*. 236(3); 604-10 (**1997**).

147 Daniel K.G., Harbach R.H., Guida W.C., Dou Q.P.; *Front Biosci*. 9; 2652-62 (**2004a**).

148 Daniel K.G., Gupta P., Harbach R.H., Guida W.C., Dou Q.P.; *Biochem Pharmacol*. 67(6); 1139-51 (**2004b**).

149 Khan G.N., Merajver S.D.; *Curr Pharm Des*. 13(35); 3584-90 (**2007**).

phase II clinical trials highlighting good results, opening the way to the synthesis of various copper chelating compounds as antitumor agents.

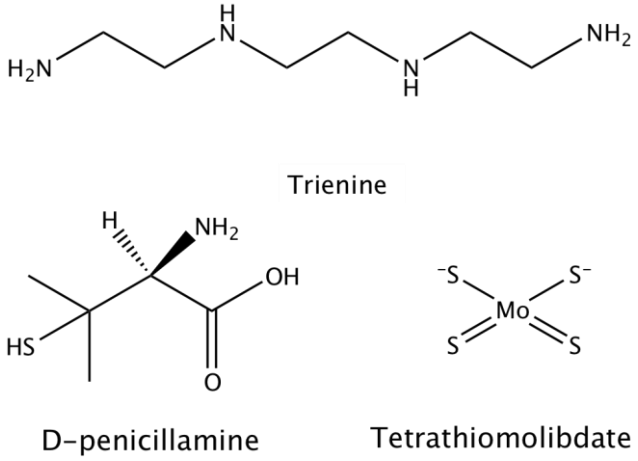

Figure 8. Copper chelating agents that have reached clinical trials.

1.3 COPPER COMPLEXES AS AN ALTERNATIVE TO PLATINUM-BASED DRUGS IN ANTICANCER THERAPY

A large variety of metal-based antitumor compounds have been studied with the aim to overcome the drawbacks related to platinum-based drugs, including complexes of essential metals like copper. The rationale beyond the use of copper is also related to the fact that it is an endogenous metal, so it results in principle less noxious than the exogenous platinum. Moreover, the properties that make copper toxic for biological systems constitute also the basis for the development of copper complexes with an antineoplastic profile.[150] Last but not least, it has also to be considered the atypical biological necessity of an elevate uptake of copper for tumor cells.

Starting from 70s, different copper derivatives with various classes of ligands like phosphine or imidazole have been proposed as antitumor agents, but their activity has been investigated just in the past few years[151]. The proposed mechanisms of action of such derivatives are different from the one of platinum complexes, in the same way as biodistribution and toxicity: this is a very important aspect if we are looking for the possibility to overcome resistance to platinum drugs, with a contemporaneous reduction of side effects. The success of this new strategy is strictly related to the kind of ligand used: metal bioavailability, stability of the complex, which must be stable enough to

[150] Frausto Da Silva J.J.R., Williams R.J.P.; *The biological chemistry of elements. The inorganic chemistry of life*; Oxford: Clarendon Press (**1994**).

[151] Marzano C., Pellei M., Tisato F., Santini C.; *Anticancer Agents Med Chem*.; 9(2); 185-211 (**2009**).

reach the target but fairly labile to interact with the binding site, hard/soft proprieties of the metal, toxicity of the complex are all features that can be tuned by carefully choosing the nature of the ligands. Copper results to be a good candidate also because of its versatility as far as coordination geometry and, depending on the oxidation state, the possibility to coordinate various types of S- and N- donor ligands.

1.4 MECHANISM OF ACTION OF COPPER COMPLEXES

One of the possible target of copper complexes is surely DNA; already in 1969 it has been demonstrated that there is a big affinity between copper and DNA[152] and in 1991 it has been published a crystalline structure of a $CuCl_2$-DNA adduct in which copper is bound to a guanine[153]. Various copper complexes are still undergoing analysis as metallodrugs with DNA as target; it has been verified that planarity, hydrophobicity, nature of the co-ligand, but especially the coordination geometry play an essential role in determining the kind of bound and the type of intercalation of copper derivatives with DNA.

Antineoplastic copper complexes can promote nucleobases oxidation, phosphor-ester bound hydrolysis or oxidation of the deoxyribose sugar. In 1986 Zue and collaborators have demonstrated that copper works as a redox catalyst[154]; different studies have stated that copper promotes a scission of DNA provoking oxidative stress[155,125]. This mechanism takes to ROS formation like the hydroxylic radical or diverse metal-based intermediates ($CuOH_2^+$ or CuO^+) that break the polynucleotides chain[156]. In 1996 it has been reported the first example of Cu(II)-TACN (1,4,7-triazacyclononane) that cuts DNA in both anaerobic/aerobic conditions, with a hydrolytic scission. It is important to underline that oxidative agents produce DNA fragments that cannot be enzymatically rebounded[157]. Belicchi-Ferrari and collaborators have synthesized a panel of Cu(II) complexes derived from 5-formyluracil-thiosemicarbazones (Figure 10): their activity has been verified on DNA PBR 322 plasmid by electrophoresis[158].

---

152 Eichhorn G.L., Shin Y.A.; *J. Am. Chem. Soc.* 90; 7323 (**1968**).

153 Kagawa T.F., Geierstanger B.H., Wang A.H.J., Ho P.S.; *J. Biol. Chem*. 266; 20175 (**1991**).

154 Wang D., Lippard S.J.; *Nat. Rev. Drug Discovery*. 4; 307 (**2005**).

155 Arjmand F., Muddassir M.; *Chirality*. 23; 250 (**2011**).

156 Fleming A.M., Muller J.G., Ji I., Burrows C.; *J. Org. Biomol. Chem*. 9; 3338 (**2011**).

157 Hegg E.L., Burstyn J.N.; *Inorg. Chem*. 35; 7474 (**1996**).

158 Belicchi Ferrari M., Bisceglie F., Pelosi G., Tarasconi P.; *Polyhedro*n. 27; 1361-1367 (**2008**).

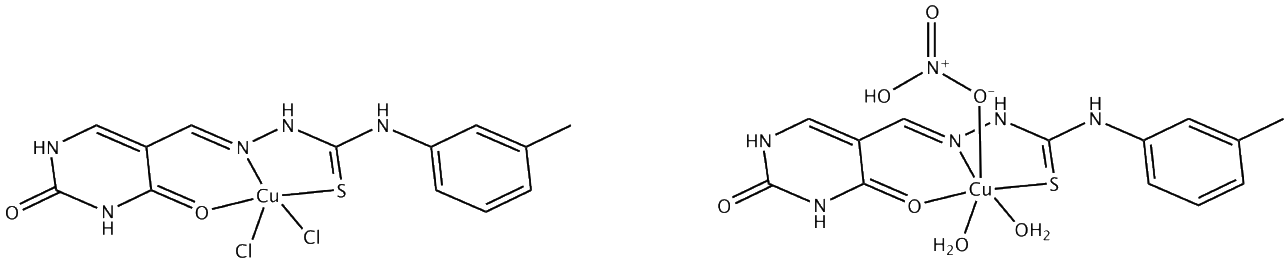

Figure 10. Molecular structure of 5-formyluracil-thiosemicarbazones copper complexes[158].

Past investigations have revealed that copper complexes, or just fragments of them, are able to interact with the nucleic acid: recently, it has been discovered that the Cu-plumbagin complexes have a cytotoxicity which is related to topoisomerase I inhibition.

Higher levels of ROS, provoked by redox cycles activation and GSH decrease, are often present in carcinogenic cells when compared to healthy ones. One of the most accredited mechanism proposed for anticancer copper complexes is based on ROS formation by the Haber-Weiss reaction[159] and/or by the ability of some copper complexes to mimic SOD activity[160]. This implies a redox imbalance, an excessive oxidative stress that the cancer cells cannot afford: cellular dead pathways are then activated and apoptosis or paraptosis occur. Generally, apoptosis is the most common process that takes cells to death but recently a new pathway, called paraptosis, has been found: this has been observed in human neoplastic cells treated with Cu(I)[161,162,163] and Cu(II)[164,165,166] complexes. However, other cellular targets have recently emerged for copper complexes, like topoisomerase I and the multiproteic proteasome 26S complex[125].

1.4.1 Copper complexes as topoisomerase inhibitors

Topoisomerases are proteins that regulate DNA metabolism and they are divided into two categories: topoisomerase I (Topo I) and II (Topo II); the essential difference between them is that the first is able to break just one of the two helices of DNA, while Topo II provokes an interruption

159 Koppenol W.H.; *Redox Rep*. 6(4); 229-234 (**2001**).

160 Devereux M., O'Shea D., O'Connor M., Grehan H., Connor G. et al.; *Polyhedron*. 26(15); 4073-4084 (**2007**).

161 Marzano C., Pellei M., Alidori S., Brossa A., Lobbia G.G., Tisato F., Santini C.; *J Inorg Biochem*. 100(2); 299-304 (**2006a**).

162 Marzano C., Pellei M., Colavito D., Alidori S., Lobbia G.G., Gandin V., Tisato F., Santini C.; *J Med Chem*. 49(25); 7317-24 (**2006b**).

163 Marzano C., Gandin V., Pellei M., Colavito D., Papini G., Lobbia G.G., Del Giudice E., Porchia M., Tisato F., Santini C.; *J Med Chem*. 51(4); 798-808 (**2008**).

164 Dallavalle F., Gaccioli F., Franchi-Gazzola R., Lanfranchi M., Marchiò L., Pellinghelli M.A., Tegoni M.; *J Inorg Biochem.* 92(2); 95-104 (**2002**).

165 Tardito S., Bussolati O., Gaccioli F., Gatti R., Guizzardi S., Uggeri J., Marchiò L., Lanfranchi M., Franchi- Gazzola R.; *Histochem Cell Biol*. 126(4); 473-82 (**2006**).

166 Tardito S., Bussolati O., Maffini M., Tegoni M., Giannetto M., Dall'asta V., Franchi-Gazzola R., Lanfranchi M., Pellinghelli M.A., Mucchino C., Mori G., Marchio L.; *J Med Chem*. 50(8); 1916-24 (**2007**).

of both helices[167]. These proteins are essential because they are involved into the overwinding/underwinding of DNA, so they could be an interesting clinical target for chemotherapy and, in fact, their inhibitors have a central role in diverse therapeutic regimes. Different literature data reported that a copper-salicylaldoxime, which inhibits leukemia L1210 cells proliferation, interferes with Topo II forming a dimer, which causes an interruption in a single helix of DNA to which the enzyme is bound[168]. Heterocycle α-thiosemicarbazones and relative copper complexes can inhibit Topo II in *in vitro*/*in vivo* assays with IC_{50} values below the one of etoposide, a Topo II inhibitor[169]. Different α-heterocycle-N4 substituted-thiosemicarbazones have been recently studied, together with the relative copper complexes, for their ability to decrease proliferation of breast cancer cells[170]: results have shown that [Cu(TSC)Cl] complexes are more active than the corresponding free ligand. It has been supposed that they act binding the ATP-hydrolysis domain of the enzyme interfering with the hydrolysis of the enzyme.

1.4.2 26S proteasome inhibitors

The 26S proteasome is an ATP-dependent multifunctional complex which is located in both nucleus and cytoplasm: it selectively degrades intracellular proteins including signaling molecules, tumor suppressors, cellular cycle regulators, transcriptional factors, anti-apoptotic proteins. The proteasome is composed of a proteolytic core, called 20S proteasome, enclosed between two regulatory complexes called 19S[171]: these complexes associate in presence of ATP[172,173]. 20S proteasome has a hollow cylindrical structure composed of 4 rings stacked on each other; all rings contain seven subunits: the most external are made of α-subunits, the inner ones are made of β[174] (Figure 11). α-subunits are the selective barrier between the catalytic core of the proteasome and cytoplasm, and they monitor the entry/exit of substrates; they are also able to recognize the proteins to allow their degradation process to begin. β-subunits contain the active site which faces the innermost part of the cylinder: so, the only access way that allows substrates to reach this

167 Qin Y., Meng L., Hu C., Duan W., Zuo Z., Lin L., Zhang X., Ding J.; *Mol. Cancer Ther.* 6; 2429 (**2007**).

168 Jayaraju D., Kondapi A.K.; *Curr. Sci*. 81; 787 (**2001**).

169 Marzano C., Severin E., Pani B., Guiotto A., Bordin F.; *Environ Mol Mutagen*. 29(3); 256-64 (**1997**).

170 Zeglis B.M., Divilov V., Lewis J.S.; *J. Med. Chem*. 54; 2391 (**2011**).

171 Hölzl H., Kapelari B., Kellermann J., Seemüller E., Sümegi M., Udvardy A., Medalia O., Sperling J., Müller S.A., Engel A., Baumeister W.; *J Cell Biol*. 150(1); 119-30 (**2000**).

172 Coux O., Tanaka K., Goldberg A.L.; *Annu Rev Biochem*. 65; 801-47(**1996**).

173 Voges D., Zwickl P., Baumeister W.; *Annu Rev Biochem*. 68; 1015-68 (**1999**).

174 Baumeister W., Walz J., Zühl F., Seemüller E.; *Cell*. 92(3); 367-80 (**1998**).

narrow chamber is through cannels of α-subunits[175,176]. Because of the position of the catalytic site inside the cylinder, 26S proteasome has a high selectivity for just few substrates, so it avoids an uncontrolled degradation process of a large panel of cellular proteins[177].

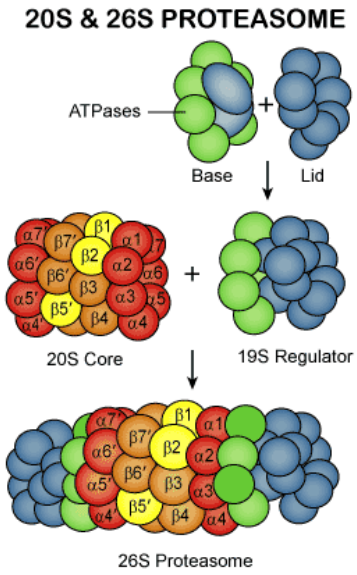

Figure 11. Scheme of the structure of 20S and 26S proteasome.

The 20S core contains six active sites, three in each of two β rings (β_1, β_2, β_5) and they differ for the catalytic activity: β_1 has a "caspases-like" activity and it cuts after acidic residues; β_5 breaks the polypeptide after hydrophobic amino acids like chymotrypsin; β_2 cuts after basic residues[178].

19S regulatory complexes are made of a base and a top[179]; the base is associated to 20S proteasome and it is made of 8 polypeptides, with 6 ATP-ase homologs included: they interact with the α-subunits and they determine the ATP-dependent opening of the channel allowing the access of polypeptides in the catalytic chamber[180].

The 26S complex is responsible of different proteins degradation, like the mutated, damaged and misfolded one; it is also essential for cellular mechanisms like cells development control, apoptosis control, regulation of genic expression and development of inflammatory response[181,182]. The use

175 Groll M., Ditzel L., Löwe J., Stock D., Bochtler M., Bartunik H.D., Huber R.; *Nature*. 386(6624); 463-71 (**1997**).

176 Jung T., Catalgol B., Grune T.; *Mol Aspects Med*. 30(4); 191-296 (**2009**).

177 Kisselev A.F., Goldberg A.L.; *Chem Biol*. 8(8); 739-58 (**2001**).

178 Keiji T.; *Proc Jpn Acad Ser B Phys Biol Sci*. 85(1); 12–36 (**2009**).

179 Glickman M.H., Rubin D.M., Coux O., Wefes I., Pfeifer G., Cjeka Z., Baumeister W., Fried V.A., Finley D.; *Cell*. 94(5); 615-23(**1998**).

180 Köhler A., Cascio P., Leggett D.S., Woo K.M., Goldberg A.L., Finley D.; *Mol Cell*. 7(6); 1143-52 (**2001**).

181 Orlowski R.Z., Dees E.C.; *Breast Cancer Res*. 5(1); 1-7 (**2003**).

182 Nalepa G., Rolfe M., Harper J.W.; *Nat Rev Drug Discov*. 5; 596-613 (**2006**).

of inhibitors that are able to affect this complex could present a new antitumor strategy: it has been noticed that the treatment of non-tumor cells with an inhibitor of this enzyme leads to a block of the cellular cycle, while tumor cells undergo apoptosis[183].

The first case of Cu-complex has been reported by Dou and collaborators[184]: they have described a copper-mixture, derived from Cu(II) salts and (8-OHQ) bidentate ligands, which is active just against carcinogenic cells; since that, different complexes have been synthesized: dithiocarbamate[185], phosphinic complexes[132,186,125] and copper(II) complexes of type Cu[(N-N)(A-A) with (A-A)= N-O or O-O[187] donor ligands, which have an high selectivity for this enzyme.

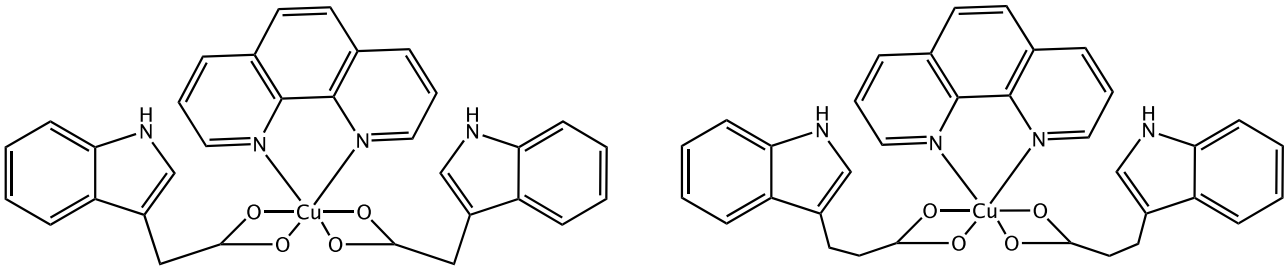

Figure 12. Molecular structure of Cu[(N-N)(O-O)] derivative[187].

1.5 S-DONOR SYSTEMS: THIOSEMICARBAZONES (TSCs)

Thiosemicarbazones (TSCs) are a class of compounds well known for their medical properties: they have been studied for their antiviral, antifungal and antitumor activity[44,45]. Metisazone ([(1-methyl-2-oxoindolo-3-ylidene)amino]thiourea) (Figure 12) was for instance approved with the name of Marboran™, to treat smallpox[161]. Subsequently, Sulfathiazole (Figure 13) was developed as antibacterial agent[188].

183 Adams J.; *Drug Discov Today*. 8(7); 307-1 (**2003**).

184 Dou Q.P., Goldfarb R.H.; *Drugs*. 5; 828 (**2002**).

185 Frezza M., Hindo S., Chen D., Dvenport A., Schmitt S., Tomco D., Dou Q.P.; *Curr. Pharm. Des*. 16; 1813 (**2010**).

186 Tardito S., Isella C., Medico E., Marchiò L., Bevilacqua E., Hatzoglou M., Bussolati O., Franchi-Gazzola R.; *J Biol Chem*. 284(36); 24306-19 (**2009**).

187 Zhang Z., Bi C., Schmitt S.M., Fan Y., Dong L., Zuo J., Dou Q.P.; *J. Biol. Inorg. Chem*. 17; 1257 (**2012**).

188 Pfau Cj.; *Chemotherapy of Viral Infections*. 61; 147-204 (**1982**).

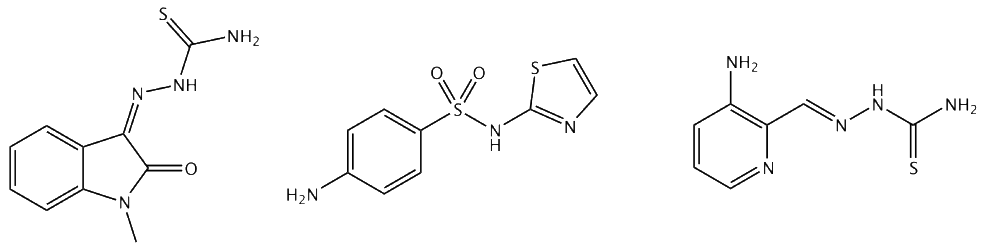

Figure 13. Molecular structure of Metisazone, Sulfathiazole and Triapine.

TSCs play an essential role in biological processes typical of mammalian cells because they inhibit ribonucleotide reductase, which is necessary for DNA precursors synthesis[57]: this enzyme is highly expressed in carcinogenic cells and this makes it a good and well-defined target for antitumor therapy. Mammalian ribonucleotide reductase is made of two different proteins, R1 and R2: the first contains polythiols while the second has a non-heme iron ion and a free tyrosyl radical, which is the active center of the enzyme; the stability of such radical depends on the presence of a binuclear Fe(III) center[189]. TSCs are able to inhibit R2: it was first supposed that they coordinate iron by the N,N,S chelating motif with consequent inhibition of its activity[190]; moreover, some thiosemicarbazones increase their activity if bounded to specific metal ions[191]. Triapine (Figure 13) has reached out phase II clinical trial against diverse types of cancer. Other TSCs derivatives have been investigated as iron chelators, like dipyridyl and quinoline/quinazoline derivatives[192], reporting very promising results.

189 Matesanz A.I., Souza P.; *Mini Rev Med Chem*., 9(12); 1389-96 (**2009**).

190 Liberta A.E., West D.X.; *Biometals*. 5(2); 121-6 (**1992**).

191 Arora S., Agarwal S., Singhal S.; *International Journal of Pharmacy and Pharmaceutical Sciences*. 6(9); (**2014**).

192 Mrozek-Wilczkiewicz A. et al.; *European Journal of Medicinal Chemistry* 171; 180-194 (**2019**).

AIM OF THE PROJECT: This project fits into a larger context: the research of new metal-based antitumor agents. Despite its great success, *cis*platin has a high toxicity and it is also cause of severe collateral effects. Meanwhile, copper complexes have emerged as potential antitumor agents[117,57,153]: the starting idea is to use this metal ion to reduce toxicity induced by exogenous metals such as platinum, gold or ruthenium, that easily accumulate in the organism. In this project, different thiosemicarbazones derivatives (Figure 14) and the relative copper complexes have been investigated to evaluate their antitumor activity. Their antiproliferative activity has been studied in both 2D and 3D cell cultures: cytotoxicity tests have been developed on a large panel of carcinogenic human cell lines and from preliminary data it has been possible to speculate about preliminary structure-activity relationships (SARs). Uptake experiments on cell have been developed and, in the end, the action mechanism has been studied by biochemical and microscopy tests, unveiling a possible cellular target.

As a prosecution of this work, in order to increase the water solubility of the copper complexes, a modification on the thiosemicarbazonic scaffold has been made, inserting a sulphonyl group; the corresponding copper(II) complexes have been synthesized and both ligands and complexes have been tested to evaluate their antitumor activity.

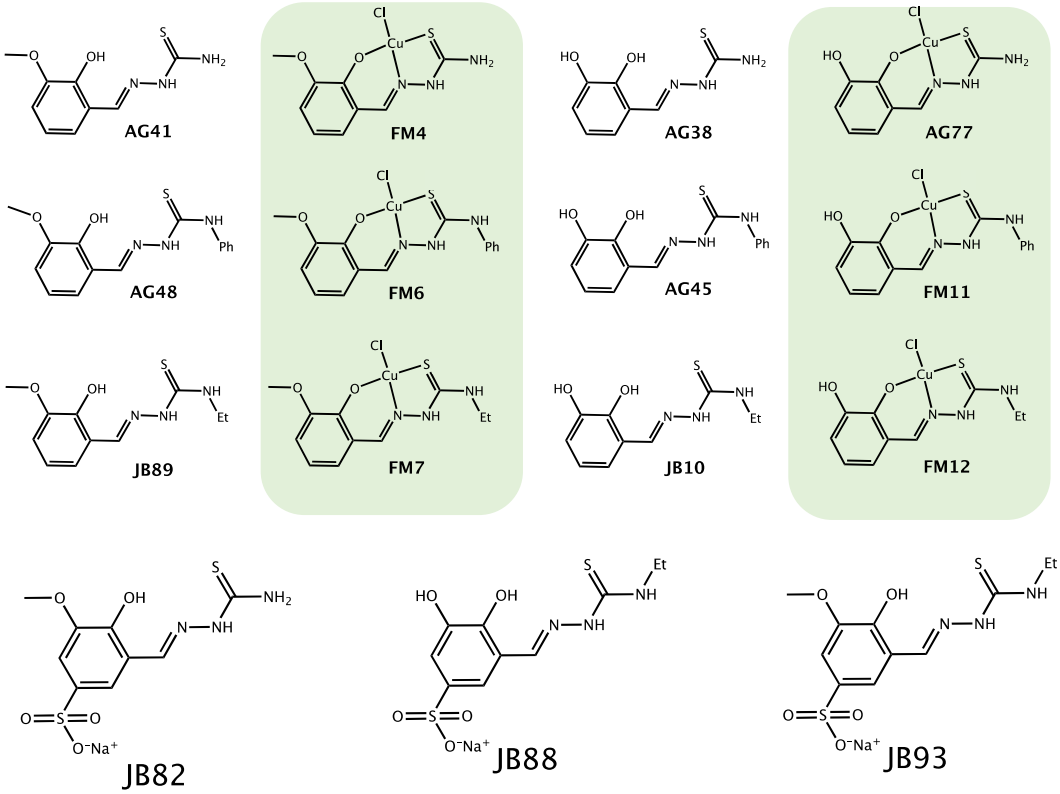

Figure 14. Molecular structure of thiosemicarbazones ligands, their copper(II) complexes and the 5-sulphonyl derivatives.

2. EXPERIMENTAL SECTION

2.1 MATERIALS AND METHODS

2.1.1 Chemistry

All reagents of commercial quality were purchased from Sigma-Aldrich and used without further purification. The purity of the synthesized compounds was determined by elemental analysis and verified to be ≥ 95%. ^{1}H-NMR spectra were recorded at 25 °C on a Bruker Avance 400 FT spectrophotometer. The ATR-IR spectra were recorded by means of a Nicolet-Nexus (Thermo Fisher) spectrophotometer by using a diamond crystal plate in the range of 4000-400 cm^{-1}. Elemental analyses were performed by using a FlashEA 1112 series CHNS/O analyzer (Thermo Fisher) with gas-chromatographic separation. Electrospray mass spectral analyses (ESI-MS) were performed with an electrospray ionization (ESI) time-of-flight Micromass 4LCZ spectrometer. Samples were dissolved in methanol. MS spectra were acquired with a DSQII Thermo Fisher apparatus, equipped with a single quadrupole analyzer in positive EI mode, by means of a DEP-probe (Direct Exposure Probe) equipped with a Re-filament. The UV-vis spectra were collected using a Thermo Evolution 260 Bio spectrophotometer provided with a thermostatting Peltier device, and quartz cuvettes with 1 cm path length.

2.1.2 Crystallography

Single crystals of **FM4 ·H_2O** and {$Na[CuLCl]_2Cl$}, with HL=**AG41**, were mounted on a glass fibre and the intensity data were collected with a SMART APEX2 diffractometer equipped with a Bruker AXS CCD detector using Mo-Ka radiation and a graphite crystal monochromator [λ(Mo-Kα) = 0.71073 Å]. The SAINT[193] software was used for the integration of reflection intensities and scaling, and SADABS[194] for the absorption correction. The structures were solved by direct methods using SIR97[195] and refined by full-matrix least-squares on all F2 using SHELXL97[196] implemented in the WinGX package[197]. All the non-hydrogen atoms in the molecules were refined anisotropically. The hydrogen atoms were partly found and partly placed in ideal positions using riding models. The structures were solved by direct methods and difference Fourier synthesis using the SHELX suite of

193 SAINT: SAX, Area Detector Integration, Siemens Analytical Instruments Inc., Madison, Wisconsin, USA

194 Sheldrick G. SADABS: Siemens Area Detector Absorption Correction Software, University of Goettingen, Germany, 1996.

195 Altomare A., Burla C., Camalli M., Cascarano G.L., Giacovazzo C., Guagliardi A., Moliterni A.G.G., Polidori, G.; *Spagna, R. J. Appl. Crystallogr*. 32; 115-119 (**1999**).

196 Sheldrick G.M.; *Acta Cryst.* A64; 112-122 (**2008**).

197 Farrugia L.J.; *J. Appl. Crystallogr.* 32; 837-838 (**1999**).

programs as implemented within the WINGX software. Thermal ellipsoid plots were generated using the program ORTEP-333 integrated within the WinGX suite of programs.

2.2 CHEMISTRY

General procedure for the synthesis of the ligands[198]: the aldehyde is dissolved into absolute ethanol, together with few drops of glacial acetic acid and it is heated up to reflux; an equimolar amount of the proper thiosemicarbazide is added and it is left reacting for 3 hours. The precipitate is collected by filtration, washed with diethyl ether and dried by vacuum.

***2-hydroxy-3-methoxybenzaldehyde thiosemicarbazone,* AG41**: white powder (yield= 80%). ^{1}H-NMR (DMSO-d_6, 25°C, 400 MHz) ppm: 11.39 (s, 1H, NH), 9.17 (s, br, OH), 8.40 (s, 1H CH), 8.10 (s, 1H, NH_2), 7.88 (s, 1H, NH_2), 7.54 (d, 1H, CH_{arom}), 6.97 (d, 1H, CH_{arom}), 6.77 (t, 1H, CH_{arom}), 3.81 (s, 3H, OCH_3). MS-EI (70 eV, positive ions): m/z = 224.7 $[M]^+$. IR (ATR, cm^{-1}): ν_{OH+NH2}= 3457, 3339; ν_{NH} = 3157; $\nu_{C=N}$= 1585; $\nu_{C=S}$= 1055, 802.

***2-hydroxy-3-methoxybenzaldehyde 4-phenyl-thiosemicarbazone*, AG48**: white powder (yield = 83%). ^{1}H-NMR (DMSO-d_6, 25°C, 400 MHz) ppm: 11.80 (s, 1H, NH), 10.03 (s,1H, NH), 9.26 (s, 1H, OH), 8.51 (s, 1H, CH), 7.69 (d, 1H, CH_{arom}), 7.56 (d, 2H, CH_{arom}), 7.36 (t, 2H, CH_{arom}), 7.20 (t, 1H, CH_{arom}), 6.98 (d, 1H, CH_{arom}), 6.79 (t, 1H, CH_{arom}), 3.82 (s, 3H, OCH_3). MS-EI (70 eV, positive ions) m/z = 301.0 $[M]^+$. IR (ATR, cm^{-1}): ν_{NH} = 3299; $\nu_{C=N}$ = 1594, 1580; $\nu_{C=S}$= 1066, 781.

***2-hydroxy-3-methoxybenzaldehyde 4-ethyl-thiosemicarbazone,* JB89**: white powder (yield=94%). ^{1}H-NMR (DMSO-d_6, 25°C, 400 MHz) ppm: 11.39 (s, 1H, NH), 9.20 (s, br, OH), 8.45 (s, 1H, NH), 8.39 (s, 1H, CH), 7.55 (d, 1H, CH_{arom}), 6.96 (d, 1H, CH_{arom}), 6.79 (t, 1H, CH_{arom}), 3.81 (s, 3H, OCH_3), 3.57 (m, 2H, CH_2), 1.14 (t, 3H, CH_3). MS-EI (70 eV, positive ions) m/z = 253.1 $[M]^+$. IR (ATR, cm^{-1}): ν_{NH} = 3305; $\nu_{C=N}$ = 1522; $\nu_{C=S}$= 1063, 784.

198 Rogolino D., Bacchi A., De Luca L., Rispoli G., Sechi M., Stevaert A., Naesens L., Carcelli M.; *J. Biol. Inorg. Chem.* 20; 1109-1121 (**2015**).

2,3-dihydroxybenzaldehyde thiosemicarbazone, **AG38:** white powder (yield= 85%). ^{1}H-NMR (DMSO-d6, 25°C, 400 MHz) ppm: 6.63 (t, 1H, CH_{arom}), 6.77 (d, 1H, CH_{arom}), 7.34 (d,1H, CH_{arom}), 7.86 (s, 1H, NH_2), 8.09 (s, 1H, NH_2), 8.36 (s, 1H, CH), 8.91 (s, 1H, OH), 9.50 (s, 1H, OH), 11.37 (s, 1H, NH). MS-EI (70 eV, positive ions): m/z = 211.0 $[M]^+$. IR (ATR, cm^{-1}): $\nu_{OH+\nu NH}$= 3286, 3173; ν_{NH} = 2994; $\nu_{C=N}$= 1608; $\nu_{C=S}$= 1234, 822.

2,3-dihydroxybenzaldehyde **4-phenyl-thiosemicarbazone, AG45**: white powder (yield = 83%). ^{1}H-NMR (DMSO-d_6, 25°C, 400 MHz) ppm: 11.76 (s, 1H, NH), 10.01 (s, 1H, NH), 9.53 (s, 1H, OH), 9.00 (s, 1H, OH), 8.49 (s, 1H, CH), 7.58 (d, 1H, CH_{arom}), 7.49 (m, 2H, CH_{arom}), 7.36 (t, 2H, CH_{arom}), 7.19 (t, 1H, CH_{arom}), 6.82 (d, 1H, CH_{arom}), 6.66 (t, 1H, CH_{arom}). MS-EI (70 eV, positive ions) m/z = 287.3 $[M]^+$. IR (ATR, cm^{-1}): $\nu_{OH}+\nu_{NH2}$= 3442, 3392; ν_{NH} = 3131, 2974; $\nu_{C=N}$ = 1541; $\nu_{C=S}$= 1201, 727.

2,3-dihydroxybenzaldehyde 4-ethyl-thiosemicarbazone, **JB10**: white powder (yield= 77%).^{1}H-NMR (DMSO-d_6, 25°C, 400 MHz) ppm: 11.31 (s, 1H, NH), 9.45 (s, br, OH), 8.90 (s, br, OH), 8.37 (s, 2H, CH+NH), 7.35 (d, 1H, CH_{arom}), 6.80 (d, 1H, CH_{arom}), 6.66 (t, 1H, CH_{arom}), 3.58 (m, 2H, CH_2), 1.14 (s, 3H, CH_3). MS-EI (70 eV, positive ions) m/z = 239.1 $[M]^+$. IR (ATR, cm^{-1}): $\nu_{OH}+\nu_{NH2}$= 3445; ν_{NH} = 3127, 2974; $\nu_{C=N}$ = 1522; $\nu_{C=S}$= 1050, 774.

General procedure for the synthesis of copper complexes: 0.150 g of the ligand is dissolved into degassed methanol under nitrogen atmosphere and 1M NaOH is added until pH is around 8. An equimolar amount of $CuCl_2{\cdot}2H_2O$ in methanol solution is added dropwise and immediately a green precipitate is formed; it is left reacting for 3 hours, then the green solid is isolated by filtration under nitrogen atmosphere and it is dried by vacuum.

[CuLCl]·3H$_2$O (HL = AG41), **FM4**: dark green powder (yield= 52%). MS-ESI (positive ions): m/z = 287 ($[CuL]^+$; 345 $[CuLCl+Na]^+$. IR (ATR, cm^{-1}): ν_{NH}= 3280, 3168; $\nu_{C=N+(N-H)}$= 1634, 1604; ν_{CS}= 1217. Anal. Calcd. for $C_9H_{10}N_3O_2SCuCl \cdot 3H_2O$: C 28.65; H 4.27; N 11.14. Found: C 28.82; H 4.09; N 10.96. Crystals

of [CuLCl]·H_2O (HL = **AG41**) suitable for X-ray diffraction analysis were obtained by slow evaporation of a methanol solution.

***[CuLCl]·1/2H₂O (HL = AG48)*, FM6**: dark green powder (yield= 77%). MS-ESI (positive ions): m/z= 363 $[CuL]^+$; 662 $[CuL_2]^+$. IR (ATR, cm^{-1}): ν_{NH}= 3182, 3019; $\nu_{C=N+(N-H)}$= 1605, 1576; ν_{CS}= 1217. Anal. Calcd. for $C_{15}H_{14}N_3O_2SCuCl$ 1/2H_2O: C 44.12; H 3.70; N 10.29. Found: C 44.42; H 3.80; N 10.09.

***[CuLCl]·1.5H₂O (HL = JB89)*, FM7**: dark green powder (yield= 71%). MS-ESI (positive ions): m/z= 315 $[CuL]^+$; 373 $[CuLCl+Na]^+$. IR (ATR, cm^{-1}): ν_{NH} = 3347, 3299; $\nu_{C=N+(N-H)}$= 1605, 1586; ν_{CS}= 1219. Anal. Calcd. for $C_{11}H_{14}N_3O_2SCuCl$ ·1.5 H_2O: C 34.92, H 4.53, N 11.11. Found: C 34.84, H 3.98, N 10.87.

***[CuLCl]·1.5H₂O (HL = AG38)*, AG77**: dark green powder (yield= 67%). MS-ESI (positive ions): m/z= 273 $[CuL]^+$; 295 $[CuHLCl+Na]^+$; 331 $[CuLCl+Na]^+$. IR (ATR, cm^{-1}): ν_{NH} = 3347, 3287; $\nu_{C=N+(N-H)}$= 1640; ν_{CS}= 1230. Anal. Calcd. for $C_8H_8N_3O_2SCuCl$ ·1.5 H_2O: C 28.58; H 3.30; N 12.50. Found: C 28.82; H 3.06; N 12.57.

***[CuLCl]·1.5H₂O (HL = AG45)*, FM11**: dark green powder (yield= 66%). MS-ESI (positive ions): m/z= 349 $[CuL]^+$. IR (ATR, cm^{-1}): ν_{NH} = 3360, 3207; $\nu_{C=N+\ (N-H)}$= 1610; ν_{CS}= 1207. Anal. Calcd. for $C_{14}H_{12}N_3O_2SCuCl$ ·1.5 H_2O: C 40.78; H 3.67; N 10.19. Found: C 40.85; H 3.53; N 9.97.

***[CuLCl]·H₂O (HL = JB10)*, FM12**: dark green powder (yield= 55%). MS-ESI (positive ions): m/z= 301 $[CuL]^+$. IR (ATR, cm^{-1}): ν_{NH} = 3351, 3271; $\nu_{C=N+(N-H)}$= 1621; ν_{CS}= 1223. Anal. Calcd. for $C_{10}H_{12}N_3O_2SCuCl$ ·H_2O: C 33.80; H 3.97; N 11.83. Found: C 33.93; H 3.92; N 11.70.

General procedure for sulphonated ligand: 6 eq. of conc.H_2SO_4 is added dropwise to 1 eq. of the proper ligand with vigorous stirring at 0°C; the red solution is left reacting for 3 hours. A NaOH solution is slowly added to the mixture until pH=6. The solvent is removed by rotavapor and the solid residue is extracted with cold methanol; the mixture is filtered, and all solvent is removed by vacuum to give a yellow solid.

2-hydroxy-3-methoxy-5-sodium sulfonatebenzaldehyde thiosemicarbazone, **JB82**: yellow powder (yield=35%). ^{1}H-NMR (H_2O-d_2, 25°C, 400 MHz) ppm: 8.38 (s, 1H, CH), 7.75 (s, 1H, CH_{arom}), 7.07 (s, 1H, CH_{arom}), 3.74 (s, 3H, OCH_3). ^{13}C-NMR (MeOH-d, 25°C, 400MHz) ppm: 177.21, 160.30, 151.93, 151.35, 143.51, 128.67, 116.39, 108.72, 54.67. ESI-MS (neg ions): m/z = 304 [HL-Na^+]. IR (ATR, cm^{-1}): ν_{OH}= 3458; ν_{NH2}= 3422, 3268; ν_{NH}= 3157; $\nu_{C=N}$= 1599; ν_{CS}= 1047, 623. Anal. Calcd. for $C_9H_{10}N_3O_5S2Na \cdot 1.5\ H_2O$: C 30.09; H 3.38; N 11.38; S 17.49. Found: C 30.56; H 3.60; N 11.90; S 16.82.

2,-3-dihydroxy-5-sodium sulfonatebenzaldehyde 4-ethyl-thiosemicarbazone, **JB88**: orange powder (yield= 30%). ^{1}H-NMR (DMSO-d_6, 25°C, 400 MHz) ppm: 11.30 (s, 1H, OH), 9.58 (s, br, OH), 9.15 (s, 1H, NH), 8.38 (s, 1H, CH), 8.27 (s, 1H, NH), 7.45 (s, 1H, CH_{arom}), 7.14 (s, 1H, CH_{arom}), 3.59 (m, 2H, CH_2), 1.14 (t, 3H, CH_3). ^{13}C-NMR (DMSO-d_6, 25°C, 400 MHz) ppm: 176.99, 145.84, 144.93, 141.52, 140.03, 119.72, 115.14, 114.83, 29.39, 15.06. ESI-MS (neg ions): m/z= 318 $[HL]^-$. IR (ATR, cm^{-1}): ν_{OH}= 3586; ν_{NH}=3506, 3450; ν_{NH}= 3318; $\nu_{C=N}$= 1539; $\nu_{C=S}$= 1046, 711. Anal. Calcd. for $C_{10}H_{12}O_5N_3S_2Na \cdot 1.5\ H_2O$: C 32.61; H 4.10; N 11.41. Found: C 32.60; H 3.38; N 10.90.

2-hydroxy-3-methoxy-5-sodium sulfonatebenzaldehyde 4-ethyl-thiosemicarbazone, **JB93**: yellow powder (yield=25%). ^{1}H-NMR (DMSO-d_6, 25°C, 400 MHz) ppm: 15.53 (s, br, OH), 10.93 (s, 1H, NH), 8.50 (s, 1H, CH), 7.76 (s, 1H, NH), 7.44 (s, 1H, CH_{arom}), 6.76 (s, 1H, CH_{arom}), 3.63 (s, 3H, OCH_3), 3.52 (m, 2H, CH_2), 1.09 (t, 3H, CH_3). ^{13}C-NMR (DMSO-d_6, 25°C, 400 MHz) ppm: 160.21, 151.36, 144.43, 129.67, 123.52, 119.92, 109.91, 109.40, 55.62, 49.07, 38.10, 15.31. ESI-MS (neg ions): m/z= 332 $[HL]^-$. IR (ATR, cm^{-1}): ν_{OH}= 3342; ν_{NH}=3288; ν_{NH}= 2952; $\nu_{C=N}$= 1562; $\nu_{C=S}$= 1044, 600. Anal. Calcd. for $C_{11}H_{14}N_3O_5S_2Na \cdot 2H_2O$: C 33.01; H 3.88; N 10.23; S 17.36. Found: C 32.64; H 3.72; N 10.01; S 16.93.

General procedure for the sulfonated copper complexes: 1 eq. of the proper ligand is dissolved into degassed methanol under nitrogen atmosphere, together with few drops of 1M NaOH as catalyst; an equimolar amount of $CuCl_2 \cdot 2H_2O$ in methanolic solution is added dropwise the mixture is left

reacting at rt for 3 hours. Solution is concentrated by vacuum and it is cooled to promote precipitation; the solid is isolated by filtration under nitrogen atmosphere.

***[CuLCl]$_2$·2.5H$_2$O (HL = JB82)*, JB91**: dark green powder (yield= 58%). ESI-MS (neg ions): m/z= 365 [(HL-Na)+Cl]. IR (ATR, cm^{-1}): ν_{OH}= 3421; ν_{NH2}=3324; ν_{NH}= 2944; $\nu_{C=N}$= 1617; $\nu_{C=S}$= 1036, 603. Anal. Calcd. for $C_{18}H_{20}O_{10}N_6S_4Cu_2Cl_2 \cdot 2.5\ H_2O$: C 25.38; H 2.96; N 9.87. Found: C 25.09; H 2.53; N 9.12. ICP%$_{Cu}$ =15.0%. Crystals suitable for X-ray diffraction analysis were obtained by slow evaporation of a methanolic solution of JB91.

***[CuLCl]$_2$·CH$_3$OH (HL = JB88)*, JB94**: dark green powder (yield=35%). ESI-MS (neg ions): m/z= 353 [(HL-Na)+Cl]. IR (ATR, cm^{-1}): ν_{OH}= 3337, 3218; ν_{NH}=3052; ν_{NH}= 2944; $\nu_{C=N}$= 1614; $\nu_{C=S}$= 1031, 610. Anal. Calcd. for $C_{20}H_{24}O_{10}N_6S_4Cu_2Cl_2 \cdot CH_3OH$: C 29.10; H 3.26; N 9.70. Found: C 29.41; H 3.31; N 9.88. ICP%$_{Cu}$ =18.4%. Crystals suitable for X-ray diffraction analysis were obtained by slow evaporation of a solution of JB94 in methanol.

2.3 STUDIES IN SOLUTION

HEPES 25 mM buffer methanol:water 9:1 (*v/v*) solution at pH 7.4 was prepared as follows: solid HEPES (0.59 g) was suspended in 100 mL of a methanol:water 9:1 (*v/v*) mixture. Few drops of concentrated (10 N) aqueous NaOH solution was added until pH 7.4 was reached, where complete dissolution of the solid was observed. The pH was measured using a Thermo Orion 720A pH-meter connected with a Hamilton glass electrode. A 0.1 M KCl solution in methanol:water 9:1 (*v/v*) was used to fill the reference compartment of the electrode. Calibration of the glass electrode using buffers in methanol:water 9:1 (v/v) solutions was performed immediately before its use. Stock solutions of the ligands **HL^1** and **HL^4** (C_L = *ca*. 1.1 mM) have been prepared by weight in DMF and used within few days. Stock solutions of $CuCl_2$ and $ZnCl_2$ in water (C_{Cu} *ca.* 0.016 M, C_{Zn} *ca.* 0.018 M) were prepared by weight of the salts and their titre determined using standardized EDTA solutions. Titrant metal solutions were obtained by dilution of the stock solutions in methanol:water 9:1 (*v/v*), and prepared at *ca.* 0.55 mM concentration.

The complex formation equilibria at pH 7.4 for **AG41** and **AG38** with Cu(II) and Zn(II) were studied by direct spectrophotometric titrations of a solution of the ligands with the metal ions, as follows.

Solutions of the ligands (C^0_L = 40 μM) were prepared in the cuvette by diluting the ligands stock solutions in HEPES 25 mM buffer methanol:water 9:1 (*v/v*, pH 7.4). Total volume of samples in the cuvette was *ca*. 2.7 mL. The obtained ligand solutions were titrated with Cu(II) or Zn(II) titrant solutions up to a metal:ligand ratio of 2.4 – 2.7. For each addition of titrant the absorption spectrum was collected in the 250-500 nm range. The equilibria of the Cu(II)/Zn(II)/**AG41** system were studied by a competitive UV-Visible spectrophotometric titration, as follows. A solution of the ligand **AG41** (C^0_L = 41 μM) was prepared in the cuvette by diluting the ligand stock solution in HEPES 25 mM buffer methanol:water 9:1 (*v/v*, pH 7.4). A proper amount of the Zn(II) stock solution was added to the ligand solution to obtain a Zn(II) and **AG41** in 2:1 ratio. The obtained titrant solution was titrated with Cu(II) up to a Cu(II):ligand ratio of 1.1. In all experiments, for each addition of the titrant the absorption spectrum was collected in the 250-500 nm range. All titrations were performed in triplicate.

Job's plot experiments were carried out by preparing 11 solutions with constant $C_{Cu/Zn} + C_L$ (*ca*. 40 μM, L = **AG41** or **AG38**), and variable $\chi = C_L/(C_L+C_{Cu/Zn})$ molar fractions in the 0 – 1 range. All samples were prepared in HEPES 25 mM buffer methanol:water 9:1 (*v/v*) solution at pH 7.4.

The logarithms of the conditional stability constants were calculated from the spectral dataset using the HypSpec2014 software. For each system, data from different titrations were treated together. In the treatment of the competitive titration of the Zn(II):**AG41** system with Cu(II), the formation constants and the molar absorption spectra of the [Zn(**AG38**)] and [Zn(**AG38**)$_2$] complexes (charges omitted, see below) were used as fixed parameters. In all other titrations the molar spectrum of the ligand has been used as the only fixed parameter. Speciation diagrams were calculated using the Hyss 2009 software.

2.4 *IN VITRO* BIOLOGICAL ASSAYS

2.4.1 Experiments with Human Cells

Complexes and organic ligands were solubilized in stock DMSO solutions (10 mg/mL) and added to the culture medium to a final solvent concentration of 0.5%, which had no effects on cell viability. Cisplatin and oxaliplatin were solubilized in 0.9% NaCl solutions. MTT (3-(4,5-dimethylthiazol-2-yl)-2,5-diphenyltetrazolium bromide), fluorogenic peptide proteasomal substrates (N-Suc-Leu-Leu-Val-Tyr-AMC, Boc-Gln-Ala-Arg-AMC, and Z-Leu-Leu-Glu-AMC; AMC = 7-amido-4-methylcoumarin), cisplatin and oxaliplatin were obtained from Sigma Chemical Co, St. Louis, USA.

2.4.2 Cell Cultures

Human colon (HCT-15 and LoVo) carcinoma cell lines along with human melanoma cells (A375) and nontransformed embryonic kidney (HEK293) were obtained from American Type Culture Collection (ATCC, Rockville, MD, USA). Human pancreatic (BxPC3 and PSN1) carcinoma cells were obtained from European Collection of Cell Culture (ECACC, Salisbury, UK). The human thyroid carcinoma cell line (BCPAP) was provided by the Leibniz-Institut DSMZ—Deutsche Sammlung von Mikroorganismen und Zellkulturen GmbH (Braunschweig, Germany). Human ovarian 2008 cancer cells were kindly provided by Prof. G. Marverti (Dept. of Biomedical Science of Modena University, Modena, Italy). The LoVo-OXP cells were obtained as previously described[199]. Cell lines were maintained in culture in the logarithmic phase at 37 °C in a 5% carbon dioxide atmosphere using the following media added of 10% fetal calf serum (Euroclone, Milan, Italy), antibiotics (50 units/mL penicillin and 50 µg/mL streptomycin), and 2 mM L-glutamine: (i) RPMI-1640 medium (Euroclone) for HCT-15, PSN1, BCPAP, BxPC3 and 2008 cells; (ii) F-12 HAM'S (Sigma Chemical Co.) for A549, LoVo and LoVo-OXP cells; iii) DMEM (Sigma Chemical Co.) for A375 and HEK293 cells.

2.4.3 Spheroid Cultures

Spheroid cultures were obtained by seeding 2.5×10^3 HCT-15 or PSN1 cells/well in round bottom non-tissue culture treated 96 well-plate (Greiner Bio-one, Kremsmünster, Austria) in phenol red free RPMI-1640 medium (Sigma Chemical Co.), containing 10% FCS and supplemented with 20% methyl cellulose stock solution.

2.4.4 MTT Assay

The growth inhibitory effect towards 2D tumor cell lines was evaluated by means of the MTT assay as previously described[200]. IC_{50} values were calculated by four parameters logistic (4-PL) model.

2.4.5 Acid Phosphatase (APH) Assay

An APH modified assay was used for determining cell viability in 3D spheroids, as previously described[201]. IC_{50} values were calculated with four parameters logistic (4-PL) model.

---

199 Gandin V., Pellei M., Tisato F., Porchia M., Santini C., Marzano, C.; *J. Cell. Mol. Med.* 16; 142-151 (**2012**).

200 Alley M.C., Scudiero D.A., Monks A., Hursey M.L., Czerwinski M.J., Fine D.L., Abbott B.J., Mayo J.G., Shoemaker R.H., Boyd M.R.; *Cancer. Res.* 48; 589-601 (**1988**).

201 Gandin V., Ceresa C., Esposito G., Indraccolo S., Porchia M., Tisato F., Santini C., Pellei M., Marzano C.; *Sci. Rep.* 7; 13936 (**2017**).

2.4.6 Cellular accumulation and distribution

LoVo cells (2.5×10^6) were seeded in 75 cm^2 flasks in growth medium (20 mL). After overnight incubation, the medium was replaced and the cells were treated with the tested compounds for 24 or 36 h. Cell monolayers were washed with cold PBS, harvested and counted. Cell nuclei were isolated by means of nuclei isolation kit Nuclei EZ Prep (Sigma Co.) and also cellular mitochondrial fractions were isolated by Mitochondria Isolation Kit (Sigma Co.). The samples were treated with highly pure nitric acid (Cu: ≤0.005 $\mu g \cdot kg^{-1}$, TraceSELECT® Ultra, Sigma Chemical Co.) and transferred into a microwave teflon vessel. Afterwards, samples were mineralized by using a speed wave MWS-3 Berghof instrument (Eningen, Germany). After cooling, each mineralized sample was analyzed for copper content by means of a Varian AA Duo graphite furnace atomic absorption spectrometer (Varian, Palo Alto, CA; USA), at 324 nm. The calibration curve was obtained using known concentrations of standard solutions purchased from Sigma Chemical Co.

2.4.7 Comet Assay

Single-cell gel electrophoresis for detection of DNA damage was performed using the Comet assay reagent kit (Trevigen Inc., Gaithersburg, MD, US) according to the manufacturer's instructions. Briefly, LoVo (10^5) cells were seeded in 25 cm^2 flasks in growth medium (6 mL). After 24 h, cells were incubated for 6 h with IC_{50} concentrations of tested compounds. Subsequently, cells were washed twice with cold PBS, harvested, centrifuged, and resuspended at 1×10^5 cell/mL in 1% low melting point agarose (LMPA, Trevigen). Then 50 µL of cells−LMPA mixture was layered onto frozen microscope slides, which were pre-coated with 1% normal agarose. After the agar had been allowed to set at 4 °C, the slides were immersed in lysis buffer (100 mM Na_2EDTA, 2.5 M NaCl, 10 mM Tris pH 10.0, and 1% Triton X-100) for 1 h at 4 °C. The slides were then incubated in an alkaline electrophoresis solution (1 mM EDTA, 300 mM NaOH, pH > 13) at 4 °C for 40 min, followed by electrophoresis (1 V/cm) at 4 °C for 30 min. The slides were washed with a neutralization buffer three times before immersion in absolute ethanol for 20 min and air-dried at room temperature. The DNA was stained with SYBR Green (1 µg/mL) for 5 min at 4 °C. A total of 25 comets per slide, randomly captured, were examined at 40x magnification in a fluorescence microscope (Olympus BX41, Milano, Italy; excitation, 495 nm; emission, 521 nm) connected through a black and white camera to a computer-based image analysis system. DNA damage was measured as tail length (distance of DNA migration from the middle of the body of the nuclear core) using Cell-F software (Olympus).

2.4.8 Proteasome activity

In vitro inhibition of purified 26S proteasome. The purified rabbit 26S proteasome (Sigma Aldrich) was incubated for 60 min at 37 °C in an assay buffer (50 mM Tris-HCl, pH 7.5, 250 mM sucrose, 5 mM $MgCl_2$, 1 mM DTT, and 0.5 mM EDTA), in the presence of increasing concentrations of the tested complexes or Lactacystin. Afterwards, fluorogenic peptides were added and substrate hydrolysis was measured after 30 min by monitoring spectrofluorometrically the release of AMC (excitation at 370 nm, emission at 460 nm).

Inhibition of 26S proteasome in intact cancer cells. Human colon adenocarcinoma LoVo (10^6) cells were treated for 24 h with IC_{50} concentrations of tested compounds. Afterward, cells were harvested and homogenized in a lysis buffer (50 mM Tris-HCl, pH 7.5, 250 mM sucrose, 5 mM $MgCl_2$, 1 mM DTT, and 0.5 mM EDTA), and the protein concentration in the cytosolic extract was determined by the BioRad protein assay (BioRad). Protein aliquots (100 µg) were stained at 37 °C for 30 min with a fluorescent proteasome substrate specific for CT-like activity and the hydrolysis was measured as described above.

2.4.9 Quantification of thiols

LoVo cells (2×10^5) were seeded in a six-well plate in growth medium (4 mL). After 24 h, cells were incubated for 24 h with increasing concentrations of tested compounds. Subsequently, the thiol content was measured as previously described[202].

2.4.10 Total and oxidized intracellular glutathione

LoVo cells (3.5×10^5) were seeded in 6-well microplates in growth medium (4 mL). Following 24 h of exposure with the tested complexes, cells were washed twice with PBS, treated with 6% metaphosphoric acid and scraped. Samples were centrifuged and the supernatants were neutralized with Na_3PO_4 and assayed for total and oxidized glutathione following the procedure reported by Bindoli et al.[203] Aliquots of pellets were dissolved in RIPA buffer and the protein content was determined.

---

[202] Rigobello M.P., Gandin V., Folda A., Rundloef A.K., Fernandes A.P., Bindoli A., Marzano C.; *Free Radic. Biol. Med.* 47; 710-721 (**2009**).

[203] Bindoli A., Callegaro M.T., Barzon E., Benetti M., Rigobello M.P.; *Arch. Biochem. Biophys.* 342; 22-28 (**1997**).

2.4.11 Protein disulfide isomerase (PDI) activity

The reductase activity of PDI was assayed by measuring the PDI-catalysed reduction of insulin in the presence of increasing concentrations of the tested compounds by using PROTEOSTAT PDI assay kit (Enzo Life Sciences, Lausen, Switzerland). Experiments were performed according to the manufacturer's instructions. Briefly, copper complexes or Bacitracin (at increasing concentrations) were added to an insulin PDI solution. Subsequently, DTT was added to start PDI reduction activity and after 30 min of incubation, the reaction was stopped by adding the stop reagent mixture. The insulin precipitate was labelled with the fluorescent Proteostat PDI detection reagent and fluorescence intensity was measured at 500 nm excitation and 603 nm emission. IC_{50} values were calculated by four parameters logistic (4-PL) model.

2.4.12 Transmission electron microscopy (TEM) analyses

About 10^6 LoVo cells were seeded in 24-well plates and, after 24 h incubation, were treated with the tested compounds and incubated for additional 24 h. Cells were then washed with cold PBS, harvested and directly fixed with 1.5% glutaraldehyde buffer with 0.2 M sodium cacodylate, pH 7.4. After washing with buffer and postfixation with 1% OsO_4 in 0.2 M cacodylate buffer, specimens were dehydrated and embedded in epoxy resin (Epon Araldite). Sagittal serial sections (1 µm) were counterstained with toluidine blue; thin sections (90 nm) were given contrast by staining with uranyl acetate and lead citrate. Micrographs were taken with a Hitachi H-600 electron microscope (Hitachi, Tokyo, Japan) operating at 75 kV. All photos were typeset in Corel Draw 11.

2.4.13 Nuclear DNA Fragmentation

LoVo cells (10^4/well) were treated in a 96-well plate at 37 °C for 24 h with IC_{50} doses of tested compounds. Afterward, the plate was centrifuged for 10 min, the supernatant removed, and the pellet treated according to the manufacturer's instructions of an ELISAplus cell death detection kit (Roche). The extent of nuclear fragmentation was measured in a plate reader following absorbance at 405 minus 492 nm.

2.5 Experiments with animals

In vivo anticancer activity toward Lewis Lung Carcinoma (LLC)

The mice were purchased from Charles River, Italy, housed in steel cages under controlled environmental conditions (constant temperature, humidity, and 12 h dark/light cycle), and

alimented with commercial standard feed and tap water ad libitum. The LLC cell line was purchased from ECACC, United Kingdom. The LLC cell line was maintained in DMEM (Euroclone, Pero, Italy) supplemented with 10% heat-inactivated foetal bovine serum (Euroclone, Pero, Italy), 10 mM L-glutamine, 100 U/mL penicillin, and 100 µg/mL streptomycin in a 5% CO_2 air incubator at 37 °C. The LLC was implanted intramuscularly (i.m.) as a 2×10^6 cell inoculum into the right hind leg of 8-week old male and female C57BL mice (24 ± 3 g body weight). After 7 days from tumor implantation (tumor visible), mice were randomly divided into 4 groups (8 animals per group) and treated with a daily i.p. injection of **1** (3 and 6 mg kg^{-1} in 20% Cremophor EL (v/v), 30% PEG400 (v/v) and 50% saline solution (v/v)), cisplatin (1.5 mg kg^{-1} in 0.9% NaCl solution), or the vehicle solution 20% Cremophor EL (v/v), 30% PEG400 (v/v) and 50% saline solution (v/v). At day 15, animals were sacrificed, the legs were amputated at the proximal end of the femur, and the inhibition of tumor growth was determined according to the difference in weight of the tumor-bearing leg and the healthy leg of the animals expressed as a percentage referring to the control animals. Body weight measured every 2 days, starting from day 7, was taken as a parameter for systemic toxicity. All of the values are the means ± SD of not less than three measurements. Multiple comparisons were made by the Tukey−Kramer test (**, $p < 0.01$; * $p < 0.05$).

3.RESULTS and DISCUSSION

3.1 Cu(II)-THIOSEMICARBAZONE COMPLEXES

3.1.1 Synthesis and crystal structure analysis

As already stated in the introduction section, thiosemicarbazone derivatives have emerged for their chemical versatility and biological activity, comprising the antitumor one[104]. Such compounds and, especially, their metal complexes, have different ways of action when compared to *cis*platin, since they may have several cellular targets. Among others, results obtained with salicylic derivatives are very promising, and they can offer interesting opportunities in term of coordinating properties. [204,205,206] Looking at the literature background, we have decided ,therefore, to focus on the salicylic-thiosemicarbazone scaffold and to introduce a second substituent on the aromatic ring, an hydroxylic or a methoxy moiety, in order to modulate the activity of the free ligands and, accordingly, of the related metal complexes. In particular, we explored the use of 2,3-dihydroxy/2-hydroxy-3-methoxy-benzaldehyde; moreover, the use of several substituents at the N4 position has been studied to evaluate a possible structure-activity relationship. A first panel of molecules has been designed and their molecular structures are schematically depicted in Figure 15.

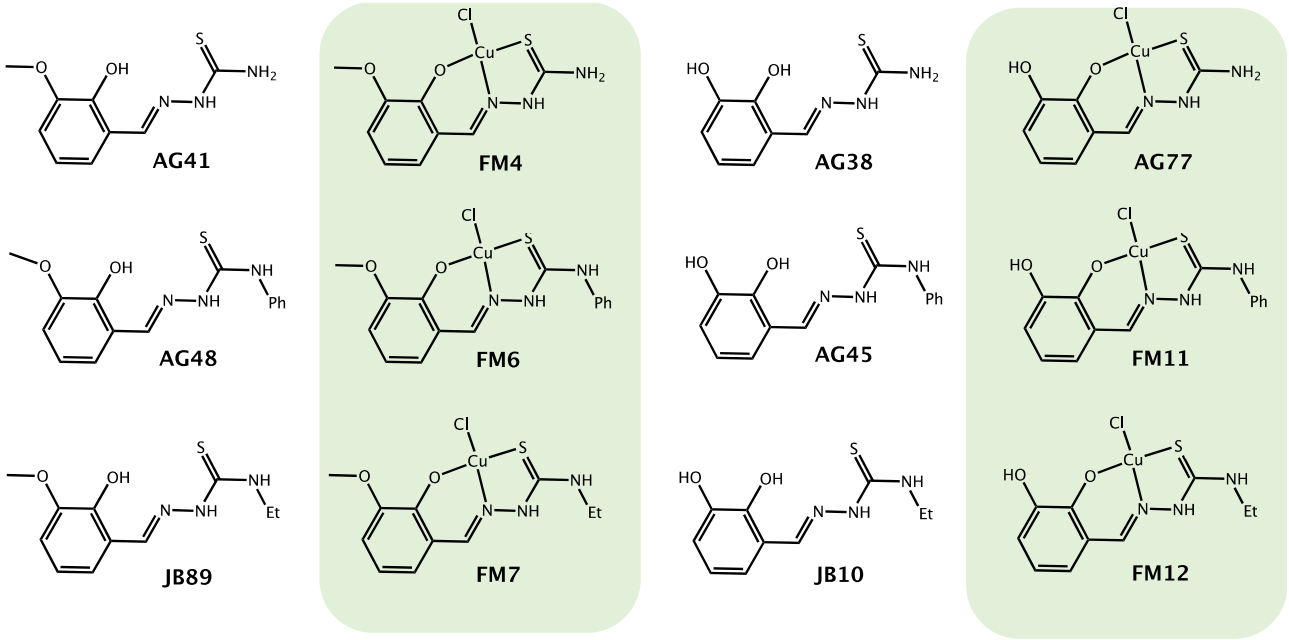

Figure 15. Structure of the thiosemicarbazones derivatives studied, and their copper complexes (green).

204 Dilovic´ I., Rubc˘ic´ M., Vrdoljak V., Pavelic´ S. K., Kralj M., Piantanidab I., Cindric´ M.; *Bioorg. Med. Chem. 16*; 5189-5198 (**2008**).

205 Qi J., Gou Y., Zhang Y., Yang K., Chen S., Liu L., Wu X., Wang T., Zhang W., Yang F.; *J. Med. Chem.* 59; 7497-7511 (**2016**).

206 Gatti A., Habtemariam A., Romero-Canelón I., Song J.-I., Heer B., Clarkson G. J., Rogolino D., Sadler P. J., Carcelli M.; *Organomet.* 37; 891-899 (**2018**).

The synthesis of the ligands is achieved by reacting the aldehyde (1 eq.) with the proper N4 functionalized thiosemicarbazide (1 eq.) in ethanol, together with few drops of acetic acid as catalyst[207]. All ligands have been characterized by usual spectroscopic techniques (ATR-IR, ESI-MS, $^{1}H/^{13}C$-NMR). Below it is reported the proton NMR (DMSO-d_6, 25°C, 400 MHz) spectrum of derivative **JB10** as an example (Figure 16): the signal relative to the proton of the aldehyde (≅ 11 ppm) disappeared, while a new one appears at 8.37 ppm, which is attributed to the iminic proton: this means that the condensation reaction occurred, as confirmed by the ATR-IR analysis, with the presence of the stretching band of C=N at 1528 cm^{-1}. The NMR analysis in DMSO also confirms that ligands are present only as *E*-form in solution[4]. Thiosemicarbazones are species that are used to give a thione-thiol equilibrium in solution: in this case only the thione form is present, as can be inferred also by IR analysis: the stretching band of NH at 3121 cm^{-1} and the absence of the S-H stretching band at 2600 cm^{-1} confirm what we have stated with the NMR analysis; moreover, a strong stretching band at ≅1050 cm^{-1} and a bending one at ≅721 cm^{-1}, which are attributable to the C=S bond, are present.

[207] Rogolino D., Bacchi A., De Luca L., Rispoli G., Sechi M., Stevaert A., Naesens L., Carcelli M.; *J. Biol. Inorg. Chem.* 20; 1109-1121 (**2015**).

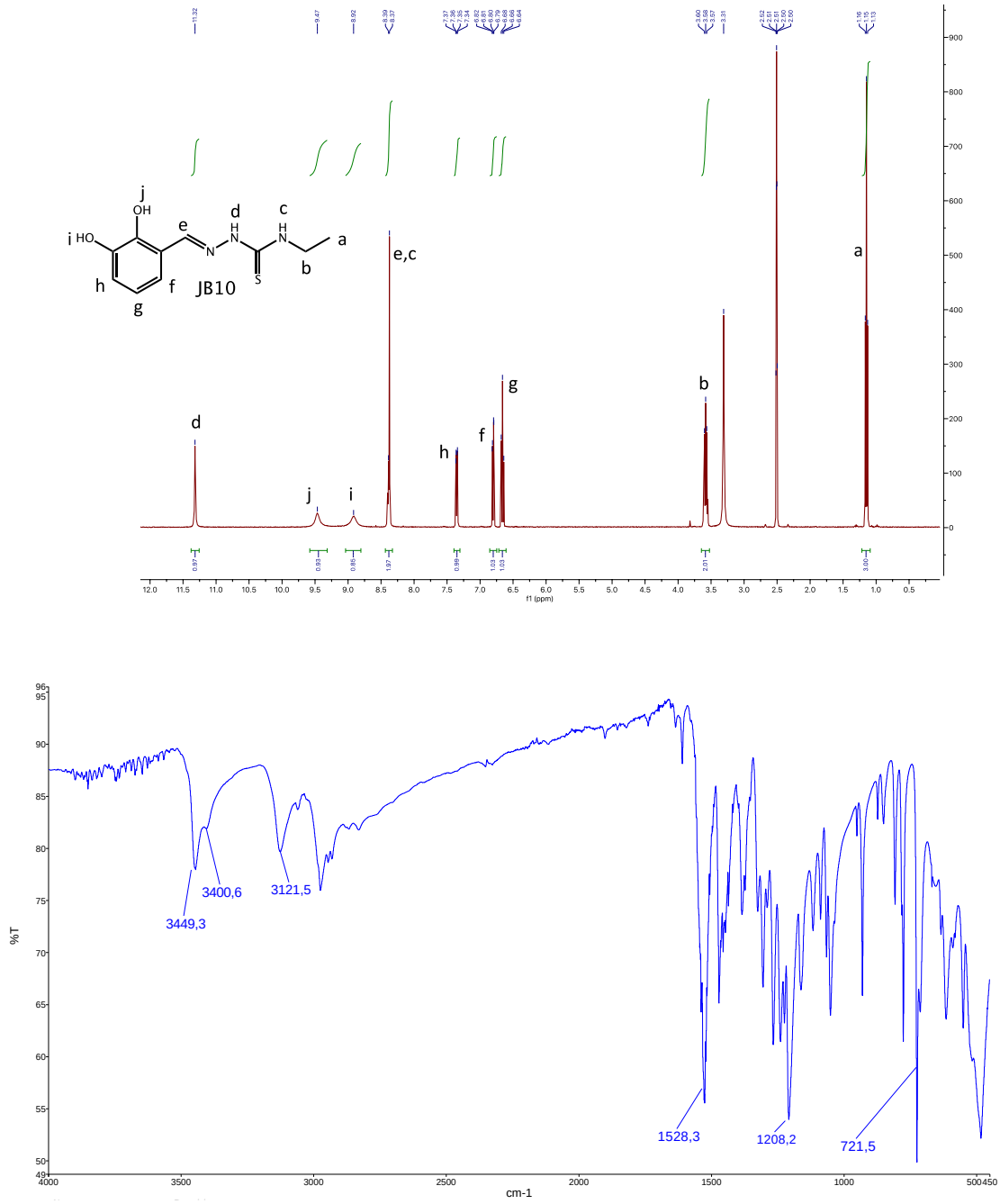

*Figure 16. [1]H-NMR (400 MHz, DMSO) spectrum, on the top, and the ATR-IR spectrum, on the bottom, of derivative **JB10**.*

Once the nature of ligands is ascertained, copper(II) complexes have been synthesized accordingly the next procedure: 1 eq. of the thiosemicarbazone is dissolved into degassed methanol under nitrogen flux and 1M NaOH is added until pH is around 8 in order to promote ligand deprotonation. The inert atmosphere is a necessary condition to avoid cyclization of the ligand and/or reduction of the metal[208]. An equimolar amount of $CuCl_2 \cdot 2H_2O$ in methanol is slowly added and immediately a

[208] Chattopadhyay S.K. , Mak T.C.W.; *Inorganic Chemistry Communications* 3; 111–113 (**2000**).

green solid is formed; it is left reacting for 3 hours, then the precipitate is isolated by filtration under nitrogen atmosphere and dried by vacuum. All copper complexes resulted to be paramagnetic; in the ATR-IR spectrum of **FM12** (Figure 17) we can see that several stretching bands result to be shifted to higher wavenumbers with respect to the parent ligand: the band relative to the iminic bond is shifted of about 62 cm^{-1} to higher values, in the same way as the C=S stretching bands, which are shifted of 174 cm^{-1}, indicating the involvement of these groups in the coordination of the metal. The absorptions of the OH group (around 3400 cm^{-1} in the free ligand) disappeared, evidently because the ligand is subjected to deprotonation upon complexation.

*Figure 17. ATR-IR spectra of **JB10**, reported in red, and **FM12**, reported in green.*

In the ESI-Mass spectra of all copper (II) complexes, recorded in methanol in positive ion mode, there are peaks relative to the species $[CuL]^+$, corresponding to the loss of a chloride ion. Overall, the elemental analysis data suggested that all complexes resulted to have the same stoichiometry, with ratio between ligand and metal ion 1:1, with the mono-deprotonated ligand behaving as *O,N,S* tridentate and a chloride ion completing the coordination sphere of the Cu(II) ion. This structure was confirmed also by single crystal X-ray diffraction analysis on **FM4**·H_2O (Figure 18). Interestingly, slow evaporation of mother liqueur of FM7 leaded to crystals of $[Na(CuLCl)_2Cl]$ with HL= **JB89**, suitable for X-ray diffraction analysis (Figure 18).

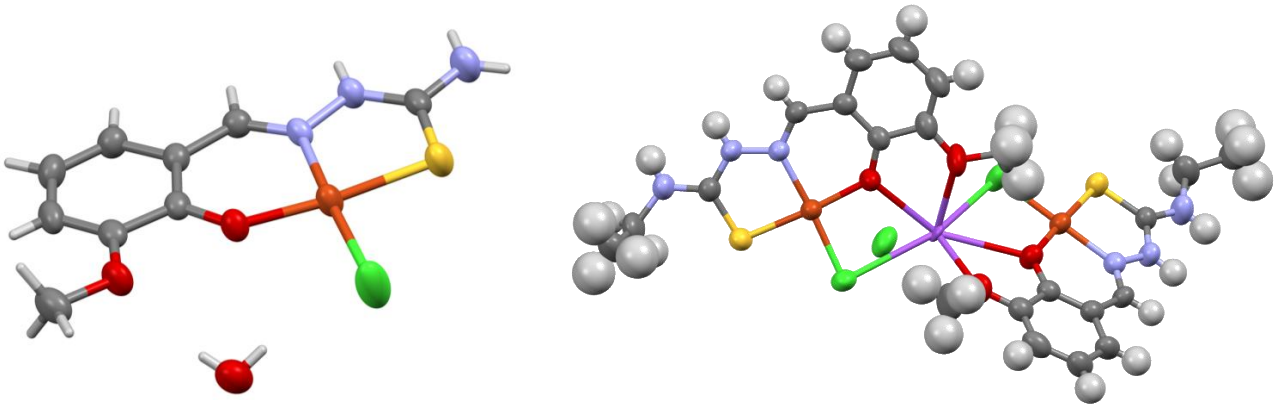

*Figure 18. ORTEP plot of the crystal structure of **FM4** (probability 50%), on the left, and of Na[CuLCl]$_2$Cl (HL=**JB89**) (probability 50%), on the right.*

In the crystal structure of **FM4**·H_2O, the copper(II) ion presents a square-planar geometry; the ligand is in its *E*-form with respect to the iminic bond: the ligand behaves as *O,N,S* tridentate through the deprotonated salicylic group, the iminic nitrogen and the sulfur one, forming a six-member and a five-member chelating ring, respectively. The N2 nitrogen of the thiosemicarbazide moiety is protonated and the C=S bond is consequently rather short (1.697 Å), in agreement with a thionic form of the ligand. The packing is mainly determined by a water molecule which forms hydrogen bonds acting as a donor through its two hydrogens towards the methoxy oxygen and the chlorine atom. Water also behaves as an acceptor of the hydrazine hydrogen belonging to a close-by molecule. Another noteworthy hydrogen bond (3.298 Å) is found between the chlorine atom and the terminal amino group of an adjacent molecule.

In the crystal structure of Na[CuLCl]$_2$Cl (HL=**JB89**), the sodium ion plays a key role, since it is responsible of the packing by coordinating oxygens and chlorine of two different [CuLCl] units, which taken singularly are structurally very similar to the one of **FM4**·H_2O (Figure 18).

The sodium ion is surrounded by four oxygens from the ligands, two chlorines coordinated by copper and another Cl^-, which plays the role of counterion to Na^+.

3.1.2 Studies in solution

Studies in solution have been carried out in order to evaluate the complex formation constants of Cu(II) ions with ligands **AG41** (**L_1**) and **AG38** (**L_2**); metal:ligand systems were investigated by means of spectrophotometric titrations of the ligand solutions with the metal ions. As described later, it was necessary to use a competitive Zn(II)/Cu(II) titration strategy, hence the stability of zinc

complexes has also been determined. The buffered conditions have made difficult to establish if the ligand is protonated or not, therefore the free ligand and the complexed form are reported as **L_1** and **L_2**, where L represents the thiosemicarbazone in its different protonated states, with omitted charges. UV-visible spectra of the free ligands have been collected: they show a strong absorption bands at *ca*. 300-325 nm, with ε_{L1}= 32000 $M^{-1}cm^{-1}$ and ε_{L2}= 19000 $M^{-1}cm^{-1}$. Generally, with the addition of metal ions, a band at *ca*. 370-400 nm appears in all titration: this is indicative of the formation of the complexed species and it could be due to intra-ligand charge transition or to the ligand-metal one.

We started with the Cu(II)/**HL_1** system: as it has been characterized in the solid state, such system forms the 1:1 metal to ligand species and the same species are expected to be observed in solution; the spectral dataset in this case shows two bands, one at *ca*. 320 nm and another at *ca*. 390 nm, and they respectively decrease and increase upon addition of the metal ion solution (Figure 19).

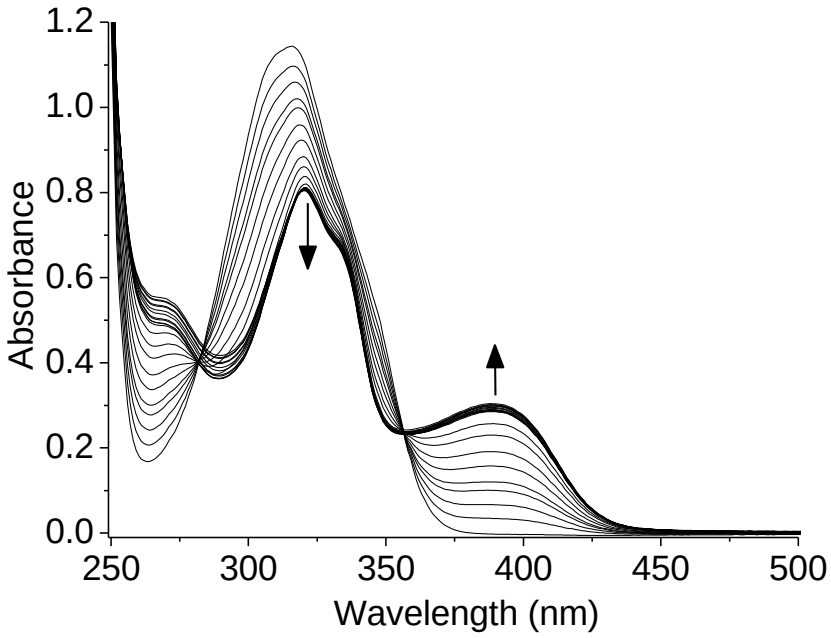

Figure 19. UV-visible spectra for the titration of HL_1 with Cu(II) in MeOH: 9:1 (v/v) at pH 7.4 (25 mM HEPES buffer. HL_1 = 41 μM, HL_1:Cu(II) = 1:0-2.1).

Evaluation of the absorbance at 388 nm and the Job's plot (Figure 20) suggests the formation of the predominant Cu(II):L_1, 1:1 specie, but the endpoint of the titration is very defined, and this makes impossible the determination of the formation constant (data not shown).

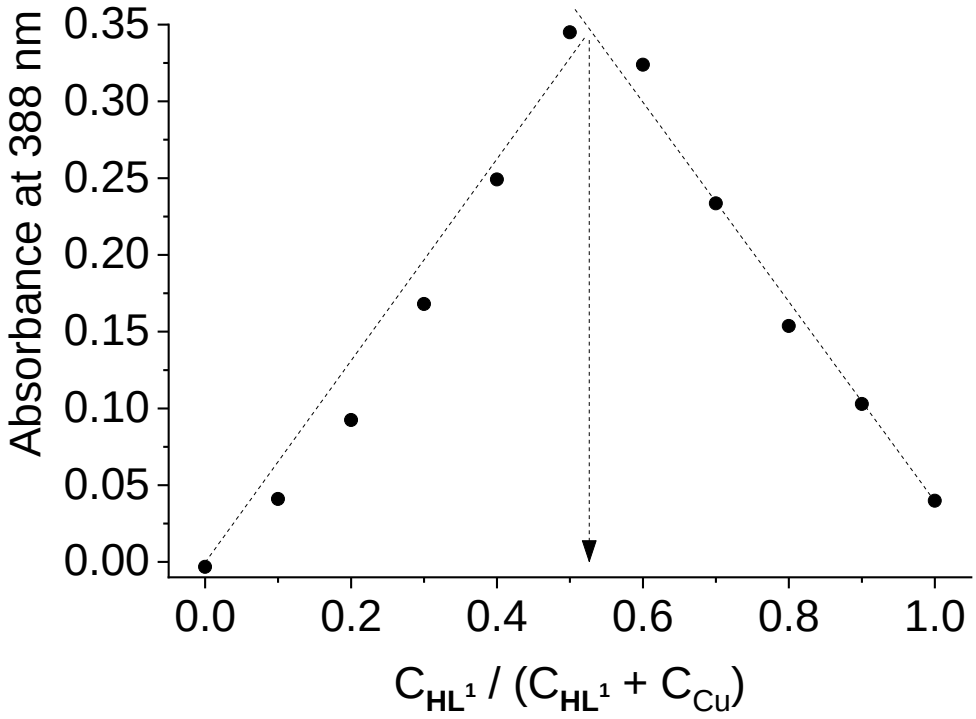

*Figure 20. Job's plot of the absorbance values at 388 nm for the Cu(II)/**HL_1** system in methanol:water 9:1 (v/v) at pH 7.4 (25 mM HEPES buffer. CL_1 = 41 µM).*

In order to determine it, Zn(II) has been used as competing ion; it has been possible to study the ZnL_1+Cu → CuL_1+Zn equilibrium and, then, to determine the formation constant of the copper complex starting from the zinc one. First of all, zinc titration of **HL_1** has been performed and it has revealed a behavior similar to the one of Cu(II); treatment of data has suggested that the ZnL_1 species is formed, and the formation constant has been determined (**Table 1**). Afterwards, a titration of the HL_1/Zn(II) system (HL_1:Zn = 1:2) with Cu(II) followed: we observed an interconversion of the principal species ZnL_1 into CuL_1 and this is supported by the decrease of a band at *ca*. 375 nm and the contemporaneous increase of the one at *ca*. 390 nm (Figure 21).

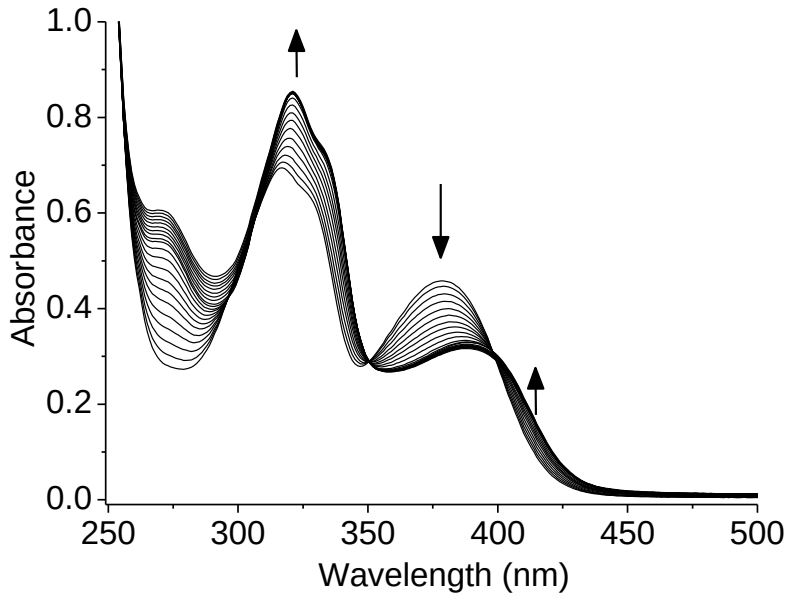

Figure 21. UV-visible spectra for the titration of a Zn(II)/HL_1 2:1 solution with Cu(II) in methanol:water 9:1 (v/v) at pH 7.4 (25 mM HEPES buffer. CL_1 = 41 μM, Zn(II):Cu(II) = 1:0-1.1).

The best fitting of the experimental data has been obtained with the equimolar ratio of **HL_1** and Cu(II) and the constant has been determined (**Table 1**).

Different results have been found with the **HL_2** titration with Cu(II): indeed, the 2,3-dihydroxybenzyl group of the ligand could work as a second coordination site for metal ions, so there's the possibility to observe the formation of Cu_2L^2 species. Actually, after the addition of a first equivalent of copper we can note the same behavior of **HL_1**: the band at *ca*. 310 nm decreases while the one at *ca*. 390 nm increases; but, after the addition of a second equivalent of the metal ion, the band at *ca*. 390 nm decreases and there's the appearance of a shoulder at 355-360 nm, together with an isosbestic point at *ca*. 374 nm. We can deduce that two predominant species are formed, CuL^2 and Cu_2L^2. The corresponding formation constants have been calculated, together with the one of ZnL^2, and they are all reported in **Table 1**.

	HL_1	**HL_2**
[Cu(L)]	7.90(3)	7.32(18)
$[Cu(L)_2]$	-	13.0(2)
[Zn(L)]	5.97(2)	6.91(11)
$[Zn(L)_2]$	-	12.0(2)

*Table 1. Logarithms of the formation constant of zinc and copper(II) complexes with ligands **AG41** (HL_1) and **AG38** (HL_2) in HEPES buffer (25 mM) in MeOH:H_2O 9:1. Standard deviation reported in parentheses.*

3.1.3 Evaluation of the *in vitro* cytotoxicity

The new thiosemicarbazone derivatives and the relative copper(II) derivatives have been tested for their cytotoxicity by means of MTT assay on different human cancer cell lines: ovarian (2008), colon (HCT-15), pancreatic (PSN-1 and BxPC3), thyroid (BCPAP) and also melanoma (A375); *cis*platin (**CDDP**) has been used as reference compound and it has been evaluated in the same conditions. IC_{50} values are obtained after 72 hours' exposure and they're reported in **Table 2**. O-vanillin derivatives **AG41**, **AG48** and **JB89** possess IC_{50} values in the low-micromolar range, while the remaining ligands have given results non-reproducible and non-reliable, so their IC_{50} values have not been calculated: probably this is due to their low solubility and extensive precipitation in the assay medium. As expected, better results have been obtained with the copper-based compounds: they have revealed a good *in vitro* antitumor potential, with IC_{50} values in the nanomolar range, as reported in **Table 2**.

	IC_{50} (μM) ± S.D.					
	2008	**HCT-15**	**PSN-1**	**A375**	**BxPC3**	**BCPAP**
AG41	0.78±0.21	0.51±0.14	0.51±0.12	0.10±0.030	0.005±0.001	0.51±0.09
FM4	0.013±0.008	0.004±0.001	0.008±0.002	0.003±0.0004	0.03±0.01	0.033±0.01
AG48	4.85±1.12	3.97±0.38	6.82±1.08	2.11±0.4	0.98±0.25	3.15±0.62
FM6	0.035±0.011	0.017±0.006	0.32±0.10	0.009±0.001	0.002±0.0005	0.84±0.16
JB89	1.97±0.66	2.22±0.76	3.13±1.11	2.23±0.78	1.11±0.76	0.51±0.090
FM7	0.010±0.001	0.036±0.012	0.021±0.090	0.019±0.004	0.015±0.006	0.041±0.011
AG38	ND	ND	ND	ND	ND	ND
AG77	0.098±0.004	0.091±0.06	0.36±0.010	0.029±0.006	0.011±0.004	0.35±0.09
AG45	ND	ND	ND	ND	ND	ND
FM11	0.71±0.15	0.82±0.14	0.51±0.12	0.28±0.09	0.11±0.09	0.83±0.11
JB10	ND	ND	ND	ND	ND	ND
FM12	0.16±0.04	0.23±0.09	0.029±0.008	0.069±0.020	0.029±0.011	0.072±0.012
CDDP	2.17 ± 1.37	13.92±1.68	12.10±2.87	3.11±0.98	13.98±1.23	6.65±2.85

Table 2. Cytotoxicity was assessed by MTT test. IC_{50} values are calculated by a four parameters logistic model (P<0.05). S.D.= standard deviation.

Looking at the data, we can say that the 2-hydroxy-3-methoxybenzyl copper(II) complexes are more cytotoxic than the corresponding 2,3-dihydroxybenzyl ones.

Interesting results emerge from the comparison with data relative to *cis*platin: copper(II) complexes result to be considerably more cytotoxic than cisplatin, their IC_{50} values can be even 3 order of magnitude lower. **FM4** resulted to be the most cytotoxic compound, and, in particular, considering BxPC3, PSN1 and HCT-15 cell lines, IC_{50} values are about 466, 1510 and 3480 folds more effective than **CDDP**. **FM11**, instead, resulted to be the weakest compound, even if its activity is 16 times superior than *cis*platin.

The activity of complexes has also been evaluated on human colon cancer cell lines LoVo and LoVo-OXP, which are respectively sensitive and resistant to oxaliplatin, which is the key compound in FOLFOX (folinic acid, 5-fluorouracil and oxaliplatin) chemotherapeutic regimen[209]. The use of such drug is limited by the resistance of carcinogenic cells, apart from the diverse side effects that it may provoke. Cytotoxic tests on sensitive and resistant cells have been developed after 72 hours' exposure to copper(II) derivatives by MTT test: all complexes exhibit a similar activity on both cell lines and IC_{50} values, together with RF (resistance factor, *i.e*. ratio between IC_{50} value of resistant cells and the one of the sensitive ones) are reported in **Table 3**. RF values are from 6 to 50 times lower than that of oxaliplatin (**OXP**) and this means an absence of cross-resistance phenomena.

	IC_{50} (μM) ± S.D.		
	LoVo	**LoVo OXP**	**RF**
FM4	0.031±0.001	0.004±0.001	0.13
FM6	0.029±0.008	0.030±0.010	1.03
FM7	0.036±0.009	0.008±0.002	0.22
AG77	0.020±0.001	0.020±0.001	1
FM11	0.21±0.08	0.09±0.01	0.43
FM12	0.030±0.001	0.02±0.01	0.67
OXP	2.17 ± 1.37	13.92±1.68	6.41

Table 3. Cross-resistance profiles. IC50 values were calculated by a four parameters logistic model (P < 0.05). S.D.= standard deviation.

[209] Raymond E., Faivre S., Chaney S., Woynarowski J., Cvitkovic E.; *Mol. Cancer Ther. 1*; 227-235 (**2002**).

The problem of using platinum derivatives like oxaliplatin also concerns the toxic effects on non-cancerous cells, that they can provoke. In order to evaluate if the new derivatives are cytotoxic for non-tumor cells, copper complexes have been screened against kidney HEK293 non-tumor cells and the SI (selectivity index, *i.e*. ratio between IC_{50} values of non-tumor cells and IC_{50} values of the tumor ones, considering values obtained in LoVo cell lines) has been determined, as reported in **Table 4**. Surprisingly, only copper(II) derivatives with the 2-hydroxy-3-methoxybenzyl group (**FM6** and **FM7**) are less cytotoxic on HEK293 cell line, with SI values better than the one calculated for *cis*platin, while the 2,3-dihydroxybenzyl derivatives have shown absence of any preferential activity against carcinogenic cells.

	IC_{50} (μM) ± DS	
	HEK293	**SI**
FM4	0.009±0.002	0.3
FM6	0.093±0.011	3.2
FM7	0.11±0.080	3.05
AG77	0.007±0.001	0.3
FM11	0.021±0.010	0.1
FM12	0.034±0.001	1.1
CDDP	24.38±3.45	2.1

Table 4. Cytotoxicity in HEK293 human non-cancerous cells. IC_{50} values were calculated by a four parameters logistic model (P < 0.05). D.S. = standard deviation.

Copper(II)-based compounds have also been tested on 3D spheroids of colon (HTC-15) and pancreatic (PSN1) cell lines: a 3D cell culture is in fact able to better mimic the environment of *in vivo* tumors and it results to be more predictive than the conventional 2D ones[210]. So, 3D cell cultures were exposed for 72 hours to copper(II) complexes and **CDDP**, then cell viability has been assessed by means of the acid phosphatase (APH) assay. Results are reported in **Table 5** and they suggest that compounds are extremely effective, being about 60 times more active than *cis*platin; these results confirm a very good antitumor potential for the synthesized derivatives.

[210] Kankotia S., Stacpoole P.W.; *Biochim. Biophys. Acta 1846*; 617-629 (**2014**).

	$IC_{50}(\mu M)\pm$ S.D.	
	HCT-15	**PSN-1**
FM4	1.08±0.38	0.90±0.02
FM6	3.56±1.67	1.17±0.11
FM7	1.25±0.98	0.90±0.3
AG77	1.17±0.62	0.94±0.27
FM11	1.69±0.45	1.18±0.23
FM12	1.28±0.62	0.91±0.01
CDDP	68.2±4.57	52.6±3.78

Table 5. Activity in 3D cell cultures. IC_{50} values were calculated from the dose-survival curves by four parameters logistic model ($P < 0.05$). S.D. = standard deviation.

3.1.4 Evaluation of cellular uptake

With the aim to correlate the cytotoxic activity of complexes and their ability to permeate carcinogenic cells and distribute in their compartments, uptake and distribution studies have been developed on LoVo cell lines. Copper(II) complexes derived from o-vanilline thiosemicarbazones **FM4**, **FM6** and **FM7** were able to accumulate in a time- and dose-dependent manner, and significantly better than the corresponding copper(II) complexes with 2,3-dihydroxybenzaldehyde thiosemicarbazones, which poorly permeated cancer cells, independently of exposure time (Figure 22A-B); in particular, derivative **FM4** resulted to be the most internalized one. However, comparing data related to the cytotoxic activity and those of the cellular uptake it is not possible to evidence a direct correlation between them.

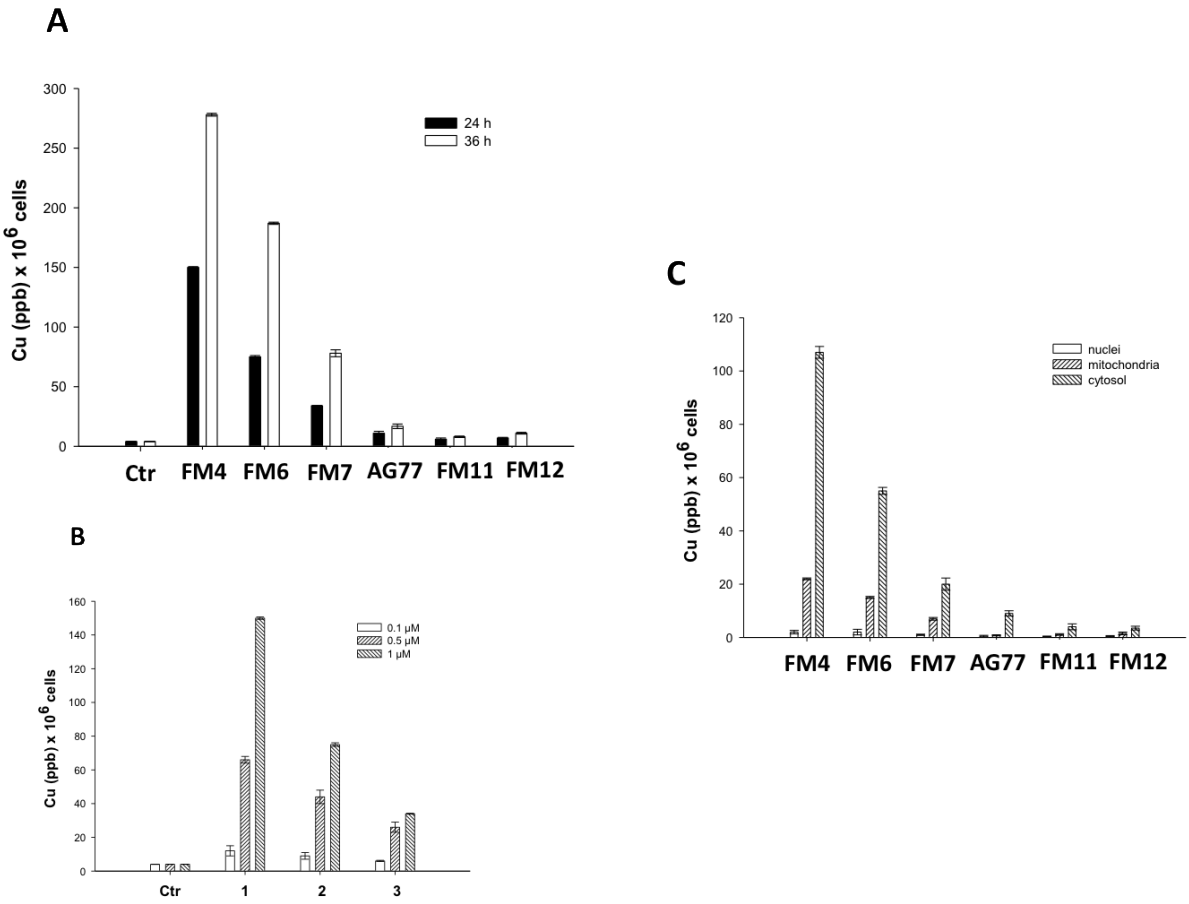

Figure 22. Cellular uptake (A, B) and distribution studies (C) in cancer cells.

Cancer cells compartments, such as nuclei, mitochondria and cytosol, have been studied to verify copper accumulation levels after exposure to thiosemicarbazones complexes: **FM4**, **FM6** and **FM7** (*i.e*. 2-hydroxy-3-methoxybenzyl derivatives) do preferentially accumulate into mitochondrial fraction and, to a lesser extent, in the cytosol (Figure 22C), while low concentration of copper are found in the nucleus. Again, 2,3-dihydroxybenzyl derivatives are poorly able to accumulate in tumor cells and their compartments.

3.1.5 Mechanistic studies of Cu(II) thiosemicarbazone complexes

DNA is classified as one of the possible targets for Cu(II) complexes; therefore, it is interesting to evaluate the ability of our metal-based derivatives to interact with the nucleic acids. To do that, LoVo cancer cells have been exposed to copper derivatives for 6 and 12 hours, then DNA fragmentation has been evaluated by Alkaline Comet Assay (alkaline single cell electrophoresis). Results have been compared to the one of dichloro(1,10-phenanthroline) copper(II), Cu(phen), used as reference in view of its known nuclease activity (Figure 23). Cells treated with our compounds

did not showed an increase in DNA fragmentation, since no evidence of increasing in electrophoretic migration is observed, while those exposed to Cu(phen) displayed a significant DNA fragmentation.

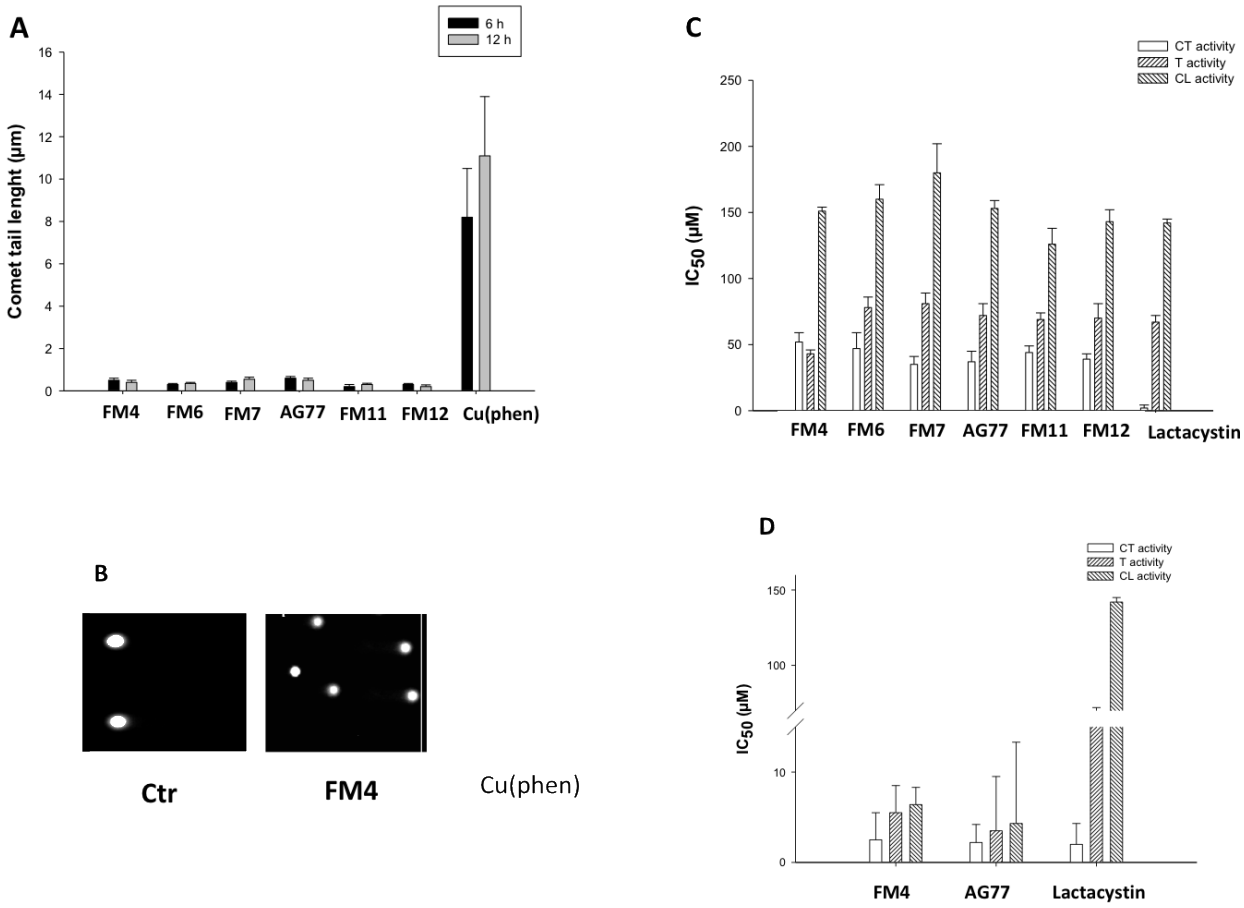

Figure 23. Mechanistic studies: DNA interaction (A and B) and proteasome inhibition (C and D). The error bars indicate the standard deviation.

It has been previously demonstrated that some metal complexes act by inhibiting the proteolytic proteasome activity[130]. We have investigated about the ability of the copper(II) complexes to act like chymotrypsin on isolated rabbit 26S proteasome, using Lactacystin, a well-known proteasome inhibitor, as positive control. LoVo cells have been exposed to increasing concentration of our derivatives for 24 hours, then the chymotryptic-like (CT-L), trypsin-like (T-L) and caspase-like (C-L) activities were assessed. *In vitro* results have revealed that all complexes are not very effective in reducing CT-L activity for 26S proteasome, having IC_{50} values 25 times higher than that of the positive control (Figure 23C); contrariwise, they've proved to be very effective in intact cells, being able to inhibit 50% of all catalytic activities at low micromolar concentrations: IC_{50} values for CT-L

activity are similar to the one of Lactacystin and **FM4** and **AG77** were even more powerful than the control against T-L and C-L activities (Figure 23D).

As previously discussed in the introduction, several studies[107-109] have reported that one of the possible mechanisms of action of copper complexes consists in modifying the cellular redox homeostasis and subjecting cells to an oxidative stress status, causing the death of cellular systems. In order to verify if our copper(II) derivatives may act as ROS accumulation enhancer, during biodistribution studies of our copper derivatives inside the cell, we have detected that it does accumulate into mitochondria, which have a key role in redox balance, so we have considered appropriate to evaluate their ability to interfere with the cellular redox homeostasis. All the complexes resulted to be ineffective in modulating cellular sulphydryl content and the total glutathione amount; apparently, they induce higher level of oxidized glutathione than in control cells and this effect is more pronounced with the 2,3-dihydroxybenzyl derivatives (Figure 24A-B).

We have also evaluated the morphological changes induced by copper complexes in LoVo cells by mean of TEM analysis. Upon treating cells with **FM4** for 24 hours with a concentration corresponding to $IC_{50,}$ an intensive swelling of mitochondria, and a consequent decreasing in electron density of the matrix regions and inner membrane, has been observed (Figure 24C). A massive induced swelling of endoplasmic reticulum (ER) membrane, sign of ER stress, has been found.

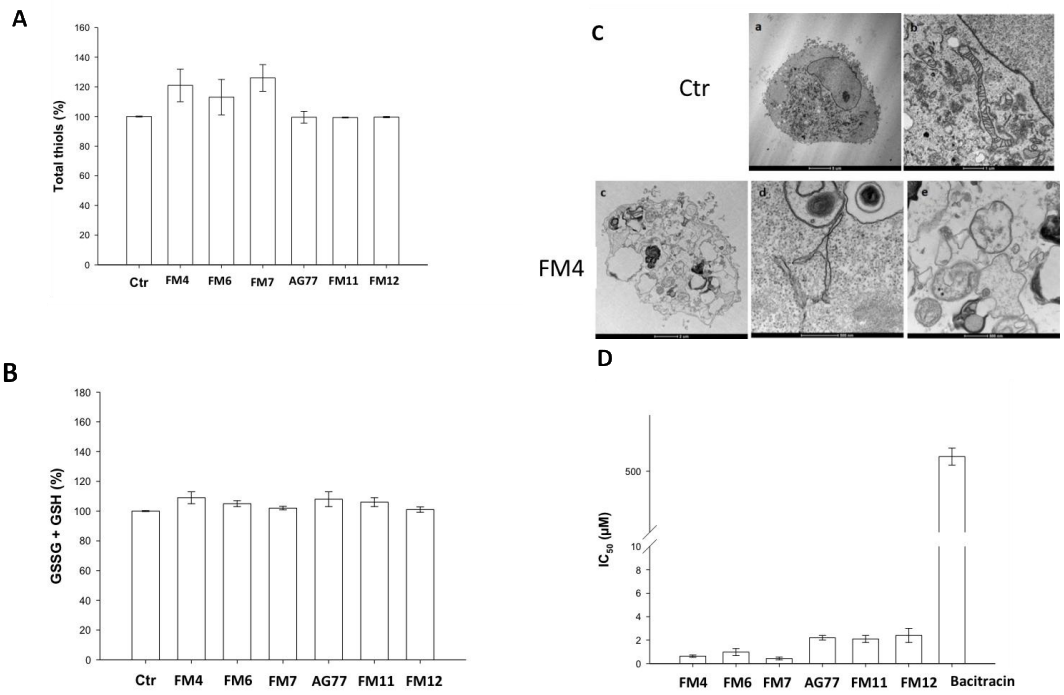

Figure 24. Mechanistic studies: cellular redox state (A and B), TEM analysis (C) and PDI inhibition (D).

It is well known that one of the most important protein which acts as an effective crosstalk between ER and mitochondria is Protein Disulfide Isomerase (PDI). PDI has several functions in the ER as catalyst of redox transfer, disulfide isomerization and oxidative protein folding, and as molecular chaperone. Even if there are many reports that underline the ability of this enzyme to bind and reduce copper metal ions[211], the impact of binding on the enzymatic activity is not fully characterized; also, PDI expression contributes to copper resistance in diverse organisms[212]. Basing on all these information, we have supposed that our copper derivatives may interfere with the disulfide bond catalytic activity of the enzyme. Results suggested that all analyzed complexes can effectively inhibit the protein, resulting to be even more powerful than Bacitracin, which is a well-known PDI inhibitor (Figure 24D): their IC_{50} values are up to three orders of magnitude lower than that of Bacitracin, being active in the low micromolar range.

3.1.6 *In vivo* preliminary studies of FM4

Basing on preliminary data obtained, which show a high potential of metal complexes as anticancer agents, we have decided to make a step forward and evaluate preliminary *in vivo* antitumor activity. In order to do that, among all derivatives, just the 2-hydroxy-3-methoxybenzyl thiosemicarbazone Cu(II) complex **FM4** has been chosen, because of its promising *in vitro* antitumor activity and its preferential cytotoxicity toward carcinogenic cells; its antitumor activity has been evaluated on a highly aggressive syngeneic murine *Lewis Lung Cancer* (LLC), a solid tumor. The tumor growth inhibition induced by **FM4** has been compared to the one induced by *cis*platin; after seven days of tumor inoculation, tumor-bearing mice were randomized into vehicle control and treatment groups.

	Daily dose ($mg \cdot kg^{-1}$)	Average tumor weight (mean±S.D., g)	Inhibition of tumor growth (%)
control[a]	-	0.459±0.13	-
FM4	3	0.239±0.08	48.0
FM4	6	0.118±0.09	74.3
CDDP	1.5	0.114±0.08	75.2

Table 6. *In vivo* antitumor activity. [a]vehicle (20% Cremophor EL (v/v), 20% PEG400 (v/v) and 60% saline solution (v/v)).

211 Narindrasorasak S., Yao P., Sarkar B.; *Biochem. Biophys. Res. Commun. 311*; 405-414 (**2003**).

212 Furlong E.J., Lo A.W., Kurth F., Premkumar L., Totsika M., Achard M.E.S., Halili M.A., Heras B., Whitten A.E., Choudhury H.G., Schembri M.A., Martin J.L.; *Nat Commun.*, 8; 16065 (**2017**).

Control mice are treated with vehicle solution (20% Cremophor EL (v/v), 60% saline solution (v/v) and 20% PEG400 (v/v)) or CDDP (1.5 mg/kg in saline solution). After 15 days, tumor growth has been evaluated and results reported in **Table 6**. Administration of 6 mg/kg of **FM4** induces about 75% reduction of the tumor mass, the same result obtained by using 1.5 mg/kg of CDDP; however, it is well-known that *cis*platin provokes anorexia while treatment with the copper(II) complex does not provoke a substantial body weight loss (<10%) throughout the therapeutic experimentation.

3.2 WATER-SOLUBLE Cu(II)-COMPLEXES

3.2.1 Synthesis and crystal structure analysis

With the previously described set of molecules we got promising results from the 2-hydroxy-3-methoxybenzyl derivatives, but we have faced some solubility problems with the *in* vivo assay. In order to overcome these drawbacks, we have decided to take a step forward and to increase the water-solubility of the previous set of thiosemicarbazones modifying the molecular structure of the ligands, by the insertion of an hydrophilic group in para position with respect to the 2-hydroxylic one. We have chosen to introduce a sulfonate group, isolating the derivatives as sodium salts (Figure 25). Thiosemicarbazones that have reported the better results in the previous analysis (i.e. **AG41**, **JB89**, **AG38**) have been selected and we have functionalized them by addition of 6 eq. of concentrated H_2SO_4 to the thiosemicarbazone at 0°C. The mixture is left reacting at rt for 3 hours; it is quenched by slow addition of ice, then pH values is raised to ≅7 by slow addition of a concentrated solution of NaOH. After solvent removal, the final product is isolated by extraction with cold methanol to give yellow to orange powders, characterized by $^{1}H/^{13}C$-NMR, ESI-MS, ATR-IR and Elemental Analysis.

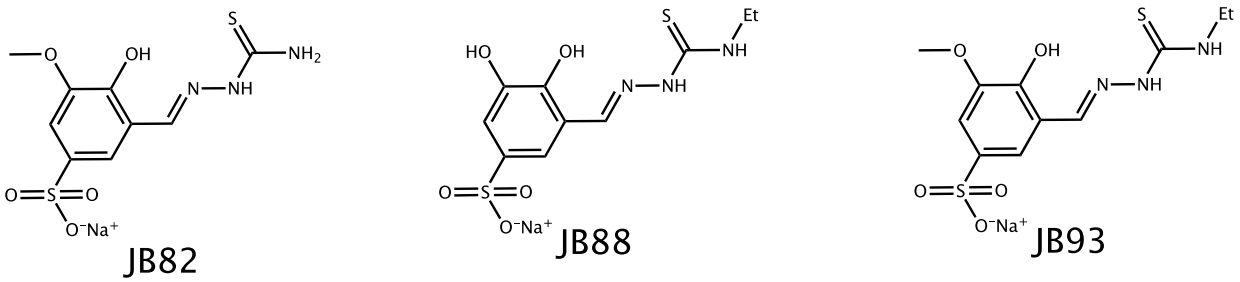

Figure 25. Structure of benzenesulfonate thiosemicarbazonic derivatives.

Even in their sulfonated forms, such ligands present only the *E*-form in solution and, even in this case, the thione-thiol equilibrium is in favor of the thione one, the only present form in solution. A

comparison of IR spectra of **JB10** and **JB88** reveals that the stretching band of iminic group C=N results to be shifted from 1522 cm^{-1} in the parent ligand to 1539 cm^{-1}. Elemental analysis has been carried out on the isolated powders and results confirmed that all ligands have been isolated in the sodium salt form and that they have different grade of hydration, from 1.5 to 2.5 water molecules. ESI-MS analysis (negative ions mode) has confirmed the nature of the ligand, reporting a m/z peak relative to the specie $[L]^-$.

Once verified the nature of the benzenesulfonate thiosemicarbazones, we synthetized the related Cu(II) complexes: 1 eq. of the ligand is made reacting with an equimolar amount of $CuCl_2 \cdot 2H_2O$ at pH around 8 in nitrogen atmosphere; the mixture is left reacting a rt for 4 hours and a green precipitate is isolated by filtration. Characterization of the isolated powders has followed and from ^{1}H-NMR analysis it has emerged that all complexes have a paramagnetic nature, as for the first set of metal-based compounds, indicating also in this case the presence of Cu(II) in the complexes. By a comparison of the IR spectra of a free ligand and the relative metal complex it is possible to guess which is the chelating motif adopted by this class of ligands; matching the spectra of **JB88** and **JB94** it is possible to notice that some stretching bands are shifted at both higher and lower values (Figure 26): OH band passes from 3586 to 3337 cm^{-1}, C=N bond has a stretching band at 1537 cm^{-1} in the free ligand, while it is shifted to 1611 cm^{-1} in the complex and, the band relative to the C=S group is shifted from 1043 to 1028 cm^{-1}. We can, then, suppose that even in this case an O,N,S chelating motif is involved in coordination of the metal core.

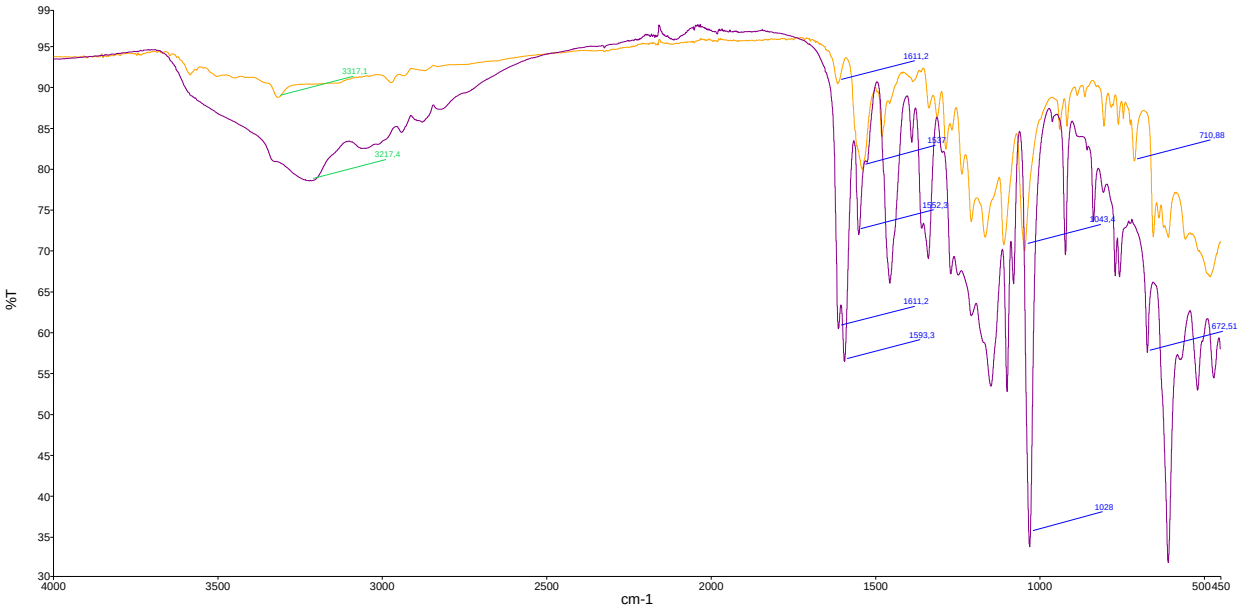

*Figure 26. ATR-IR spectra of the free ligand (**JB88**, orange) and the complexed form (**JB94**, violet).*

To verify the purity of the copper(II) compounds, elemental analysis has been carried out and it emerges that all the metal-based derivatives resulted to have different hydration grades.
Moreover, diverse crystallization attempts of the copper(II) complexes have been developed in order to evaluate their solid-state structures and crystals suitable for X-ray analysis have been obtained by slow evaporation of methanolic solutions of derivatives **JB91** and **JB94** (Figure 27).

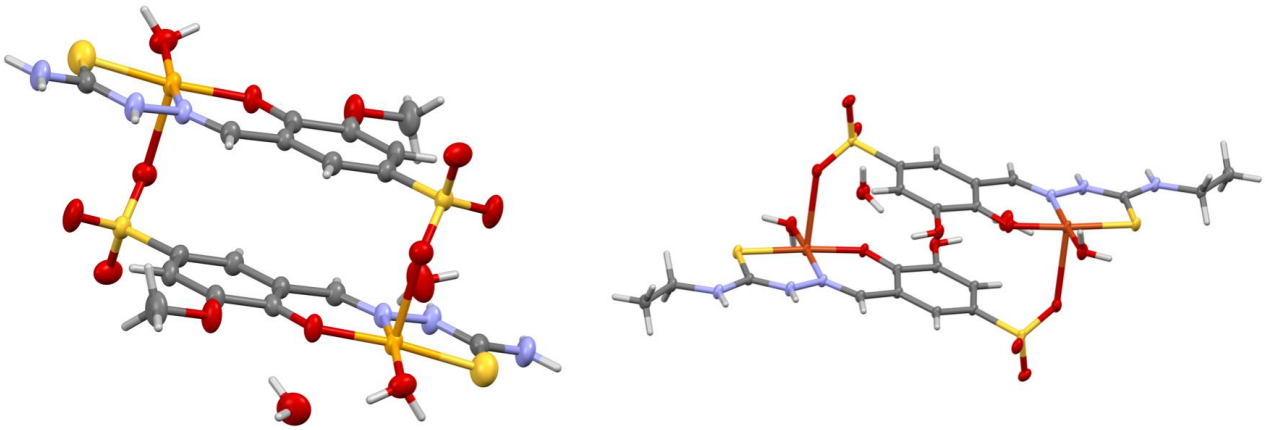

*Figure 27. X-rays structures of **JB91** (on the left) and **JB94** (on the right).*

Both ligands have the same coordinative behavior as their parent forms: the copper(II) ion is surrounded by a six-member chelating ring that involves the orto- hydroxy group in a deprotonated form, as well as the protonated N2 of the thiosemicarbazide moiety: the C=S bond results to be rather short (1.619 Å for **JB91** and 1.710 Å for **JB94**) in accord with a thione form, with the final ligand resulting in the *O,N,S* chelating motif. The complex forms a dimer with a second complex unit: in fact, the apical coordination position of the metal ion is occupied by an oxygen atom derived from the SO_3^- group of a ligand of an adjacent complex molecule. The equatorial coordination is ,then, completed by a water molecule.
The *in vitro* and *in vivo* antitumor activity of the sulphonyl derivatives are actually ongoing.

Notes:

*Studies in solution of ligands **AG48** and **AG41** have been developed in collaboration with Prof. Matteo Tegoni (University of Parma, SCVSA Department), while in vitro/in vivo biological assays, together with the investigation on the mechanism of action, have been developed by Prof. Valentina Gandin and Prof. Marzano Cristina (University of Padova, Department of Pharmaceutical and*

Pharmacological Sciences). All experiments with animals were reviewed and approved by the internal Review Board (OPBA) and authorized by the Italian Ministry of Health (authorization n. 640/2016-PR), accordingly with the current national and European regulations and guidelines for the care and use of laboratory animals (D.L. 26/2014; 86/609/EEC Directive).

2,3-dihydro-6,7-dihydroxy-1H-isoindol-1-ones as influenza virus PA_N endonuclease inhibitors

1.INTRODUCTION

1.0 PREMISE

In autumn 1918 an unexpected pandemic, the so-called "Spanish flu", spread all around the world, killing between 20 and 40 million people in just 8 months[213]. More recently, in early April 2009, an unusual series of deaths has been reported to the Mexican Ministry of Health[214]: a new pandemic had to be faced, induced, in this case, by the 2009 H1N1 virus, also called "swine-flu"[215,216]. A permanent risk of sudden influenza pandemics is still present, but these are rare extreme situations; a more common but still relevant cause of morbidity and mortality could be found in seasonal influenza A or B. Vaccination is a widely used prophylactic measure, whereas two classes of anti-influenza drugs are available, acting on the viral M2 ion-channel, like amantadine and rimantadine, or on the viral neuraminidase (NA), like zanamivir and oseltamivir. However, the M2 inhibitors have limited clinical utility due to their central nervous system side effects; in addition, resistance is a growing concern for both M2 inhibitors and oseltamivir[217,218,219]. Therefore, there is an urgent need for new antiviral compounds, preferably based upon novel pharmacophores and different modes of action. In this work we have explored the use of a novel class of antiviral compounds, based on the isoindol-1-one scaffold, as inhibitors of an influenza virus enzyme, PA_N endonuclease.

213 Crosby A.; *America's Forgotten Pandemic*, Cambridge University Press, Cambridge, (**1989**).

214 Viboud C., Alonso W.J., Simonsen L.; *PLoS Med* 3(4); e89 (**2006**).

215 Chowell G. *et al.*; *N. Engl. J. Med.* 361; 674–679 (**2009**).

216 Garten R.J. *et al.*; *Science* 32; 197–201 (**2009**).

217 Deyde V.M. et al.; *J. Infect. Dis.* 196; 249-257 (**2007**).

218 Moscona A.; *N. Engl. J. Med.* 360; 953-956 (**2009**).

219 Memoli M.J. et al.; *J. Infect Dis.* 203; 348−357 (**2011**).

1.1 INFLUENZA VIRUS

1.1.1 Influenza virus structure

Influenza is a single-stranded negative-sense, enveloped RNA virus of the *Orthomyxoviridae* family[220]. The major serotypes are called A, B , C: such classification is based on the antigenic specificity of the nucleoprotein (NP) antigen[221]. Influenza C is poorly characterized and there are just few studies in pediatric population[222], while A and B affect 5-10% of adult and 20-30% of pediatric population every year[223].

Influenza virion consists of a spherical capsule of about 100 nm diameter (Figure 1) and its envelope is made of a lipidic bilayer membrane in which three viral transmembrane proteins are located: neuraminidase (NA), hemagglutinin (HA) and matrix protein 2 (M2). HA is the most abundant one and it is involved into the virus binding to the host cell surface by sialic-acid residues and into the fusion of the viral envelope with the endosomal membrane of the host cell. NA is a glycoprotein responsible of the cleavage of sialic-acid receptors from the host cell membrane and the consequent release of progeny virions; M2 is a pH-activated proton channel involved in the acidification of the interior of the virion, leading to its uncoating[224,225]. Adherent to the inner part of the lipidic bilayer we find the matrix protein 1 (M1), which helps the encapsulation of the viral genome into the particle: it bridges interactions between genomic materials and the membrane[226].

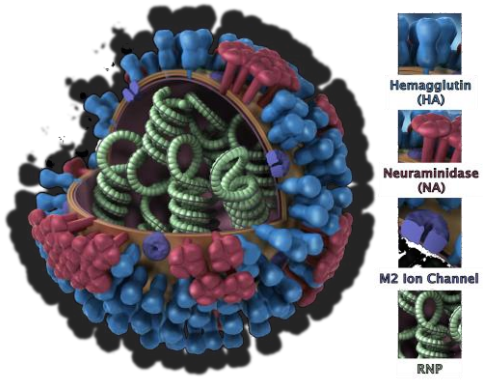

Figure 24.Cartoon of the virion spherical structure.

220 Lamb A.R. et al.; *Lippincott Williams & Wilkins: Philadelphia* 1487-1531 (**2001**).

221 World Health Organization; *Bull. World Health Organ.* 58; 585-591 (**1980**).

222 Salez N. et al.; *J. Infect.* 69; 182-189 (**2014**).

223 World Health Organization. Influenza (seasonal) - Fact sheet N°211.

224 Sakaguchi T. et al.; *Proc. Natl. Acad. Sci. U.S.A.* 94; 5000-5005 (**1997**).

225 Zebedee S.L., Lamb R.A.; *Proc. Natl. Acad. Sci. U.S.A.* 86; 1061-1065 (**1989**).

226 Yasuda J. et al.; *Virology* 196; 249-255 (**1993**).

The viral genome consists of eight vRNA strands in the form of ribonucleoprotein complexes (vRNPs) (Figure 2) and each one consists of a single negative-oriented RNA segment, covered of nucleoproteins copies, that is bound to the polymerase complex, which is the real responsible for the viral replication process[227,228,229]. The RNA-dependent RNA polymerase of viruses is encoded by the three largest RNA segments, while the three-intermediate size RNAs encode HA, NA and NP; the largest of the remaining segments encodes M1 and M2, while the smaller encodes NS1 and NS2/NEP[230], two non-structural proteins.

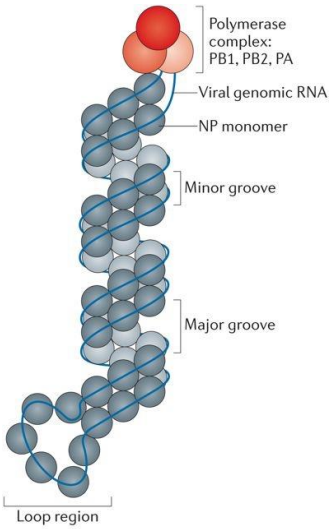

Figure 25.Cartoon of the vRNA : it consists of a single negative-stranded helix, with a loop region on one side; on the other it is bound to the polymerase complex (red) which consists of three subunits: two basic, PB1 and PB2, and an acidic one, PA.

1.1.2 Influenza virus lifecycle

The viral lifecycle can be divided into five main stages (Figure 3): i) the virus permeates the cellular membrane and enters the host cell; ii) the vRNPs enter the nucleus; iii) the viral genome is transcribed and replicated; iv) vRNPs are exported from the nucleus; v) assembly and budding of viral progeny at the host cell plasma membrane.

The viral membrane protein HA recognizes the terminal sialic acid residues of host glycolipids and glycoproteins, allowing the adhesion of influenza virus particle to the host cell; an endocytosis occurs and, then, the virus is transported inside the cell by an endosome. The viral M2 protein functions as a proton channel that lowers the pH in the endosomes, causing virion uncoating and

227 Ronconi L., Sadler P.J.; *Coord. Chem. Rev.* 251; 1633-1648 (**2007**).

228 Steitz T.A.; *Nature* 391; 231-232 (**1998**).

229 Pingoud A. et al.; *Cell. Mol. Life Sci.* 62; 685-707 (**2005**).

230 Chen W. et al.; *Nat. Med.* 7; 1306-1312 (**2001**).

genome release in the host cytoplasm[231]. vRNP has, then, to enter the nucleus[232] and, once inside, it has the primary role of transcribing viral mRNAs to produce viral proteins and to replicate cRNA (complementary genomic RNA) to generate progeny vRNPs. Hence, influenza vRNPs are subjected to the primary transcription process: they are transcribed to produce viral mRNA for *de novo* viral protein synthesis[233]. This, thus, is a primer-dependent process and primers are obtained from the "cap-snatching" mechanism by the viral polymerase complex[234,235,236]: PB2 subunit binds the 5'-7 methylguanosine cap of a pre-mRNA and, then, the PA catalytic site of endonuclease cleaves 10-15 nucleotides downstream. The RNA primer, now, is subjected to polymerization by the PB1 subunit, using vRNA as template. A chimeric mRNA, which is a hybrid between the viral and the host cell ones, is synthesized and it is, then, transported to the cytoplasm to undergo translation into viral proteins. Once synthesized, the new proteins enter, again, the nucleus where other cycles of transcription and replication take place. These newly synthetized vRNP complexes are then exported from the nucleus to the cytoplasm; then, the new virus is packed from the host cell membrane, together with host-cell phospholipids and the viral membrane proteins HA, NA and M2, and it is released from the cell surface by the enzyme Neuraminidase (NA).

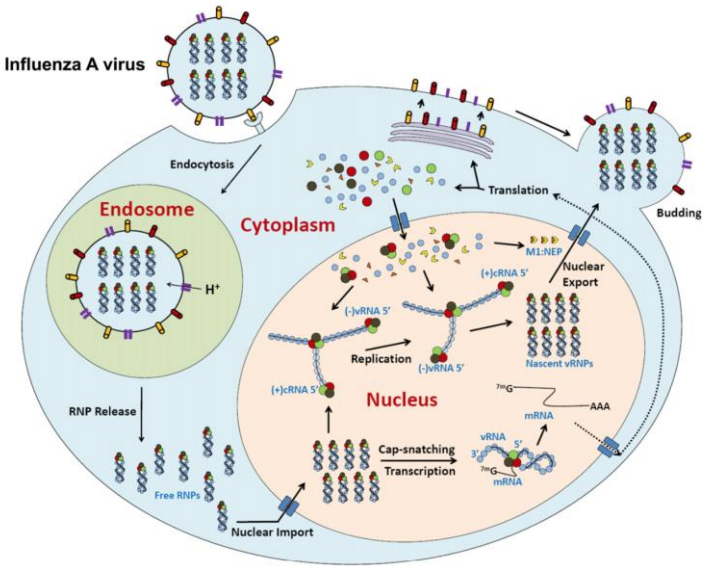

Figure 26. Schematic representation of influenza viral lifecycle.

231 Eisfeld A.J., Neumann G., Kawaoka Y.; *Nat. Rev. Microbiol.* 13; 28-41 (**2015**).

232 Boulo S. et al.; *Virus Res.* 124(1-2); 12-21 (**2007**).

233 Mark G.E. et al.; *J. Virol.* 29; 744-752 (**1979**).

234 Bouloy M. et al.; *Proc. Natl Acad. Sci. USA* 75; 4886-4890 (**1978**).

235 Plotch S.J. et al.; *Proc. Natl Acad. Sci. USA* 76; 1618-1622 (**1979**).

236 Plotch S.J. et al.; *Cell* 23; 847-858 (**1981**).

1.2 TREATMENT OF INFLUENZA VIRUS INFECTIONS

Nowadays, vaccination is considered to be the best way to prevent mortality and morbidity provoked by influenza virus severe infections. However, continuous manifestations of mutations in the RNA genome of influenza are the reasons why vaccines require an annual updating and result to be just partially protective in elderly and immunocompromised population[237], as well as pregnant woman[238].

The available used seasonal influenza vaccines are made up to contain the A/H1N1, A/H3N2 and B strains but they are not able to provide a long lasting and protective immunity, moreover, strains selection is based on prediction and surveillance, then there results to be a discrepancy, although mild, between circulating viruses and vaccines strains, with a consequent drop of efficacy[239]. Moreover, current vaccines are not efficient against zoonotic influenza viruses that may provoke severe pandemics. Antiviral drugs, therefore, result to be crucial in the first period of pandemics, when vaccines are still not available. The available antiviral drugs are classified on the basis of their molecular targets; thus, they can be divided into: i) M2 ion channel blockers; ii) NA and iii) RNA polymerase/endonuclease inhibitors. They are briefly described in the following sections.

1.2.1 M2 ion channel blockers

As already mentioned, M2 is a multifunctional protein involved in the viral lifecycle: it is responsible for virus entry, assembly and budding; it is a homotetramer that consists of a proton-selective ion channel in the middle of four helices[240]. As pH activated proton channel, it is responsible for the acidification of virus particles inside the endosome to unpack the viral genome[241,242].

237 Simonsen L. et al.; *Lancet. Infect. Dis.* 7; 658-666 (**2007**).

238 Madhi S.A. et al.; *N. Engl. J. Med.* 371; 918-931 (**2014**).

239 De Jong J.C. et al.; *J. med. Virol.* 61; 94-99 (**2000**).

240 Sakaguchi T. et al.; *Proc. Natl. Acad. Sci. U.S.A.* 94; 5000-5005 (**1997**).

241 Helenius A.; *Cell* 69; 577-578 (**1992**).

242 Pinto L.H., Holsinger L.J., Lamb R.A.; *Cell* 69; 517-528 (**1992**).

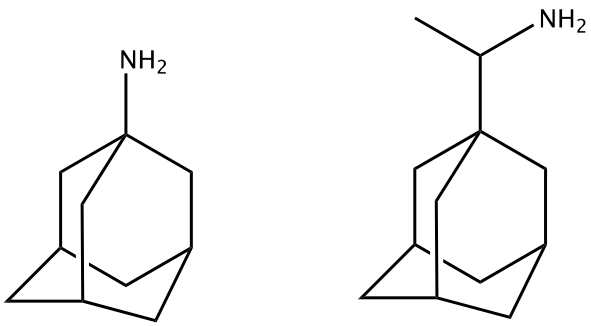

Figure 27. M2 ion channel inhibitors as antiviral drug.

Two compounds, amantadine and rimantadine (Figure 4) are used as M2 inhibitors: they bind the inner pocket of the protein, occluding the pore[243,244]; thus, such compounds have a limited use because of widespread resistance, as in 2009 pandemic H1N1 virus[245,246,247] that has been caused by a mutation in the transmembrane domain of M2 protein[248,249].

1.2.2 NA protein inhibitors

The neuraminidase influenza virus protein is a homotetrameric mushroom-shaped glycoprotein with a domain bound to the viral membrane and it contains the catalytic site in its globular head. This enzyme cleaves sialic acid moieties from glycans surface of the host cell membrane in order to easily allow virus release from infected cells[250]. Inhibitors of this protein work by mimic its substrate and impairing the enzymatic activity.

Zanamivir has been the first drug that has been used as antiviral in prophylaxis and in treatment of influenza virus; it was the first licensed neuraminidase inhibitor[251] and it is available in Italy with the commercial name *Relenza* as inhalation powder: this is a limit due to the low oral bioavailability.

243 Stouffer A. et al.; Nature 451; 596-599 (**2008**).

244 Pielak R.M., Oxenoid K., Chou J.J.; *Structures* 19; 1655-1663 (**2011**).

245 Deyde V.M. et al.; *J. Infect. Dis.* 196; 249-257 (**2007**).

246 Memoli M.J. et al.; *J. Infect Dis.* 203; 348−357 (**2011**).

247 Moscona A.; *N. Engl. J. Med.* 360; 953-956 (**2009**).

248 Belshe R.B. et al.; *J. Virol.* 62; 1508-1512 (**1988**).

249 Hay A.J. et al.; *J. Antimicrob. Chemother.* 18 Suppl B; 19-29 (**1986**).

250 Palese P. et al.; *Virol. J.* 10; 321 (**2013**).

251 Von Itzstein M. et al.; *Natur*e 363; 418-423 (**1993**).

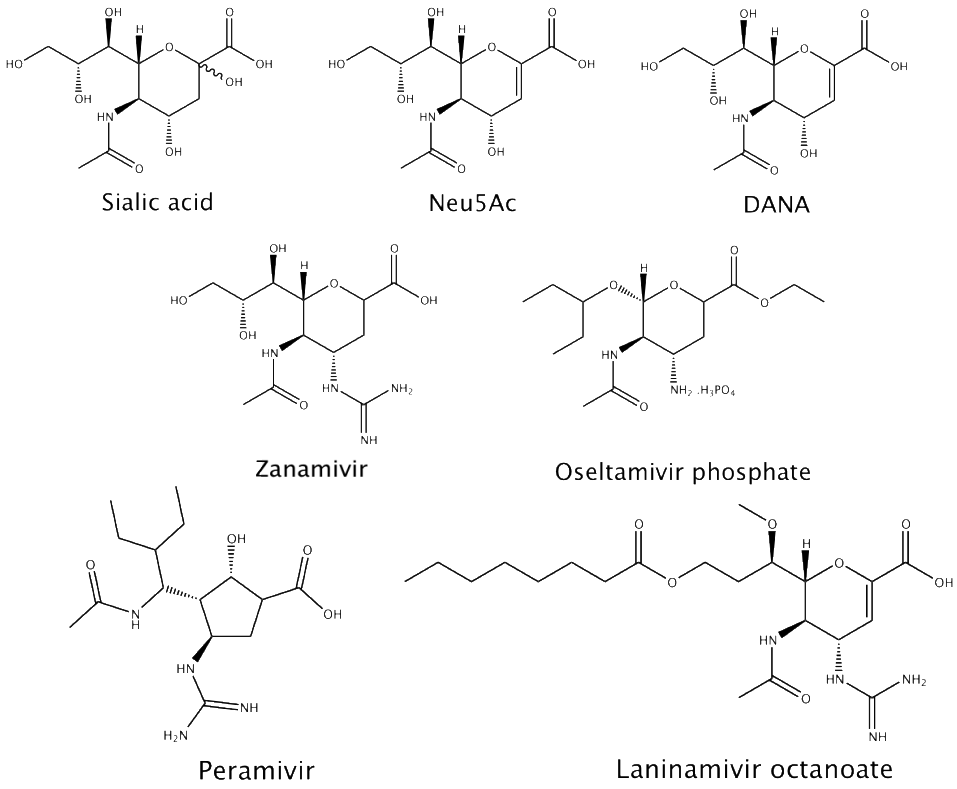

Figure 28. Sialic acid and the most common NA inhibitors molecular structure.

Oseltamivir[252,253] is an antiviral drug commercialized as phosphate salt in rigid capsules or oral suspension (*Tamiflu*, Roche); the limit in its use is caused by the rapid appearance of resistance. **Peramivir**, known as *Rapivab*, has been developed by BioCryst Pharmaceuticals and it has been approved for intravenous administration; together with **Laninamivir**, they're the most recent neuraminidase inhibitors that have reached out clinical trials[254,255] , however, NA mutations that affect **Oseltamivir** are able to impair also the **Peramivir**.[256]

1.2.3 RNA polymerase or endonuclease inhibitors

The influenza virus RNA polymerase is a key enzyme in viral replication; it consists of a 250 kDa heterotrimer made up of three subunits: two basic units, called PB1 and PB2, and an acidic one, PA[257,258]. The catalytic site of this enzyme resides in the N terminal domain of PA (PA_N) endonuclease

252 Kim C.U. et al.; *J. Am. Chem. Soc.* 119; 681-690 (**1997**).

253 Li W. et al.; *Antimicrob. Agents Chemother.* 42; 647-653 (**1998**).

254 Yamashita M. et al.; *Antimicrob. Agents Chemother.* 53; 186-192 (**2009**).

255 Babu Y.S. et al.; *J. Med. Chem.* 43; 3482-3486 (**2000**).

256 Nguyen H.T. et al.; *Antimicrob. Agents Chemother.* 54; 3671-3677 (**2010**).

257 Pflug A. et al.; *Nature* 516; 355-360 (**2014**).

258 Boivin S. et al.; *J. Biol. Chem.* 285; 28411-28417 (**2010**).

subunit and it is responsible for the so-called "*cap-snatching*" mechanism (Figure 6): it consists of a cleavage of 10 to 20 nucleotides from the 5' end of the host cell mRNA and a rebound to the 3' cap of the viral RNA, producing the so-called chimeric viral mRNA, which is a hybrid of the virus and the host cell ones.

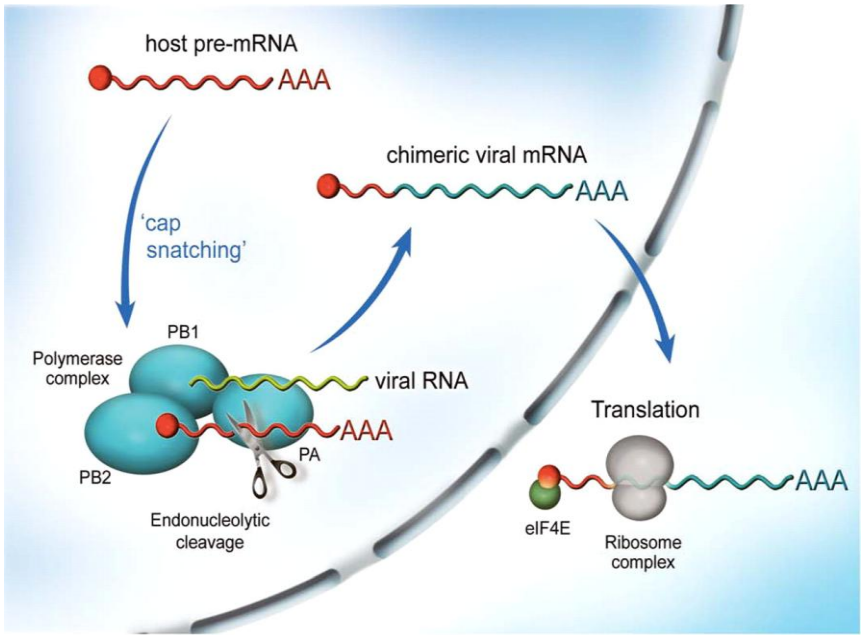

Figure 29. Scheme of the "cap-snatching" mechanism.

Thanks to this process, the ribosome complex that deals with the host cell mRNA replication is able to recognize the nucleotides sequence and it starts the replication process of the chimeric RNA, giving rise to virus replication. PB2 is responsible for the starting binding of RNAs to polymerase, while PB1 is the subunit that performs the real synthesis of RNA. Diverse RNA-polymerase inhibitors have been developed during the years (Figure 7).

Ribavirin, known as *Tribavirin,* has been first discovered in 1972 and it has been approved in 1986 for medical use[259]; this drug belongs to the World Health Organization's List of Essential Medicine and it is the most safe and effective drug in the health system. Studies on its mode of action are still going on and it has recently been demonstrated that it causes lethal mutations in the influenza virus genome because it is able to mimic the purine scaffold[260]. However, its clinical use is limited by diverse potential side effects[261]

259 Fischer J., Ganellin C.R.; *Analogue-based Drug Discovery*. John Wiley & Sons. p. 504 (**2006**).

260 Chegun P.P et al.; *Nat. Commun*. 5; 4794 (**2014**).

261 NIH, National Library Of Medicine, US. Hazardous Substances Databank Number: 6513. (http://toxnet.nlm.nih.gov/).

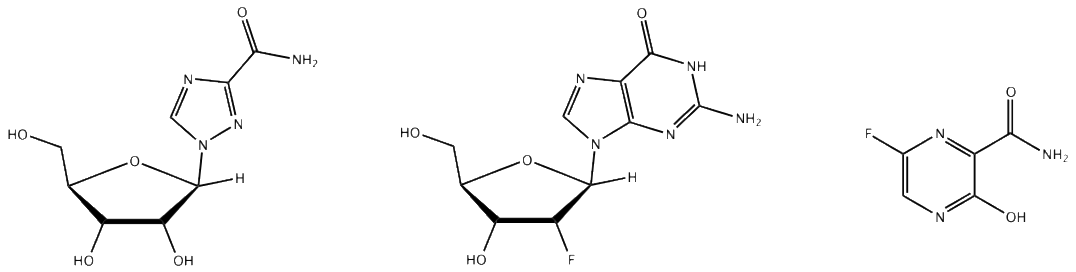

Figure 30. Molecular structures of the most successful RNA polymerase/endonuclease inhibitors.

Favipiravir (**T-705**), as nucleobase mimetic, is recognized as purine nucleotide[262] by viral RNA polymerase but its action mechanism is still unclear[263264] This compound has reached out Phase III clinical trials in both Europe and USA, and it results to be active against influenza A, B and C viruses[265], as well as the 2009 pandemic H1N1, the avian H5N1[266] and H7N9[267]. It is ,also, resulted to have a good *in vitro* activity on M2 ion channel blockers/NA inhibitors resistant viruses[268]. Favipiravir also impairs replication of Ebolavirus[269,270], bunyaviruses[271], arenaviruses[272], alphaviruses[273], flaviviruses[274], noroviruses[275] and picornaviruses[276].

1.3 PA_N ENDONUCLEASE AS A NEW ATTRACTIVE TARGET

Although there is a quite good availability of antiviral drugs, the emergence of viral resistance makes urgent the development of novel compounds[277,278,279,280]. The research has, then, moved forward in

262 Sangawa H. et al.; *Antimicrob. Agents Chemother.* 57; 5202-5208 (**2013**).

263 Baranovich T. et al.; *J. Virol.* 87; 3741-3751 (**2013**).

264 Jin Z. et al.; *PLoS One* 8; e68347 (**2013**).

265 Furuta Y. et al.; *Antimicrob. Agents Chemother.* 46; 977-981 (**2002**).

266 Kiso M. et al.; *Proc. Natl. Acad. Sci. U.S.A.* 107; 882-887 (**2010**).

267 Cao R. et al.; *Antivira Chem. Chemother.* (**2013**).

268 Sleeman K. et al.; *Antimicrob. Agents Chemother.* 54; 2517-2524 (**2010**).

269 Ostereich L. et al.; *Antiviral. Res.* 105; 71-21 (**2014**).

270 Smither S.J. et al.; *Antiviral. Res.* 104; 153-155 (**2014**).

271 Gowen B.B. et al.; *Antimicrob. Agents Chemother.* 51; 3168-3176 (**2007**).

272 Gowen B.B. et al.; *PLoS One* 3; e2614 (**2008**).

273 Julander J.G. et al.; *Antiviral. Res.* 82; 169-171 (**2009**).

274 Julander J.G. et al.; *Antimicrob. Agents Chemother.* 53; 202-209 (**2009**).

275 Rocha-Pereira J. et al.; *Biochem. Biophys. Res. Commun.* 424; 777-780 (**2012**).

276 Furuta Y. et al.; *Antimicrob. Agents Chemother.* 46; 977-981 (**2002**).

277 Krug R.M., Aramini J.M.; *Trends Pharmacol. Sci.* 30; 269-277 (**2009**).

278 Klumpp K.; *Expert Opin. Ther, Pat.* 14(8); 1153-1168 (**2004**).

279 De Clercq E.; *Nature Rev.* 5; 1015-1025 (**2006**).

280 De Clercq E., Neyts J.; *Trends Pharmacol. Sci.* 28; 280-285 (**2007**).

order to design antivirals with a possible molecular target different from M2 and NA: in this scenario, influenza virus polymerase emerges as good target for new drug development. The PA subunit, in particular, results to be a very attractive target because of its uniqueness: in fact, there is no analogue in the host cell, thus PA designed inhibitors would not impair the normal host cell activity; moreover, its catalytic site is highly conserved among all viruses subtypes[281].

PA subunit consists of a N-terminal (PA_N) and a C-terminal (PA_C) domain connected by a long flexible peptide: crystallographic structure of PA_N has revealed that it is a 25 kDa domain that contains seven α-helices and five β-strands which form an highly negative-charged pocket that is able to coordinate bivalent metal ions. Its metal-dependent nature has been confirmed, but it remains unclear which kind of metals and how many of them are necessary for its catalytic activity. As reported in Figure 8a, Yuan et al.[282] have been able to obtain a structure which contains just one Mg^{2+} ion coordinated by Glu80, Asp108, and three water molecules. The same situation has been identified by Zhao et al.[283] (Figure 8b), while Tefsen and colleagues[284] have found just one manganese ion coordinated by Glu119 side chain and by an oxygen from Glu80, one nitrogen from His41 and both oxygens from the side chain of Asp108 (Figure 8c).

281 Parkers K.E.B. et al.; *J. Med. Chem.* 46; 1153-1164 (**2003**).

282 Yuan P. et al.; *Nature* 458; 909-913 (**2009**).

283 Zhao C. et al.; *J. Virol.* 83; 9024-9030 (**2009**).

284 Tefsen B. et al.; *J. Virol.* 88; 1935-1941 (**2014**).

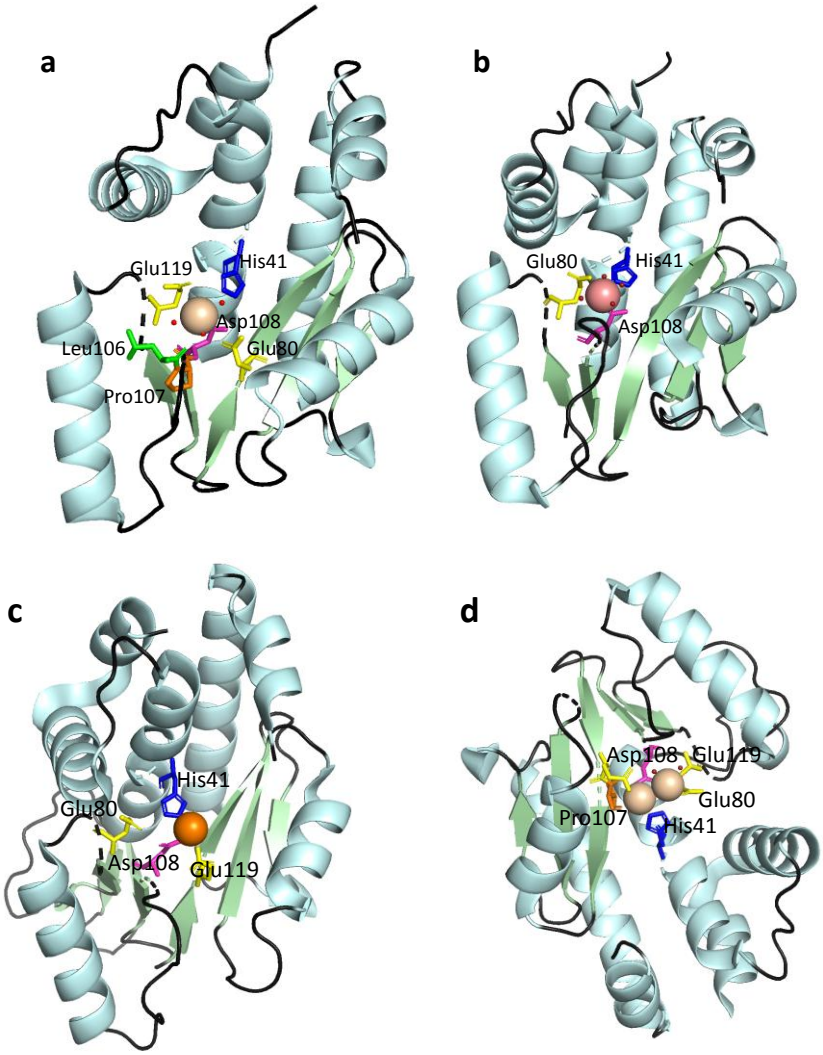

Figure 31. Comparison of the crystalline structures of the catalytic site of influenza virus PA endonuclease found by Yuan[282], Zhao[283], Tefsen[284] and Dias[285].

Contrariwise, Dias et al.[285] have reported two manganese metal ions in the pocket: the first is equivalent to the magnesium ion reported by Yuan, while the second is coordinated by Asp108, Glu119, Ile120 and three water molecules (Figure 8d). An explanation of the discrepancy in the number and kind of bivalent metal ions found in the active site has been given by Crépin and co-workers[286]: they support the theory that PA_N has two binding sites with high affinity for divalent metal ions, the first one has an higher affinity than the other and the pocket prefers to bind Mn^{2+} instead of Mg^{2+} because of the lower affinity of the last one for His[287,288,289].

285 Dias A. et al.; *Nature* 458; 914-918 (**2009**).

286 Crépin T. et al.; *J. Virol.* 84; 9096-9104 (**2010**).

287 Yang T.Y. et al.; *J. Am. Chem. Soc.* 125; 3168-3180 (**2003**).

288 Bock C.W. et al.; *J. Am. Chem. Soc.* 121; 7360-7372 (**1999**).

289 Harding M.M. et al.; *Crystallogr. Rev.* 16; 247-302 (**2010**).

Doan et al.[290] have studied the role of divalent metal ions in RNA cleavage process by PA endonuclease, highlighting that metal ions activate the PA endonuclease in a cooperative way: two interacting metal-binding sites able to coordinate M^{2+} are present in the catalytic core of endonuclease. Moreover, both metal ions are necessary to the normal development of PA endonuclease activity and each one has a specific role in nucleic acid hydrolysis, according to the two-metal ion mechanism firstly described by Steitz to explain the phosphoryl transfer catalyzed by a DNA polymerase[291].

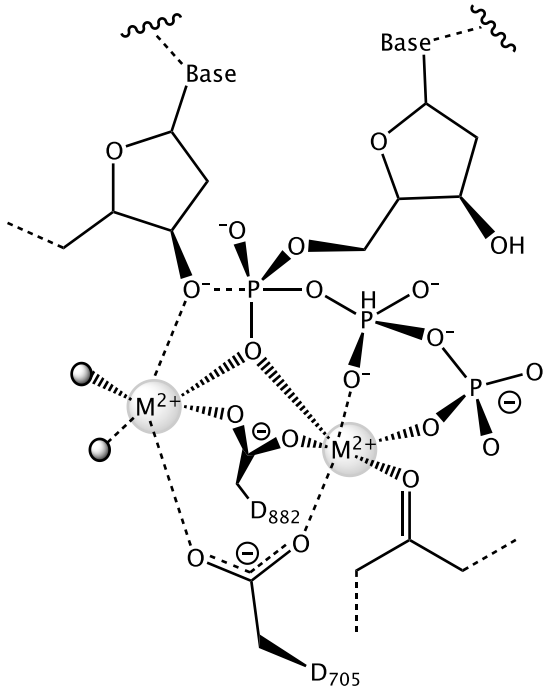

Figure 32. Representation of the cooperative interaction of the two metal ions in the catalytic site of PA_N endonuclease domain.

According to this mechanism, protein residues present in the active pocket are able to coordinate and, at the same time, orientate two M^{2+} ions for catalysis, together with the penultimate residue of the substrate, the 3'-terminal, and a nucleophile water molecule. The coordination sphere of both metals is surrounded by water molecules and the scissile phosphate: this makes the formation of the OH^- group easier and, thus, it promotes the stabilization of the transition state. Each metal has a specific role: M_A is responsible for the formation of the hydroxyl group, which is in a good orientation toward the phosphorus, thanks to Glu357 and Tyr497, in order to make an in-line attack to the scissile phosphate. Meanwhile, M_B plays the role of Lewis acid, since it facilitates the exit of

[290] Doan L. et al.; *Biochemistry* 38; 5612-5619 (**1999**).

[291] Steitz T.A.; *Procl. Natl. Acad. Sci.* USA 90; 6498-6502 (**1993**).

the 3' oxyanion[292]; it has also a second role: it is, in fact, involved into the stabilization of the pentacovalent intermediate[293].

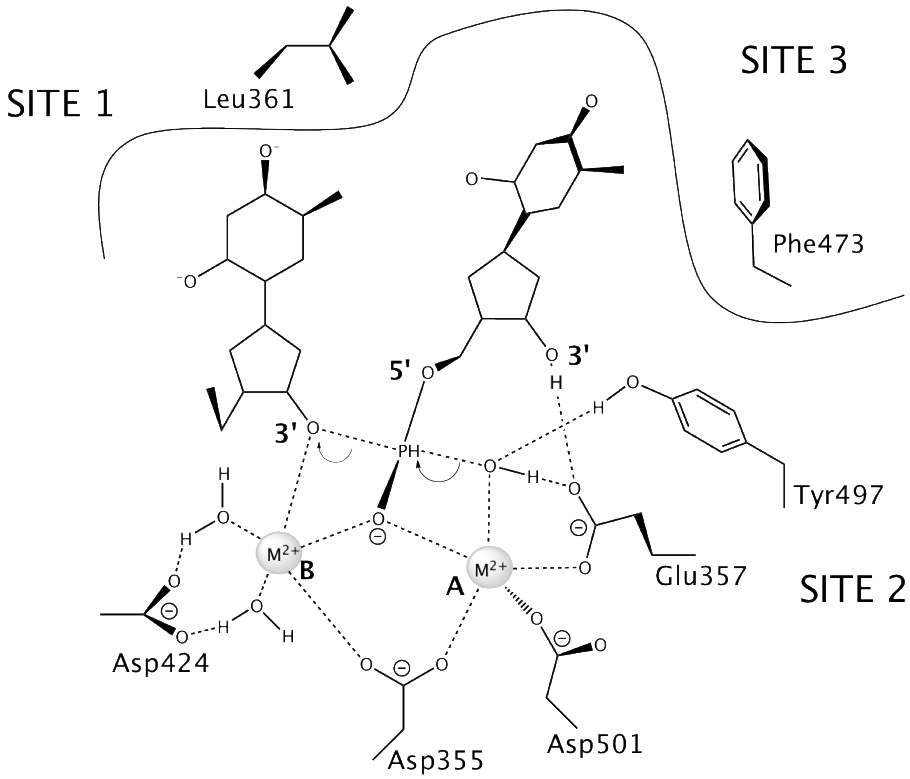

Figure 33. Two metal ions catalyzed mechanism: pentacoordinate transition state (intermediate) with the aminoacidic residues as found in crystallographic studies[291].

Magnesium is a common metal cofactor in a wide range of enzymes like those involved into nucleic acid biochemistry[294,295]; the choice of such metal as cofactor could be due to its small ionic radius, that makes it fits in diverse pockets of enzymes, and, then, to its high charge density, which make it a hard metal ion that can be coordinated by oxygen/nitrogen atoms of several aminoacidic residues of the protein. Moreover, this ion present no redox activity so that it cannot interfere with biological redox processes, it is a good Lewis acid and it has a slow ligand exchange; magnesium has a good affinity for water molecules and the 6-coordination number makes it a good candidate for interaction with nucleic acid substrates, leading to hydrolytic processes and condensation reactions under physiological conditions. Like we said before, Mg^{2+} results to be a hard ion, so it can directly bind side chains of the protein through carboxylates groups or by making a bridge by binding water

292 Herschlag D., Jencks W.P.; *J. Am. Chem. Soc* 109; 4665-4674 (**1987**).

293 Westheimer F.A.; *An. Chem. Res.* 1; 70-79 (**1968**).

294 Cowan J.A.; *Biometals* 15; 225 (**2002**).

295 Yang W., Lee J.Y., Nowotny M.; *Mol. Cell* 22; 5 (**2006**).

molecules[112]: these kind of interactions result to be present in enzymes like polymerases, nucleases, integrases that are all involved into the process of viral genome replication[296]. Mn^{2+} can substitute magnesium ions in DNA binding, cutting and pasting processes in *in vitro* assays, but Mg^{2+} is supposed to be the real *in vivo* cofactor. Since Mg^{2+} has such an essential role in these types of metalloenzymes, a good strategy to provide viral inhibitors consists in targeting the metal cofactors[114,297,298]: in such scenario, coordination chemistry results to be a perfect tool for the design of innovative therapeutic agents[299,300].[301] Metal chelators that are able to simultaneously chelate the two magnesium ions would impair the activity of the enzyme involved in viral replication, blocking its lifecycle. This strategy resulted to be successful in many cases, as the lunch on the market of Raltegravir and Dolutegravir as HIV integrase antiviral drugs has demonstrated[302].

1.4 PA_N ENDONUCLEASE INHIBITORS

The chelation of the bivalent metal ions present in the active center has been pursued also in the case of PA_N endonuclease to impair the activity of the enzyme. As described before, each metal ions present in the active pocket results to have a well-defined role in the cap-snatching process: in order to obtain efficient inhibition, it is necessary to contemporary chelate both metal ions.

Moreover, several classes of PA endonuclease inhibitors have been explored and all have in common donor oxygen atoms with a defined geometry and orientation: they can interact with the metal cofactors blocking the access to the substrate. An overview on the most important classes is reported below.

1.4.1 α,β-diketo acid family

This is the first class discovered by Merk about two decades ago: during an intense drug discovery screening it has been highlighted the ability of such compounds to impair the activity of the superfamily of nucleases and polynucleotidyl transferases[303].

296 Kirschberg T., Parrish J.; *Curr. Opin. Drug Discov. Dev*. 10; 460 (**2007**).

297 White R.J., Margolis P.S., Trias J., Yuan Z.; *Curr.Opin.Pharmacol*. 3; 502 (**2003**).

298 Rouffet M., Cohen S.M.; *Dalton Trans*. 40; 3445 (**2011**).

299 Hocharoen L., Cowan J.A.; *Chem.: Eur. J.* 8670 (**2009**).

300 Ronconi L., Sadler J.P.; *Coord. Chem. Rev*. 251; 1633 (**2007**).

301 Rogolino D. et al.; *Coord. Chem. Rev.* 256; 3063-3086 (**2012**).

302 Rogolino D. et al.; *Coord. Chem. Rev.* 256; 3063-3086 (**2012**).

303 Tomassini J. et al.; *Antimicrob. Agents Chemother.* 38; 2827–2837 (**1995**).

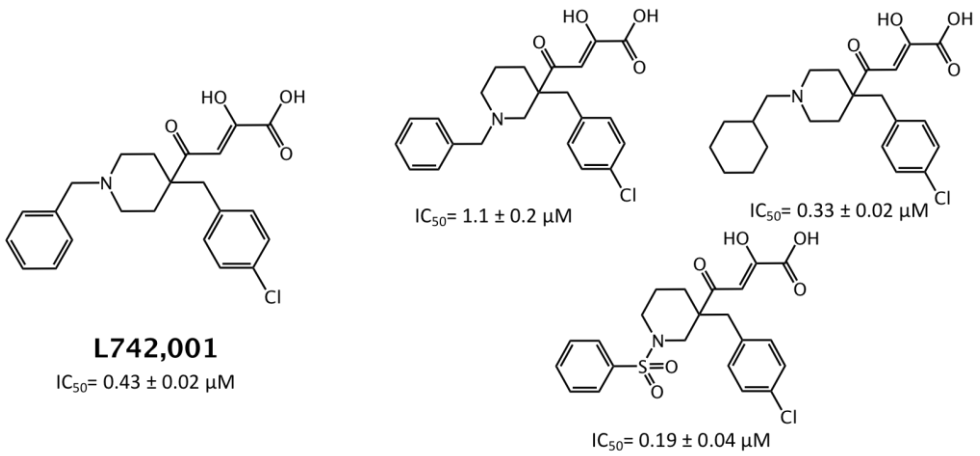

Figure 11. Molecular structure of the most active 2,4-dioxobutanoic acids.

4-substituted 2,4-dioxobutanoic acids (Figure 11) are able to selectively inhibit influenza cap-snatching mechanism with IC_{50} values from 0.19 to 29.0 μM. **L-742,001** (Figure 11) results to be one of the most potent compound, with IC_{50} value of 0.43 μM in cell culture. This compound results, also, to have good solubility[304].

A better understanding of the inhibition mechanism of L-742,001 has been made thanks to XRD studies on crystals of PA_N in complex with the inhibitor[305,306]: the diketoacid portion chelates the two metal ions, the central oxygen is shared by two ions and the carboxyl group forms salt bridge to Lys134; benzyl and chlorobenzyl substituents expand to diverse pockets around the active site, with the chlorobenzyl causing a shift in Tyr24. A structure with 2009 pandemic H1N1 PA endonuclease revealed that L-742,001 and analogues have a similar binding mode, but diverse substituents occupy different sub-pockets: this highlights the plasticity of the catalytic site cavity[307]. Recently, L-742,001 has been discovered to be unsuitable for further development and clinical applications, but it still remains a good starting point for the design of novel PA_N endonuclease inhibitors.

1.4.2 Flutimide and its derivatives

In 1994, a natural compound, a substituted 2,6-diketopiperazine called Flutimide, has been isolated from a fungal species, *Delitschia confertaspora.*[308] Different studies have revealed that Flutimide is

304 Hastings J.C. et al.; *Antimicrob. Agents Chemother.* 40; 1304–1307 (**1996**).

305 Dubois R.M. et al.; *PLoS Pathog.* 8; e1002830 (**2011**).

306 Kowalinski E. et al.; *PLoS Pathog.* 8; e1002831 (**2012**).

307 Lee H.K. et al.; *J. Clin. Microbiol.* 49; 3555–3559 (**2011**).

308 Pelaez F., Polishook J.D. et al.; *Mycotaxon* 50; 115-122 (**1994**).

able to selectively inhibit the cap-dependent endonuclease of transcriptase, without affecting neither the initiation or the elongation of influenza virus mRNA synthesis. Such compound has revealed an inhibitory activity on influenza A/PR/8/34 polymerase with IC_{50} value of 5.5 μM; moreover, it has shown no toxic effect, with $CC_{50} \geq$ 100 μM, in virus yield assays on influenza A infection of MDCK cells (EC_{50}=5.9 μM).

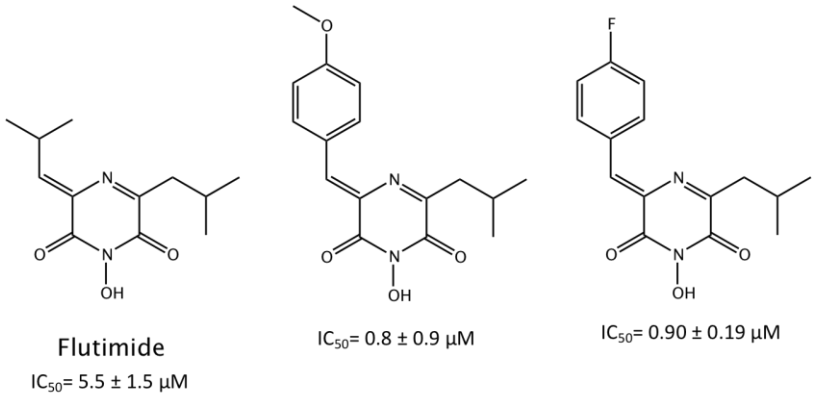

Figure 12. Molecular structure of Flutimide and two of its most active analogues.

As for the diketoacids family, different analogues have been synthesized by introducing functionalized benzyl groups at 3 or 5 position[309,310,311], leading to even more potent compounds (Figure 12).

1.4.3 N-hydroxamic acids family and catechins

During a high-throughput *in vitro* screening, it has been highlighted the inhibitory activity of N-hydroxamic acid derivatives on the capped RNA-dependent transcription of influenza A and B with the hit compound **1** (Figure 13) having an IC_{50} value of about 40 μM on both types. SAR studies of this derivative have revealed that the hydroxamic moiety, together with the phenolic hydroxyl and the nitrogen atom of quinoline, are essential for activity; moreover, the insertion of the hydroxamic acid on a cyclic ring scaffold can enhance the activity, as verified for **2** and **3**, which mimic the binding motif of Flutimide. However, these compounds resulted to be toxic, then no further investigation of antiviral *in vivo* activity has been developed.

309 Tomassini J.E. et al.; *Antimicrob. Agents Chemother.* 40; 1189–1193 (**1996**).

310 Singh S.B. and Tomassini J.E.; *J. Org. Chem.* 66; 5504–5516 (**2001**).

311 Baranov M.S. et al.; *Cheminform* 70; 3714–3719 (**2014**).

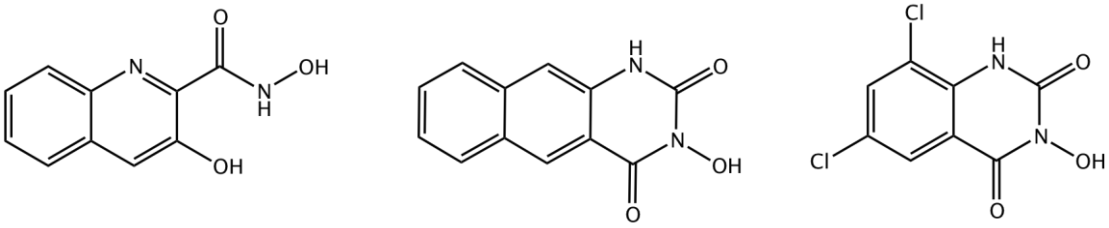

Figure 13. N-hydroxamic acid analogues and the relative IC_{50} values.

Catechins, too, were found to impair influenza A replication and viral RNA synthesis: this has been attributed to the alteration of the physical properties of the viral membrane[312]. Recent studies have revealed that ECG ((-)-epicatechin gallate) and EGCG ((-)-epigallocatechin gallate) have an inhibitory activity on PA endonuclease: docking studies confirmed the hypothesis that the galloyl group chelates both metal ions by the three adjacent oxygen atoms[313]. By a screening of several types of phytochemicals, three of them have been identified as PA endonuclease inhibitors: marchantins (Ms), perrottetins (Pes) and plagiochins (Pls)[314].

1.4.4 3-hydroxypyridinone and analogues

X-ray crystallography fragment screening first, and, then, FRET-based endonuclease inhibition assays have led to the discovery of compound **9** as a hit derivative[315,316]. Phenyl and substituted-phenyl have been introduced on the 3-hydroxypyridin-2(1H)-one at the 4-,5- and 6-position to try to make more efficient interactions with the diverse hydrophobic pockets that surround the active site. Among all, compounds that are bis-substituted at 5- and 6-position, like compounds **10** and **11** (Figure 14), resulted to be the most active, while the 4-position substituted compounds resulted to have almost lost their activity.

312 Song J.M. et al.; *Antiviral Res.* 68; 66–74 (**2005**).

313 Kuzuhara T. et al.; *PLoS Curr.* 1; RRN1052 (**2009**).

314 Iwai Y. et al.; *PLoS One* 6; e19825 (**2011**).

315 Bauman J.D. et al.; *ACS Chem. Biol*. 8; 2501–2508 (**2011**).

316 Parhi A.K. et al.; *Bioorg. Med. Chem*. 21; 6435–6446 (**2013**).

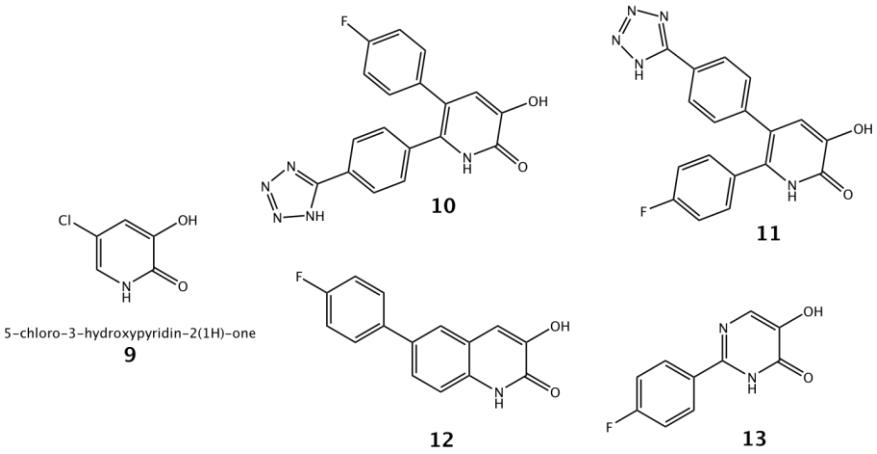

Figure 14 .3-hydroxypyridinone analogues molecular structures.

A step forward has been made by trying to change the ring skeleton by the introduction of nitrogen heterocycles: 5-hydroxypyrimidin-4(3H)-one analogues have been synthesized and analyzed in enzymatic assay[317,318]. Modifications on the 3-hydroxyquinolin-2(1H)-one have led to two potent derivatives, **12** and **13** (IC_{50}= 0.5 μM, both) which have a p-fluorophenyl group at 6-and7-position respectively. From X-ray data it has been possible to elucidate the chelating motif of **13**: the ketone group at 2-position and the 3-hydroxyl are involved into metal coordination, while the NH group of quinoline core coordinates the water molecule that chelates a metal ion.

Nowadays, none of the worldwide approved antiviral drugs acts by impairing the activity of PA_N endonuclease; recently, two PA inhibitors (*i.e.* Baloxavir marboxil and AL-794, S-033188) have reached out advanced steps in clinical trials, highlighting the validity of this innovative molecular target[319]. Moreover, Baloxavir marboxil has reached out phase III clinical trials[320] and it has been approved in 2008 in Japan as antiviral therapeutic agent[321]. Even if steps forward in this field have been made in the past years, there is still an urgent need of new antiviral compounds possible based on novel molecular scaffold: this is mainly due to the resistance that viruses have developed against the most common therapy.

317 Sagong H.Y. et al.; *ACS Med. Chem. Lett*. 4; 547–550 (**2013**).

318 Sagong H.Y. et al.; *J. Med. Chem*. 57; 8086–8098 (**2014**).

319 Wu X., Sun Q., Zhang C., Yang S., Li L., Jia Z.; *Theranostics* 7; 826-845 (**2017**).

320 Portsmouth S., Kawaguchi K., Arai M., Tsuchiya K., Uehara T.; *Open Forum Infect. Dis.* 4(Suppl. 1); S734(**2017**).

321 Heo Y.A.; *Drugs* 78; 693-697 (**2018**).

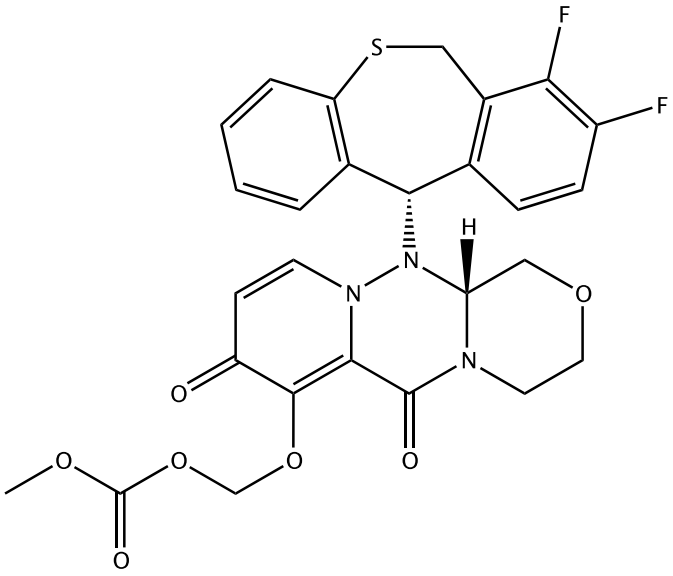

Figure 15. Chemical structure of Baloxavir marboxil.

AIM OF THE PROJECT. The research has moved forward, and interesting results are reported by Zhao and co-workers[322]: they've have explored a novel molecular scaffold, the 2,3-dihydro-6,7-dihydroxy-1H-isoindol-1-one one, as inhibitor for the HIV Integrase in order to impair its activity, then the viral replication process. From preliminary enzymatic assay results seem to be really promising, revealing IC_{50} values in the low micromolar range. From data reported, it is possible to infer that the use of a 2,3-dihydro-6,7-dihydroxy-1H-isoindol-1-one scaffold could be a good strategy to simultaneously chelate both the metal ions present in the active site of a magnesium-dependent enzyme. We have, then, decide to use the same scaffold modifying it in order to increase the affinity for Influenza virus PA endonuclease active center. The panel shown in Figure 16 has been synthesized and preliminary IC_{50} values for PA endonuclease inhibition have been estimated by a FRET-based assay.

322 Zhao X.Z. et al.; *J. Med. Chem.* 51; 251-259 (**2008**).

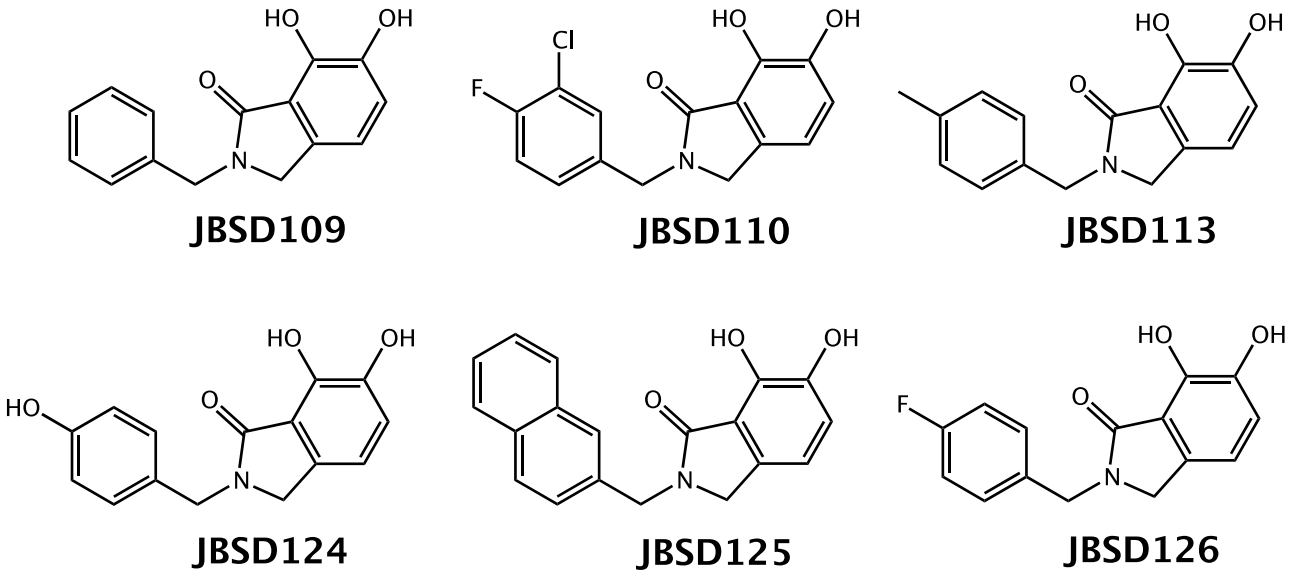

Figure 16. 2,3-Dihydro-6,7-dihydroxy-1H-isoindol-1-one derivatives as Mg^{2+} targeting PA_N endonuclease inhibitors.

On the basis of enzymatic *in vitro* assays, a second panel of molecules has been, then, synthesized in order to highlight the role of the substituent at the 4-position on the aromatic ring as well as the length of the spacer between the isoindol-1-one moiety and the benzylic one. Biological assays on this second panel of molecules are still ongoing at KU Leuven University (Prof. Lieve Naesens).

2. EXPERIMENTAL SECTION

2.1 MATERIALS AND METHODS

2.1.1 Chemistry

All reagents of commercial quality were purchased from Sigma-Aldrich and used without further purification. The purity of the synthesized compounds was determined by elemental analysis and verified to be ≥ 95%. 1H-NMR spectra were recorded at 25 °C on a Bruker Avance 500 FT spectrophotometer. The ATR-IR spectra were recorded by means of a Nicolet-Nexus (Thermo Fisher) spectrophotometer by using a diamond crystal plate in the range of 4000-400 cm^{-1}. Elemental analyses were performed by using a FlashEA 1112 series CHNS/O analyzer (Thermo Fisher) with gas-chromatographic separation. The purity of all compounds used in assays was determined to be ≥95% by ^{1}H NMR spectroscopy and confirmed by high-resolution mass spectrometry (HRMS) experiments using an Agilent 6230 Accurate-Mass LC-TOFMS at the U.C. San Diego Molecular Mass Spectrometry Facility (MMSF). Electrospray mass spectral analyses (ESI-MS) were performed with an electrospray ionization (ESI) time-of-flight Micromass 4LCZ spectrometer. Samples were dissolved in methanol. MS spectra were acquired with a DSQII Thermo Fisher apparatus, equipped with a single quadrupole analyzer in positive EI mode, by means of a DEP-probe (Direct Exposure Probe) equipped with a Re-filament. The UV-vis spectra were collected using a Thermo Evolution 260 Bio spectrophotometer provided with a thermostatting Peltier device, and quartz cuvettes with 1 cm path length.

2.1.2 Protein expression and purification

Pandemic H1N1 N-terminal PA endonuclease was expressed from a pET-28a parent vector containing a kanamycin-resistance reporter gene, expression inducible by the Lac 1 operon. The endonuclease was expressed as an 8-histidine tagged fusion protein. Transformation protocol was adapted from pET system manual (Novagen) using single competent BL21 cells. Briefly, 1 µL of 25 ng/µL recombinant plasmid was used for transformation. Cells were mixed by flicking with plasmid and were heat shocked at 42 oC for 30 sec followed by incubation on ice for 5 minutes. Outgrowth was plated on LB agarose plates contain 50 µg/mL kanamycin, and was incubated overnight at 37 oC. One colony was scraped from the LB plate and added to 50 mL of SOC broth containing 50 µg/mL kanamycin, and was incubated for 5 h at 37 °C with shaking at 125 rpm. Glycerol stocks of this culture were prepared (0.9 mL cultured media + 0.1 mL 80% glycerol) and flash frozen for future expressions. 100 mL of SOC media containing 50 µg/mL kanamycin was combined with 1 mL frozen glycerol stock or 1 mL the previously mentioned 5 h growth, and was incubated with shaking at 100-

125 rpm overnight at 37 °C as a starter culture. This starter culture was then equally divided into 4×1L batches of expression media (TB media with added 0.2% dextrose, 0.1 mM $MnCl_2$, and 0.1 mM $MgSO_4$) containing 50 μg/mL kanamycin. Cells were grown to the beginning of log phase (OD_{600} = between 0.6-0.8) at 37 °C with shaking at 100-125 rpm. Expression of PA endonuclease was then induced by the addition of IPTG to a final concentration of 0.8 mM. The media was grown with shaking overnight at ~18 °C. After approximately 18 h the cells were harvested by centrifuging at 2000g for 30 min at 4 °C. The resulting paste was stored at -80 °C prior to lysis.

Cell paste was thawed on ice for 2 h and re-suspended in 25-35 mL of lysis buffer (20 mM Na_2PO_4, 500 mM NaCl, 25 mM imidazole, 1 mM $MgCl_2$, 2 mM dithiothreitol (DTT), 0.2% Triton-X, pH=7.4) plus EDTA free protease inhibitor (Roche) and lysed by sonication - 5×25 sec pulses with 2 min rest periods on ice. To the cell lysates was added DNAse1 to a final concentration of 10-100 μg/mL, and the lysates were shaken at 125 rpm for 30-60 min on ice until the consistency of the lysate became free-flowing. Cell debris was then pelleted by centrifugation at 10000 rpm 35-45 min at 4 °C. The supernatant was decanted from the pellet, and a HisTrap HP (Parmacia) column was utilized to isolate His-tagged fusion protein from the cell lysates according to the manufacturer's recommendations. Briefly, cell-free lysates from 4L of growth were loaded on 1×5mL column that had previously been charged with Ni ions. The column was then washed with binding buffer (20 mM Na2PO4, 500 mM NaCl, 25 mM imidazole, pH=7.4) until fraction absorbance reached a steady baseline. Fusion protein was then eluted over a 45 min gradient at a flow rate of 4 mL/min, from 0-100% elution buffer (20 mM Na2PO4, 500 mM NaCl, 500 mM imidazole, pH=7.4). Pure target protein eluted between 50- 60% elution buffer. Isolated protein was flash-frozen and stored at -80 °C. SDS-PAGE analysis showed a single band of pure protein running at ~23kD.

2.1.3 Endonuclease activity assay

Endonuclease activity assays were carried out in Black Costar 96-well plates. Each well contained a total volume of 100 μL comprised of: buffer (20 mM Tris, 150 mM NaCl, 2 mM $MnCl_2$, 10 mM β-mercaptoethanol, 0.2% Triton-X100, pH=8.0), influenza PA endonuclease (25 nM), inhibitor (various concentrations) in buffer, and fluorescent ssDNA-oligo substrate (200 nM). A single-stranded, 17-mer DNA substrate labeled with a 5'-FAM fluorophore and a 3'- TAMRA quencher ([6-FAM]AATCGCAGGCAGCACTC[TAM]) synthesized by Sigma-Aldrich was employed to measure endonucleic cleavage. Upon addition of the substrate, the change in fluorescence was measured over 45 min at 37 °C (excitation: 485 nm; emission 528 nm). The positive control wells contained no

inhibitor for preliminary screens and were set as an arbitrary 100% activity. Later screens employed EGCG (Epigallocatechin 3-gallate), a previously validated inhibitor, as a positive control. The gain was set to 100 and the first 10 data points (10 min) were excluded from the activity calculations. Dose-response curves were generated, fitted, and analyzed using Origin8 graphing software.

3.2 CHEMISTRY

***1,2-dimethoxy-4-(methoxymethyl)benzene,* JBSD104:** In a Schleck flask, under N_2 atmosphere, 3,4-dimethoxy-benzyl alcohol (3.74 mL, 1 eq, 25.7 mmol) is dissolved in dry THF and it is cooled to 0°C. Sodium hydride 99% (1.0 g, 1 Eq, 25.7 mmol) is added portion wise to the solution which turns to grey. It is left reacting for 30 minutes at 0°C. Iodomethane (2.09 mL, 1.30 eq, 33.4 mol) is added dropwise to the solution, which is allowed to return to room temperature and it is left reacting for 3 hours, monitoring by TLC (Hex:AcOEt, 8:2). The reaction is quenched by ice-water and ethyl acetate addition. The organic phase is washed with water, then brine, and it is dried on $MgSO_4$. After salt removal, solution is taken to dryness by vacuum and the residue dark brown oil is purified by column chromatography (Hex:AcOEt, 8:2) to give the product as a colorless oil (yeld=96%). ^{1}H-NMR ($CDCl_3$-d, 500 MHz, 25°C), ppm: 6.87-6.79 (m, 3H, CH_{arom}), 4.36 (s, 2H, CH_2), 3.86 (s, 3H, OCH_3), 3.84 (s, 3H, OCH_3), 3.34 (s, 3H, OCH_3). ^{13}C-NMR ($CDCl_3$-d, 500 MHz, 25°C), ppm: 149.08, 148.66, 130.08, 122.49, 120.38, 111.06, 111.041, 74.69, 57.96, 55.96, 55.87.

***Methyl-2,3-dimethoxy-6-(methoxymethyl)benzoate*, JBSD105:** In a Schleck flask, under N_2 atmosphere, **JBSD104** (2.001 g, 1 eq, 10.98 mmol) is dissolved in dry diethyl ether (30 mL); the mixture is cooled to 0°C. n-butyl lithium (1.6 M solution in hexane) (10 mL, 1.501 eq, 16.48 mmol) is added dropwise to the solution, which becomes cream-colored. It is left reacting for 3 hours. The solution is cooled to -78 °C and methyl chloroformate (4.00 mL, 4.700 eq, 51.61 mmol) is added; it is allowed to return to rt, and it is left reacting for 20 hours. Water is added until the solution becomes colorless; the organic phase is extracted, dried with $MgSO_4$, filtered and the solvent is removed by vacuum. The residual oil is purified by column chromatography (Hex:AcOEt, 1:1) , to

give the product as a pale yellow oil (yield= 42%). ^{1}H-NMR ($CDCl_3$-d, 500 MHz, 25°C), ppm: 7.04 (d, 1H, CH_{arom}), 6.69 (d, 1H, CH_{arom}), 4.39 (s, 2H, CH_2), 3.91 (s, 3H, OCH_3), 3.86 (s, 6H, OCH_3), 3.32 (s, 3H, OCH_3). ^{13}C-NMR ($CDCl_3$-d, 500 MHz, 25°C), ppm: 186.78, 167.92, 152.43, 128.43, 124.35, 113.29, 72.22, 61.65, 58.29, 56.04, 52.30.

***Methyl 6-(chloromethyl)-2,3-dimethoxybenzoate,* JBSD106:** In a round bottom flask, **JBSD105** (1.0329 g, 1 eq, 4.2991 mmol) is dissolved in dry diethyl ether (5 mL), together with dry zinc(II) chloride (352 mg, 0.601 eq, 2.58 mmol); the solution is cooled to 0 °C. Then, acetyl chloride (990 µL, 3.24 eq, 13.9 mmol) is added dropwise to the solution, which turns to orange; the mixture is left reacting for 30 minutes at 0 °C. Aluminum(III) oxide (1.0 g, 2.3 eq, 9.8 mmol) is added and the mixture is filtered on a small pad of Al_2O_3. The solvent is completely removed, and the residual oil is purified by column chromatography (Hex:AcOEt, 1:1) to give a pale yellow oil (yield=64%). ^{1}H-NMR ($CDCl_3$-d, 500 MHz, 25°C), ppm: 7.10 (d, 1H, CH_{arom}), 6.69 (d, 1H, CH_{arom}), 4.59 (s, 2H, CH_2), 3.95 (s, 3H, OCH_3 r), 3.87 (s, 6H, OCH_3). ^{13}C-NMR ($CDCl_3$-d, 500 MHz, 25°C), ppm: 167.31, 153.17, 128.75, 127.50, 125.86, 113.49, 61.67, 56.02, 52.62, 43.77.

General procedure for the synthesis of 6,7-dimethoxyisoindolin-1-ones: **JBSD106** is dissolved in acetonitrile (6 mL) and triethylamine (2 eq) is added; the mixture is heated up to reflux. An equimolar amount of the amine is added, and the mixture is left reacting for 7 hours. The solvent is removed by rotavapor and the residue is portioned between water and CH_2Cl_2; the organic phase is extracted and dried with $MgSO_4$, filtered on a Buchner funnel and dried by vacuum. The residue is purified by column chromatography.

***2-benzyl-6,7-dimethoxyisoindolin-1-one*, JBSD107:** yellow powder (yield=52%). ^{1}H-NMR ($CDCl_3$-d, 500 MHz, 25°C), ppm: 7.34-7.25 (m, 5H, CH_{arom}), 7.06 (d, 1H, CH_{arom}), 6.99 (d, 1H, CH_{arom}), 4.74 (s, 2H, CH_2), 4.15 (s, 2H, CH_2), 4.11 (s, 3H, CH_3), 3.88 (s, 3H, CH_3). ^{13}C-NMR ($CDCl_3$-d, 500 MHz, 25°C), ppm: 166.77, 152.44, 147.48, 137.20, 134.60, 128.84, 128.33, 127.71, 124.95, 117.85, 116.54, 56.89,

48.57, 46.44. HR-RSI-TOFMS : m/z= 306.11 ($M+Na^+$). IR (ATR, cm^{-1}): ν_{CHarom}= 3002; $\nu_{C=O}$= 1677; ν_{C-N}= 1263. M.p.: 85-87°C.

***2-(3-chloro-4-fluorobenzyl)-6,7-dimethoxyisoindolin-1-one*, JBSD108:** yellow powder (yield= 20%). ^{1}H-NMR ($CDCl_3$-d, 500 MHz, 25°C), ppm: 7.33 (d, 1H, CH_{arom}), 7.16 (s, 1H, CH_{arom}), 7.07-7.00 (m, 3H, CH_{arom}), 4.66 (s, 2H, CH_2), 4.16 (s, 2H, CH_2), 4.08 (s, 3H, OCH_3), 3.86 (s, 3H, OCH_3). ^{13}C-NMR ($CDCl_3$-d, 500 MHz, 25°C), ppm: 166.84, 152.55, 147.53, 134.42, 144.32, 130.37, 128.08, 128.03, 124.60, 117.95, 117.03, 116.86, 116.77, 62.63, 56.87, 48.57, 45.39. HR-RSI-TOFMS : m/z= 358.06 ($M+Na^+$).

***6,7-dimethoxy-2-(4-methylbenzyl)isoindolin-1-one*, JBSD112:** yellow powder (yield= 40%). ^{1}H-NMR ($CDCl_3$-d, 500 MHz, 25°C), ppm: 7.19 (d, 2H, CH_{arom}), 7.12 (d, 2H, CH_{arom}), 7.05 (d, 1H, CH_{arom}), 6.98 (d, 1H, CH_{arom}), 4.70 (s, 2H, CH_2), 4.14 (s, 2H, CH_2), 4.11 (s, 3H, OCH_3), 3.87 (s, 3H, OCH_3), 2.32 (s, 3H, CH_3). ^{13}C-NMR ($CDCl_3$-d, 500 MHz, 25°C), ppm: 166.70, 152.39, 147.39, 137.38, 134.67, 134.17, 129.47, 128.33, 125.01, 117.86, 116.47, 62.65, 56.85, 48.49, 46.12, 21.18. HR-RSI-TOFMS : m/z= 320.12 ($M+Na^+$).

***2-(4-hydroxybenzyl)-6,7-dimethoxyisoindolin-1-one,* JBSD119:** yellow powder (yield= 51%). ^{1}H-NMR ($CDCl_3$-d, 500 MHz, 25°C), ppm: 7.13 (d, 2H, CH_{arom}), 7.05 (d, 1H, CH_{arom}), 6.99 (d, 1H, CH_{arom}), 6.80 (d, 2H, CH_{arom}), 4.65 (s, 2H, CH_2), 4.15 (s, 2H, CH_2), 4.08 (s, 3H, OCH_3), 3.87 (s, 3H, OCH_3). ^{13}C-NMR ($CDCl_3$-d, 500 MHz, 25°C), ppm: 167.03, 156.10, 152.44, 147.31, 134.59, 129.64, 128.38, 124.92, 122.50, 117.95, 116.68, 115.87, 62.56, 56.85, 48.67, 46.10. HR-RSI-TOFMS : m/z= 322.10 ($M+Na^+$).

***2-(4-fluorobenzyl)-6,7-dimethoxyisoindolin-1-one,* JBSD120:** pale-orange powder (yield= 32%). ^{1}H-NMR ($CDCl_3$-d, 500 MHz, 25°C), ppm: 7.27 (d, 2H, CH_{arom}), 7.06 (d, 1H, CH_{arom}), 7.02-6.98 (m, 3H, CH_{arom}), 4.70 (s, 2H, CH_2), 4.15 (s, 2H, CH_2), 4.10 (s, 3H, OCH_3), 3.88 (s, 3H, OCH_3). ^{13}C-NMR ($CDCl_3$-d, 500 MHz, 25°C), ppm: 166.74, 152.43, 147.37, 134.45, 129.95, 124.79, 117.95, 116.57, 115.73,

115.56, 62.59, 56.81, 48.49, 45.65. HR-RSI-TOFMS : m/z= 324.10 ($M+Na^+$). IR (ATR, cm^{-1}): ν_{CHarom}= 2958; $\nu_{C=O}$= 1676; ν_{C-N}= 1268; ν_{C-F}= 818. M.p.: 128-130°C.

6,7-dimethoxy-2-(naphthalen-2-ylmethyl)isoindolin-1-one, **JBSD121:** pale-orange powder (yield= 20%). ^{1}H-NMR ($CDCl_3$-d, 500 MHz, 25°C), ppm: 7.90-7.79 (m, 3H, CH_{arom}), 7.74 (s, 1H, CH_{arom}), 7.48-7.42 (m, 3H, CH_{arom}), 7.05 (d, 1H, CH_{arom}), 6.97 (d, 1H, CH_{arom}), 4.90 (s, 2H, CH_2), 4.17 (s, 2H, CH_2), 4.14 (s, 3H, OCH_3), 3.88 (s, 3H, OCH_3). ^{13}C-NMR ($CDCl_3$-d, 500 MHz, 25°C), ppm: 166.86, 152.46, 147.48, 134.72, 134.61, 132.41, 132.92, 128.78, 127.81, 127.06, 126.35, 126.09, 124.94, 117.89, 116.58, 62.71, 56.88, 48.61, 46.62. HR-RSI-TOFMS : m/z= 356.12 ($M+Na^+$).

6,7-dimethoxy-2-(naphthalen-1-ylmethyl)isoindolin-1-one**, JB137:** yellow powder (yield= 47%). ^{1}H-NMR ($CDCl_3$-d, 500 MHz, 25°C), ppm: 8.27 (d, 1H, CH_{arom}), 7.87 (t, 2H, CH_{arom}), 7.58-7.44 (m, 4H, CH_{arom}), 7.04 (d, 1H, CH_{arom}), 6.93 (d, 1H, CH_{arom}), 5.22 (s, 2H, CH_2), 4.16 (s, 3H, OCH_3), 4.04 (s, 2H, CH_2), 3.80 (s, 3H, OCH_3).

6,7-dimethoxy-2-(4-(trifluoromethyl)benzyl)isoindolin-1-one, **JB139:** pale-yellow powder (yield= 47%).^{1}H-NMR ($CDCl_3$-d, 500 MHz, 25°C), ppm: 7.57 (d, 2H, CH_{arom}), 7.41 (d, 2H, CH_{arom}), 7.08 (d, 1H, CH_{arom}), 7.01 (d, 1H, CH_{arom}), 4.79 (s, 2H, CH_2), 4.17 (s, 2H, CH_2), 4.10 (s, 3H, OCH_3), 3.88 (s, 3H, OCH3. ^{13}C-NMR ($CDCl_3$-d, 500 MHz, 25°C), ppm: 166.94, 152.58, 147.64, 141.34, 134.40, 129.95, 128.49, 125.81, 124.60, 117.89, 116.87, 62.63, 55.97, 56.91, 48.67, 46.05. IR (ATR, cm^{-1}): ν_{CHarom}=2954, 2915, 2848; $\nu_{C=O}$= 1676; ν_{C-N}= 1271. M.p.:109-112°C.

6,7-dimethoxy-2-(4-nitrobenzyl)isoindolin-1-one, **JB140:** pale solid (yield=10%).^{1}H-NMR ($CDCl_3$-d, 500 MHz, 25°C), ppm: 8.17 (d, 2H, CH_{arom}), 7.46 (d, 2H, CH_{arom}), 7.09 (d, 1H, CH_{arom}), 7.03 (d, 1H, CH_{arom}), 4.83 (s, 2H, CH_2), 4.20 (s, 2H, CH_2), 4.09 (s, 3H, OCH_3), 3.88 (s, 3H, OCH_3). IR (ATR, cm^{-1}): ν_{CHarom}=2924, 2848; $\nu_{C=O}$= 1683; ν_{NO2}= 1492, 1341; ν_{C-N}= 1262. Anal. Calcd. for $C_{17}H_{16}N_2O_5 \cdot ¾\ H_2O$: C 59.73, H 5.16, N 8.20. Found: C 59.46, H 5.16, N 7.55. M.p.:115-117°C.

***2-(4-hydroxyphenethyl)-6,7-dimethoxyisoindolin-1-one*, JB141:** yellow powder (yield=22%). ^{1}H-NMR ($CDCl_3$-d, 500 MHz, 25°C), ppm: 7.06-6.99 (m, 4H, CH_{arom}), 6.78 (d, 2H, CH_{arom}), 6.29 (s, br, OH), 4.13 (s, 2H, CH_2), 4.05 (s, 3H, OCH_3), 3.87 (s, 3H, OCH_3), 3.76 (t, 2H, CH_2), 2.87 (t, 2H, CH_2). ^{13}C-NMR ($CDCl_3$-d, 500 MHz, 25°C), ppm: 167.05, 154.97, 152.43, 134.64, 129.78, 125.13, 117.75, 116.62, 115.71, 62.59, 56.90, 49.72, 44.43, 33.90. IR (ATR, cm^{-1}): ν_{OH}=3317; ν_{CHarom}=2996, 2926; $\nu_{C=O}$= 1656; ν_{C-N}= 1267. Anal. Calcd. for $C_{18}H_{19}NO_4 \cdot ½\ H_2O$: C 67.07, H 6.25, N 4.35. Found: C 67.23, H 6.15, N 4.23. M.p.: 174-176°C.

General procedure to get 6,7-dihydroxyisoindolin-1-ones: 6,7-dimethoxyisoindolin-1-ones are dissolved in dry dichloromethane (5 mL), in a dried round bottom double-necked flask; the solution is purged with nitrogen flux for 30 min, then it is cooled to -78° C. Boron tribromide 99% (8.5 eq) is slowly added to the solution, which is allowed to return to r.t. After 4 hours volatiles are eliminated by vacuum, then the solid is quenched with methanol; it is dried by rotovap and the solid is portioned between water and EtO_2. The organic phase is extracted, washed with water and dried by rotovap to give the final product.

***2-benzyl-6,7-dihydroxyisoindolin-1-one,* JBSD109:** pale-grey powder (yield= 40%). ^{1}H-NMR ($CDCl_3$-d, 500 MHz, 25°C), ppm: 7.35-7.25 (m, 5H, CH_{arom}), 7.04 (d, 1H, CH_{arom}), 6.75 (d, 1H, CH_{arom}), 4.72 (s, 2H, CH_2), 4.20 (s, 2H, CH_2). ^{13}C-NMR ($CDCl_3$-d, 500 MHz, 25°C), ppm: 143.21, 142.07, 136.61, 132.10, 128.97, 128.16, 127.94, 119.67, 117.53, 114.49, 49.80, 46.16. HR-RSI-TOFMS : m/z= 356.09 ($M+Na^+$). IR (ATR, cm^{-1}): ν_{OH}= 3336; ν_{CHarom}= 3028, 2915; $\nu_{C=O}$= 1661; ν_{C-N}= 1270. Anal. Calcd. for $C_{15}H_{13}NO_3$: C 70.55, H 5.10, N 5.49. Found: C 70.10, H 5.26, N 5.10. M.p.: 148-152°C.

***2-(3-chloro-4-fluorobenzyl)-6,7-dihydroxyisoindolin-1-one*, JBSD110:** beige powder (yield= 90%). ^{1}H-NMR ($CDCl_3$-d, 500 MHz, 25°C), ppm: 7.32 (d, 1H, CH_{arom}), 7.17-7.08 (m, 3H, CH_{arom}), 7.05 (d, 1H, CH_{arom}), 6.77 (d, 1H, CH_{arom}), 4.66 (s, 2H, CH_2), 4.20 (s, 2H, CH_2). ^{13}C-NMR ($CDCl_3$-d, 500 MHz, 25°C),

ppm: 168.49, 157.98, 156.02, 144.99, 143.53, 136.14, 132.85, 130.32, 120.07, 119.95, 118.28, 114.29, 49.24, 44.57. HR-RSI-TOFMS : m/z= 308.04 ($M+H^+$). IR (ATR, cm^{-1}): ν_{OH}= 3302; ν_{CHarom}= 2922; $\nu_{C=O}$= 1660; ν_{C-N}= 1246; ν_{C-F}= 783; ν_{C-Cl}= 668. Anal. Calcd. for $C_{15}H_{11}NO_3FCl$: C 58.55, H 3.60, N 4.60. Found: C 58.21, H 3.96, N 4.20. M.p.: 157-161°C.

6,7-dihydroxy-2-(4-methylbenzyl)isoindolin-1-one, **JBSD113:** beige powder (yield= 85%). ^{1}H-NMR ($CDCl_3$-d, 500 MHz, 25°C), ppm: 7.17-7.13 (m, 4H, CH_{arom}), 7.02 (d, 1H, CH_{arom}), 6.74 (d, 1H, CH_{arom}), 4.67 (s, 2H, CH_2), 4.17 (s, 2H, CH_2), 2.32 (s, 3H, CH_3). ^{13}C-NMR ($CDCl_3$-d, 500 MHz, 25°C), ppm: 154.97, 143.25, 142.06, 137.70, 135.42, 133.55, 132.13, 129.62, 128.18, 119.66, 114.46, 49.72, 45.89, 21.18. HR-RSI-TOFMS : m/z= 292.09 ($M+Na^+$). IR (ATR, cm^{-1}): ν_{OH}= 3229; ν_{CHarom}= 2920; $\nu_{C=O}$= 1640; ν_{C-N}= 1303. Anal. Calcd. for $C_{18}H_{19}NO_3$: C 72.64, H 6.39, N 4.71. Found: C 73.10, H 6.71, N 4.41. M.p.: 124-127°C.

6,7-dihydroxy-2-(4-hydroxybenzyl)isoindolin-1-one, **JBSD124:** beige powder (yield= 54%). ^{1}H-NMR ($CDCl_3$-d, 500 MHz, 25°C), ppm: 7.16 (d, 2H, CH_{arom}), 7.03 (d, 1H, CH_{arom}), 6.80 (d, 2H, CH_{arom}), 6.75 (d, 1H, CH_{arom}), 4.64 (s, 2H, CH_2). ^{13}C-NMR ($CDCl_3$-d, 500 MHz, 25°C), ppm: 168.38, 157.20, 144.84, 143.43, 132.61, 129.65, 128.14, 120.00, 118.53, 115.89, 114.29, 48.93, 45.08. HR-RSI-TOFMS : m/z= 272.09 ($M+Na^+$). IR (ATR, cm^{-1}): ν_{OH}= 3454; ν_{CHarom}= 2973; $\nu_{C=O}$= 1652; ν_{C-N}= 1265; ν_{C-OH}= 1076. Anal. Calcd. for $C_{15}H_{13}NO_4 \cdot 1/3\ H_2O$: C 64.98, H 4.97, N 5.05. Found: C 65.02, H 5.21, N 4.65. M.p.: 209-211°C.

6,7-dihydroxy-2-(naphthalen-2-ylmethyl)isoindolin-1-one**, JBSD125:** beige powder (yield= 87%). ^{1}H-NMR ($CDCl_3$-d, 500 MHz, 25°C), ppm: 7.83-7.80 (m, 3H, CH_{arom}), 7.73 (s, 1H, CH_{arom}), 7.49-7.47 (m, 2H, CH_{arom}), 7.40 (d, 1H, CH_{arom}), 7.04 (d, 1H, CH_{arom}), 6.74 (d, 1H, CH_{arom}), 4.88 (s, 2H, CH_2), 4.21 (s, 3H, CH_2). ^{13}C-NMR ($CDCl_3$-d, 500 MHz, 25°C), ppm: 166.86, 152.46, 147.48, 134.72, 134.61, 132.41, 132.92, 128.78, 127.81, 127.06, 126.35, 126.09, 124.94, 117.89, 116.58, 62.71, 56.88. HR-RSI-TOFMS : m/z= 306.11 ($M+Na^+$). IR (ATR, cm^{-1}): ν_{OH}= 3166, 3383; ν_{CHarom}= 2921, 2851; $\nu_{C=O}$= 1652;

ν_{C-N}= 1259. Anal. Calcd. for $C_{19}H_{15}NO_3$· 1/8 H_2O: C 74.19, H 5.00, N 4.55. Found: C 74.35, H 5.35, N 4.56. M.p.: 193-196°C.

***2-(4-fluorobenzyl)-6,7-dihydroxyisoindolin-1-one*, JBSD126:** pale-grey powder (yield= 58%). ^{1}H-NMR ($CDCl_3$-d, 500 MHz, 25°C), ppm: 7.30 (d, 2H, CH_{arom}), 7.18 (d, 2H, CH_{arom}), 6.96 (d, 1H, CH_{arom}), 6.76 (d, 1H, CH_{arom}), 4.63 (s, 2H, CH_2), 4.19 (s, 2H, CH_2). ^{13}C-NMR ($CDCl_3$-d, 500 MHz, 25°C), ppm: 169.80, 143.34, 142.14, 132.44, 131.99, 129.92, 119.88, 117.42, 115.96, 115.79, 114.53, 49.73, 45.47. HR-RSI-TOFMS : m/z= 274.08 ($M+H^+$). IR (ATR, cm^{-1}): ν_{OH}= 3336; ν_{CHarom}= 2959, 2923, 2857; $\nu_{C=O}$= 1661; ν_{C-N}= 1270; ν_{C-F}= 781. Anal. Calcd. for $C_{15}H_{12}NO_3F$: C 65.93, H 4.40, N 5.13. Found: C 65.98, H 4.64, N 4.86. M.p.: 155-158°C.

***6,7-dihydroxy-2-(naphthalen-1-ylmethyl)isoindolin-1-one,* JB142:** pale-beige powder (yield=27%). ^{1}H-NMR ($CDCl_3$-d, 500 MHz, 25°C), ppm: 8.19 (d, 1H, CH_{arom}), 7.87-7.83 (m, 2H, CH_{arom}), 7.54 (t, 1H, CH_{arom}), 7.45 (t, 1H, CH_{arom}), 7.44 (d, 1H, CH_{arom}), 6.99 (d, 1H, CH_{arom}), 6.68 (d, 1H, CH_{arom}), 5.16 (s, 2H, CH_2), 4.07 (s, 2H, CH_2). ^{13}C-NMR ($CDCl_3$-d, 500 MHz, 25°C), ppm: 169.38, 143.18, 142.04, 134.02, 132.17, 132.05, 131.52, 129.22, 128.85, 127.51, 127.04, 126.29, 125.30, 123.62, 119.60, 117.54, 114.45, 49.86, 44.41. ESI-MS (pos ions): m/z = 327 [$HL+Na^+$]. IR (ATR, cm^{-1}): ν_{OH}= 3322; ν_{CHarom}= 2980, 2920, 2850; $\nu_{C=O}$= 1652; ν_{C-N}= 1259. Anal. Calcd. for $C_{19}H_{15}NO_3$ · 4/3 H_2O: C 62.13, H 5.76, N 4.53. Found: C 62.56, H 5.57, N 4.36. M.p.: 165-167°C.

***6,7-dihydroxy-2-(4-hydroxyphenethyl)isoindolin-1-one*, JB143:** pale powder (yield=25%).^{1}H-NMR (MeOD-d, 500 MHz, 25°C), ppm: 7.03 (d, 2H, CH_{arom}), 6.93 (d, 2H, CH_{arom}), 6.73 (d, 1H, CH_{arom}), 6.67 (d, 1H, CH_{arom}), 4.15 (s, 2H, CH_2), 3.93 (t, 2H, $CH_{2\text{-ethyl}}$), 2.84 (t, 2H, $CH_{2\text{-ethyl}}$). ^{13}C-NMR (MeOD-d, 500 MHz, 25°C), ppm: 169.79, 155.77, 144.06, 142.94, 132.65, 129.54, 129.42, 129.39, 119.63, 115.05, 113.54, 50.20, 43.88, 33.42. ESI-MS (pos ions): m/z= 308 $[HL+Na]^+$. IR (ATR, cm^{-1}): ν_{OH}= 3322, 3550, 3480; ν_{CHarom}= 2917, 2848; $\nu_{C=O}$= 1645; ν_{C-N}= 1224. Anal. Calcd. for $C_{19}H_{15}NO_3$ · 11/4 H_2O: C 64.31, H 5.82, N 3.95. Found: C 64.41, H 5.53, N 3.50. M.p.:204-209°C.

***6,7-dihydroxy-2-(4-nitrobenzyl)isoindolin-1-one*, JB144:** pale powder (yield=24%). ^{1}H-NMR ($CDCl_3$-d, 500 MHz, 25°C), ppm: 8.20 (d, 2H, CH_{arom}), 7.45 (d, 2H, CH_{arom}), 7.07 (d, 1H, CH_{arom}), 6.80(d, 1H, CH_{arom}), 4.82 (s, 2H, CH_2), 4.24 (s, 2H, CH_2). ^{13}C-NMR ($CDCl_3$-d, 500 MHz, 25°C), ppm: 170.04, 144.07, 143.45, 142.16, 131.79, 128.73, 124.26, 120.09, 116.98, 114.70, 50.01, 45.60, 29.78. ESI-MS (pos ions): m/z= 323 $[HL+Na]^+$ Anal. Calcd. for $C_{15}H_{12}N_2O_5 \cdot H_2O$: C 56.60, H 4.43, N 8.33. Found: C 56.68, H 4.92, N 8.03. M.p.:160-165°C.

***6,7-dihydroxy-2-(4-(trifluoromethyl)benzyl)isoindolin-1-one,* JB146:** brown powder (yield=80%). ^{1}H-NMR (DMSO-d_6, 500 MHz, 25°C), ppm: 7.89 (d, 2H, CH_{arom}), 7.33 (d, 2H, CH_{arom}), 6.93 (d, 1H, CH_{arom}), 6.74 (d, 1H, CH_{arom}), 4.68 (s, 2H, CH_2), 4.21 (s, 2H, CH_2). ESI-MS (pos ions): m/z = 324 $[HL+H^+]$.

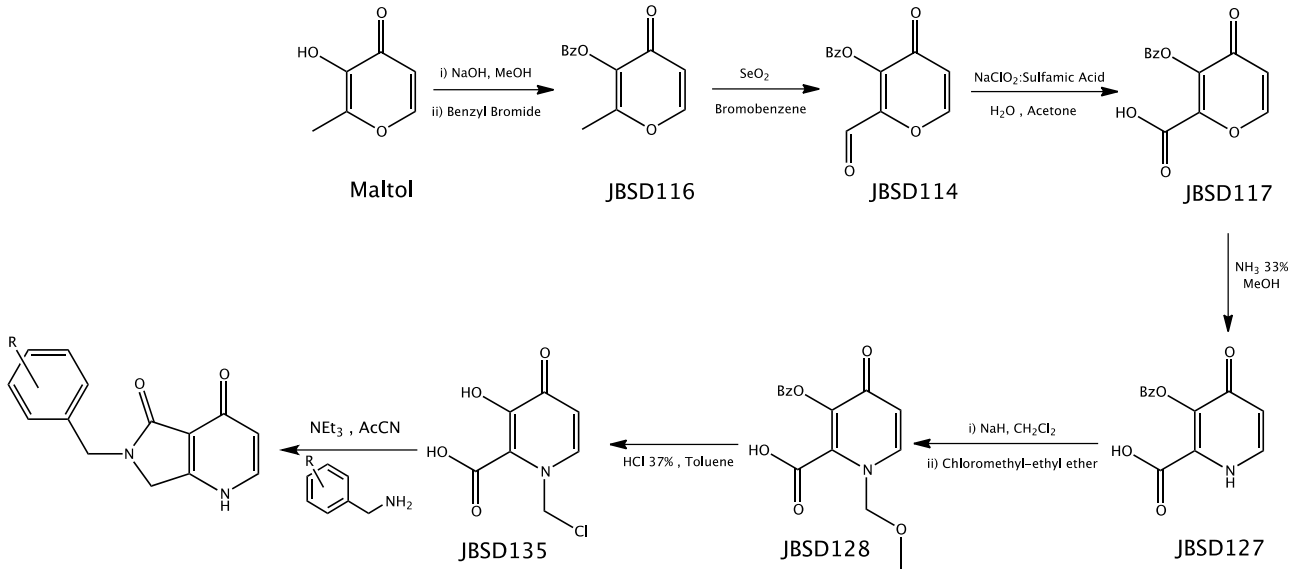

***Benzyl-maltol,* JBSD116:** Maltol (100 g, 1 eq, 0.793 mol) is dissolved in methanol (1 L) at 30°C; a 1M sodium hydroxide (30.2 g, 0.952 eq, 0.755 mol) solution is slowly added. Benzyl bromide (107 mL, 0.87 eq, 0.69 mol) is added dropwise to the solution, which is heated up to 58°C and it is left reacting overnight. The solution is cooled to room temperature and the solvent is removed by rotovap. The solid residue is dissolved in 100 ml of CH_2Cl_2, washed with 5% NaOH (2x50 ml), then water (2x50 ml); the organic phase is dried with $MgSO_4$, filtered and the solvent is removed by vacuum. The red solid is left decanting in Et_2O for one night; it is filtered on Buchner funnel and dried by vacuum to

give a yellow solid (yield= 70%). ^{1}H-NMR (DMSO-d_6, 500 MHz, 25°C), ppm: 8.01 (d, 1H, CH), 7.37-7.30 (m, 5H, CH_{arom}), 6.33 (d, 1H, CH), 4.99 (s, 2H, CH_2), 2.08 (s, 3H, CH_3). ^{13}C-NMR (DMSO-d_6, 500 MHz, 25°C), ppm: 174.50, 159.80, 155.54, 143.67, 137.441, 129.33, 129.03, 128.72, 116.96, 73.20, 15.00. ESI-MS (pos ions): m/z= 239 $[HL+Na]^+$. IR (ATR, cm^{-1}): ν_{CH}= 3074, 2961, 2886; $\nu_{C=O}$=1640; ν_{C-O}= 1250; ν_{C-Opir}= 1179. Anal. Calcd. for $C_{13}H_{12}O_3$: C 72.22, H 5.55. Found: C 72.11, H 5.58. M.p.:54-57°C.

3-(benzyloxy)-4-oxo-4H-pyran-2-carbaldehyde, **JBSD114: JBSD116** (5.1166 g, 1 eq, 23.66 mmol) and selenium dioxide (7.716 g, 2.939 eq, 69.53 mmol) are dissolved into bromobenzene (80 mL) and the mixture is heated up to reflux and it is left reacting for 19 hours. The solution is allowed to return to room temperature, and it is filtered to remove the black solid. The dark red solution is dried by rotavap and the dark brown oil is purified by column chromatography (Hex:AcOEt, 1:1) to get a brown oil (yield= 27%). ^{1}H-NMR (DMSO-d_6, 500 MHz, 25°C), ppm: 9.87 (s, 1H, $CH_{aldehyde}$), 7.73 (d, 1H, CH), 7.35 (br, 5H, CH_{arom}), 6.49 (d, 1H, CH), 5.51 (s, 2H, CH_2). ^{13}C-NMR (DMSO-d_6, 500 MHz, 25°C), ppm: 182.72, 177.04, 154.29, 151.94, 135.09, 129.31, 128.99, 128.66, 128.55, 118.4 , 75.09. ESI-MS (pos ions): m/z= 255 $[HL+Na]^+$.

3-(benzyloxy)-4-oxo-4H-pyran-2-carboxylic acid, **JBSD117:** sodium chlorite (1.8342 g, 2.132 eq, 20.28 mmol) and sulfamic acid (2.8109 g, 3.043 eq, 28.95 mmol) are dissolved in H_2O (20 mL) at 0°C. **JBSD114** (2.1902 g, 1 eq, 9.5135 mmol) is dissolved in Acetone (20 mL) and it is added dropwise to the aqueous solution; the mixture is left reacting for 30 min. A white precipitate is formed and it is isolated by filtration, washed with cold water, then diethyl ether; it is dried by vacuum (yield=45%).^{1}H-NMR (DMSO-d_6, 500 MHz, 25°C), ppm: 8.20 (d, 1H, CH), 7.44 (d, 2H, CH_{arom}), 7.37-7.31 (m, 3H, CH_{arom}), 6.55 (d, 1H, CH), 5.10 (s, 2H, CH_2). ^{13}C-NMR (DMSO-d_6, 500 MHz, 25°C), ppm: 176.01, 161.21, 156.20, 147.89, 137.01, 128.75, 128.67, 128.57, 117.54, 74.04. ESI-MS (pos ions): m/z= 246 $[HL+H]^+$. M.p.:164-166°C.

***3-(benzyloxy)-4-oxo-1,4-dihydropyridine-2-carboxylic acid,* JBSD127: JBSD117** (1.0028 g, 1 eq, 4.0728 mmol), methanol (10 mL) and ammonia solution (8 mL) are placed in a high pressure vessel; the yellow solution is heated up to 95°C and it is left reacting for 17 hour. The solution is allowed to return to room temperature and all the solvent is removed by vacuum. The residue is dissolved in water and 37% HCl is added until pH=1. Solution is cooled to 4°C and a thin precipitate is formed; the solid is isolated by filtration on Buchner funnel and dried by vacuum (yield=54%). ^{1}H-NMR (DMSO-d_6, 500 MHz, 25°C), ppm: 8.11 (d, 1H, CH), 7.44 (d, 2H, CH_{arom}), 7.36-7.31 (m, 3H, , CH_{arom}), 7.22 (d, 1H, CH), 5.10 (s, 2H, CH_2). ESI-MS (pos ions): m/z= 247 $[HL+H]^+$. IR (ATR, cm^{-1}): ν_{NH}= 3310; ν_{OH}= 3144; ν_{CH}= 3091, 3019, 2851; $\nu_{C=Oacid}$= 1724; $\nu_{C=O}$=1604; ν_{C-O}= 1214. Anal. Calcd. for $C_{13}H_{11}NO_4$ ·1/2 H_2O: C 57.35, H 5.18, N 5.14. Found: C 57.41, H 4.90, N 5.18.

***3-(benzyloxy)-1-(ethoxymethyl)-4-oxo-1,4-dihydropyridine-2-carboxylic acid,* JBSD128: JBSD127** (397.21 mg, 1 eq, 1.6197 mmol) is dissolved into dry DMF (4 mL) in a dried double-necked round bottom flask, under nitrogen flux; it is heated up to 50°C. Sodium hydride (38.87 mg, 1 eq, 1.6197 mmol) is added and it is left reacting for 15 min. Chloromethyl-ethyl ether (225 µL, 1.5 Eq, 2.4296 mmol) is added dropwise over a period of 10 min and it is left reacting for 2 days monitoring by TLC (MeOH: CH_2Cl_2, 1:9). Water is added and then it is extracted with chloroform; the organic phase is washed with brine (20 ml x2) then H_2O (20 ml x2). All chloroform is removed by vacuum to get the final product as a pale-brown powder (yield= 51%). ^{1}H-NMR (DMSO-d_6, 400 MHz, 25°C), ppm: 7.70 (d, 1H, CH), 7.64 (s, 1H, OH), 7.43 (m, 5H, CH_{arom}), 6.17 (d, 1H, CH), 5.17 (s, 2H, CH_2), 5.00 (s, 2H, $CH_{2\text{-}ether}$), 3.38-3.35 (m, 2H, $CH_{2\text{-}ethyl}$), 1.06 (t, 3H, CH_3). M.p.:235-237°C.

***1-(chloromethyl)-3-hydroxy-4-oxo-1,4-dihydropyridine-2-carboxylic acid*, JB135: JBSD128** (153 mg, 1 eq, 504 µmol) is dissolved into a mixture of toluene (5 mL) and HCl (5 mL); it is vigorously stirred for 1 hour at rt, monitoring by TLC (MeOH:CH_2Cl_2, 1:9). The aqueous phase is extracted and dried by rotovap. The residue is extracted with water/chloroform, the aqueous phase is extracted and

dried by vacuum to give the product as a white powder (yield= 58%).^{1}H-NMR (DMSO-d_6, 400 MHz, 25°C), ppm: 8.25 (d, 1H, CH), 7.24 (d, 1H, CH), 5.51 (s, 2H, $CH_{2\text{-ether}}$).

3.RESULTS and DISCUSSION

3.1 2,3-DIHYDRO-6,7-DIHYDROXY-1H-ISOINDOL-1-ONE-BASED INHIBITORS

3.1.1 Synthesis and Characterization

In a previous work from Zhao et collaborators[120] the isoindol-1-one scaffold has been explored as an innovative chelating motif for magnesium ions that are present in the active pocket of HIV integrase. Data obtained with this scaffold were really promising, with IC_{50} values in the low micromolar range. In view of the structural similarities of the catalytic site of HIV integrase and influenza endonuclease, we have decided to study the activity of the same class of derivatives against PA_N endonuclease, which shares with HIV integrase structural homologies and the same "two-metal ion" catalytic mechanism. Several are the favorable features of this kind of molecular skeleton: the presence of three donor oxygen atoms, which have a good affinity for Mg^{2+} metal ions, with a good preorganization (*i.e.* well-defined geometry and rigidity) and orientation in order to chelate both metal cofactors at the same time (a two-metal binding region, Figure 17). Moreover, the presence of a lipophilic portion, the benzyl group, can enhance the activity of derivatives because it can interact with different pockets that surround the catalytic center (Figure 17).

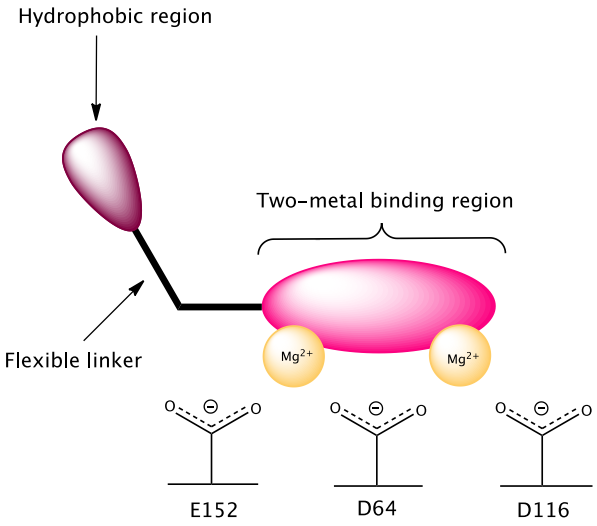

Figure 17. Schematic representation of the chelating ligand, with the two-metal binding region and the hydrophobic moiety.

In order to highlight a possible relationship between the activity of the isoindol-1-ones and their chemical structures, the use of several substituents at the 4-position on the aromatic ring has been explored.

A synthetic pathway already reported in the literature has been followed [323], with some modifications, as highlighted in Scheme 1.

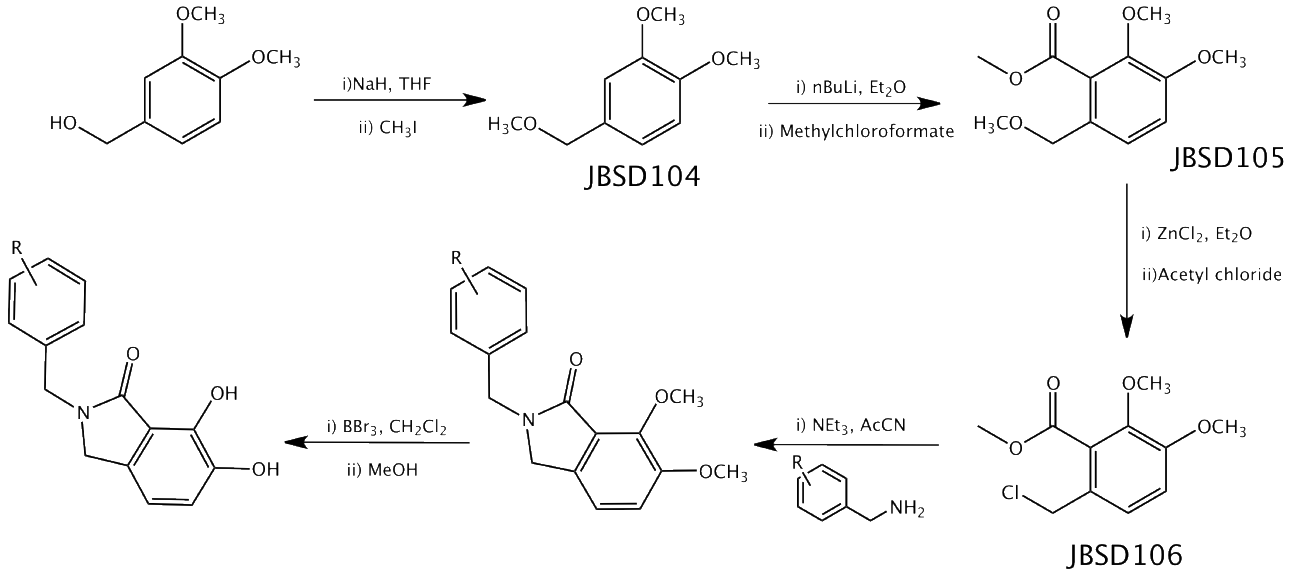

Scheme 34. Synthetic pathway for the synthesis of the isoindol-1-ones.

First, the hydroxyl group of 3,4-dimethoxybenzyl alcohol has been subjected to a protection reaction to be converted to the methoxy form; several attempts have been made in order to improve this synthetic step and we have been finally able to quantitatively isolate derivative **JBSD104**. NaH is added portionwise to a solution of 3,4-dimethoxybenzyl alcohol in distilled THF, under nitrogen atmosphere at 0°C, then iodomethane is added dropwise and the solution is stirred at room temperature for 4 hours. The final colorless oil is obtained by purification on column chromatography (Hex:AcOEt, 8:2) and it has been fully characterized by common spectroscopic techniques. In the ^{1}H-NMR (Figure 18) it can be seen the singlet at 3.37 ppm, which is related to the methoxy group, that gives confirmation of the success of the reaction; all the other signals are in the expected range (Figure 18).

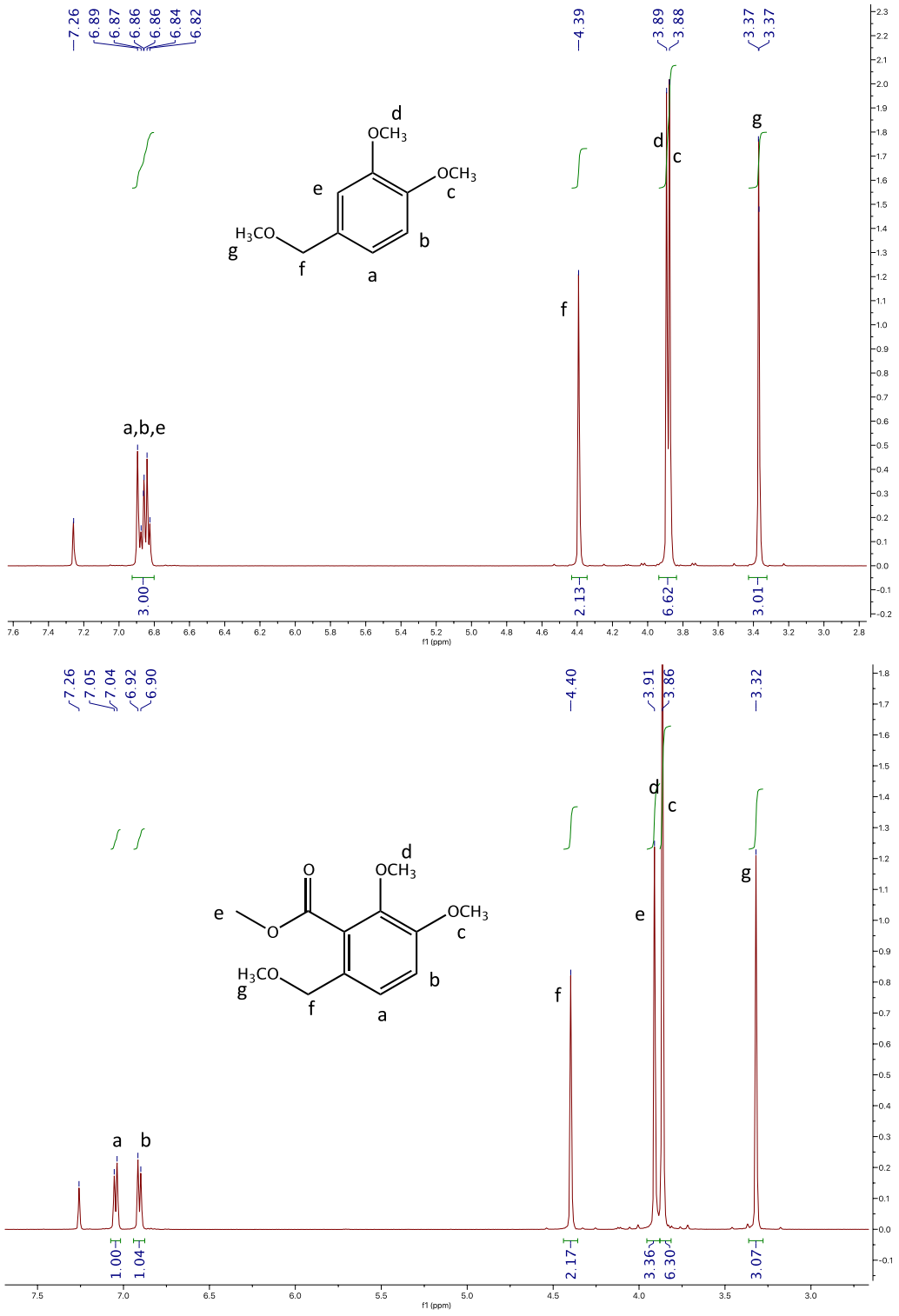

*Figure 18. ^{1}H-NMR ($CDCl_3$-d, 500 MHz, 25°C) spectra of derivatives **JBSD104** (on the top) and **JBSD105** (on the bottom).*

Then, after a proper lithiation reaction, **JBSD104** has been made reacting with methyl chloroformate under inert conditions at -80°C; the final product **JBSD105** is obtained as pale-yellow oil by column chromatography (Hex:AcOEt, 8:2). In the ^{1}H-NMR spectrum (Figure 18, bottom) we can see that the singlet relative to the aromatic proton (*e*) of the parent compound disappeared, while a singlet

relative to the OCH_3 (e) arises at 3.91 ppm. One species is present in solution, confirming that the formylation occurred only at the 2-position.

In order to get the chloride form **JBSD106**, several synthetic attempts have been made to find the best molar ratio between zinc chloride and **JBSD105** (Table 1):

JBSD105	1	1	1	1
$ZnCl_2$	0.01	0.4	1	0.5

Yield	25%	57%	**0%**	**84%**

*Table 1. Summary of molar ratios explored between $ZnCl_2$ and **JBSD105** with the relative yields*

We have finally been able to isolate in high yield the chloride form **JBSD106** by adding acetyl chloride to a mixture of **JBSD105**:$ZnCl_2$, 1:0.5, under nitrogen atmosphere. After filtration on Al_2O_3, the final product has been isolated as a yellow oil by purification on column chromatography (Hex:AcOEt, 1:1). ^{1}H-NMR (Figure 19) has confirmed that the S_N2 reaction occurred.

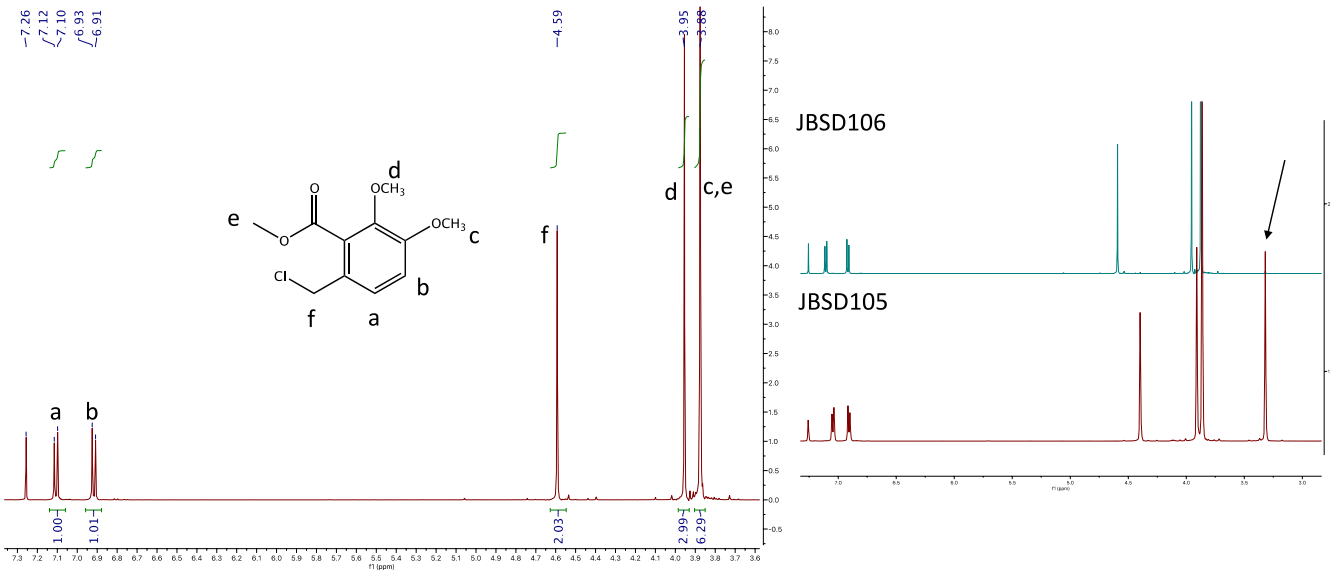

*Figure 19. ^{1}H-NMR spectrum ($CDCl_3$-d, 500 MHz, 25°C) of **JBSD106** and the comparison with **JBSD105**.*

The shift of the signal relative to the methylene CH_2 of about 0.19 ppm to higher ppm (from 4.40 to 4.59 ppm) and the disappearance of the singlet at 3.32 ppm relative to the OCH_3 group bounded to

the methylene carbon are evidences that the substitution has occurred as expected and as confirmed also by ESI-MS analysis.

Compound **JBSD106** is now made reacting with different 4-substituted benzyl amines in order to isolate the set of 6,7-dimethoxy derivatives represented in Figure 20:

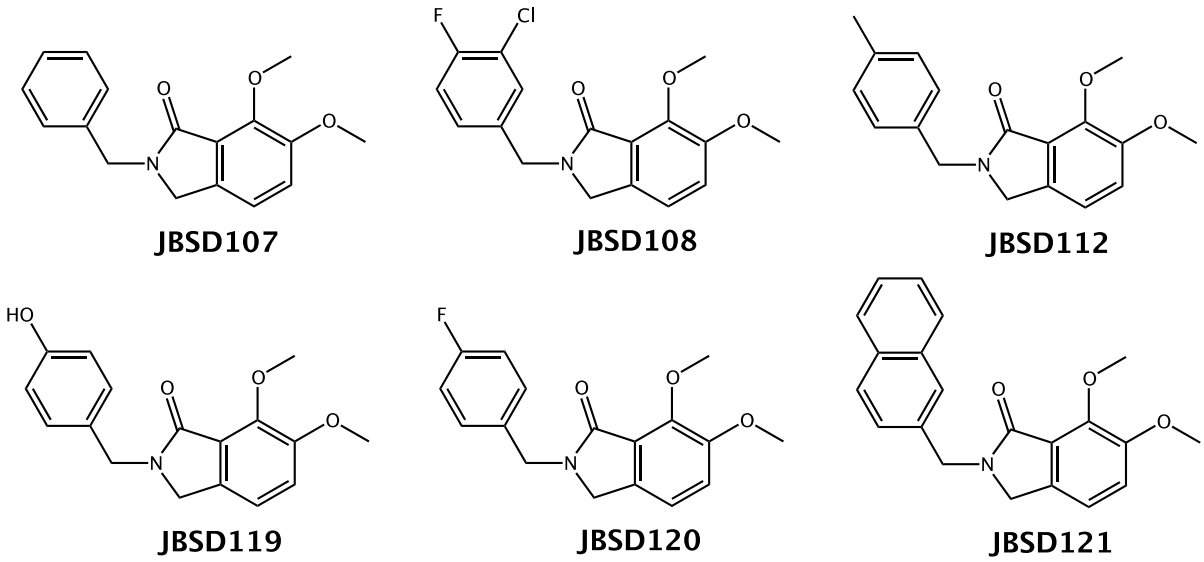

Figure 20. 2,3-dihydro-6,7-dimethoxy-1H-isoindol-1-ones molecular structures.

JBSD106 is made reacting with the corresponding benzylamine in acetonitrile, in presence of triethylamine; all compounds are purified by column chromatography (Hex:AcOEt) and they have been characterized through the most common techniques, like $^{1}H/^{13}C$-NMR, ATR-IR and ESI-MS.

In Figure 21 it is reported the ^{1}H-NMR spectrum of **JBSD107** as an example. This spectrum shows the expected signals pattern typical of such class of compounds[323].

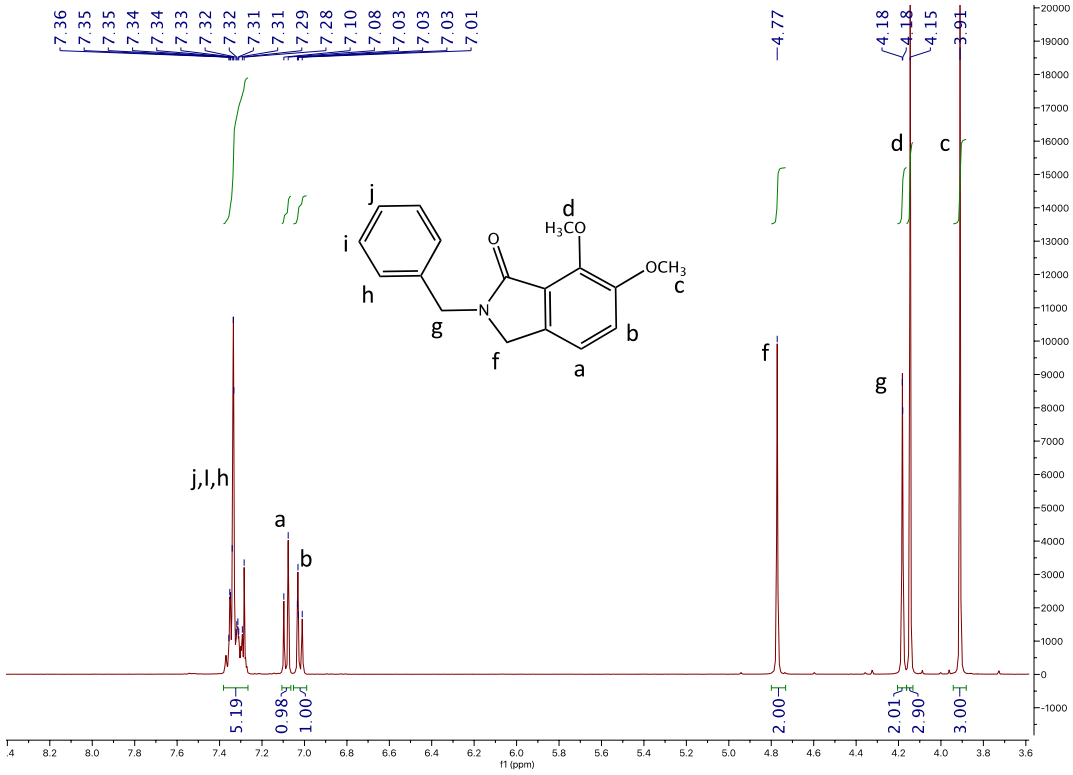

*Figure 21. 1H-NMR ($CDCl_3$-d, 500 MHz, 25°C) of derivative **JBSD107**.*

In the IR spectrum it is possible to see the stretching bands relative to the C=O and C-N bonds at 1674 and 1263 cm^{-1}, respectively.

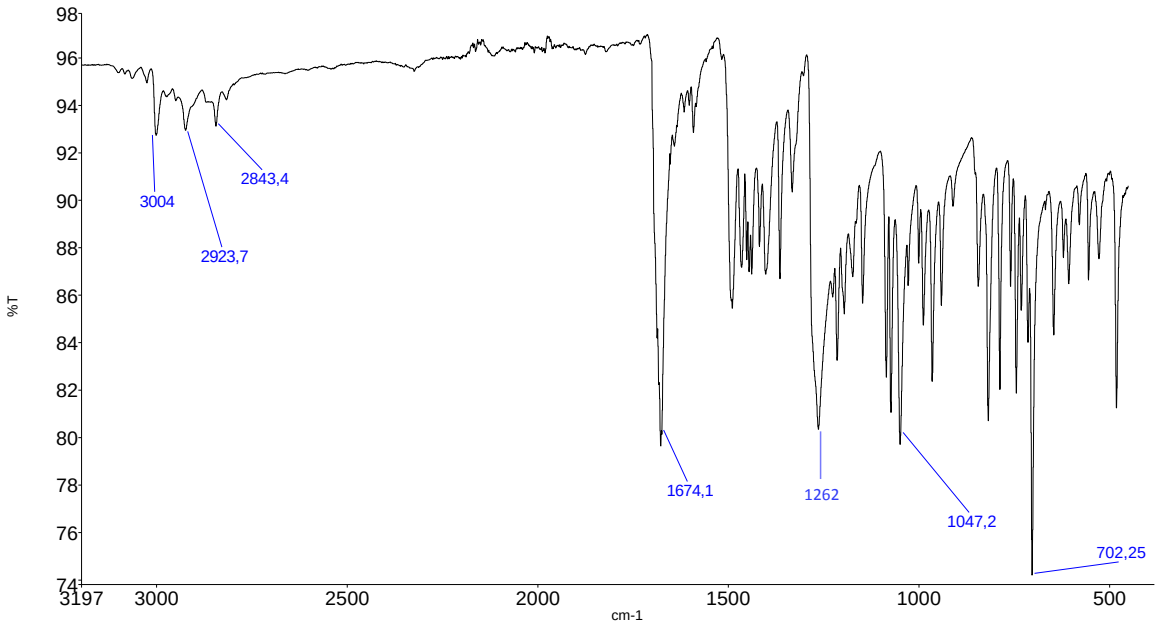

*Figure 22. ATR-IR spectrum of derivatives **JBSD107**.*

Crystals suitable for X-ray analysis have been obtained by slow evaporation of a solution of **JBSD108** (Hex:AcOEt, 3:7): it is possible to notice that the isoindol-1-one portion and the 3,4-substituted phenyl group do not lay on the same plane, but they are on planes forming an angle of about 88° (Figure 23).

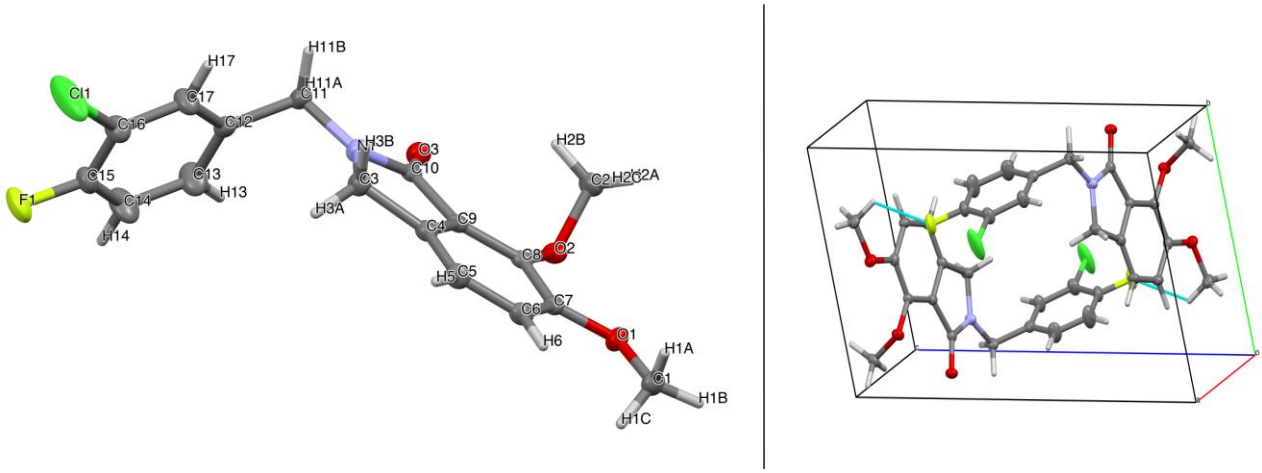

*Figure 23. Crystalline structure (100 K) of **JBSD108** (on the left) and of the corresponding unit cell (on the right).*

The unit cell results to be P_{-1}, with a intermolecular halogen bond of 2.62 Å between the fluorine atom F_1 and H_{1C} of a methoxy group of an adjacent molecule; no hydrogen bonds are present, while there is a CH- π interaction between H_{1A} of the methoxy group and C_4 of the isoindol-1-one portion. Once confirmed the nature of the isolated products, we have proceeded with a deprotection reaction of the methoxyl groups: BBr_3 is added dropwise to a solution of the 6,7-dimethoxy derivative in CH_2Cl_2 under inert atmosphere; the final 6,7-dihydroxy derivatives have been isolated by H_2O/Et_2O extraction, taking the organic phase to dryness. By a comparison of the NMR spectra of **JBSD107** and the relative 6,7-dihydroxy compound, **JBSD109** (Figure 24), it is possible to notice that the two singlets relative to the methoxy groups, at 4.15 and 3.91 ppm, disappeared, while a broad signal at 5.55 pm appears, which can be attributed to the two hydroxyl groups.

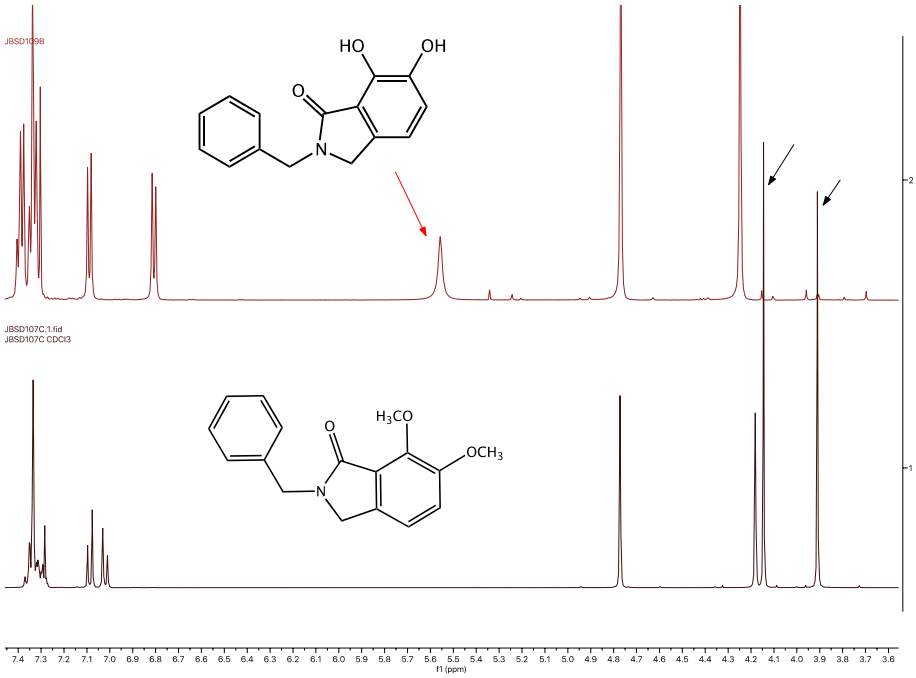

*Figure 24. Comparison of ^{1}H-NMR ($CDCl_3$-d, 500 MHz, 25°C) spectra of **JBSD107** (bottom) and the relative 6,7-dihydroxy form **JBSD109** (on the top).*

In order to get some single crystals suitable for X-ray analysis, several crystallization attempts have been carried out and we have finally been able to isolate crystals of **JBSD109** from slow evaporation of a methanolic solution of the ligand.

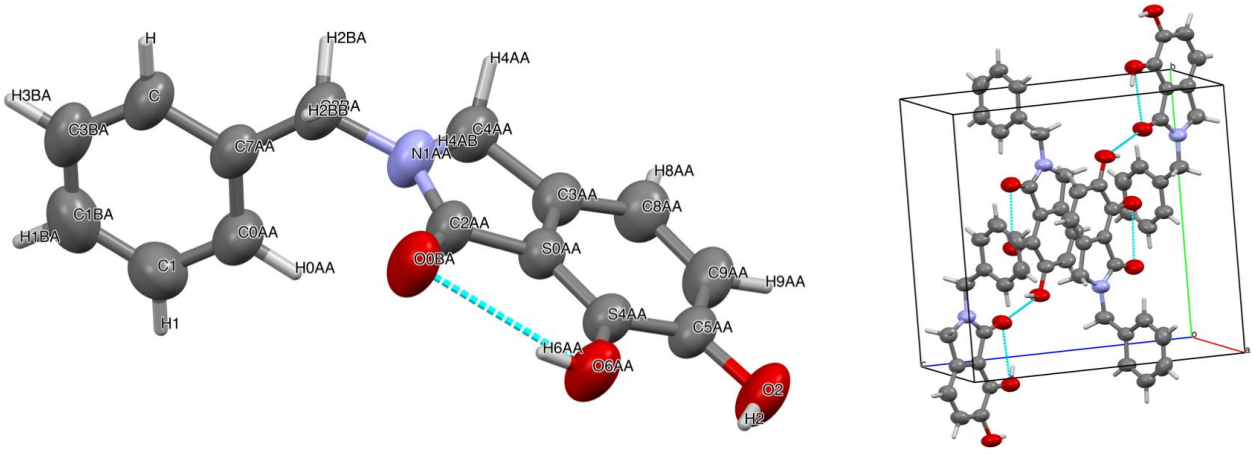

*Figure 25. Crystalline structure (273 K) of derivative **JBSD109** and its unit cell (on the right).*

In Figure 25 it is reported the crystal structure obtained by X-ray diffraction analysis. It is possible to notice that, like in the 6,7-dimethoxy form, the insoindol-1-one scaffold and the phenyl group are on two different planes, with an angle between them of about 88.2°; there is an intramolecular hydrogen bond between O_{0BA} and H_{6AA} (Figure 25). Looking at the packing motif of **JBSD109**, the unit

cell results to be $P2_1/c$ and it is present an intermolecular hydrogen bond between O_{0BA} and H_2 of an adjacent molecule; it is also present a CH-π interaction between H_{8AA} and C_{1BA} of the phenyl group of an adjacent molecule.

The purity of the final compounds has been verified by elemental analysis, as reported in the experimental section. In Figure 26 the structures of the isolated products are reported.

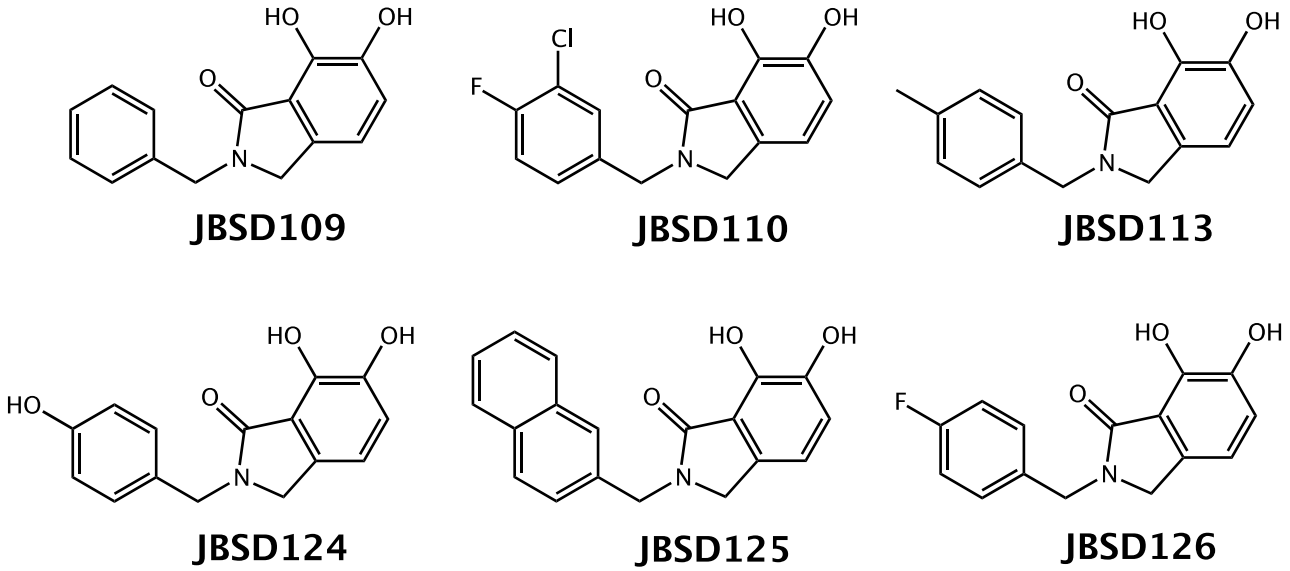

Figure 26. 2,3-dihydro-6,7-dihydroxy-1H-isoindol-1-one molecular structures.

3.2 BIOLOGICAL ASSAYS

3.2.1 FRET-based endonuclease assay

In order to evaluate PA_N endonuclease inhibitory activity of the synthesized molecules, a FRET-based endonuclease assay has been performed[323]. In this assay it is used a single strand DNA (ssDNA) substrate which is labeled with an emitter and a quencher fluorophore at opposite ends: when the substrate enters the enzyme, it is subjected to the cap-snatching mechanism (Figure 27), then the removal of the emitter turns on its fluorescence and allows to record a signal; once the competitive inhibitor is added, it would be able to remove the substrate from the catalytic active site of PA_N endonuclease and to chelate both metal ions: therefore, a decrease in fluorescence occurs, depending on the concentration of the inhibitor.

[323] Credille C.V., Chen Y., Cohen S.M.; *J. Med. Chem.* 59(13); 6444-6454 (**2016**).

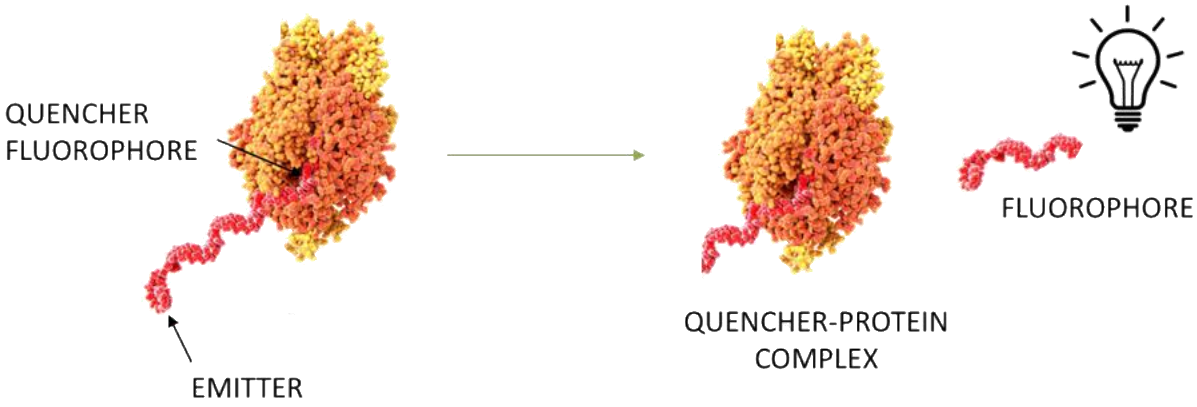

Figure 27. Scheme of the FRET-based assay: once the functionalized ss-DNA oligo-substrate enters the active site of the enzyme is subjected to the cap-snatching mechanism and the fluorophore is released in solution, with a turn on of its fluorescence.

Several solutions at different concentrations (ranging from 100 to 0.001 μM) of the derivatives have been tested; the change in fluorescence was measured over 45 minutes at 37°C ($\lambda_{excitation}$: 490nm; $\lambda_{emission}$ 520nm; 13.5 nm window). Dose-response curves were generated, fitted, and analyzed using Origin8 graphing software and final results are reported in Table 2.

	IC_{50} (nM)	S.D.
JBSD109	**39.39**	0.14
JBSD110	24.76	0.18
JBSD113	**22.30**	0.21
JBSD124	27.57	0.24
JBSD125	**30.47**	0.19
JBSD126	**22.49**	0.11

Table 2. IC_{50} values determined by FRET-based endonuclease assay. S.D.: standard deviation

Data obtained from a preliminary analysis on the inhibitory activity of the derivatives have revealed that the presence of a 4-positioned substituent on the aromatic ring can enhance the activity of the compound: in fact, **JBSD109**, with an unsubstituted phenyl moiety, and **JBSD125**, with a naphtyl substituent, result to have the lowest activity of the panel. The best profile is obtained with a methyl group (**JBSD113**) or a fluorine (**JBSD126**) substituent on the benzyl group. Results revealed that a functionalization of the aromatic ring is useful in order to establish additional interactions with the

enzymatic side chain, so that to increase the stability of the enzyme-inhibitor complex and efficiently impair the PA endonuclease activity.

In order to enlarge the available data set and possibly highlight a structure-activity relationship, we have decided to make a step forward and explore different 4-position substituents: a new panel of molecules has been synthesized and completely characterized (Figure 28).

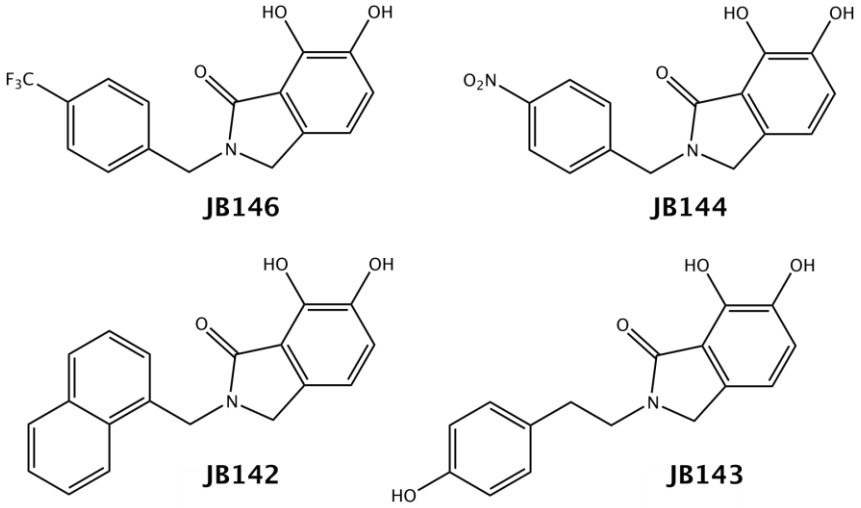

Figure 28. Second generation 2,3-dihydro-6,7-dihydroxy-1H-isoindol-1-one molecular structures.

As reported in Figure 28, we have chosen the 4-hydroxybenzyl group, to study a possible relationship between the activity of the inhibitor and the length of the spacer between the isoindol-1-one scaffold and the benzyl group. Moreover, we have explored the use of the 1-naphthalenyl group instead of the 2-bound one to verify if a changing in the orientation of the condensed system could afflict the inhibitory features of the compound. Moreover, we considered the presence of a NO_2 or a CF_3 group to investigate the role of the substituent at the 4-position of the benzyl moiety. All derivatives are actually being tested in in vitro enzymatic assays at University of California San Diego (USA, Prof. Seth Cohen) to verify their inhibitory activity on PA_N endonuclease.

Biological data obtained from previous analysis are in the nanomolar range and therefore very promising: these results underline that the isoindol-1-one scaffold can be used to develop efficient antivirals active against influenza virus PA_N endonuclease. On the basis of these considerations, we have decided to increase the affinity of the ligand for the magnesium ions making some modifications on the chelating moiety, designing a class of ligands with a new scaffold, as highlighted in Figure 29.

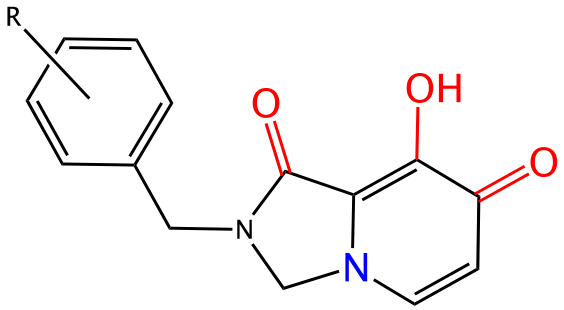

Figure 29. Molecular scaffold of the new influenza virus PA_N endonuclease inhibitors.

Both the insertion of a second nitrogen atom in the five-member ring and the replacement of a carbonyl group in place of the second hydroxyl one give a more rigid structure to the molecules, enhancing the chelating efficiency of the ligand.

Investigations about the synthetic pathway necessary to isolate a panel of molecules similar to the parent one are still ongoing. Details are given in the experimental section.

Notes:

This project has been developed at University of California San Diego in professor Seth M. Cohen's laboratory. Studies of the enzymatic activity of the derivatives has been carried out in collaboration with Dr. Christine Morrison (UCSD).